Functional Analysis of the GRAS Gene *LATERAL SUPPRESSOR* in Root Development of *Arabidopsis* and tomato



Rahere Thoma

Functional Analysis of the GRAS Gene *LATERAL SUPPRESSOR* in Root Development of *Arabidopsis* and tomato

Inaugural-Dissertation

zur

Erlangung des Doktorgrades

der Mathematisch-Naturwissenschaftlichen Fakultät

der Universität zu Köln

vorgelegt von

Rahere Thoma

aus Solingen

Köln, 2020



Max Planck Institute for
Plant Breeding Research



IMPRS Cologne

Die vorliegende Arbeit wurde am Max-Planck-Institut für Pflanzenzüchtungsforschung in Köln in der Arbeitsgruppe von Prof. Dr. Klaus Theres angefertigt.

Berichterstatter:	Prof. Dr. Klaus Theres
(Gutachter)	
	Prof. Dr. Wolfgang Werr
Vorsitzende der Prüfungskomission:	Prof. Dr. Ute Höcker
Tag der mündlichen Prüfung:	16.07.2019

Abstract

The genetic regulation of axillary meristem (AM) initiation is highly conserved throughout the majority of higher plants. Especially the GRAS gene LATERAL SUPPRESSOR (LAS), and its orthologues in various species constitute a nice example of this mechanistic conservation. LAS and its orthologues act as branching regulators, which promote the initiation of axillary meristems during vegetative development. Yet, the molecular mechanisms of LAS function are unknown. This study explored new perspectives, to gain a deeper understanding of the molecular basis of LAS function. Instead of focusing on AM initiation, the root was chosen as a promising new developmental context to analyze LAS function. Root-specific expression of LAS appears to be similarly conserved as LAS contribution to AM initiation, hence the root provides a new approach to study LAS function. Here, the previously identified cis-regulatory element B, located 2 kb downstream of *LAS*, is shown to be indispensable for *LAS* expression in the *Arabidopsis* root. *LAS* expression domains in the root mirror the cone-shaped domain of auxin response maxima in the tips of primary and lateral roots, showing transcript accumulation in the quiescent center, the columella stem cells and the mature columella cells. Monitoring of protein localization revealed that LAS protein accumulates in the nucleus and the cytoplasm. Also, LAS is a cell-to-cell mobile protein, trafficking from the columella in the LRC. Additionally, the *LAS* locus encodes for a long noncoding antisense transcript, which is expressed in exactly the same domains as *LAS*. One notable difference between *LAS* expression domains in the tips of primary and lateral roots is the significantly elevated expression level in young lateral roots. This might correlate with the increased vertical growth trajectories of LRs in *las-4* mutants, which is the only phenotypic deviation found in roots. LAS is thought to act as an inhibitor of cell differentiation. This hypothesis was tested by ectopic expression of *LAS* in the root apical meristem (RAM), which constitutes a powerful system to analyze cell differentiation. Ectopic expression reveals, that LAS promotes cell differentiation, and surprisingly cell differentiation also occurs in cells that express *LAS* endogenously. This indicated that LAS function might be dosage dependent. To test the applicability of root-derived knowledge about LAS protein characteristics, nuclear-targeted versions of LAS (LAS-NLS) were employed to analyze the relevance of protein movement during AM initiation. Interestingly, LAS-NLS versions were not able to complement the *las-4* mutant branching phenotype. Addition of the nuclear targeting domain seems not to affect movement of the LAS protein, because in the root LAS-NLS versions are still cell-to-cell mobile. Interestingly, there is a positive correlation between dosage and function, based on the analysis of transgene copy-number in relation to *las-4* complementation. Higher copy-number correlates with the loss of *las-4* complementation. To account for the reoccurring theme of dosage-dependent function a spillover-model of LAS function is proposed. In this model, LAS is kept in check by a second interacting protein. If the buffering capacity of the interacting protein is compromised or exceeded, LAS might extend its functional scope, probably counteracting its own endogenous function.

Zusammenfassung

In den meisten höheren Pflanzen ist die Bildung von Achselmeristemen (AMs) ein genetisch hoch konservierter Mechanismus. Dies spiegelt sich besonders in der Funktionsweise des GRAS Gens LATERAL SUPPRESSOR (LAS) wider. LAS und seine orthologen Gene beeinflussen AM Bildung immer nach dem selben Muster. Ein Verlust der Genfunktion unterdrückt die Bildung von AMs während der vegetativen Wachstumsphase. Trotz dieses eindeutigen Ursache-Wirkung Zusammenhangs ist die Funktion von LAS auf molekularer Ebene unklar. Ziel dieser Studie ist es, einen neuen Ansatz zu finden, welcher eine funktionale Analyse von LAS ermöglicht. Alle bisherigen Studien zu LAS beschränkten sich auf den Prozess der AM Bildung. Eine in vielen Studien genannte, aber nicht weiter beachtete Eigenschaft von LAS und seinen orthologen Genen ist das Vorkommen von Expressions-Domänen in Wurzelgewebe. Wurzel-spezifische LAS Expression scheint in einem ähnlichen Maß konservier zu sein, wie der Zusammenhang zwischen LAS Funktion und AM Bildung. Die Wurzel bietet besonders im Bezug auf molekulare Analysen gewisse Vorteile gegenüber dem Sprossgewebe, und stellt deswegen einen vielversprechenden neuen entwicklungsbiologischen Ansatz zur funktionalen Analyse von LAS dar. Hier wird gezeigt, dass das, in einer früheren Studie beschriebene, regulatorische Element B unverzichtbar für die Expression von *LAS* in der Wurzel von *Arabidopsis* ist. Wurzelgewebe, welche LAS Transkript aufweisen, sind deckungsgleich mit den kegelförmigen Domänen in den Spitzen von Haupt- und Seitenwurzeln, welche durch ein Maximum von Auxin gesteuerter Gen Expression gekennzeichnet sind. Der kegelförmige Bereich umfasst das Ruhende Zentrum, die Columella-Stamzellen und die differenzierten Columella Zellen. Die Charakterisierung der Protein-Akkumulation ergab, dass LAS sowohl im Zellkern, als auch im Cytoplasma auftritt. Eine weitere neuentdeckte Eigenschaft ist die Fähigkeit des LAS Proteins, sich in benachbarte Zellen zu bewegen. Im Fall der Wurzelspitze wandert LAS von der Columella in die Zellen der lateralen Wurzelkappe. Außerdem wird gezeigt, dass der LAS Locus zusätzlich für ein langes nicht-kodierendes *antisense* Transkript kodiert, welches in denselben Domänen wie *LAS* exprimiert wird. Haupt- und Seitenwurzeln zeigen bezüglich der *LAS* Expression einen gravierenden Unterschied. In Seitenwurzeln wird *LAS* sehr viel stärker als in Hauptwurzeln exprimiert. Dies könnte in Zusammenhang stehen mit dem Phänotyp der Funktionsverlust-Mutante *las-4*, welche eine deutlich gesteigerte vertikale Wuchsrichtung der Seitenwurzeln zeigt. Unterdrückung von Zell-Differenzierung ist die gängige Interpretation der Funktionsweise von LAS. Diese Hypothese wurde durch ektopische Expression von *LAS* im Wurzelspitzenmeristem (RAM) getestet. Das RAM ist aufgrund seiner zellulären Organisation ein klassisches System um Zell-Differenzierung zu analysieren. Die ektopische Expression ergab, dass LAS Zell-Differenzierung fördert. Überraschenderweise tritt Zell-Differenzierung auch in Zellen auf, welche *LAS* bereits endogen exprimieren. Dieses Ergebnis deutet daraufhin, dass die Funktion von LAS von der Menge des gebildeten Proteins beeinflusst werden kann. Die Übertragbarkeit der neugewonnenen Erkenntnisse zu Eigenschaften des LAS Proteins wurde im Kontext der AM Bildung getestet. Zellkern-spezifische LAS Versionen (LAS-NLS) wurden auf ihre Fähigkeit getestet,

den AM Bildungsdefekt in der *las-4* Mutante zu komplementieren. Die LAS-NLS Versionen konnten den AM Bildungsdefekt in *las-4* nicht retten. Hierbei ist hervorzuheben, dass die gezielt Zellkern-gerichtete Lokalisierung von LAS-NLS, unerwarteterweise, nicht die Wanderungseigenschaften des Proteins beinträchtigte. Eine Analyse der Anzahl der Transgen Insertionen ergab, dass eine positive Korrelation zwischen einer hohen Anzahl von Insertionen und der Beeinträchtigung der *las-4* Komplementation besteht. Aufgrund des in verschiedenen und voneinander unabhängigen Experimenten beobachteten Dosis-Funktion-Zusammenhanges, im Hinblick auf die Funktion von LAS, wurde ein Spillover-Modell als Erklärungsversuch vorgeschlagen. In diesem Model steht die Funktion von LAS in Zusammenhang mit einem zweiten interagierenden Protein, welches LAS Funktion stabilisiert. Wenn die stabilisierende Wirkung entfällt, eröffnen sich neue Funktionspotentiale für LAS, welche unter Umständen der endogenen Funktion entgegenwirken können.

Contents

Abstract I

Zusammenfassung II

List of Figures VI

Abbreviations VIII

1 Introduction 1

1.1 Plant development in a nutshell . . . 1
1.2 Organization and molecular set up of the shoot apical meristem . . . 1
1.3 Boundaries and the initiation of lateral branches . . . 4
1.4 Regulation of *LATERAL SUPPRESSOR* expression in the shoot apical meristem 8
1.5 Organization and maintenance of the root apical meristem . . . 10
1.6 Looking beyond - differences between primary and lateral growth axes . . . 14
1.7 Aim of this work . . . 17

2 Materials and Methods 19

2.1 Sharing of Data, Scripts and Plasmids . . . 19
2.2 Material . . . 19
2.3 Methods . . . 25

3 Results 36

3.1 Exploring *LATERAL SUPPRESSOR* expression domains in the *Arabidopsis* root 36
Root specific expression of *LAS* depends on regulatory element B . . . 36
LAS root expression domains on cellular level . . . 37
What is the basis of *LATERAL SUPPRESSOR* movement? . . . 43
3.2 Phenotypic analysis of *las-4* root system development . . . 45
Loss of *LATERAL SUPPRESSOR* effects the orientation of lateral roots . . . 45
Increased vertical growth trajectories in *las-4* lateral roots . . . 47
3.3 Analysis of cell differentiation in the root apical meristem after ectopic *LATERAL SUPPRESSOR* expression . . . 49
Prolonged 17-β-estradiol treatment leads to a reduced primary root growth rate in non-transgenic plants . . . 52

Ectopic *LAS* expression in the root endodermis is sufficient to reduce growth rates in primary and lateral roots . . . 52
Ectopic *LAS* expression promotes increased horizontal growth in lateral roots . . 54
LAS-Tq2 is ubiquitously detected in the root apical meristem and not restricted to the endodermis . . . 58
LAS-Tq2 promotes stem cell differentiation in the root stem cell niche . . . 60
3.4 Analyzing LATERAL SUPPRESSOR function in tomato root development . . . 62
The *ls-1* mutant displays altered growth trajectories in primary and lateral roots 62
Reduced primary root growth rate, but no reduction of LR number in *ls-1* . . . 65
Minor reduction of gravitropism in primary roots of *ls-1* mutants . . . 67
Lateral roots in *ls-1* display a severe reduction in gravitropism . . . 70
Detection of an *Ls/LAS* antisense transcript in root tips of tomato and *Arabidopsis* 73
3.5 Biological relevance of LAS movement in the context of axillary meristem initiation 75
Inhibition of LAS movement . . . 75
LAS-NLS versions rescue axillary meristem initiation in a dose dependent manner 75

4 Discussion **80**
4.1 Cellular differences in *LATERAL SUPPRESSOR* expression domains in leaf axils and root tips . . . 80
4.2 LATERAL SUPPRESSOR - a putative suppressor of auxin signaling or modifier of auxin fluxes? . . . 81
4.3 Comparison of *Arabidopsis las-4* mutants and tomato *ls-1* mutants . . . 83
4.4 Potential LATERAL SUPPRESSOR functions - deduced from ectopic expression analysis . . . 86
4.5 The role of the *LAS/Ls* antisense transcript . . . 89
4.6 Does LATERAL SUPPRESSOR movement plays a role during axillary meristem formation? . . . 90
4.7 Conclusions . . . 93

5 Supplementary Data **94**

References **117**

Danksagung/Acknowledgments **133**

Eidesstattliche Erklärung **134**

List of Figures

1 SAM and shoot apex organization . . . 8
2 Distribution and function of cis-regulatory elements at the *LAS* locus . . . 10
3 RAM organization, developmental timeline and terminology for direction . . . 13
4 Model of GSA control . . . 16

5 Region B regulates *LAS* expression in root tissues . . . 38
6 *LAS* is expressed in a cone shaped domain covering the quiescent center, columella stem cells and the columella . . . 40
7 LATERAL SUPPRESSOR protein is detected in the lateral root cap . . . 42
8 Cell-to-cell movement of LAS protein . . . 44
9 *las-4* causes a reduction in the lateral root branching angle and less curvature during lateral root growth . . . 46
10 Lateral roots in *las-4* display increased vertical growth trajectories . . . 48
11 Driving *LAS* expression by the *SCR* promoter changes root system architecture 50
12 17-β-estradiol and induction of *LAS* expression reduce root growth . . . 54
13 Induction of *LAS* expression has no effect on LR number . . . 55
14 LRs display enlarged horizontal growth angles after induction of *LAS* expression 57
15 *SCR* promoter driven *LAS* does not reproduce the endogenous SCR domain . . . 59
16 LAS promotes differentiation of apical stem cells and promotes formative divisions in the ground tissue . . . 61
17 Increased horizontal growth trajectories of roots in the *ls-1* mutant . . . 63
18 Reduced growth rate, but no reduction in LR number . . . 66
19 Minor reduction of gravitropic response and less LR development in primary roots of the *ls-1* mutant after root bending . . . 68
20 Loss of gravitropism in LRs of *ls-1* mutants . . . 71
21 *asLAS* is expressed in the same domain as *LAS* . . . 74
22 LAS-NLS versions partially rescue the *las-4* axillary meristem initiation defect . 76
23 Correlation between transgene zygosity and AM initiation rescue . . . 78

24 Spillover model . . . 93

S1 Expression of *LATERAL SUPPRESSOR* orthologues in monocots . . . 94
S2 Vns-LAS localization during lateral root morphogenesis . . . 95

S3 LAS-Vns signal during lateral root primordium emergence 96
S4 LAS-Vns protein localization during lateral root morphogenesis 97
S5 Differences in Vns-LAS protein levels between primary and lateral root QCs . . 98
S6 Root traits 99
S7 Specific deviation from gravity oriented root growth and effect on LR growth rate in *pSCR>>LAS-Tq2* plants after *LAS* induction 100
S8 Increased horizontal growth in side shoots of plants expressing *pSCR>>LAS-Tq2* 101
S9 Loss of QC fate in LAS inducing conditions 102
S10 LRs in the *ls-1* mutant did not respond to gravity 103
S11 DEGs in *ls-1* mutant primary root tips 103
S12 *Ls* antisense transcript in tomato roots 104
S13 5′ RACE of *asLAS* and *asLs* transcripts 105
S14 *aspLAS:erSclt* expression in LRs and pericycle/ground tissue cell lineages 106
S15 LAS-NLS versions are expressed in endogenous root expression domains 108
S16 Summary statistics 110

Abbreviations

βE 17-β-estradiol

μM micromolar

μg microgram

μm micrometer

2,4-D 2,4-dichlorophenoxyacetic acid

ACR4 ARABIDOPSIS CRINKLY4

AGO agravitropic offset mechanism

AHK ARABIDOPSIS HISTIDINE KINASE

AHP6 ARABIDOPSIS HISTIDINE PHOSPHO-TRANSFER PROTEIN 6

AM axillary meristem

AMS *Arabidopsis* MS

AP2/ERF APETALA2/ETHYLENE RESPONSE FACTOR

ARF AUXIN RESPONSE FACTOR

ARR1 ARABIDOPSIS RESPONSE REGULATOR1

as antisense transcript

ATAF1/2 ARABIDOPSIS TRANSCRIPTION ACTIVATION FACTOR1/2

AUX/IAA AUXIN/INDOLE-3-ACETIC ACID

avgAbsAng average absolute angle

axr auxin-resistant

BAM1 BARLEY ANY MERISTEM1

biChro biChromium

Bl Blind

BlT1 Blue Insensitive Trait 1

bp base pairs

br biological replicate

C cortex

CaMV cauliflower mosaic virus

catg category

CDF4 CYCLING DOF FACTOR4

cDNA complementary DNA

CKX2 CYTOKININ OXIDASE 2

CLE40 CLAVATA3/EMBRYO SURROUNDING REGION40

CLSM confocal laser scanning microscopy

CLV CLAVATA

cm centimeter

Col columella

Col-0 Columbia-0

CosG Cosmid G

CRN CORYNE

CSCs columella stem cells

CUC CUP-SHAPED COTYLEDON

cv. cultivar

CZ central zone

DAG days after germination

deg degree

DEGs differentially expressed genes

DMSO Dimethyl sulfoxide

DNA Deoxyribonucleic acid

DR5 DIRECT REPEAT5

DRN DORNRÖSCHEN

DRNL DORNRÖSCHEN-LIKE

En endodermis

Ep epidermis

er endoplasmic reticulum

ER endoplasmic reticulum

FC fold change

FLC FLOWERING LOCUS C

FPKM Fragments Per Kilobase Million

g gravity

GAI GIBBERELLIN-ACID INSENSITIVE

GH GRETCHEN HAGEN

GRAS *G*AI, *R*GA and *S*CR

gravAng gravity angle

GSA gravitropic setpoint angle

Gt ground tissue

Gty genotype

GUS β-glucuronidase

h hour

HD-ZIP homeodomain–leucine zipper protein

HDAC histone deacetylase

HY5 ELONGATED HYPOCOTYL5

IAA indole-3-acetic acid

IM inflorescence meristem

IPT8 ISOPENTENYLTRANSFERASE 8

IPX interacting protein

IQR inter-quartile range

kb kilo base

KN1 KNOTTED1

KNOX *KNOTTED1*-like homebox

LAS LATERAL SUPPRESSOR

LES lateral root cap/epidermis stem cell

LHP1 LIKE HETEROCHROMATIN PROTEIN 1

lncRNA long noncoding RNA

LR lateral root

LRBA LR branching angle

LRC lateral root cap

LRP lateral root primordium

LRR leucine rich repeat

MC middle cortex

ml milliliter

mm millimeter

MOC1 MONOCULM 1

MP MONOPTEROS

MpFGMYB FEMALE GAMETOPHYTE MYB

mPSPI modified pseudo-Schiff propidium iodide

mRNA messenger RNA

MS Murashige and Skoog medium

n/a not analyzed

NAC *N*AM, *A*TAF1/2 and *C*UC2

NAM NO APICAL MERISTEM

NLS NUCLEAR LOCALIZATION SIGNAL

nm nanometer

NPA N-1-naphthylphthalamic acid

nph4 non-phototropic hypocotyl4

OC organizing center

ORF open reading frame

OZ oscillation zone

p(x) p value of x

Pc pericycle

PC principal component

PCA Principal component analysis

PI Propidium iodide

PIN PIN-FORMED

PLT PLETHORA

PR primary root

PRC2 Polycomb repressive complex 2

Prp protophloem

Prv provascular cells

Prx protoxylem

Pty phenotype

PZ peripheral zone

QC quiescent center

qPCR quantitative real-time PCR

RACE rapid amplification of cDNA ends

RAM root apical meristem

RAX REGULATOR OF AXILLARY MERISTEMS

respAng response angle

REV REVOLUTA

RGA REPRESSOR of GA1

RNA Ribonucleic acid

RSA root system architecture

RZ rib zone

S. lycopersicum Solanum lycopersicum

S. penn. Solanum pennellii

SCL SCARECROW-LIKE

Sclt Scarlet

SCR SCARECROW

SEU SEUSS

SHR SHORT ROOT

SHY2 SHORT HYPOCOTYL 2

SIC SICKLE

SIEL SHORT-ROOT INTERACTING EMBRYONIC LETHAL

SlPAP27 PURPLE ACID PHOSPHATASE27-4a

SNP single nucleotide polymorphism

SPY SPINDLY

STM SHOOTMERISTEMLESS

SUF SUPPRESSOR OF FEMINIZATION

SV40 SIMIAN VIRUS 40

Swc shootward stem cell

T1 1^{st} transgenic generation after transformation

T2 2^{nd} transgenic generation after transformation

TA transit amplifier

tdTom tandemTomato

ti po time point

TIR1/AFB TRANSPORT INHIBITOR RESISTANT 1/AUXIN SIGNALING F-BOX

Tq2 mTurquoise2

Tr Cell shape tracing

trmt treatment

TSS transcription start site

UTR untranslated region

Vns Venus

WOX WUS HOMEOBOX

wt wild type

Xist X-inactive-specific transcript

Y1H yeast-one-hybrid

yuc-1D yucca-1D

1. Introduction

1.1 Plant development in a nutshell

Periodic formation of lateral organs is a general feature of plant development and modifications of this mechanism contribute to the large variety of different body plans within the plant kingdom (McSteen and Leyser, 2005). During postembryonic development, shoots and roots produce repeating units, phytomers and lateral roots (LRs), which enable establishment of lateral growth axes. Axis elongation and lateral organ formation is dependent on the activities of the primary shoot and root meristems, which contain organized groups of dividing cells, encompassing the stem cells (Heidstra and Sabatini, 2014). Shoot apical meristem (SAM) and root apical meristem (RAM) initiation at the apical and basal poles of the embryo are key events of apical-basal axis formation in plant development (Jürgens, 1995). Because these pivotal meristems are initiated during embryogenesis, they are referred to as primary meristems (Talbert et al., 1995). Apical-basal axis elongation and lateral organ production during postembryonic development relies on progeny of SAM or RAM stem cells, enforcing the plant to prevent stem cell differentiation. This postembryonic plasticity sets plants apart from animals, because being sessile organisms plants need to be able to modify their development in response to environmental cues.

1.2 Organization and molecular set up of the shoot apical meristem

The SAM is the very tip of the shoot apex and resembles a dome-shaped structure. The first visible trace of an organ primordium is a protrusion in the otherwise smooth SAM surface. Also, this marks the transition from the SAM to the more basal shoot tissue, or from undifferentiated to differentiated cells, respectively (Medford, 1992). In *Arabidopsis*, one of the broadly studied plant model systems, the expression of the *KNOTTED1*-like homeobox (KNOX) transcription factor *SHOOTMERISTEMLESS* (*STM*) defines the SAM domain. All cells in the SAM express *STM* and either belong to the stem cell pool or display a meristematic (proliferating) character. *stm* mutant analysis and *STM* overexpression studies demonstrated that *STM* is necessary for SAM initiation during embryogenesis (Long et al., 1996), and maintenance of the SAM during postembryonic development through inhibition of differentiation (Lenhard et al., 2002).

The SAM is organized into three discrete cell layers. On top, the epidermal layer (L1), from which all epidermal cells are derived, followed by the sub epidermal layer (L2), which generates sub epidermal tissue and gametes. Beneath the L2, cells form a multi layered tissue, still referred to as layer (L3), which gives rise to the ground tissue and the vasculature. Each individual layer represents a separate cell lineage. The important determinant to achieve cell lineage partitioning is the cell division plane orientation, which prevents the invasion of daughter cells from one layer into neighboring layers. In L1 and L2, cell divisions occur almost exclusively along the anticlinal plane (perpendicular to the surface), whereas in the L3 cell division occurs along all possible planes, oblique, anticlinal or periclinal (Fig. 1a ; Stahl and Simon, 2004).

The layered cell organization, reflects cellular ontogeny in the SAM, whereas the zonation of cells according to specific characteristics differentiates specific areas, independent of the lineage dependency. Geometrically, the SAM has a circular cross section, and the central zone is located in the center at the very top of the dome. The central zone stretches across all three layers and contains the stem cells of each individual layer. One characteristic of stem cells is their lower cell division frequency, compared to cells located in the periphery of the SAM that display a higher cell division frequency. The peripheral zone radially extends from the central zone towards the first visible organ primordium, which arises from the flank of the shoot apex (Reddy et al., 2004; Burian et al., 2016). Cells in deeper cell layers within the SAM, exclusively L3 tissue, are grouped into the rib zone (Fig. 1b). Even though, all cells in the SAM are continuously dividing, the frequency of cell divisions indicates the different tasks assigned to each zone. Slower divisions in the central zone are sufficient to maintain the stem cell population, and at the same time provide enough daughter cells for organ initiation in the peripheral zone. Further, a longer cell cycle duration, reduces the probability to accumulate mutations in the stem cell line, because over time less replication rounds occur. In the peripheral zone, the shortening of cell cycle duration acts than as an amplifier of cell number to ensure proper organ initiation, thereby releasing division pressure from the stem cells. The term transit amplifier (TA) was coined to describe this kind of meristematic cell, taking also into account that this is only a temporary cell state between loss of stem cell fate and start of cell differentiation (Stahl and Simon, 2004).

How does the plant manage to protect SAM stem cells from differentiation? Isolation of mutant alleles of the homeodomain transcription factor *WUSCHEL* (*WUS*), was the first step towards a plant specific stem cell niche concept. The niche is a micro environment that provides cues, which are a necessity for stem cell fate and maintenance. Loss of niche factors leads to a loss of stem cells. *WUS* RNA was detected in a specific group of L3 cells, exactly below the central zone. *wus* mutants are able to initiate SAMs, but their activity fades rapidly, because they fail to maintain a sufficient stem cell number for proper development (Laux et al., 1996; Mayer et al., 1998). STM partially rescues *wus* mutants by providing the cues for reinitiation of stem cells, which differentiate quickly because *WUS* function is lacking. This repeating cycle explains the characteristic stop-and-go development seen in *wus* mutants (Laux et al., 1996). The domain of *WUS* RNA accumulation was termed organizing center

(OC), because of its importance for stem cell maintenance (Mayer et al., 1998). Notably, the stem cell harboring zone and the OC constitute two spatially distinct domains within the SAM, suggesting communication between both cell populations along the apical-basal axis. Therefore, *WUS* either enables transmission of a stem cell fate promoting signal, or acts itself as a mobile signal. Comparison of the domains of *WUS* RNA accumulation and WUS protein localization revealed that in fact WUS protein moves through plasmodesmata from the OC into the central zone, acting as a non-cell autonomous factor for stem cell maintenance (Yadav et al., 2011; Daum et al., 2014). In addition to stem cell maintenance, *WUS* is also able to induce stem cell identity, as shown by *WUS* misexpression experiments (Schoof et al., 2000).

Genetic studies revealed additional genes controlling stem cell fate, however, defects in these genes had the opposite effect on stem cell maintenance compared to *wus*. Loss of either one of three *CLAVATA* (*CLV*) genes, caused an over accumulation of stem cells in the SAM (Clark et al., 1997; Kayes and Clark, 1998; Fletcher et al., 1999). *CLV3* turned out to be a stem cell derived signal, encoding for a short secreted peptide, that is only expressed in the central zone (Fletcher et al., 1999). Recognition of the CLV3 peptide signal was shown to be dependent on a set of membrane-localized, leucine rich repeat (LRR) based receptor complexes. Expression of the receptor kinase CLV1 is restricted to the OC (Clark et al., 1997). CLV1 homodimers are able to bind the CLV3 peptide with their extracellular domain (Ogawa et al., 2008; Shinohara and Matsubayashi, 2015). *CLV2* also encodes for an LRR receptor, however it lacks the intracellular kinase domain and it is expressed throughout many different plant tissues (Jeong et al., 1999). CLV2 forms a heterodimeric complex with CORYNE (CRN), which is a membrane localized pseudokinase that is expressed in the whole SAM (Müller et al., 2008; Nimchuk et al., 2011). *crn* mutants phenotypically mimic the *clv* mutants, indicating their importance for stem cell regulation (Müller et al., 2008; Bleckmann et al., 2010). Whether CLV3 is a ligand of the CLV2-CRN receptor-pseudokinase complex is still under debate based on opposing results from two studies (Guo et al., 2010; Shinohara and Matsubayashi, 2015). The role of the CLV2-CRN receptor-pseudokinase complex remains enigmatic. Genetic studies support the presence of two independent pathways, one based on CLV1, the other one based on CLV2-CRN (Müller et al., 2008). On molecular level, each of these mutants displays increased *WUS* expression, which is the cause of the increased number of stem cells (Brand et al., 2000; Schoof et al., 2000; Müller et al., 2008). These genetic studies showed, that a negative feedback loop keeps the stem cell population at a constant size. WUS migrates from the OC through plasmodesmata into the stem cell harboring layers L1, L2 and L3 to promote stem cell fate. In turn, stem cells express *CLV3*, which will be processed to become a secreted peptide signal that is received by specific plasma membrane located LRR receptor complexes in the OC. CLV/CRN receptor complexes trigger a yet unresolved signaling cascade to suppress *WUS*, closing the negative feedback loop.

The described CLV-WUS negative feedback loop represents just the minimal working solution and many more layers of complex regulation are required for proper SAM function. For example, two receptor kinases closely related to CLV1, BARLEY ANY MERISTEM1 (BAM1) and BAM2 were shown to be necessary for stem cell maintenance. *bam1 bam2* double mutants

displayed smaller meristems, an indication for a decreased number of stem cells (DeYoung et al., 2006). However, higher order mutant combinations with CLV pathway genes revealed complex interactions. *bam1 bam2* suppressed the *clv3* phenotype, displayed no effect in combination with *clv2*, but enhanced the *clv1* phenotype (Deyoung and Clark, 2008). Careful molecular and genetic studies revealed that *BAM* genes are able to partially complement *clv1*, based on ectopic expression in the OC. *BAM* gene expression is normally suppressed through CLV1, explaining the drastic phenotype of the triple mutant (Nimchuk et al., 2015). Further, the CLV-WUS negative feedback loop is the convergence point for many developmental cues that tweak signaling components to increase or decrease the stem cell population in the SAM. For example, changes in soil nitrate availability trigger a root-borne long-range cytokinin based signal to modulate *WUS* expression and the size of the SAM stem cell pool (Landrein et al., 2018).

1.3 Boundaries and the initiation of lateral branches

Cells located at the edge of the peripheral zone are integrated into organ primordia. Integration into an organ primordium coincides with the transition from meristematic tissue into differentiating tissue (Burian et al., 2016). Organ primordia appear as small bulges on the otherwise smooth SAM surface. In between the adaxial side of the protruding primordium and the dome-like structure of the SAM a leaf axil is formed. An unique morphological feature of the leaf axil, is the specific arrangement of cells, that results in a surface with negative Gaussian curvature (Kwiatkowska, 2004). Leaf axils are a unique tissue, because they are the launching pads for lateral branches. Cells in the leaf axil share similar characteristics, like less frequent cell divisions. Further, leaf axil cells form a tissue that acts as a barrier, separating meristematic cells from the differentiating cells in the organ primordium, hence the term boundary was coined. Prerequisite to generate a side shoot is the initiation of a secondary meristem in the boundary, also referred to as axillary meristem (AM; Wang et al., 2016). The AM harbors SAM derived stem cells, which establish a secondary branch-specific lineage during branch outgrowth (Burian et al., 2016). Initiation of AMs relies therefore on the formation of a new stem cell niche, and poses the question about the fate of AM stem cell predecessors. Two different scenarios for AM initiation were proposed, the 'detached meristem' concept and the '*de novo*' concept. The detached meristem concept states that AM precursors cells keep their pluripotent stem cell character when they leave the SAM stem cell niche. In contrast, the '*de novo*' concept emphasizes positional information, placement in the boundary, as the determining cue for AM initiation independent of the differentiation stage of a given cell (Long and Barton, 2000).

In *Arabidopsis*, continuous expression of *STM* is required to initiate AMs (Fig. 1c). *STM* expression fades rapidly in newly initiating organ primordia, but in the boundary *STM* expression is maintained. The boundary specific *STM* expression domain displays differences regarding the distribution of *STM* transcripts, and the age of the leaf axil. From P1 to P15,

STM is detected throughout the whole boundary. From P16 onwards, *STM* expression is focused to a central group of cells at the adaxial leaf base, which overlaps with the position of the later developing AM (Long and Barton, 2000; Greb et al., 2003). The dependence of AM initiation from *STM* expression was shown through the analysis of mutant plants carrying the weak *stm-bum1* allele, which failed to initiate AMs (Shi et al., 2016). However, *STM* expression is very broad and unspecific in the shoot apex, meaning that additional factors are needed to provide domain specific information.

Mutant screenings conducted in tomato, identified two main branching regulators. The first branching regulator, *LATERAL SUPPRESSOR* (*Ls*) encodes a putative transcriptional regulator that belongs to the GRAS (*GIBBERELLIN-ACID INSENSITIVE* (*GAI*); *REPRESSOR of GA1* (*RGA*); *SCARECROW* (*SCR*)) gene family (Pysh et al., 1999; Schumacher et al., 1999). GRAS genes represent a plant specific family of transcriptional regulators, which are important for plant growth and development (Pysh et al., 1999; Niu et al., 2017). The *ls-1* mutant, presumably a *Ls* loss-of-function allele, develops no side shoots in leaf axils during vegetative development (Fig. 1c). Additionally, during reproductive growth the proper development of flowers is disturbed, with lower total flower number per inflorescence, reduced fertility and a lack of petals (Schumacher et al., 1999). The *Ls* pathway is highly conserved in higher plants and defective AM initiation during vegetative development is found in various species with described mutants of *Ls* orthologous genes, like *Arabidopsis*, rice and *Antirrhinum majus* (snapdragon; Greb et al., 2003; Li et al., 2003; Mizzotti et al., 2017). In *Arabidopsis*, *LATERAL SUPPRESSOR* (*LAS*) transcripts accumulate in leaf primordia/leaf axils from P1 to P20/22, in a band-shaped domain (Greb et al., 2003). Similarly, expression of *MONOCULM 1* (*MOC1*) in rice and *Ls* in tomato is restricted to leaf primordia/leaf axils (Li et al., 2003; Busch et al., 2011). In other species, the expression of *Ls* orthologous resembles the transcript accumulation of *STM* in the *Arabidopsis* shoot apex, as seen in snapdragon and *Helianthus annuus* (wild sunflower; Fambrini et al., 2017; Mizzotti et al., 2017). The molecular function of *LAS*, also with respect to detached vs *de novo* mode of AM initiation, is still an open question. Being a GRAS family member, *LAS* is expected to affect gene expression (Pysh et al., 1999; Niu et al., 2017). However, evidence supporting a role for LAS in regulating gene expression through direct DNA binding or through interaction with transcription factors is preliminary and has to be extended (Rossmann, 2013). With respect to the molecular role of LAS, an indication was derived from a study done in tomato. Rossmann et al. (2015) compared cell fate in distal leaflet boundaries, a tissue that is affected by loss of Ls function, in wild-type and *ls* mutant backgrounds. The distal leaflet boundary displays functional similarity to leaf axils, because in tomato ectopic shoots can arise from that specific region. This suggested that *Ls* might act as an inhibitor of cell differentiation, to keep cells competent for later recruitment into a new stem cell niche (Rossmann et al., 2015). In *Arabidopsis las* mutants, *STM* transcript accumulation in primordia/leaf axils lack the focused expression domain at the adaxial leaf base from P16 onwards. Similarly, expression of *REVOLUTA* (*REV*), a homeodomain–leucine zipper protein (HD-ZIP), is lost in an *STM* equivalent domain, from P16 onwards, in *las* mutants (Ratcliffe

et al., 2000; Greb et al., 2003). Among other phenotypic alterations *rev* mutants frequently fail to develop side shoots during vegetative development (Fig. 1c; Talbert et al., 1995). Therefore, LAS is needed to promote boundary specific changes in transcript accumulation of *STM* and *REV*. The regulatory mechanisms behind these dynamics of transcript accumulation in the boundary are largely unknown, but it was shown that REV is able to directly promote *STM* expression (Tian et al., 2014).

In *Arabidopsis*, the NAC (*NO APICAL MERISTEM* (*NAM*); *ARABIDOPSIS TRANSCRIPTION ACTIVATION FACTOR1/2* (*ATAF1/2*); *CUP-SHAPED COTYLEDON2* (*CUC2*)) transcription factors CUC1, CUC2 and CUC3 are all expressed in SAM boundaries, and loss-of-function mutants display fusion of adjacent organs. Organ fusion reflects the loss of a separating tissue, like the boundary in the leaf axil, between two organs (Aida et al., 1997; Takada et al., 2001; Vroemen et al., 2003; Raman et al., 2008). *cuc3* mutants display loss of AM formation during vegetative development, but *LAS* transcript accumulation was wild type-like in boundaries of leaf primordia/leaf axils. This indicated that CUC3 and LAS act in separate pathways during AM formation (Raman et al., 2008). Single mutants of either *cuc1* or *cuc2* resembled wild type plants with respect to AM initiation. Interestingly, overexpression of the post transcriptional *CUC* inhibitors *MIR164A/MIR164B* in the *cuc3* mutant enhanced the branching defect. miR164 binding to their complementary binding sites within *CUC1* and *CUC2* transcripts leads to mRNA cleavage and degradation (Kasschau et al., 2003). This indicated that all three *CUC* genes play a role during AM formation. Further, *LAS* transcript accumulation in leaf primordia/leaf axils was strongly reduced. In contrast, *mir164a-4 mir164b-1 mir164c-1* triple mutants displayed enhanced *LAS* expression in the SAM. These results indicated that both CUC1 and CUC2 act as positive regulators of *LAS* expression during AM formation, and it was shown that CUC2 directly binds to *LAS* regulatory elements (Fig. 1c; Raman et al., 2008; Tian et al., 2014). Interestingly, *CUC* genes are required for SAM initiation during embryogenesis, suggesting that meristem initiation in general relies on a specific mechanism, independent of developmental stage (Aida et al., 1997). For proper cotyledon development, *CUC1* expression during embryogenesis is regulated by the *APETALA2/ETHYLENE RESPONSE FACTOR* (*AP2/ERF*) transcription factor DORNRÖSCHEN (DRN; Ikeda et al., 2006). Both, DRN as well as its paralog DORNRÖSCHEN-LIKE (DRNL) are required during vegetative development for AM initiation based on the phenotypic analysis of loss-of-function alleles. DRN has been shown to directly activate the expression of *CUC2*, and DRN as well as DRNL have been shown to directly promote *STM* expression in a REV dependent manner (Fig. 1c; (Zhang et al., 2018)). Recurrence of such gene modules corroborates the similarities between SAM initiation during embryogenesis and AM initiation during postembryonic development.

The second identified tomato branching regulator, Blind (Bl), belongs to the R2R3 class of MYB transcription factors. *bl* mutants display defective AM initiation during vegetative development in 40-90% of their leaf axils (Schmitz et al., 2002). Orthologues of *Bl* have been

described in *Arabidopsis*, *Capsicum annuum* (pepper) and sunflower. Mutations in Bl orthologues in *Arabidopsis* and pepper lead to branching defects during vegetative development, indicating the conservation of Bl as a branching regulator (Müller et al., 2006; Jeifetz et al., 2011; Fambrini et al., 2017). Similar to *Ls*, *Bl* is expressed in a band shaped domain in the boundaries of leaf primordia/leaves (Busch et al., 2011). The *Arabidopsis* genome contains six genes with high amino acid similarity to Bl (Busch et al., 2011; Müller et al., 2006). *AtMYB36* and *AtMYB68* only displayed root specific expression, and recent studies have shown that MYB36 is a master regulator of root endodermis differentiation and Casparian strip formation (Liberman et al., 2015; Kamiya et al., 2015). The other four *AtMYBs* displayed unspecific expression across various tissues, but genetic analysis showed that the paralogues *AtMYB37* (*REGULATOR OF AXILLARY MERISTEMS1* (*RAX1*)), *AtMYB38* (*RAX2*) and *AtMYB84* (*RAX3*) regulate vegetative branching in *Arabidopsis* (Müller et al., 2006). *rax1* single mutants and higher order mutant combinations including the *rax1* mutant display increasingly stronger AM initiation defects (Fig. 1c). The *rax1 rax2 rax3* triple mutant has the strongest AM initiation defect, also affecting cauline branches (Müller et al., 2006). Only *RAX1* and *RAX3*, display band shaped expression domains in the boundaries of leaf primordia/leaves. Similar to *las*, boundary specific expression of *STM* is lost in the *rax1 rax2 rax3* triple mutant (Müller et al., 2006). The molecular function of the *RAX* genes is not solved. Recently, a study focusing on flower development in *Arabidopsis* demonstrated that RAX1 directly binds as a negative regulator to the *CLV1* promoter, boosting indirectly the expression of *WUS*. Doing so might stabilize the establishment of a functional floral stem cell niche (Denay et al., 2018). The same mechanism might be in place during the formation of the AM stem cell niche. Further, RAX1 binds as a positive regulator to the *CUC2* promoter (Tian et al., 2014). However, the *las rax1* double mutant displays an enhanced branching defect with branchless cauline leaves, indicating that both branching regulators act through separate pathways (Müller et al., 2006). Interestingly, RAX2 was identified in a separate study as Blue Insensitive Trait 1 (BIT1), a cryptochrome steered positive regulator of blue light-dependent gene expression (Hong et al., 2008). However, the impact of light signaling on AM initiation was not further explored, yet.

How do cells know that they are part of a boundary tissue? The phytohormone auxin is hypothesized, to act as a morphogen-like substance during plant development. The differential distribution of auxin across plant tissues, a consequence of polar auxin transport, generates concentration gradients, which might trigger concentration dependent auxin signaling (Weijers and Wagner, 2016). In the context of AM initiation in *Arabidopsis* and tomato, it was demonstrated that the boundary regions during vegetative development represent auxin minima. The auxin minimum within a tissue is characterized by the domain displaying the lowest intracellular auxin concentration. Further, auxin mediated transcriptional changes should be at a minimum, as well. Maintenance of auxin minima is a consequence of regulated polar auxin transport, that actively channels auxin out of the boundary domain. It seems that maintenance of an auxin minimum is required to sensitize cells for cytokinin signaling spikes, which promote AM initiation (Wang et al., 2014b,c). It has been shown that cytokinin is able to

directly promote *LAS* expression through the B-type ARABIDOPSIS RESPONSE REGULATOR1 (ARR1). Further, AM initiation in *rax1* single mutants or *rax1 rax2 rax3* triple mutants was partially rescued through boundary specific expression of the cytokinin biosynthesis gene ISOPENTENYLTRANSFERASE 8 (IPT8; Tian et al., 2014; Wang et al., 2014c).

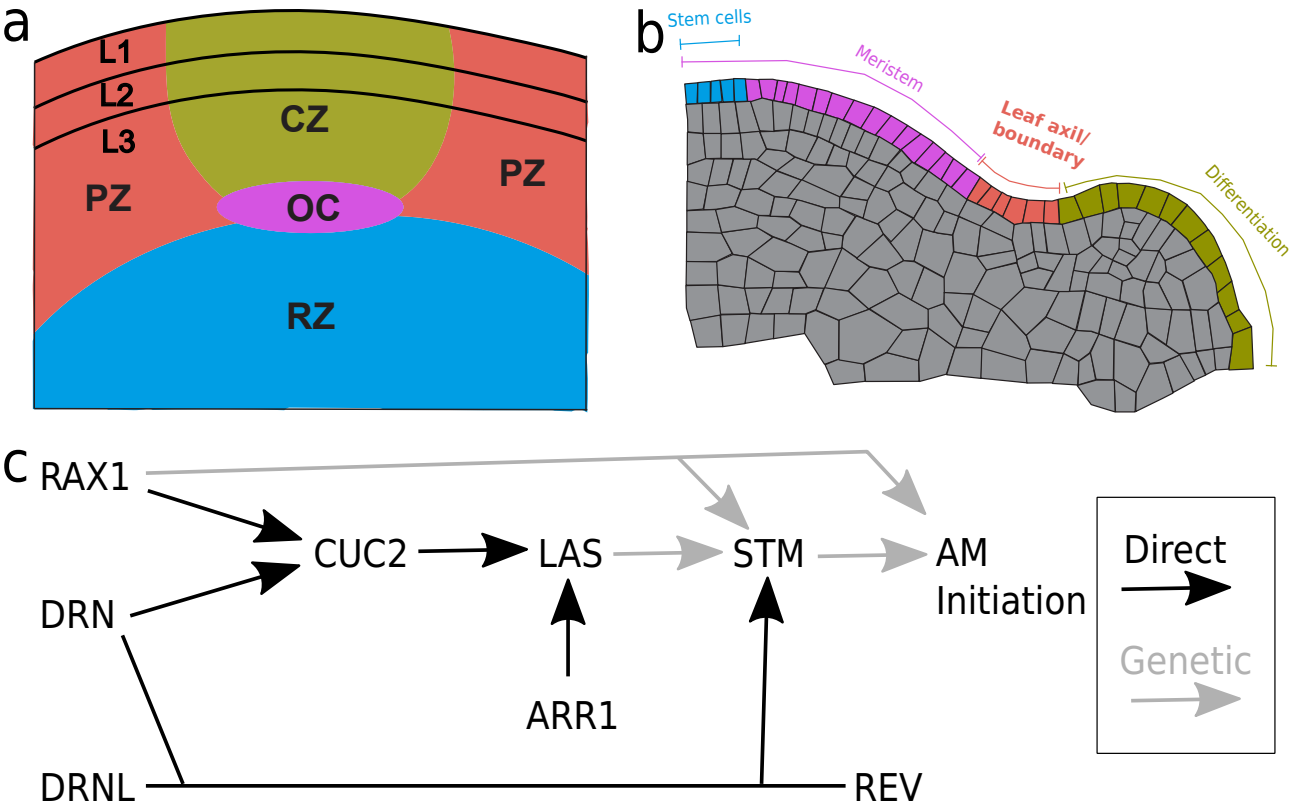


Figure 1: SAM and shoot apex organization. **a**, Cartoon of SAM organization showing the layered organization (L1, L2 and L3), and the zonation into central zone (CZ), peripheral zone (PZ), organizing center (OC) and rib zone (RZ). Cartoon was modified from Sparks (2017b). **b**, Cartoon of the shot apex, showing the zonation into stem cell niche, meristem/TAs, leaf axil/boundary and leaf, based on cell differentiation status. **c**, Simple genetic regulatory network based on the description in the subsections above. A black arrow indicates direct activation through binding to the promoter of the target gene. A grey arrow indicates genetic interaction with unknown mechanism.

1.4 Regulation of *LATERAL SUPPRESSOR* expression in the shoot apical meristem

Analysis of the regulatory elements controlling *LAS* expression in the leaf axil, revealed the presence of 5′ promoter (upstream) and 3′ (downstream) enhancer elements at the *LAS* locus. Both, the 5′ promoter and the 3′ enhancer consisted of two separate regulatory units (Fig. 2; Raatz et al., 2011). Goldshmidt et al. (2008) demonstrated that the 5′ promoter, around 3 kb in size, was sufficient to promote *LAS* expression in the boundaries of floral primordia and floral organs. However, this study provides no evidence supporting boundary sepcific *LAS* expression during vegetative development, nor proper rescue of the AM initiation defect

when employing just the 5′ promoter to drive *LAS* expression in a *las* mutant background. In contrast, Raatz et al. (2011) demonstrated that the 5′ promoter alone was insufficient to restore AM initiation in most of the rosette leaf axils in *las-4*. A weak complementation was observed in the topmost (youngest) rosette leaf axils. In contrast, the 3′ enhancer was sufficient to fully restore AM initiation in *las-4*. The role of the 5′ promoter during vegetative development remains unsolved. Based on the rescue experiment it confers *LAS* expression at least in the youngest rosette leaf axils shortly before the floral transition. During this short time window, the 5′ promoter displays similarities to a shadow promoter. A shadow promoter or enhancer, describes redundant cis-regulatory elements that only become apparent in a sensitized genetic background (Hobert, 2010). In case of the *LAS* locus, this refers to the situation when region C is removed, yet, regions A and D are still present, conferring proper *LAS* expression shortly before the floral transition. The buffering capacity of regions A and D is clearly restricted to primordium/leaf axils close to the shoot apex. Therefore, only region C seems to be able to confer *LAS* expression in older leaf axils with greater distance to the SAM. The 3′ enhancer was further narrowed down to a single element, termed region C. Notably, the second enhancer element, called region B, seemed of no biological relevance for AM initiation. This was further corroborated through expression analysis of a GUS reporter gene, driven either by B and C together, or just by region C alone. Independent of the introduced construct, transgenic plants displayed GUS staining in cells that were located in vegetative leaf axils. Taken together, these findings demonstrated that region B is not involved in the regulation of *LAS* expression in the context of AM initiation (Raatz et al., 2011). However, based on phylogenetic shadowing this result was unexpected, because region B displayed the highest conservation throughout evolution. Also, in all assayed species region B was always located downstream, and in close proximity to *LAS* or the *LAS* orthologue (Raatz et al., 2011).

According to the definition of a true enhancer, the orientation and location of the 3′ enhancer should be irrelevant for *LAS* expression (Picard and Schaffner, 1983; Banerji et al., 1983). Driving *LAS* expression with the 3′ enhancer as a replacement for the 5′ promoter was sufficient to restore AM initiation in *las-4*. Interestingly, analysis of the *Ls* locus in tomato revealed a similar distribution of regulatory elements, which are also organized in a 5′ promoter and an 3′ enhancer. Functional equivalence of both enhancers was demonstrated through an enhancer swapping experiment. Exchanging the *Arabidopsis* 3′ *LAS* enhancer with the corresponding tomato 3′ *Ls* enhancer, was sufficient to fully rescue AM initiation in *las-4* (Raatz et al., 2011).

The 5′ promoter and part of the 3′ enhancer, represented by region C, are sufficient to explain *LAS* expression in shoot tissues, but the biological relevance of region B remains unsolved. The lack of AMs is the only obvious phenotypic deviation discriminating *las-4* from wild type, suggesting that region B might promote *LAS* expression in a different developmental process than AM initiation. Roots represent a tissue in which *LAS* expression is found (Greb et al., 2003). This pattern holds true for species with available organism wide expression data sets of *LAS* orthologues, like in tomato, rice and *Antirrhinum majus* (snapdragon; Schumacher et al., 1999; Li et al., 2003; Mizzotti et al., 2017). Based on the high conservation of region B and

the reoccurring pattern of root expression in different species, it is attractive to speculate that region B might promote root specific expression of *LAS*. So far, studies of *LAS* function focused on AM initiation, and other tissues are still unexplored. Analyzing *LAS* function in a different developmental context, might be an alternative approach to characterize the molecular function of *LAS*, which is still an open question.

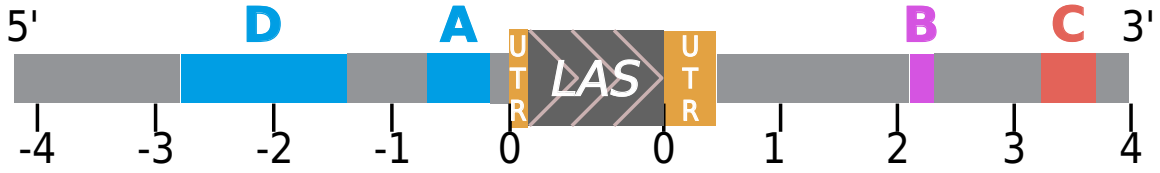


Figure 2: Distribution and function of cis-regulatory elements at the *LAS* locus. Cartoon of promoter and enhancer elements of *LAS*. Element C: Necessary for full complementation. Promotes expression in leaf axils. Elements A and D: Weak or no complementation ability. Sufficient to promote expression in close to the SAM located (young) leaf axils. Element B: no complementation ability, does not promote expression in leaf axils, function unknown. Tips of open triangles indicate the 5′ to 3′ orientation of the *LAS* gene. Ruler below showes distance in kb. Cartoon was modified from Raatz et al. (2011).

1.5 Organization and maintenance of the root apical meristem

The cellular organization of the young *Arabidopsis* root is simple and follows similar to embryogenesis a deterministic pattern. Cells are arranged along the apical-basal axes in individual cell files, which can be traced back to a single cell at the root tip. These cell files are arranged in concentric hollow cylinders, which constitute different tissues. Starting from the most external tissue, there are the epidermis, the cortex and the endodermis, each a single layered radial symmetric tissue, resembling a hollow cylinder. Inside this three layered cylinder, the pericycle and the vasculature are located. The pericycle is a single layered cylindrical tissue, similar in cellular arrangement to the outer tissues. However, its symmetry is determined by the bilateral symmetry of the underlying phloem and xylem (Fig. 6b). The three-dimensional tissue organization of the root is the result of three tightly controlled mechanisms, the timing of cell divisions, the orientation of cell divisions and the regulation of cell elongation (Benfey and Schiefelbein, 1994). Based on these parameters the root tip has been divided into two distinct zones for descriptive purposes. The meristematic zone or RAM, which includes all actively dividing cells and the differentiation zone. The transition from meristematic to differentiation is marked by a significant increase in cell length between two subsequent cells in a cell file (Fig. 3b; Dello Ioio et al., 2007). Stem cells give rise to individual cell files and surround a group of rarely dividing cells, called the quiescent center (QC; Dolan et al., 1993). Elegant laser cell ablation experiments showed, that the QC generates a non-cellautonomous signal to prevent differentiation of the surrounding stem cells, thereby acting as a stem cell niche organizer (Fig. 3a; van den Berg et al., 1997).

Similar to the shoot, genetic studies revealed the presence of a stem cell niche in the RAM. Unlike to the shoot, individual cell lineages developed different mechanisms to maintain their specific stem cell population, often related to the specific function of that tissue. The best studied system in the RAM is the distal stem cell niche, describing the preservation of the columella cell lineage . In the root, contrary to the shoot, the stem cells are located beneath a protective tissue, the root cap or columella. The columella promotes easy soil penetration of the growing root tip and serves as a sensory hub, to monitor the soil environment (Berhin et al., 2019). The *Arabidopsis* genome encodes 14 annotated proteins that share a high sequence similarity with the WUS homeodomain, and are therefore named *WUS HOMEOBOX* (*WOX*) genes. Within this family *WOX5* seemed very interesting in relation to stem cell maintenance, because it displayed specific expression in the QC (Haecker et al., 2004). Testing *wox5* mutants for stem cell maintenance defects in the root, revealed a specific loss of the columella stem cells (CSCs) through premature differentiation into columella cells. Hence, WUS and WOX5 act both in different stem cell niches to maintain stem cell fate. Functional conservation was demonstrated by promoter swapping experiments. *pWUS:WOX5* rescued the *wus* mutant and *pWOX5:WUS* rescued the *wox5* mutant (Sarkar et al., 2007). Interestingly, under standard laboratory growth conditions *wox5* mutant roots display no obvious phenotypic aberration compared to wild type roots. The root stem cell niche compensates for the loss of CSCs through an increased division frequency of the QC, to replenish missing CSCs. Lack of WOX5, however, leads to premature continuous differentiation of distal QC derivatives and a distortion of cellular organization in the root stem cell niche. Increased QC division frequency revealed a second function of WOX5 next to inhibition of CSCs differentiation. In the QC, WOX5 promotes mitotic quiescence, suppression of cell divisions, through inhibition of the expression of cell division promoting *CYCLIN D* (*CYCD*) genes, *CYCD1;1* and *CYCD3;3* (Forzani et al., 2014). WOX5 is similar to WUS a cell-to-cell mobile transcription factor, moving from the QC into the CSCs. Within the CSCs, WOX5 represses the expression of the cell differentiation promoting transcription factor CYCLING DOF FACTOR4 (CDF4) through histone deacetylation at the *CDF4* locus (Pi et al., 2015).

Interestingly, screening for mutants with an increased number of CSCs revealed more similarities between the shoot and the root stem cell niche. In young *Arabidopsis* root tips the average number of CSCs tiers averages at around one. Plants harboring mutations in either *CLV1* or *ARABIDOPSIS CRINKLY4* (*ACR4*), both receptor kinases, displayed an increased frequency of two tiered CSCs organization (Stahl et al., 2013). The spatial expression domains in relation to the stem cell niche displays differences in the shoot and the root. In the shoot, WUS expression is directly regulated through CLV-mediated signaling in the OC. In the root, the spatial distribution is changed, here CLV1 and ACR4 interfere with WOX5 signaling in the CSCs. In the shoot, CLV1 is localized in the OC, whereas in the root, CLV1 is localized only in the differentiated columella cells and the CSCs. ACR4 displays a broader expression domain and covers the whole root stem cell niche. Probably, the overlap of CLV1 and ACR4 domains in the CSCs is most important for the function of this signaling module (Stahl et al.,

2013). Accordingly, the *CLV3* paralog *CLAVATA3/EMBRYO SURROUNDING REGION40* (*CLE40*), was found to be involved in CSCs number control. cle40 mutants display, like clv1 or acr4 mutants increased frequency of two tiered CSC organization. *CLE40* is only expressed in differentiated columella cells, in contrast to *CLV3*, which is expressed in the stem cells (Stahl et al., 2009).

Two gene sets act in parallel to specify and to maintain the QC. The first gene set consists of the two *AP2/ERF* transcription factors *PLETHORA1* (*PLT1*) and *PLT2* (Horstman et al., 2014). In the postembryonic root, *PLT1* expression is restricted to the stem cell niche. *PLT2* expression is extended into the proximal meristematic zone. In the *plt1 plt2* double mutant the root stem cell niche dissipates and the meristem becomes inactive (Aida et al., 2004; Galinha et al., 2007). Expression of *PLT1* and *PLT2* is regulated by auxin through the auxin response factor (ARF) MONOPTEROS (MP). In *mp* mutants expression of *PLT1* and *PLT2* is lost. *pl1 plt2* double mutants can not be rescued through artificial auxin application, indicating that specification of the QC position through auxin can not bypass the function of PLT1 or PLT2 (Aida et al., 2004). The second gene set consists of the two GRAS domain transcriptional regulators *SCR* and *SHORT ROOT* (*SHR*). Strong loss-of-function *shr* or *scr* single mutants lose QC specific marker gene expression and the meristem becomes inactive, leading to root growth arrest (Helariutta et al., 2000; Sabatini et al., 2003). Expression domains of *SCR* and *SHR* are unaffected in *plt* mutants. Triple mutant combinations of either *shr* or *scr* with the *plt1 plt2* double mutant result in more severe root growth defects, indicating that SHR/SCR are still functional in the double mutant (Aida et al., 2004).

Root growth depends on the positioning of the transition zone as a boundary between dividing and differentiating cells in different root cell files (Fig. 3b). Genetic and pharmalogical studies revealed that the size of the meristem correlates with overall root growth. Treatment of roots with cytokinin results in a shift of the transition zone towards the stem cell niche and an early onset of cell differentiation. Consistent with that mutants in cytokinin biosynthesis genes or cytokinin signaling components display a shift of the transition zone towards the hypocotyl. A delayed onset of cell differentiation results in increased root growth. Expression domains of certain cytokinin signaling components that display an overlap with the transition zone are *ARABIDOPSIS HISTIDINE KINASE 3 AHK3*, *ARR1* and *ARR12*. Mutants of these genes display increased meristem and root length (Dello Ioio et al., 2007). Therefore, cytokinin act at the transition zone to coordinate the switch from meristematic to differentiating cells. ARR1 promotes the specific expression of the gene *SHORT HYPOCOTYL 2* (*SHY2*), an AUXIN/INDOLE-3-ACETIC ACID (AUX/IAA) protein that negatively regulates expression of *PIN-FORMED* (*PIN*) genes. Consequently, cytokinin has an direct effect on auxin distribution in the roo tip. Because SHY2 is an AUX/IAA, it is degraded by auxin signaling, thus generating a convergence point for both cytokinin and auxin signaling to determine the position of the transition zone (Dello Ioio et al., 2008). Computational simulation and genetic studies revealed that the position of the transition zone coincides with cell file specific auxin minima. Generation of auxin minima is dependent on both polar transport and degradation.

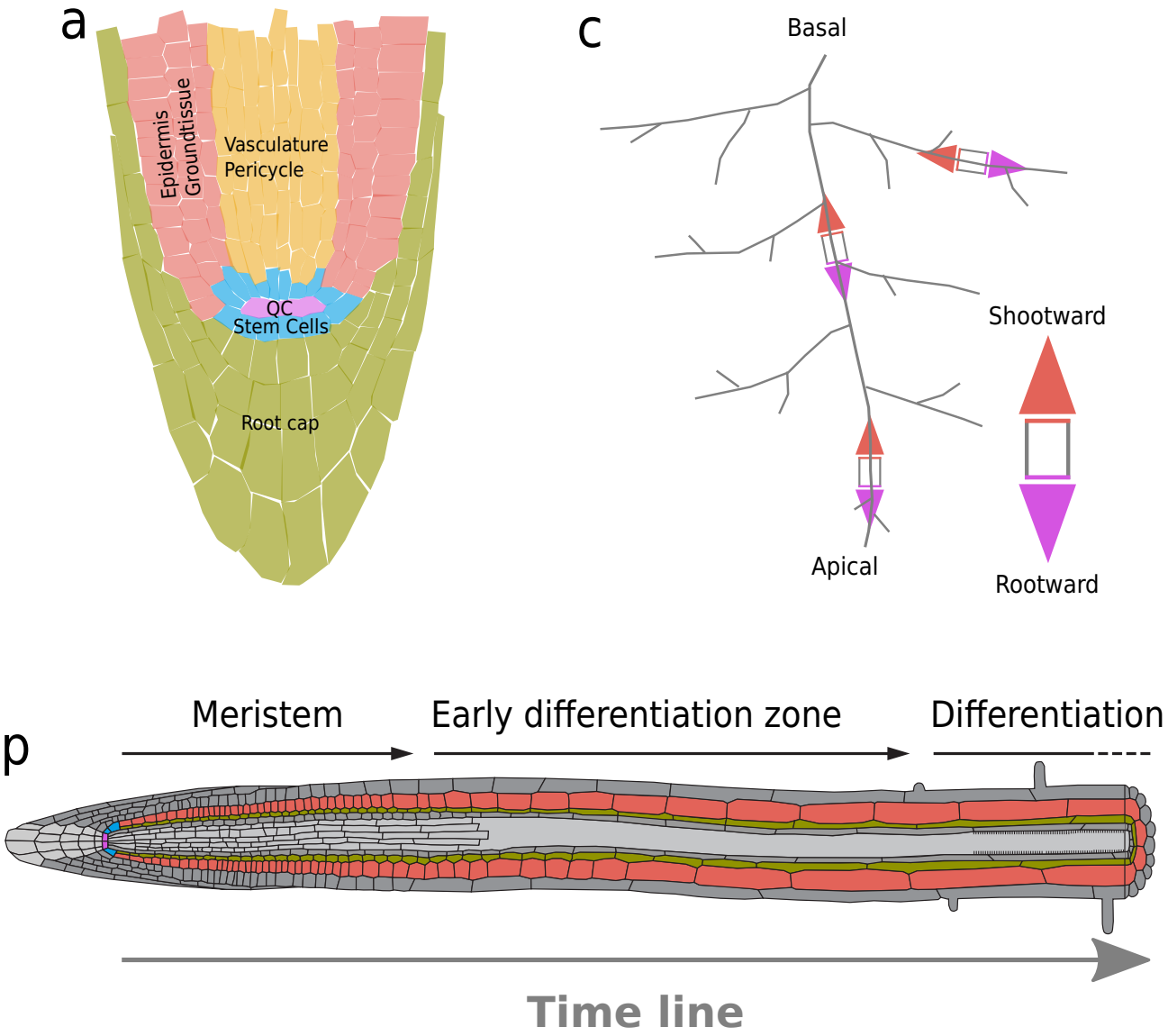


Figure 3: RAM organization, developmental timeline and terminology for direction. **a**, Cartoon of the *Arabidopsis* root stem cell niche and tissue organization. All cells bordering the QC are stem cells. The stele (vasculature and pericycle) displays bilateral symmetry, in contrast to the other radial symmetric tissues. The root cap consists of two separate tissues, the central columella and the lateral root cap. The ground tissue consists of endodermis and cortex. **b**, Cartoon of the cell-file specifc linear developmental time line in the *Arabidopsis* root. Development of the ground tissue cell lineage is highlighted. The first significant cell elongation marks the transition form meristematic to differentiating tissue for each cell file. Cartoon was modified from Peret (2017). **c**, Cartoon illustrating the usage of shootward (towards the shoot apex) and rootward (towards the root apex) in various locations of a root system. Apical and basal are used to refer to the apices (shoot tip and root tip) and bases (root-hypocotyl-junction for shoot and root) of growth axis, respectively. Cartoon was modified from Baskin et al. (2010).

A direct target, upregulated by ARR1 is GRETCHEN HAGEN 3.17 (GH3.17), a protein that catalyzes the conjugation of auxin to aspartic acid. Conjugation renders the auxin molecule inactive. Interestingly, GH3.17 is expressed only in the lateral root cap (LRC) and weakly in the differentiated epidermis (Di Mambro et al., 2017). Modifications of GH3.17 abundance in the LRC, is sufficient to change the position of the transition zone. A second gene under control of ARR1 is *PIN-FORMED 5 PIN5*, an ER localized auxin carrier, which appear to act in conjunction with GH3.17. PIN5 translocates auxin from the cytosol into the ER lumen, thus inhibiting auxin signaling through intracellular regulation of auxin accumulation. Both *gh3.17* and *pin5* mutants display a delayed transition from meristematic to differentiated cells and enhanced root growth. This demonstrates that the LRC is an important tissue to control auxin levels within the RAM to specify the position of the transition zone (Di Mambro et al., 2019). Next to suppression of auxin signaling, promotion of cell elongation is a second mechanism mediated through cytokinin signaling. Cytokinin signaling promotes the expression of *EXPANSIN* proteins and proton pumps in the transition zone. Expansins in combination with the proton pumps facilitate cell elongation through 'acid growth', and mutants in these genes display enlarged meristems and longer roots. This is consistent with the phenotypes described for mutants comprised in cytokinin biosynthesis or cytokinin signaling (Pacifici et al., 2018).

1.6 Looking beyond - differences between primary and lateral growth axes

The volume of space filled by the plant body, above and below ground, is mainly determined by the number and length of lateral growth axes. Even though the molecular mechanisms in the apical meristems providing cells for elongation are the same, their might be profound differences in the tasks assigned to individual growth axes. Different tasks might be anchorage and foraging for nutrients through LRs, or specific regulation of branching to develop a canopy for optimal light capturing. Doing so demands certain adaptations of lateral growth axes, compared to the main growth axis. A nice illustration of such a process is the differential response to gravity (Roychoudhry and Kepinski, 2015). The key observation here is that lateral branches/LRs usually deviate from the nearly vertical direction of growth seen at the tips of the main apical-basal growth axis. The direction of growth can be described with the gravitropic setpoint angle (GSA) concept introduced by Digby and Firn (1995). In this system, organ growth will be described with an angle between 0° and 180° with respect to gravity. The apices of the primary apical-basal axis will typically display GSAs close to 0° in case of the primary root or close to 180° in the case of the primary shoot. For clarity, the GSA is an inherent property and should not be confused with the gravitropic response, which is a growth response that restores vertical axis orientation after displacement. A reorientation experiment is a useful diagnostic test to determine, whether oblique growth of an axis is the consequence of active maintenance indicative for a GSA or not (Roychoudhry and Kepinski, 2015). Regarding the case of a LR that displays a GSA of 60°, which changes to an arbitrary value after rotation. If the LR will

adjust its GSA back to the initial 60°, the LR is truly maintained at an inherent GSA. If the LR fails this test, the GSA of 60° is just an arbitrary angle and would not fulfill the GSA requirement.

Maintenance of the two GSA extremes 0° and 180°, is well explained through the Cholodny-Went hypothesis of gravitropism. According to Cholodny-Went gravitropism, gravity triggers the asymmetric distribution of auxin to the lower side of an organ, which causes growth asymmetry leading to organ bending either downwards like in roots or upwards like in shoots, or positive and negative gravitropism, respectively (Evans, 1991; Morita, 2010). However, this poses the question how growth along an oblique trajectory (non-vertical GSA) is maintained. Rotating an*Arabidopsis* plant 60° along the vertical plane, immediately results in repositioning of some LRs and some side shoots in more vertical or more horizontal positions compared to their original orientation. Repositioned lateral growth axes will grow back towards their original GSA. Notably, for LRs ending up with a more vertical GSA after rotation, returning back to the initial GSA involves growth against gravity, or negative gravitropism. On the other hand, for side shoots ending up with a more vertical GSA, returning back to the initial GSA involves bending towards gravity, or positive gravitropism (Fig. 4b ;Roychoudhry et al., 2013; Roychoudhry and Kepinski, 2015). Basic Cholodny-Went based gravitropism would not account for negative gravitropism in LRs and positive gravitropism in side shoots. The same effect can be achieved through clinorotation, generating an omnilateral gravitational stimulation that triggers LRs to bend upwards and side shoots to bend downwards in relation to their preclinorotational position (Roychoudhry et al., 2013). Based on these observations Roychoudhry et al. (2013) suggested the presence of an agravitropic offset mechanism (AGO). In the proposed model, gravity sensing in lateral organs is no different to primary apices, which display vertical GSAs. However, asymmetric auxin distribution and the resulting anisotropic growth must be counteracted by an opposing growth anisotropy to achieve non-vertical growth (Fig. 4a). Notably, treatment of plants with the auxin transport inhibitor N-1-naphthylphthalamic acid (NPA), inhibited the AGO responses of lateral organs in clinorotation experiments. This indicated that auxin distribution might be involved in AGO (Roychoudhry et al., 2013). Genetic or pharmacological modification with auxin perception and signaling revealed that increased auxin signaling lead to a shift towards more vertical GSAs in LRs/side shoots. Vice versa, decreased auxin signaling/perception shifts GSAs of LRs/side shoots towards more horizontal GSAs (Roychoudhry et al., 2013). Interestingly, proper AGO response is dependent on auxin perception within the gravity sensing cells, the columella in LRs or the endodermis in side shoots, respectively (Roychoudhry et al., 2013). This is quite different to the spatial separation of gravity sensing and the location of auxin signaling in the responding cells seen in Cholodny-Went gravitropism (Morita and Tasaka, 2004).

Two recent studies reported further insights into the molecular framework of the AGO response in *Arabidopsis* LRs. The first study showed that PIN3 and PIN7, both being auxin efflux carrier proteins, display a fine-balanced polarization in the plasmamembrane of columella cells of LRs. Positive and negative graviresponse correlated with changes in the polar orientation

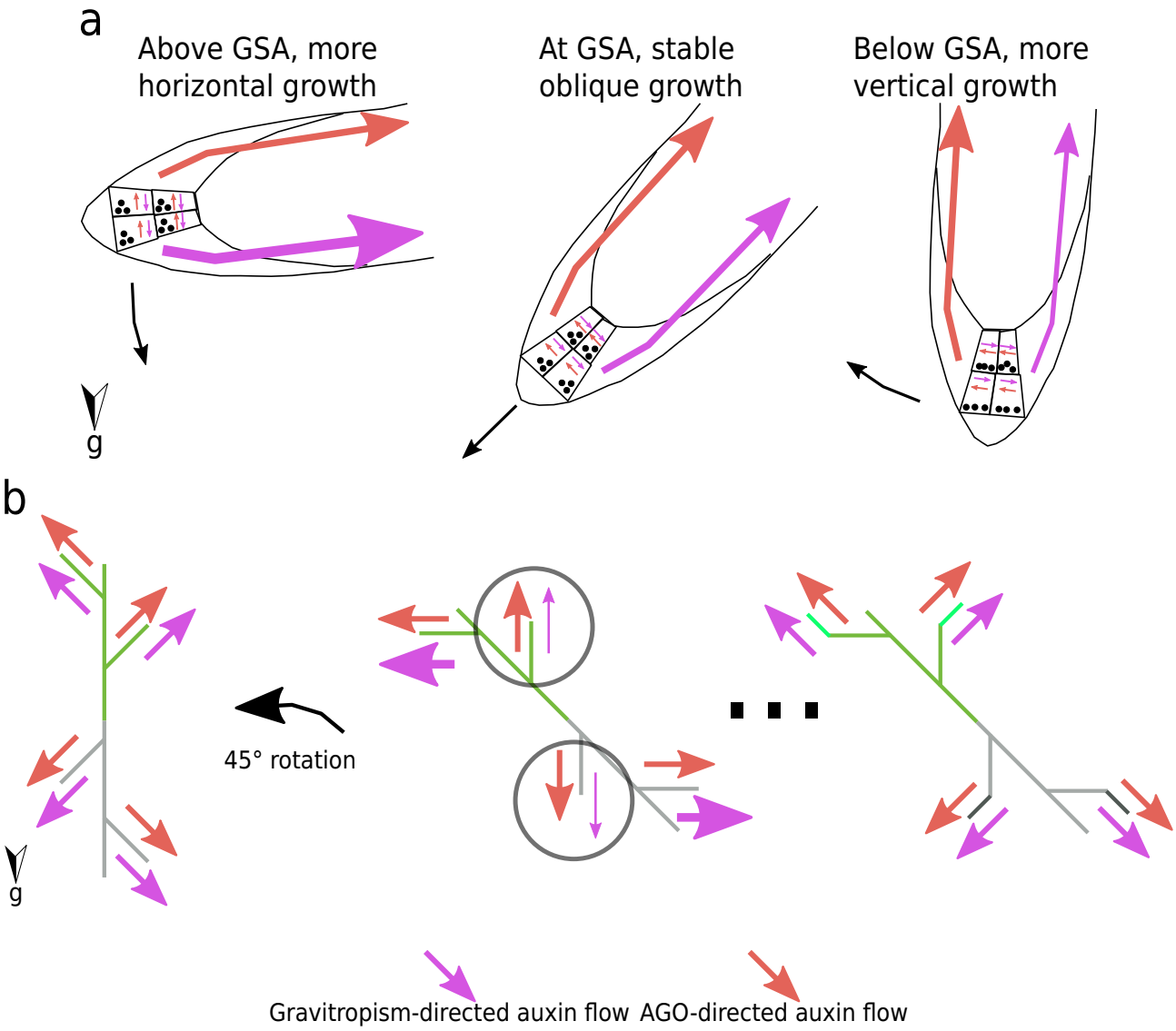


Figure 4: Model of GSA control. **a**, Model of GSA control according to Roychoudhry et al. (2019). Two auxin flows control the growth trajectory (black arrows) of the root. The auxin flow that integrates the gravitropic response is sensitive to the amount of displacement from the gravity vector. The greater the displacement from the gravity vector, the more auxin is transported along this route (arrow thickness). In contrast, the AGO mediated auxin flow stays constant independent of root orientation in relation to the gravity vector. The point at which both auxin flows establish symmetric auxin distribution in the RAM, will determine a stable growth trajectory. Black circles represent sedimenting amyloplasts. Cartoon from Roychoudhry et al. (2019). **b**, Cartoon illustrating a 45˚ rotation of a plant. After the rotation, some side shoots (green) and LRs (grey) display postive and negative gravitropism to grow back to their original growth trajectories, respectively (circles in the middle panel). The accompanying changes in the gravitropism-steered auxin flow in relation to the AGO-steered auxin flow is illustrated (thickness of arrows). Cartoon from Roychoudhry and Kepinski (2015). Arrowhead (g) in (**a**) and (**b**) denotes the direction of the gravity vector.

of PIN3 and PIN7, channeling auxin either to the lower or upper side of the LR. PIN3 contribution to auxin channeling towards the upper side of the LR, was sensitive to auxin signaling in the columella resulting in PIN3 dephosphorylation. Unphosphorylated PIN3 preferentially localized to the lower side of the columella cells, and contributed mainly to Cholodny-Went gravitropism, leading to an increased vertical LR GSA (Roychoudhry et al., 2019). The second study, explored the natural variation associated with the LR GSA establishment after emergence from the primary root. They identified a single nucleotide polymorphism (SNP) in the *CYTOKININ OXIDASE 2* (*CKX2*) gene, causing GSA variation. CKXs catalyze the irreversible degradation of cytokinins and the identified SNP inhibited the catalytic activity of CKX2. Further, cytokinin signaling was shown to interfere with cell elongation/division at the upper LR side, thus promoting more horizontal LR GSAs (Waidmann et al., 2019). One interesting difference between auxin and cytokinin signaling during LR GSA establishment is that only cytokinin elicits asymmetric signaling at the upper LR flank compared to the lower flank, whereas auxin signaling remains similar at all LR flanks (Roychoudhry et al., 2017; Waidmann et al., 2019).

As mentioned before, GSA control might be an adaptive trait that supports effective foraging for nutrients in the soil. GSA orientation in *Arabidopsis* is sensitive to nitrate and phosphate availability in the growth medium. Phosphate deficiency caused LRs to establish more vertical GSAs. Similarly, nitrate deficiency caused LRs to establish more horizontal GSAs. Both GSA responses are mediated through auxin signaling (Roychoudhry et al., 2017). *Arabidopsis* accessions carrying the *ckx2* allele, were most frequent in the Scandinavian *Arabidopsis* populations. These accessions have to deal with low oxygen availability, due to the long period of snow coverage throughout their life cycle. Growth of *Arabidopsis* in hypoxic conditions causes increased horizontal GSAs in a cytokinin dependent manner. Therefore, horizontal LR GSAs might be an adaptation to hypoxia conditions, to promote gas exchange through minimizing the distance to the soil surface (Waidmann et al., 2019).

1.7 Aim of this work

The molecular function of the branching regulator *LAS* is still obscure. Understanding *LAS* function might provide further insights into control of cell fate and pattern formation during AM initiation. Plant anatomy makes the study of boundary specific gene expression during vegetative development very challenging. Throughout vegetative development, the SAM is covered by multiple layers of leaves making boundary exposure for imaging or dissection for tissue isolation a tedious and time-consuming process. Further, it is not known whether boundaries in different leaf axils represent a homogeneous cell population. Alternatively, different boundaries may have acquired different characteristics according to the age of the subtending leaf. To circumvent these problems, the aim of this study is to explore *LAS* function in the *Arabidopsis* root, a powerful system to study developmental processes. The root was chosen based on conserved root expression domains of *LAS* and its orthologues in various species. First, *LAS* root

expression domains will be characterized by means of GFP based reporter constructs, which are suitable for confocal microscopy. In addition, a root phenotyping pipeline will be set up to characterize root traits on macroscopic level. Second, the effect of ectopic *LAS* expression in the root endodermal cell lineage will be analyzed, to explore the potential functions of LAS during cell differentiation. Third, tomato will be used as a comparative system, to study whether root specific functions of *LAS* are conserved. Eventually, root derived concepts of *LAS* function will be used to test their applicability during AM initiation.

2. Materials and Methods

2.1 Sharing of Data, Scripts and Plasmids

Data: rsml files of root tracings and raw image files (scanned root images and confocal images) can be requested by writing an email to rthoma.phd@pm.me. **Scripts**: R scripts written for analysis can be requested by writing an email to rthoma.phd@pm.me and will be deposited in the author's Github repository. **Plasmids**: Plasmids generated in this work were deposited at Addgene. Plasmids not available through Addgene can be requested by writing an email to rthoma.phd@pm.me.

Name in Thesis	Addgene Name	Link	Addgene ID
pGGB000-Venus-linker	pGGB_RT_Venus_li	https://www.addgene.org/136966/	136966
pGGD000-linker-Venus	pGGD_RT_li_Venus	https://www.addgene.org/136973/	136973
pGGC000-Tq2	pGGC_RT_Tq2CFP	https://www.addgene.org/136969/	136969
pGGD000-P2A-erTq2	pGGD_RT_biChromium	https://www.addgene.org/136974/	136974
pGGF000-RedSeed	pGGF_RT_FAST_RFP	https://www.addgene.org/136979/	136979
pGGD000-linker-Tq2	pGGD_RT_li_Tq2CFP	https://www.addgene.org/136971/	136971
pGGA000-pLexA	pGGA_RT_pLexA	https://www.addgene.org/136961/	136961
pGGC000-XVE	pGGC_RT_XVE	https://www.addgene.org/136970/	136970
pGGB000-tdTom-linker	pGGB_RT_tdTomato_li	https://www.addgene.org/136964/	136964
pGGD000-2NLS	pGGD_RT_2NLS	https://www.addgene.org/136977/	136977
pGGB000-Tq2-linker	pGGB_RT_Tq2CFP_li	https://www.addgene.org/136965/	136965
pGGC000-Sclt	pGGC_RT_mScarlet	https://www.addgene.org/136967/	136967
pGGF000-YellowSeed	pGGF_RT_FAST_Venus	https://www.addgene.org/136980/	136980

Figure M1: Reference table for plasmids deposited at Addgene.

2.2 Material

Chemicals

Chemicals used in this work were supplied by the following companies:

BayerCropScience Deutschland GmbH, Langenfeld

Bio-Budget Technologies, Krefeld

Carl Roth GmbH, Karlsruhe

Duchefa Biochemie, Haarlem, The Netherlands

Merck, Darmstadt

New England Biolabs GmbH, Frankfurt am Main

Qiagen, Hilden

Roche, Mannheim

Sigma-Aldrich Chemie GmbH, München

Thermo Fisher Scientific, Waltham, Massachusetts, USA

Expendable materials and reagents

Expendable materials and reagents used in this work were supplied by the following companies:

Incubation tubes and Petri-dishes (round, square (12 cm x 12 cm; 24 cm x 24 cm):
Eppendorf GmbH, Hamburg
Sarstedt AG & Co, Nümbrecht
Greiner-Bio-One GmbH, Frickenhausen
Nunc A/S, Roskilde, Denmark

Barrier tips, Neptune, LTF Labortechnik GmbH, Wassenburg

DNeasy® Plant Mini kit, Qiagen, Hilden

RNeasy® Plant Mini kit, Qiagen, Hilden

QIAprep® Spin Miniprep Kit, Qiagen, Hilden

QIAquick® PCR Purification Kit, Qiagen, Hilden

QIAquick® Gel Extraction Kit, Qiagen, Hilden

Microscope slides, Carl Roth GmbH, Karlsruhe

5′ RACE System for Rapid Amplification of cDNA Ends, Invitrogen, Carlsbad, USA

pCR®-Blunt-II-TOPO, Invitrogen GmbH, Karlsruhe

ExoSAP-IT®, Affymetrix, Santa Clara, USA

Power SYBR® Green PCR Master Mix: Applied Biosystems Deutschland GmbH, Darmstadt

CloneJET PCR Cloning Kit, Thermo Scientific, Waltham, Massachusetts, USA

Disposable Pasteur pipettes, Carl Roth GmbH, Karlsruhe

Enzymes

Enzymes that were most frequently used for molecular cloning were supplied by the following companies:

Phusion® HF DNA Polymerase, New England Biolabs GmbH, Frankfurt am Main

BsaI-HF®, New England Biolabs GmbH, Frankfurt am Main

T4 DNA Ligase, New England Biolabs GmbH, Frankfurt am Main

Fast Digest Eco31I, Thermo Scientific, Waltham, Massachusetts, USA

Antibiotics

Working concentrations of antibiotics used to select transformed bacteria:

Ampicillin (Amp) 100 μg/ml - 200 μg/ml

Gentamicin (Gent) 50 μg/ml

Kanamycin (Amp) 50 μg/ml

Rifampicin (Amp) 50 μg/ml

Spectinomycin (Amp) 100 μg/ml

Bacteria

The *Escherichia coli* strains used for amplification of plasmid DNA were (Source of genotypes: https://openwetware.org/wiki/E._coli_genotypes):

TOP10: F− mcrA Δ(mrr−hsdRMS−mcrBC) ϕ80lacZΔM15 ΔlacX74 nupG recA1 araD139 Δ(ara−leu)7697 galE15 galK16 rpsL(Str^R) endA1 λ $^-$

DB3.1: F− gyrA462 endA1 glnV44 Δ(sr1−recA) mcrB mrr hsdS20(r$_B$ $^-$, m$_B$ $^-$) ara14 galK2 lacY1 proA2 rpsL20(Sm^R) xyl5 Δleu mtl1

The *Agrobacterium tumefaciens* strain used for plant transformation was:

GV3103 with virulence plasmid pMP90 (Koncz and Schell, 1986)

Oligonucleotides

All oligonucleotides used in this study were ordered from Sigma-Aldrich.

Name	Sequence in 5′ to 3′ orientation
GG-seq-F	GGCTTTACACTTTATGCTTCCG
GG-seq-R	TATTACGCCAGCTGGCGAAAGG
pJET-1-2-F	CGACTCACTATAGGGAGAGCGGC
pJET-1-2-R	AAGAACATCGATTTTCCATGGCAG
M13F	GTAAAACGACGGCCAGT
M13R	GTTTTCCCAGTCACGAC
pAGM4723-LB-v2	TGGCTGGTGGCAGGATATATTG

Figure M2: Primers used for sequencing and colony-PCR.

Name	Sequence in 5′ to 3′ orientation
scr3-F	ACGTCTTTCGGATTTCGCAG
scr3-R	TAGCTTGCTCCCAGTGAGTC
AtLs2349F	ACCTCCGTCGTCTTCTTTTC
AtLs2593muR	TGGTTCGAAACAAGAACTAGT
AtLs2599F	CAGTGTATGCAAAGAACAGTTC
AtLs3070R	AACACAATTGACGGCAATGG
Q-SIC-F-v2	TCACACAGAGGTCCACCCGC
Q-SIC-R-v2	AGGGCGAGGTACCCATTGAGG
Q-Tq2VGFP-F-v2	TGCCCGAAGGCTACGTCCAG
Q-Tq2VGFP-R-v2	AGGGTGTCGCCCTCGAACTT
Q-RFP-F-v2	AGGGCGAAGGCAAGCCCTAC
Q-RFP-R-v2	AGCCAGGATGTCGAAGGCGAA

Figure M3: Primers used for copy number qRT-PCR and *las-4*/*scr-3* genotyping.

Plant material

Species	Allele	Allelic variation	Background	Reference
Arabidopsis	wt	-	Col-0	-
Arabidopsis	*las-4*	deletion and frameshift	Col-0	Greb et al. (2003)
Arabidopsis	*scr-3*	premature stop (SNP)	Col-0	Fukaki et al. (1998)
Arabidopsis	wt	*pBR47*	Col-0	Raatz et al. (2011)
Arabidopsis	wt	*pBR48*	Col-0	Raatz et al. (2011)
Tomato	wt	-	Antimold B	-
Tomato	*ls-1*	deletion	Antimold B	Schumacher et al. (1999)
Tomato	*ls-1*	deletion, *Cosmid G*	Antimold B	Schumacher et al. (1999)
Tomato	*ls-1*	deletion, *GSET6*	Antimold B	Schumacher et al. (1999)
Tomato	*ls-1*	deletion, *GSET4*	Antimold B	Schumacher et al. (1999)

Figure M4: Plant material.

Plasmids

List of all plasmids that were used to generate new constructs:

All GreenGate plasmids (Lampropoulos et al., 2013) were obtained from Addgene: GreenGate Cloning System Kit #1000000036

pAGM4723-for-GG was obtained from Hernán López (Lopez Marin, 2017)

p1R4-ML:XVE was obtained from Ari Pekka Mähönen (Siligato et al., 2016).

R2D2 was obtained from Addgene: ID #61629

p2R3a-Tq2CFP-OcsT was obtained from Addgene: ID #71268
pmScarlet-C1 was obtained from Addgene: ID #85042

pUL68 (seed coat marker) was obtained from Ivan Acosta, Group Leader, MPIPZ.

VENUS containing plasmid DNA was obtained from Alice Hasson (former member of the Theres Group).

Software and databases

A list of all-purpose software tools and databases that were used in this study:

TAIR (The Arabidopsis Information Resource, https://www.arabidopsis.org/) was used to obtain information and sequence data for *Arabidopsis* genes.

The SOL genomics network server (SGN, https://solgenomics.net/) was used to obtain the tomato genome sequence (Version 3.0) and the genome annotation (ITAG 3.2; Consortium, 2012). Further, SGN was used to BLAST tomato sequences.

Primer3web (version 4.1.0, http://primer3.ut.ee/; Untergasser et al., 2012) was used to design primers for qRT-PCR.

The National Center for Biotechnology Information server (NCBI, https://www.ncbi.nlm.nih.gov/) was used for BLAST analyses.

The Bio Analytic Resource (BAR, http://bar.utoronto.ca/) was used to access the eFP browsers of various species.

Light Cycler®480 sofware (Roche, Basel, Switzerland) was used for RT-qPCR analysis.

SeqBuilder™ software (DNASTAR, Madison, Wisconsin, USA) was used to plan molecular cloning strategies, to design primers and to do restriction analysis.

Addgene (https://www.addgene.org//) was used to order plasmids.

The BioEdit sequence alignment software (Hall et al., 1999) was used to analyze Sanger sequencing results.

Transgenic *Arabidopsis* lines generated in this study

Allele	Background	Construct	Cloning system	Selection marker	Reference
wt	Col-0	*pLAS:erGFP*	GreenGate (Lampropoulos et al., 2013)	*Basta*^{TM} (glufosinate-ammonium)	this study
las-4	Col-0	*pLAS:Vns-LAS*	GreenGate (Lampropoulos et al., 2013)	*Basta*^{TM} (glufosinate-ammonium)	this study
las-4	Col-0	*pLAS:LAS-Vns*	GreenGate (Lampropoulos et al., 2013)	*Basta*^{TM} (glufosinate-ammonium)	this study
wt	Col-0	*biChromium*	GreenGate (Lampropoulos et al., 2013)	Seed coat marker *pOLE1:OLE1-RFP*	this study
wt	Col-0	*pSCR>>LAS-Tq2*	GreenGate (Lampropoulos et al., 2013)	Seed coat marker *pOLE1:OLE1-RFP*	this study
scr-3	Col-0	*pSCR>>SCR-Tq2*	GreenGate (Lampropoulos et al., 2013)	Seed coat marker *pOLE1:OLE1-RFP*	this study
las-4	Col-0	*pLAS:tdTom-LAS-NLS*	GreenGate (Lampropoulos et al., 2013)	Seed coat marker *pOLE1:OLE1-RFP*	this study
las-4	Col-0	*pLAS:Tq2-LAS-NLS*	GreenGate (Lampropoulos et al., 2013)	Seed coat marker *pOLE1:OLE1-RFP*	this study
wt	Col-0	*aspLAS:erSclt*	GreenGate (Lampropoulos et al., 2013)	Seed coat marker *pOLE1:OLE1-RFP*	this study

Figure M5: Transgenic lines generated in this study.

2.3 Methods

Standard molecular biology methods not reported in this section, are described in Sambrook and Russel (2001).

Molecular cloning

All cloning procedures described in this part followed the standard GreenGate cloning protocol (Lampropoulos et al., 2013). If not otherwise mentioned, genomic Col-0 DNA was used as PCR template. Initial PCR products were always digested with BsaI (equal to Eco31I) prior to ligation into GreenGate entry vectors. In the case that additional BsaI sites were present in the PCR product, the fragments were domesticated, following the BsaI-based approach described in Lampropoulos et al. (2013). All entry clones were controlled by sanger sequencing. The final assembled destination vectors were controlled, by two independent restriction analysis prior to plant transformation.

Cloning of *pLAS:erGFP*

5′ *LAS* regulatory elements: PCR product of
5pLAS-GG1-F (AACAGGTCTCAACCTCGTGTGCTACACAGATTTATGTGAAAC) and
5pLAS-GG1-R (AACAGGTCTCATGTTTTGAAAAGATAGAAAAAGATGCTTTTGG) was ligated into pGGA000 to generate **pGGA000-5pLAS**.

3′ *LAS* regulatory elements: In a first step, one endogenous BsaI site had to be domesticated. PCR product 1,
3pLAS-GG5-LAS (AACAGGTCTCACTGCTCCAAAGAGAAGGACAAAAAAAACCTATATATC) and
R4 (AACAGGTCTCAATAACTATGACGTGACTAATTTAAATCG). PCR product 2,
F-4-v2 (AACAGGTCTCATTATAAATTTAAAGTGACCAT) and
3pLAS-GG5-R (AACAGGTCTCATAGTATTAGTAACAAGCATAAAGCACCAAAACCATG).
Product 1 and product 2 were combined in pGGE000 to form **pGGE000-3pLAS**.

pLAS:erGFP build: GreenGate reaction with pGGA000-5pLAS, pGGB006, pGGC014, pGGD008, pGGE000-3pLAS, pGGF001 and pAGM4723-for-GG.

Cloning of *pLAS:Vns-LAS*

linker-Venus: PCR product 1, PCR template obtained from A. Hasson,
Venus-GG-2-F (AACAGGTCTCAAACAatggtgagcaagggcgaggag) and
Venus-GG-2-R (AACAGGTCTCACtGCcttgtacagctcgtccatg). PCR product 2, PCR template pGGD001,
linker-GG2-F-v2 (AACAGGTCTCAGCaGCgGCcGCtTCaGGgAGtG) and

linker-GG2-R-v2 (AACAGGTCTCAAGCCAGCAATTGCTGCGGCAGC). Product 1 and product 2 were combined in pGGE000 to form **pGGB000-Venus-linker**.

LAS CDS: In a first step, two endogenous BsaI sites had to be domesticated. PCR product 1, cLAS-GG3-F (AACAGGTCTCAGGCTCCATGCTTACTTCCTTCAAATCCTCTAGC) and R2 (aacaggtctcaACCGGGTTAACCGGTCACCAGTTCG). PCR product 2, F2 (aacaggtctcaCGGTTCGCTGACTCTTTAGGACTCC) and R3 (aacaggtctcaCAATTGACGGCAATCGTCTCTCCTTG). PCR product 3, F3 (aacaggtctcaATTGTGTTCACTTCCTCCACA) and cLAS-GG3-R (AACAGGTCTCACTGATTTCCACGACGAAACGGAGAAGAGG). Product 1, product 2 and product 3 were combined in pGGC000 to form **pGGC000-LAS**.

pLAS:Vns-LAS build: GreenGate reaction with pGGA000-5pLAS, pGGB000-Venus-linker, pGGC000-LAS, pGGD002, pGGE000-3pLAS, pGGF001 and pAGM4723-for-GG.

Cloning of *pLAS:LAS-Vns*

Venus-linker: PCR product 1, PCR template pGGD001, linker-GG4-F (AACAGGTCTCATCAGgcGCaGCgGCcGCtTCaGGgAGtG) and linker-GG4-R (AACAGGTCTCAAGCAATTGCTGCGGCAGCcGAtC). PCR product 2, PCR template obtained from A. Hasson, PCR template pGGD001, Venus-GG4-F (AACAGGTCTCATGCTatggtgagcaagggcgaggag) and Venus-GG4-R (AACAGGTCTCAGCAGttacttgtacagctcgtccatg). Product 1 and product 2 were combined in pGGD000 to form **pGGD000-linker-Venus**.

pLAS:Vns-LAS build: GreenGate reaction with pGGA000-5pLAS, pGGB003, pGGC000-LAS, pGGD000-linker-Venus, pGGE000-3pLAS, pGGF001 and pAGM4723-for-GG.

Cloning of *biChromium*

Assembling er-mTurquoise2: PCR1, PCR template p2R3a-Tq2CFP-OcsT, Tq2CFP-GG3-F (AACAGGTCTCAGGCTCCatggtgagcaagggcgaggag) and Tq2CFP-GG3-R (AACAGGTCTCACTGActtgtacagctcgtccatgccg). Product 1 was ligated into pGGC000 to generate pGGC000-Tq2. GreenGate reaction with pGGA000-5pLAS, pGGB006, pGGC000-Tq2, pGGD008, pGGE000-3pLAS, pGGF001 and pAGM4723-for-GG to assemble **pLAS:erTq2**.

P2A in conjunction with mTurquoise2: PCR product 1, P2A, no PCR only primer annealing, P2A-GG4-Fv2 (aacaGGTCTCATCAGgcGGCAGTGGAGCTACCAATTTTAGTCTTCTCAAACAG) and P2A-GG4-Rv2 (aacaGGTCTCATGGGCCAGGGTTCTCTTCGACATCCCCGGCCTGTTTGAGAAGA). PCR product 2, PCR template pLAS:erTq2, erT-GG4-F (AACAGGTCTCACCCAatgaaagccttcacactcg) and

erT-GG4-R (AACAGGTCTCAGCAGctaaagctcatcatgacCTG). Product 1 and product 2 were combined in pGGE000 to form **pGGD000-P2A-erTq2**.

Red seed coat marker: In a first step, three endogenous BsaI sites had to be domesticated. PCR product 1, PCR template pUL68,
FAST-GG6-F (AACAGGTCTCAACTActtcaagtgtatgtaggtatag) and
FAST-R2 (AACAGGTCTCAtgtcctcaagcccaagctgac). PCR product 2, PCR template pUL68,
FAST-F2 (AACAGGTCTCAgacaagacccgaatccgagtctg) and
FAST-R3 (AACAGGTCTCAccatcatcgggtactggtccctgcc). PCR product 3, PCR template pUL68,
FAST-F3 (AACAGGTCTCAatgggccgagatcgggaccagtacc) and
FAST-R4 (AACAGGTCTCAttctttgtcggcctccttgattc). PCR product 4, PCR template pUL68,
FAST-F4 (AACAGGTCTCAagaaacctacgtcgagcagcac) and
FAST-GG6-R (AACAGGTCTCAATACtctagtaacatagatgacacc). Product 1, product 2, product 3 and product 4 were combined in pGGF000 to form **pGGF000-RedSeed**.

biChromium build: GreenGate reaction with pGGA000-5pLAS, pGGB000-Venus-linker, pGGC000-LAS, pGGD000-P2A-erTq2, pGGE000-3pLAS, pGGF000-RedSeed and pAGM4723-for-GG.

Cloning of *pSCR>>LAS-Tq2*

Assembling linker-Turquoise2: PCR1, PCR template p2R3a-Tq2CFP-OcsT,
Tq2CFP-GG4-F (AACAGGTCTCATGCTatggtgagcaagggcgaggag) and
Tq2CFP-GG4-R (AACAGGTCTCAGCAGttacttgtacagctcgtccatg).
PCR product 2, PCR template pGGD001,
linker-GG4-F (AACAGGTCTCATCAGgcGCaGCgGCcGCtTCaGGgAGtG) and
linker-GG4-R (AACAGGTCTCAAGCAATTGCTGCGGCAGCcGAtC).
Product 1 and product 2 were combined in pGGD000 to generate **pGGD000-linker-Tq2**.

New intermediate vector1: PCR product 1, PCR template pGGM000,
XbaI-Int-GG-F (aacatctagaATTGGTTGTAACATTATTCAG) and
BamHI-Int-GG-R (aacaggatccTACTGTTTATGTAAGCAGACAG).
PCR product 2, PCR template pGGZ003,
Spec-BamHI-F (AACAGGATCCatgagggaagcggtgatcgccg) and
Spec-XbaI-R (AACATCTAGAttatttgccgactaccttggtg). PCR products were digested with BamHI and XbaI, and purified. Purified products 1 and 2 were combined to generate **pGGM001**.

New intermediate vector2: PCR product 1, PCR template pGGN000,
XbaI-Int-GG-F (aacatctagaATTGGTTGTAACATTATTCAG) and
BamHI-Int-GG-R (aacaggatccTACTGTTTATGTAAGCAGACAG).
PCR product 2, PCR template pGGZ003,
Spec-BamHI-F (AACAGGATCCatgagggaagcggtgatcgccg) and
Spec-XbaI-R (AACATCTAGAttatttgccgactaccttggtg). PCR products were digested with BamHI and XbaI, and purified. Purified products 1 and 2 were combined to generate **pGGN001**.

5′ SCR regulatory sequences: PCR of
pSCR-GG1-F (AACAGGTCTCAACCTAAGGGATAGAGGAAGAGGACTTTG) and
pSCR-GG1-R (AACAGGTCTCaTGTTggagattgaagggttgttggtcgtg) was ligated into pGGA000 to generate **pGGA000-SCR**.

17-β-estradiol sensitive modules: PCR product 1, PCR template p1R4-ML:XVE,
pLexA-GG1-F (AACAGGTCTCAACCTAGCTTGGGCTGCAGGTCGAGG) and
pLexA-GG1-R (AACAGGTCTCATGTTGACTAGCTTCAGCGTGTCCTC). Product 1 was combined with pGGA000 to form **pGGA000-pLexA**.
In a first step, one endogenous BsaI site had to be domesticated. PCR product 2, PCR template p1R4-ML:XVE,
XVE-GG3-F (AACAGGTCTCAGGCTATGAAAGCGTTAACGGCCAGG) and
XVE-R2 ().
PCR product 3, PCR template p1R4-ML:XVE,
XVE-F2 (AACAGGTCTCAgatgattggactcgtctggc) and
XVE-GG3-R (AACAGGTCTCAcatcaggatctctagccaggc). Product 2 and product 3 were combined with pGGC000 to form **pGGC000-XVE**.

Intermediate-SCR-LAS-1 build: GreenGate reaction with pGGA000-SCR, pGGB003, pGGC000-XVE, pGGD002, pGGE009, pGGG001 and pGGM001.

Intermediate-SCR-LAS-2 build: GreenGate reaction with pGGG002, pGGA000-pLexA, pGGB002, pGGC000-LAS, pGGD000-linker-Tq2, pGGE001, pGGF000-RedSeed and pGGN001.

pSCR>>LAS-Tq2 build: GreenGate reaction with Intermediate-SCR-LAS-1, Intermediate-SCR-LAS-2 and pAGM4723-for-GG.

Cloning of *pSCR>>SCR-Tq2*

SCR CDS: In a first step, two endogenous BsaI sites had to be domesticated. PCR product 1,
SCR-GG3-F (AACAGGTCTCAGGCTCCATGGCGGAATCCGGCGATTTCAAC) and
SCR-R2-GG3 (AACAGGTCTCATCCCTGATAATGGCGTCAACCCATAC).
PCR product 2,
SCR-F2-GG3 (AACAGGTCTCAGGGACCTTATCCATTCCTCAACTTC) and
SCR-R3-GG3 (AACAGGTCTCAGACACCATTTTCAAGCTATGCGTTTG).
PCR product 3,
SCR-F3-GG3 (AACAGGTCTCATGTCTGCGTTTCAGGTCTTTAATG) and
SCR-GG3-R (AACAGGTCTCACTGAAGAACGAGGCGTCCAAGCTGAAG). Product 1, product 2 and product 3 were combined with pGGC000 to form **pGGC000-SCR**.

Intermediate-SCR-LAS-1 build: GreenGate reaction with pGGA000-SCR, pGGB003, pGGC000-XVE, pGGD002, pGGE009, pGGG001 and pGGM001.

Intermediate-SCR-SCR-2 build: GreenGate reaction with pGGG002, pGGA000-pLexA, pGGB002, pGGC000-SCR, pGGD000-linker-Tq2, pGGE001, pGGF000-RedSeed and pGGN001.

pSCR>>SCR-Tq2 build: GreenGate reaction with Intermediate-SCR-LAS-1, Intermediate-SCR-SCR-2 and pAGM4723-for-GG.

Cloning of *pLAS:tdTom-LAS-NLS*

linker-tandemTomato: PCR product 1, R2D2, because of the duplicated tandemTomato sequence several nested PCRs were necessary,
tdTomato-GG2-F (AACAGGTCTCAAACAatggtgagcaagggcgaggag) and
tdTomato-GG2-R (AACAGGTCTCACtGCcttgtacagctcgtccatgc). PCR product 2, PCR template pGGD001,
linker-GG2-F-v2 (AACAGGTCTCAGCaGCgGCcGCtTCaGGgAGtG) and
linker-GG2-R-v2 (AACAGGTCTCAAGCCAGCAATTGCTGCGGCAGC). Product 1 and product 2 were combined in pGGB000 to form **pGGB000-tdTom-linker**.

Duplicated NLS: PCR product 1, no PCR, only primer were annealed with each other, 2NLS,
2XSV40NLS-GG4-F (AACAggtctcatcaggtcctaagaagaagaggaaggttcctaaga) and
2XSV40NLS-GG4-R (AACAggtctcagcagtcaaaccttcctcttcttcttaggaacctt). Product 1 was ligated into pGGD000 to form **pGGD000-2NLS**.

pLAS:tdTom-LAS-NLS build: GreenGate reaction with pGGA000-5pLAS, pGGB000-tdTom-linker, pGGC000-LAS, pGGD000-2NLS, pGGE000-3pLAS, pGGF000-RedSeed and pAGM4723-for-GG.

Cloning of *pLAS:Tq2-LAS-NLS*

linker-mTurquoise2: PCR product 1,
Tq2CFP-GG2-F (AACAGGTCTCAAACAatggtgagcaagggcgaggag) and
Tq2CFP-GG2-R (AACAGGTCTCACtGCcttgtacagctcgtccatg). PCR product 2, PCR template pGGD001,
linker-GG2-F-v2 (AACAGGTCTCAGCaGCgGCcGCtTCaGGgAGtG) and
linker-GG2-R-v2 (AACAGGTCTCAAGCCAGCAATTGCTGCGGCAGC). Product 1 and product 2 were combined in pGGB000 to form **pGGB000-Tq2-linker**.

pLAS:Tq2-LAS-NLS build: GreenGate reaction with pGGA000-5pLAS, pGGB000-Tq2-linker, pGGC000-LAS, pGGD000-2NLS, pGGE000-3pLAS, pGGF000-RedSeed and pAGM4723-for-GG.

Cloning of *aspLAS:erSclt*

3′ *asLAS* regulatory elements: PCR product 1, PCR template pGGA000-5pLAS,
3pasLAS-F-GG5 (AACAGGTCTCACTGCttgaaaagatagaaaaagatgcttttgg) and
3pasLAS-R-GG5 (AACAGGTCTCATAGTcgtgtgctacacagatttatgtgaaac). Product 1 was ligated into pGGE000 to generate **pGGE000-3pasLAS**.

5′ *asLAS* regulatory elements: PCR product 1, PCR template pGGE000-3pLAS,
5pasLAS-F-GG1 (AACAGGTCTCAACCTattagtaacaagcataaagcaccaaaaccatg) and
5pasLAS-R-GG1 (AACAGGTCTCATGTTaaagagacaacctaatcttttgtgtttttaacc). Product 1 was ligated into pGGA000 to generate **pGGA000-5pasLAS**.

Scarlet: PCR product 1, PCR template pmScarlet-C1,
mScarlet-GG3-F (AACAGGTCTCaGGCTccATGGTGAGCAAGGGCGAGGCAG) and
mScarlet-GG3-R (AACAGGTCTCACTGACTTGTACAGCTCGTCCATGCC).Product 1 was ligated into pGGC000 to generate **pGGC000-Sclt**

Yellow seed coat marker: In a first step, three endogenous BsaI sites had to be domesticated. Further, to generate more diversity, the *NOS* terminator in pGGF000-RedSeed was replaced with the *Arabidopsis HSP18-2* terminator (Nagaya et al., 2009). PCR product 1, PCR template pUL68,
FAST-GG6-F (AACAGGTCTCAACTActtcaagtgtatgtaggtatag) and
FAST-R2 (AACAGGTCTCAtgtcctcaagcccaagctgac). PCR product 2, PCR template pUL68,
FAST-F2 (AACAGGTCTCAgacaagacccgaatccgagtctg) and
FAST-R3 (AACAGGTCTCAccatcatcgggtactggtccctgcc). PCR product 3, PCR template pUL68,
FAST-F3 (AACAGGTCTCAatgggccgagatcgggaccagtacc) and
FAST-v2-R1 (AACAGGTCTCAagtagtgtgctggccaccacgagtac). PCR product 4, PCR template pGGB000-Venus-linker,
FAST-v2-F1 (AACAGGTCTCAtactatggtgagcaagggcgaggag) and
FAST-v2-R2 (AACAGGTCTCAtcacttgtacagctcgtccatgcc). PCR product 5, PCR template *Arabidopsis* genomic DNA,
FAST-v2-F2 (AACAGGTCTCAgtgaatatgaagatgaagatgaaa) and
FAST-v2-R3 (AACAGGTCTCaATACcttatctttaatcatattccatag). Product 1, product 2, product 3, product 4 and product 5 were combined in pGGF000 to form **pGGF000-YellowSeed**.

aspLAS:erSclt build: GreenGate reaction with pGGA000-5pasLAS, pGGB006, pGGC000-Sclt, pGGD008, pGGE000-3pasLAS, pGGF000-YellowSeed and pAGM4723-for-GG.

Confocal Microscopy

Microscopic observations were carried out using an inverted Zeiss LSM 880 Airyscan confocal laser-scanning microscope (Carl Zeiss, Oberkochen). For analysis, images were taken with predefined microscope settings for each experiment. Adjustment of microscope settings was

done with a randomly selected transgenic line prior to the experiment, which was then used as the experiment's reference line. For each active detector, the settings were chosen, in order that the whole dynamic range was covered, yet keeping oversaturated pixels at a minimum. Further, pixel dwell time, frame size and bit depth were additional parameters that were adjusted prior to the start of the experiment. Sequential scanning was performed in all cases, in which two or more fluorophores had to be imaged in the same tissue simultaneously. For live-imaging, laser intensity was kept as low as possible and usually never exceeded 5%. The pinhole was set at 1 airy unit (AU) at 1×resolution.

Propidium iodide staining for live-imaging

Seedlings were stained prior to confocal imaging, for 5 to 20 min, in 10 *mu*g/ml propidium iodide (PI) solution. Care was taken that the root was fully submerged in the staining solution. During the staining, direct light was avoided. After the PI staining, seedlings were washed in water and mounted on microscope slides. Important to note, seedlings were never let dried out, and seedlings were only handled by grabbing the cotyledons with featherweight forceps to avoid squeezing of the root.

mPSPI staining

Modified pseudo-Schiff propidium iodide (mPSPI) staining was done as described in Truernit et al. (2008). Duration of initial fixation step: 1-5 days.

Confocal imaging of *biChromium*

Imaging of *biChromium* was done on the inverted Zeiss LSM 880 Airyscan confocal laser-scanning microscope. For imaging the 'lambda scan' and 'spectral unmixing' features of the ZEN 2012 'black edition' software (Carl Zeiss, Oberkochen) were used.

Measurement of pixel grey values to determine fluorescence intensity

To determine fluorescence intensity, raw .tiff files from the confocal imaging session were analyzed in Fiji (http://fiji.sc/). The region of interest was traced with the polygon selection tool and analyzed with the histogram function. The output of the histogram function was exported into RStudio (https://www.rstudio.com/, R version 3.4) for further analysis.

Excitation and filter settings for fluorophores

GFP, Excitation and Emission wavelength: 488 nm, 494-430 nm

Venus, Excitation and Emission wavelength: 514 nm, 525-555 nm

mTurquoise2, Excitation and Emission wavelength: 440 nm, 466-490 nm

Scarlet, Excitation and Emission wavelength: 561 nm, 580-617 nm

tandemTomato, Excitation and Emission wavelength: 561 nm, 570-610 nm

Propidium iodide, Excitation and Emission wavelength: 488 nm, 500-550 nm

GUS staining

GUS staining was done as described in Truernit et al. (2008). Staining reaction was done overnight (12 h) at 37 °C. After staining plants were immediately imaged on a light microscope.

Bacteria transformation

Transformation of *Escherichia coli* was carried out by heat-shock treatment of chemically competent cells (Hanahan, 1983). *Escherichia coli* was incubated in LB medium at 37 °C overnight (Sambrook and Russel, 2001). Concentration of applied antibiotics are listed above.

Transformation of *Agrobacterium tumefaciens* was carried out via electroporation (Bio-Rad pulser system) of electro competent cells. *Agrobacteria* were incubated in YEP or LB medium at 37 °C. Approximately 10-50 ng plasmid were used per transformation. Concentration of applied antibiotics are listed above.

Arabidopsis transformation

Arabidopsis plants were transformed according to the floral dip method described by Clough and Bent (1998). T1 transgenic seedlings were either selected by repetitive glufosinate application (250 mg/ml) or were preselected based on seed coat fluorescence (Shimada et al., 2010). Copy number determination was conducted in the T1 generation with qRT-PCR. gDNA for qRT-PCR was was isolated using the rapid-preparation-protocol described by Edwards et al. (1991). qRT-PCR was performed using the LightCycler 480 Real-Time PCR system (Roche, Applied Science), with the Power SYBR® Green PCR Master Mix (Applied Biosystems Deutschland GmbH, Darmstadt), according to the manufactures instructions. Each sample for copy number determination was pipetted in two technical replicates. Data analysis was done with the standard curve method (Applied Biosystems, User Bulletin #2, 2001). A singe copy refernce gene *SICKLE* was chosen as internal control (Zhan et al., 2012).

RNA extraction, RNAseq and bioinformatic analysis

Root tips (1 cm) of 11-day-old tomato plants were used as starting material for RNA extraction. RNA was collected in with two steel beads prepared 2 ml tubes. Harvested tissue was grounded using a Retsch MM 300 mill (Retsch, Germany). RNA was extracted with the RNeasy® Plant Mini kit (Qiagen, Hilden), following the plant-specific protocol according to the manufactures instructions. The RNA was further purified by DNaseI treatment including an RNase Inhibitor. RNA quantity was determined on a NanoDrop, and the quality was checked with a capillary electrophoresis method using an Agilent 2100 Bioanalyzer (done by the Max Planck Genome Center, Cologne).

The Max Planck Genome Center performed the library preparation including polyA enrichment of total RNA samples. The libraries were sequenced with single 150 bp reads, using the Illumina HiSeq3000 platform. Raw sequencing data was quality checked and analyzed with the 'new Tuxedo' package (default settings; Pertea et al., 2016).

HISAT2 version 2.1.0

StringTie v1.3.3b

ballgown 2.10.0

Axillary meristem scoring experiment

Prior to sowing, seeds were stratified for 2-3 days at 4 °C. Plants were grown in the greenhouse for 5-6 weeks under short day conditions (8 h light, 16 h dark). Temperature was kept at 20-25 °C during the daytime, and 15 °C during the nighttime. After 5 weeks of growth in short day conditions, plants were transferred to long day conditions (16 h light, 8 h dark) to initiate/accelerate the floral transition. After additional 1-2 weeks AM phenotypes were scored.

RNA extraction, cDNA synthesis and 5′ RACE

Root tips (1 cm) of 11-day-old tomato plants and whole roots of 8-day-old *Arabidopsis* plants were used as starting material for RNA extraction. RNA was collected in with two steel beads prepared 2 ml tubes. Harvested tissue was grounded using a Retsch MM 300 mill (Retsch, Germany). RNA was extracted with the RNeasy® Plant Mini kit (Qiagen, Hilden), following the plant-specific protocol according to the manufactures instructions. The RNA was further purified by DNaseI treatment including an RNase Inhibitor. RNA quantity was determined on a NanoDrop. The 5′ RACE System for Rapid Amplification of cDNA Ends kit (Invitrogen, Carlsbad, USA) was followed, according to the manufacturers instructions. The used gene-specific primers (GSP) are listed below:

asLS-GSP1-v1 TGATTCACTGGAAGCTACATT

asLS-GSP2-v1 TGGTTTGGGAGAGAGATTGTT

asLAS-GSP1-v1 TGATTCGTTGGAAGCGACGTT

asLAS-GSP2-v1 TTCGGTAAGGAGATTTTGGAT

Subsequently 5′ RACE amplification products were cloned into the pCR®-Blunt-II-TOPO (Invitrogen GmbH, Karlsruhe) or into theCloneJET PCR Cloning Kit (Thermo Scientific, Waltham, Massachusetts, USA). 15-25 clones were sequenced for each purified fragment.

Root system phenotyping in *Arabidopsis* and tomato

Arabidopsis growth conditions

Arabidopsis thaliana seeds were surface sterilized with 50 % bleach (v/v) (1:1000 Tween20) under continuous shaking for 5 min. Next, seeds were washed 3 times with sterile water. After the washing, seeds were in 0.15 % low-melting point agarose at 4 °C for 2-3 days. Then, seeds were sown on square Petri dishes (12 cm × 12 cm, filled with 60 ml of growth medium). *Arabidopsis* growth medium: half-strength Murashige and Skoog (1/2MS) medium (0.5×MS salts including vitamins, 1 % sucrose, 0.1 g/l Myo-Inositol, 0.5 g/l 2-(N-morpholino) ethanesulfonic acid (MES), pH 5.8 with KOH and 0.8 % phytoagar. Plates were dried with open lid for around 1 h after pouring to allow evaporation). Seeds were germinated on vertically positioned Petri dishes in a growth chamber at 21 °C in long day conditions (16h light and 8 h dark; MC785-VDB,Van den Berg). Plants were imaged at indicated time points (Figure legends).

The concentration of the 17-β-estradiol working solution was 10 muM (prepared as 20 mM stock solutions in DMSO and stored at -20 °C). 17-β-estradiol working solution was added to cooled 1/2MS medium. Plants were transferred carefully with featherweight forceps, by grabbing the cotyledons. After the transfer care was taken that the root aligned well the surface of the medium. Plants were imaged at indicated time points (Figure legends).

Tomato growth conditions

Tomato seeds were surface sterilized with 50 % bleach (v/v) (1:1000 Tween20) under continuous shaking for 5 min. Next, seeds were washed 3 times with sterile water. After the washing, seeds were transferred on 1/2MS medium and stored for 4-7 days in the dark at room temperature until they started to germinate. Seeds that displayed the same stage of development after germination were placed on big square Petri dishes, and fixed with a drop of cooled molten 1/2MS to avoid dropping of seeds Then, seeds were placed on square Petri dishes (24 cm × 24 cm, filled with 250 ml of growth medium). *Tomato* growth medium: full-strength Murashige and Skoog (1MS) medium (1×MS salts including vitamins, 3 % sucrose, 0.1 g/ll Myo-Inositol, 0.5 g/l 2-(N-morpholino) ethanesulfonic acid (MES), pH 5.8 with KOH and 1.3 % phytoagar. Plates were dried with open lid for around 1 h after pouring to allow evaporation). Seeds were germinated on vertically positioned Petri dishes in a growth chamber at 25 °C in long day conditions (16h light and 8 h dark; MC785-VDB,Van den Berg). Plants were rotated and imaged at indicated time points (Figure legends).

Image acquisition

An Epson V600 CCD flatbed color image scanner (Seiko Epson) was used for image acquisition. Image format: .tiff, 800 dpi.

Image and statistical analysis

Root systems on .tiff images were traced with the Fiji (http://fiji.sc/) plugin SmartRoot (Lobet et al., 2011). Root tracings were saved in .rsml files and imported into RStudio (https://www.rstudio.com/, R version 3.4) for statistical analysis. Data were always tested for normality based on diagnostic plots, like histograms and quantile-quantile-plots. Outlier were not removed.

3. Results

3.1 Exploring *LATERAL SUPPRESSOR* expression domains in the *Arabidopsis* root

Root specific expression of *LAS* depends on regulatory element B

Based on the analysis of expression patterns and complementation experiments, the *LAS* 5' promoter seemed sufficient to promote expression during late vegetative and throughout reproductive development (Goldshmidt et al., 2008). Whereas region C in the 3' enhancer is the key regulatory element to promote *LAS* expression during vegetative development (Raatz et al., 2011). This raised the question of the biological relevance of region B.

Various studies and online data bases report expression of *LAS* and its orthologous genes in tissues encompassing the shoot and the root. For example, in *Arabidopsis*, tomato and snapdragon, prominent abundance of *LAS*/*Ls*/*ERA* RNA was detected with semi-quantitative RT-PCR in bulk samples of complete roots (Greb et al., 2003; Schumacher et al., 1999; Mizzotti et al., 2017). Further, mining publicly available online resources, expression in roots of two monocot species was found for the *LAS* orthologues, *MONOCULM 1* (*MOC1*) in rice and *BdLAS* (BRADI1G36180) in *Brachypodium distachyon* (Fig. S1a and b).

Region B shows the highest conservation compared to the other regulatory elements, yet in *Arabidopsis* it seems not to be involved in regulating expression in the SAM (Raatz et al., 2011). Consistent detection of mRNA for *LAS* or orthologous genes in various plant species indicated that region B might control gene expression in root tissues. To test this hypothesis, two modified *LAS* promoters, *pBR47* and *pBR48*, were tested for their ability to drive root expression of a GUS reporter gene. *pBR47* contained an *LAS* promoter version consisting of the regulatory regions A, B and D, whereas in *pBR48* regulatory element B was removed (Fig. 5a). Both constructs promoted *GUS* expression in rosettes of 10 days old plants, transformed with either *pBR47* or *pBR48* (Fig. 5b and c). However, only transgenic plants carrying *pBR47* displayed additional GUS staining in the primary root tip and the tips of emerged lateral roots (LRs; Fig. 5b and c). Interestingly, both constructs showed *GUS* expression in the pericycle of transgenic plants, even though the signal was considerably weaker compared to the other stained root domains (Fig. 5d and e). *pBR47* carrying plants displayed a lower frequency of GUS staining in the pericycle compared to *pBR48* carrying plants (Fig. 5d and e). This

suggested that in *Arabidopsis* region B is capable of promoting *LAS* expression in tips of primary roots and LRs.

LAS root expression domains on cellular level

Next, *LAS* expression domains and protein localization was analyzed with confocal laser scanning microscopy (CLSM). A transcriptional reporter *pLAS:erGFP* was generated, using the *LAS* promoter described by Raatz et al. (2011) to drive GFP (Fig. 6a). GFP based reporters provide higher resolution and specificity on cellular level in living tissue compared to GUS based reporters, which are restricted to fixated tissue. *pLAS:erGFP* is a reporter for cells with endogenous *LAS* expression. Based on the GUS staining described above, tips of primary and lateral roots of transgenic plants carrying *pLAS:erGFP* were analyzed.

To avoid confusion concerning description of direction I will use throughout this thesis the terminology proposed by Baskin et al. (2010). Orientation towards the shoot apex will be denoted with shootwards, accordingly orientation towards the root apex will be denoted with rootwards. For example: The vasculature is located shootwards, whereas the columella is located rootwards in relation to the QC (Fig. 3c).

In the primary root tip, fluorescence of *pLAS:erGFP* was detected in a domain comprising the QC, CSCs and the columella (Fig. 6c and d). The columella sub-domain showed variation in GFP fluorescence, that correlated with the bilateral symmetry of the vascular tissues in the *Arabidopsis* root (Fig. 6b). Dependent on the orientation of the root tip, GFP fluorescence was detected in 3 to 4 columella cell columns (Fig. 6c). In different root tip orientations, recognizable by the presence of provascular cell columns in the shootwards meristematic tissue, GFP fluorescence was restricted to the two central columella cell columns (Fig. 6d). This might indicate, that *LAS* expression does not reproduce the radial symmetric organization of the columella. Further, GFP fluorescence was detected in individual shootward positioned stem cells (Fig. 6c). Signal in these cells occurred randomly and might indicate complex regulation of *pLAS:erGFP* expression. Alternatively, this signal could be residual GFP protein of a QC cell, which remained in daughter cells after cell division.

In tips of young LRs, GFP was detected in a similar domain compared to the primary root tip. Cellular organization of the rootward cell lineage in LR tips deviated from the organization seen in primary root tips. In the primary root tip, the columella can be represented in cross sections by a two dimensional matrix of 4 by 4 cells (Fig. 6d). In contrast, cross sections of LR tips display a columella matrix with reduced cell numbers in both dimensions (Fig. 6e and f). Expression domains in LR tips domains could follow one of two patterns. The first class displayed GFP fluorescence in a domain similar to the primary root tip (Fig. 6e). In the second class, the domain with GFP fluorescence was extended into the cell lineages of the ground tissue, LRC and epidermis (Fig. 6f). This was unique for LR tips and was never observed in primary root tips. In some cases, this resulted in asymmetric expression domains along the shootward-rootward axis (Fig. 6f). However, neither the occurrence of one of the expression

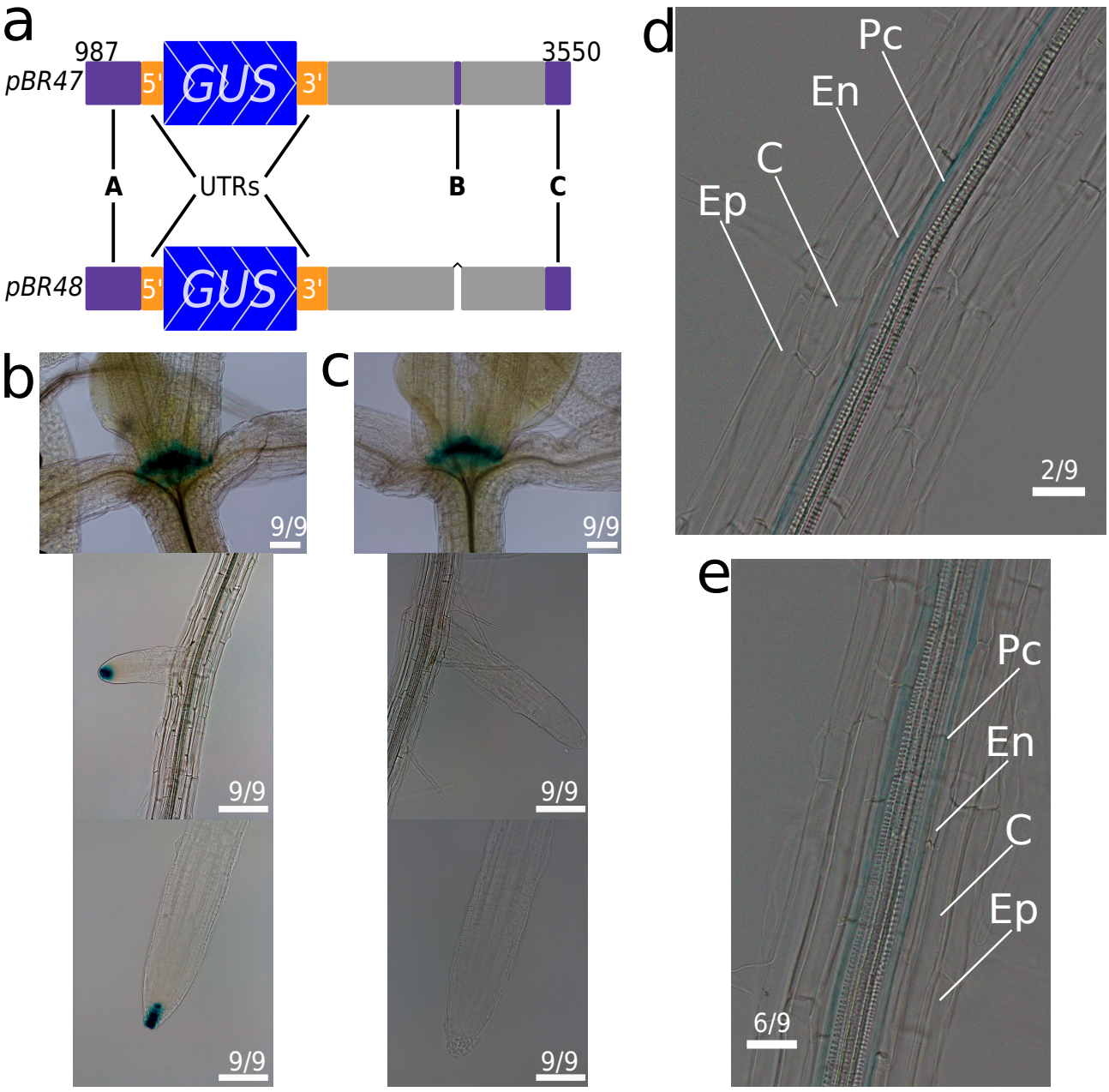


Figure 5: Region B regulates *LAS* expression in root tissues. GUS staining of 10 days old plants expressing either *pBR47* or *pBR48*. **a**, Cartoon of *pBR47* and *pBR48* as described in Raatz et al. (2011). 987 bp 5' of *LAS* start codon and 3550 bp 3' of *LAS* stop codon including the endogenous 5' and 3' untranslated regions (UTRs) driving *β-glucuronidase* (*GUS*) expression. *pBR47* contains the 5' regulatory sequence A and 3' regulatory sequences B and C. In *pBR48* region B was deleted, but otherwise identical to pBR47. **b**, GUS staining in 10 DAG *las-4* plants carrying *pBR47*. **c**, GUS staining in 10 DAG *las-4* plants carrying *pBR48*. **d**, Pericycle specific GUS staining in 10 DAG *las-4* plants carrying *pBR47*. **e**, Pericycle specific GUS staining in 10 DAG *las-4* plants carrying *pBR48*. For (**b**) and (**c**), top to bottom, young rosette, LR, primary root tip. Ratios in (**b**) to (**e**) represent the number of similar observations in independent plant samples. Scale bars in (**b**) and (**c**) indicate 100 μm and 25 μm in (**d**) and (**e**). Plants in (**b**) to (**e**) were stained for 16 h. C = cortex, En = endodermis, Ep = epidermis, Pc = pericycle.

domain classes, nor the occurrence of asymmetric expression domains could be correlated with a specific LR developmental stage or the reaction to an abiotic factor like gravity.

In order to monitor protein localization on cellular level, a set of two translational reporters was generated. For the translational reporters, the same *LAS* promoter sequences as in the transcriptional reporter *pLAS:erGFP* were utilized. Two translational fusion proteins, Vns-LAS (Vns at N-terminus) and LAS-Vns (Vns at C-terminus) were cloned to analyze protein localization (Fig. 7a and Fig. S4a). No difference in the cellular localization of plants transformed with either one of the cloned LAS protein versions could be observed, indicating that neither N-terminal nor C-terminal positioning of the fluorophore interfered with the localization of the fusion protein. Therefore, I will refer to both versions with Vns-LAS and details about fluorophore positions will be described in figure legends.

In the primary root tip, Vns-LAS fluorescence was detected in an extended domain, compared to the domain displayed by *pLAS:erGFP*. Similarly to the transcriptional reporter, Vns-LAS fluorescence was detected in the QC, CSCs and the columella. Cells of these lineages, displayed Vns-LAS fluorescence in the cytosol and the nucleus (Fig. 7b). Additionally, Vns-LAS fluorescence was detected in nuclei of the lateral root cap cells closest to the root tip (Fig. 7b). These observations indicated that LAS might be able to move from the columella to LRC, because only Vns-LAS could be detected in the LRC, whereas *pLAS:erGFP* signal was restricted to the columella.

In tips of young LRs, Vns-LAS signal was extended compared to *pLAS:erGFP*, again indicating the ability of Vns-LAS to move into neighboring cells, that lack *LAS* expression. *pLAS:erGFP* and Vns-LAS displayed partially overlapping domains, intersecting at the QC and the columella cell lineages (Fig. 7c). In this intersection, Vns-LAS fluorescence displayed sub cellular localization of the protein in cytosol and nucleus, whereas in the Vns-LAS unique domain the protein was primarily restricted to the nucleus (Fig. 7c). *pLAS:erGFP* expression displayed more variation in LRs compared to primary roots. Vns-LAS behaved similarly, however expression domains were extended compared to *pLAS:erGFP* along the shootward-rootward axis and the radial axis (Fig. 7c). This was different compared to the primary root tip, where the Vns-LAS domain was extended only along the radial axis compared to *pLAS:erGFP*. In LR tips, Vns-LAS fluorescence signal was high in the QC and decreased gradually with increasing distance to the QC along all axis. Intensity of the Vns-LAS signal was indicative of its sub cellular localization. In the intersection domain, Vns-LAS signal intensity was high and the protein was detected in the cytosol and the nucleus. Decreasing Vns-LAS signal along the shootward-rootward axis and the radial axis correlated with a gradual loss of the cytosolic protein localization and restriction of Vns-LAS to the nucleus, until the signal vanished completely in 5 to 7 cells distance to the QC (Fig. 7c).

In individual LRs that reached 5 mm or more in length, an interesting change on sub cellular localization of Vns-LAS was observed. Some columella cells only displayed Vns-LAS fluorescence in the cytosol and lost the signal in the nucleus (Fig. S2c and d). This phenomenon was restricted to individual columella cells and no obvious pattern could be associated with

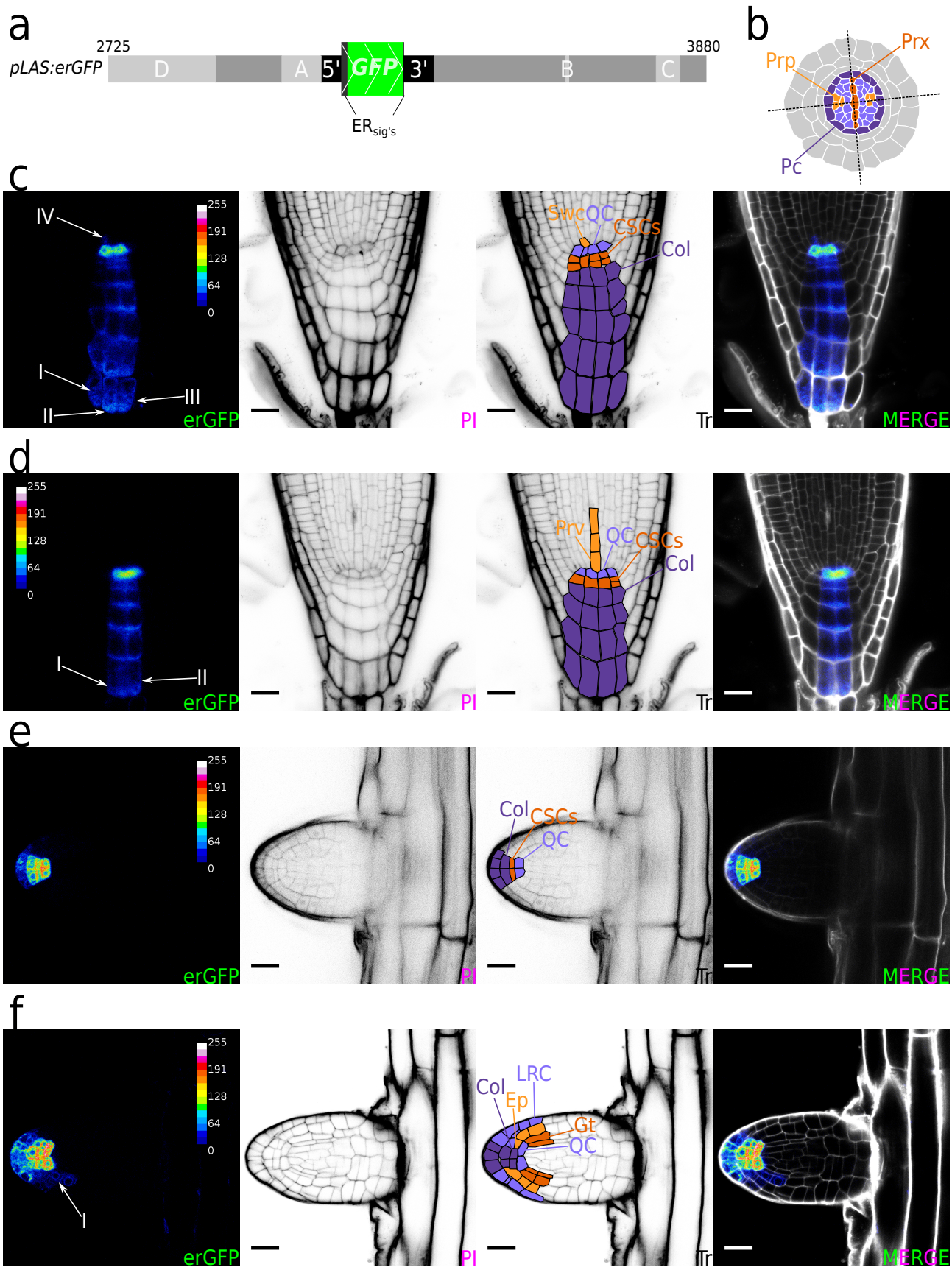


Figure 6: *LAS* is expressed in a cone shaped domain covering the quiescent center, columella stem cells and the columella. CLSM of *pLAS:erGFP* expression in root tips of transgenic plants. **a**, Cartoon of the transcriptional reporter *pLAS:erGFP*. *LAS* promoter described by Raatz et al. (2011) and endogenous UTRs of the *LAS* locus, drive expression of an ER-targeted GFP. Tips of open triangles show 5' to 3' orientation of the *GFP* ORF. FIGURE CONTINUES ON THE NEXT PAGE ...

Figure 6: continued. **b**, Cartoon of the bilateral symmetric organization found in the *Arabidopsis* root. Radial symmetric tissues are indicated in grey. Bilateral symmetry along the xylem-phloem radial axis. Dashed lines represent the two symmetry axes. Cartoon was modified from Sparks (2017a). **c**, GFP fluorescence in the primary root tip. Arrows I - III indicate fluorescence in three columella cell columns. Arrow IV: Fluorescence in a shootward stem cell. **d**, The same as in (**c**), but primary root from a different plant. Arrows I - II indicate fluorescence in two columella cell columns. **e**, GFP fluorescence in the tip of just emerged LR. **f**, The same as in (**e**), but LR from a different root system. Arrow I indicates asymmetric expression domain in the ground tissue. In (**c**) to (**f**) images were taken from roots of Col-0 plants transformed with *pLAS:erGFP* (line 180026_143), 14 days after germination. (**a**) to (**d**), panels from left to right: GFP channel with grey value heat map, PI channel, cell tracings (Tr) and image of merged GFP and PI channels. In (**f**) only cell lineages are traced without denoting stem cells. Based on cellular organization, discrimination of the columella and LRC lineage in LRs is not in all cases unambiguous. Scale bars at the bottom corners of panels represent 18 μm. Col = columella, CSCs = columella stem cells, Ep = epidermis, Gt = ground tissue, LRC = lateral root cap, Pc = pericycle, Prp = protophloem, Prv = provascular cells, Prx = protoxylem, QC = quiescent center, Swc = shootward stem cell.

it. This observation suggested that there might be mechanisms for controlling the localization of LAS protein on sub cellular level resulting in one of three possible outcomes. These are characterized by physical presence of the LAS protein in either cytosol and nucleus at the same time or restriction to exclusively one of these compartments.

Further, a noticeable pattern associated with Vns-LAS fluorescence, was the strong increase in fluorescence intensity in young LRs compared to the primary root tip. This differential fluorescence intensities were quantified, by measuring the intensity grey values in reference cell types. The QC was chosen as the reference cell type for comparison of fluorescence intensity between primary and lateral roots, because of its fixed position at the convergence point of all cell lineages in the root tip. Considering one individual root system, the QC of a young LR displayed a strong Vns-LAS intensity increase, compared to the main QC in the primary root tip (Fig. S5a and b).

Lastly, the expression domain of Vns-LAS in the pericycle was analyzed. The domain delineated by Vns-LAS fluorescence in the pericycle, extends from the early differentiation zone in the root tip, shootwards, until the root hypocotyl junction is reached. This is a physical large domain, making it difficult to cover every aspect with CLSM in great detail. Therefore the observations described below are preliminary results. Vns-LAS signal intensity in pericycle cells close to the root tip was considerable weaker compared to the intensity seen in the primary root or lateral root tip. Vns-LAS fluorescence within pericycle cells was mainly restricted to the nucleus (Figs. S2a and b, S3, S4b). Sometimes Vns-LAS signal was detected in neighboring endodermal cells (Fig. S2a and b, S3). In older (fully differentiated) shootward parts of the root, Vns-LAS signal intensity increased compared to pericycle cells close to the root tip. In lateral root primordia (LRPs) from stage I onwards, Vns-LAS signal was elevated compared to neighboring pericycle cells. Vns-LAS was present throughout every stage of LR development.

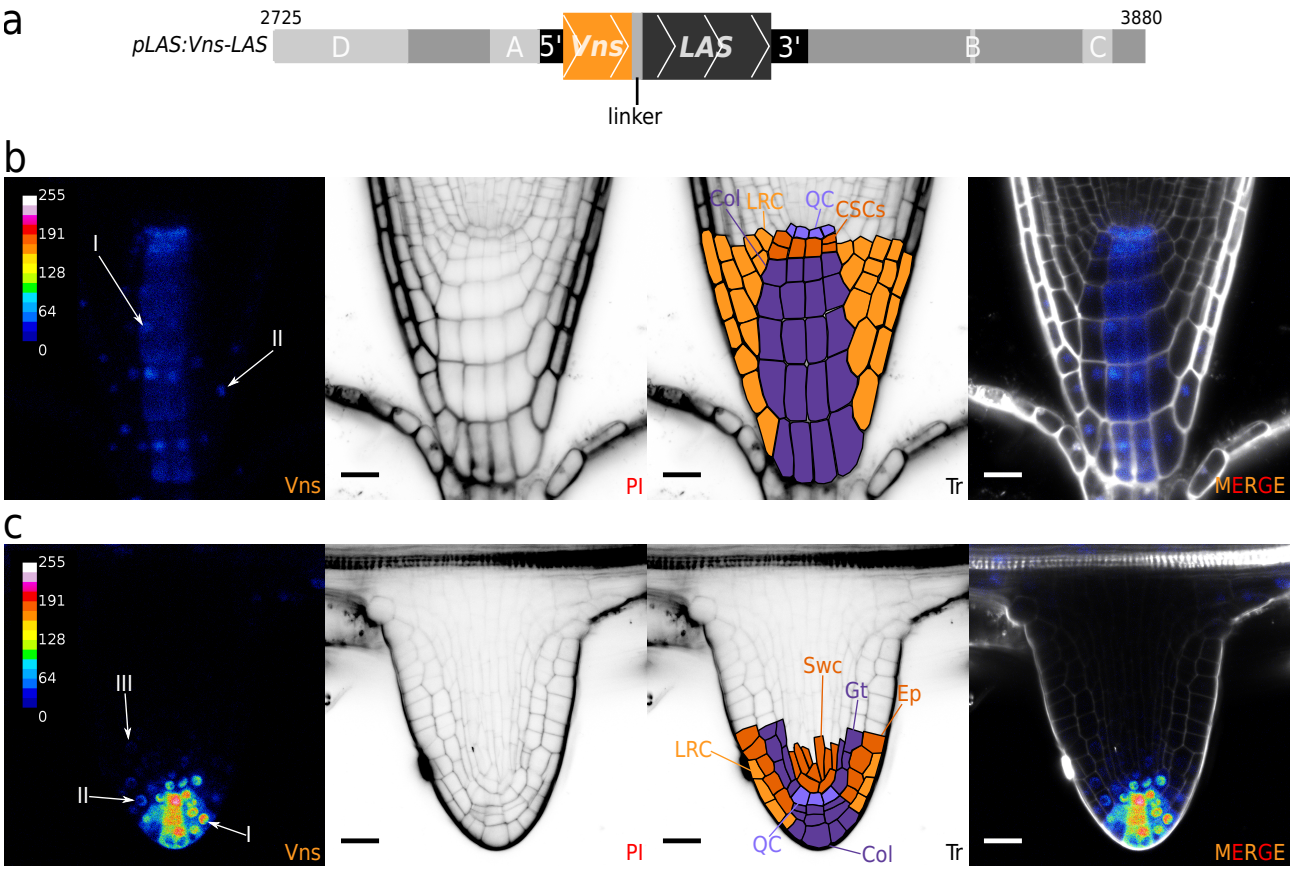


Figure 7: LATERAL SUPPRESSOR protein is detected in the lateral root cap. CLSM of Vns-LAS expression in root tips of transgenic *las-4* plants. **a**, Cartoon of the translational reporter *pLAS:Vns-LAS*. The *LAS* promoter described by Raatz et al. (2011) including endogenous UTRs of the *LAS* locus, drives expression of a translational fusion protein. The fusion protein consists of three parts. N-terminal *Vns* is connected via a flexible 99 bp *linker* sequence described by Daum et al. (2014), with the *LAS* genomic sequence. Tips of open triangles show 5' to 3' orientation of the *Vns-LAS* ORF. **b**, Vns-LAS fluorescence in the primary root tip. Arrow I: Columella cell displaying sub cellular protein localization in the cytosol and the nucleus. Arrow II: LRC cell with protein localization restricted to the nucleus. **c**, Vns-LAS fluorescence in the LR tip. Arrow I: Columella cell displaying sub cellular protein localization in the cytosol and the nucleus. Arrow II: Epidermal cell with protein localization restricted to the nucleus. Arrow III: Ground tissue cell with nuclear protein localization and decreased fluorescence intensity. In (**b**) to (**c**) images were taken from roots of *las-4* mutant plants transformed with *pLAS:Vns-LAS* (line 170138_4), 7 days after germination. (**b**) and (**c**), panels from left to right: Vns channel with grey value heat map, PI channel, cell tracings (Tr) and image of merged Vns and PI channels. Based on cellular organization, discrimination of the columella and LRC lineage in LRs is not in all cases unambiguous. Scale bars at the bottom corners of panels represent 18 μm. Col = columella, CSCs = columella stem cells, Ep = epidermis, Gt = ground tissue, LRC = lateral root cap, QC = quiescent center, Swc = shootward stem cells.

Sub cellular localization of Vns-LAS during LR development was restricted to the nuclei of LRP cells (Figs. S2a and b, S4b-e). Interestingly, in LRP stages II to IV, cells from the overlaying endodermis and cortex in physical contact with the developing LRP, displayed strong Vns-LAS signal in their nuclei. The Vns-LAS signal intensity in these overlying tissues was usually stronger compared to the signal seen in cells of the LRP (Figs. S2b, S4c-e). When the LRP penetrated the epidermis, the Vns-LAS fluorescence domain transformed into the domain seen in LR tips. This was accompanied by a strong increase of the Vns-LAS signal (Fig. S3).

What is the basis of *LATERAL SUPPRESSOR* movement?

In the primary root tip, signal for both reporters, Vns-LAS and *pLAS:erGFP*, was detected in a domain composed of the QC, CSCs and columella. Notably, exclusively Vns-LAS was detected also in the LRC. This observation indicated the possible translocation of *LAS* gene products, on mRNA or protein level, from *LAS* expressing cells into neighboring, *LAS* non-expressing cells. To discriminate between the possibilities of inter-cellular mRNA translocation and inter-cellular protein movement, an artificial bi-cistronic *LAS* gene driven by the *LAS* promoter, called *biChromium*, was engineered (Fig. 8a). The two proteins encoded by *biChromium* are a translational LAS fusion protein (Vns-LAS$_{biChro}$) and an ER-targeted Tq2 (erTq2$_{biChro}$). With this set up, transcriptional and translational domains can be monitored simultaneously. The critical step is the separation of both *biChromium* reporter units, in order to get two independent functional proteins. Separation of the two encoded proteins is achieved via the 2A peptide 'ribosomal skip' mechanism. 2A peptides to force the ribosome to skip the formation of a peptide bond at the C-terminus of the 2A peptide, without termination of translation. This separates the 2A peptide and optional N-terminal fused proteins from the next peptide downstream, making it a versatile system for co-expression of two proteins from the same mRNA (Donnelly et al., 2001; Kim et al., 2011). The advantage of this bi-cistronic reporter system for inter-cellular translocation studies, is the linkage of both *biChromium* proteins on the same mRNA. Based on the cellular colocalization of both *biChromium* proteins, protein movement and RNA translocation can be discriminated. If *biChromium* mRNA (containing endogenous *LAS* mRNA) would be translocated from the columella, a *LAS* expressing tissue, into a tissue with no *LAS* expression like the LRC, one would expect to detect both *biChromium* proteins in all cell types. If the translocation takes place on protein level, only Vns-LAS$_{biChro}$ would be present in the LRC.

In the primary root tip, erTq2$_{biChro}$ is detected in the same cell lineages as the transcriptional reporter *pLAS:erGFP*. This domain comprised of the QC, CSCs and columella (Fig. 8b). In contrast, Vns-LAS$_{biChro}$ was detected additionally in the LRC lineage, recreating the same domain, displayed by Vns-LAS (Fig. 8b). On sub cellular level, localization of Vns-LAS$_{biChro}$ mimicked Vns-LAS behavior as well. In the QC, CSCs and columella, signal was detected in the cytosol and the nucleus, whereas in the LRC the signal was more restricted to the nucleus (Fig. 8b). In tips of young LRs, erTq2$_{biChro}$ was detected in the QC and rootward cell lineages (Fig. 8c). Again, this was nearly identical to the domain displayed by *pLAS:erGFP* in tips of

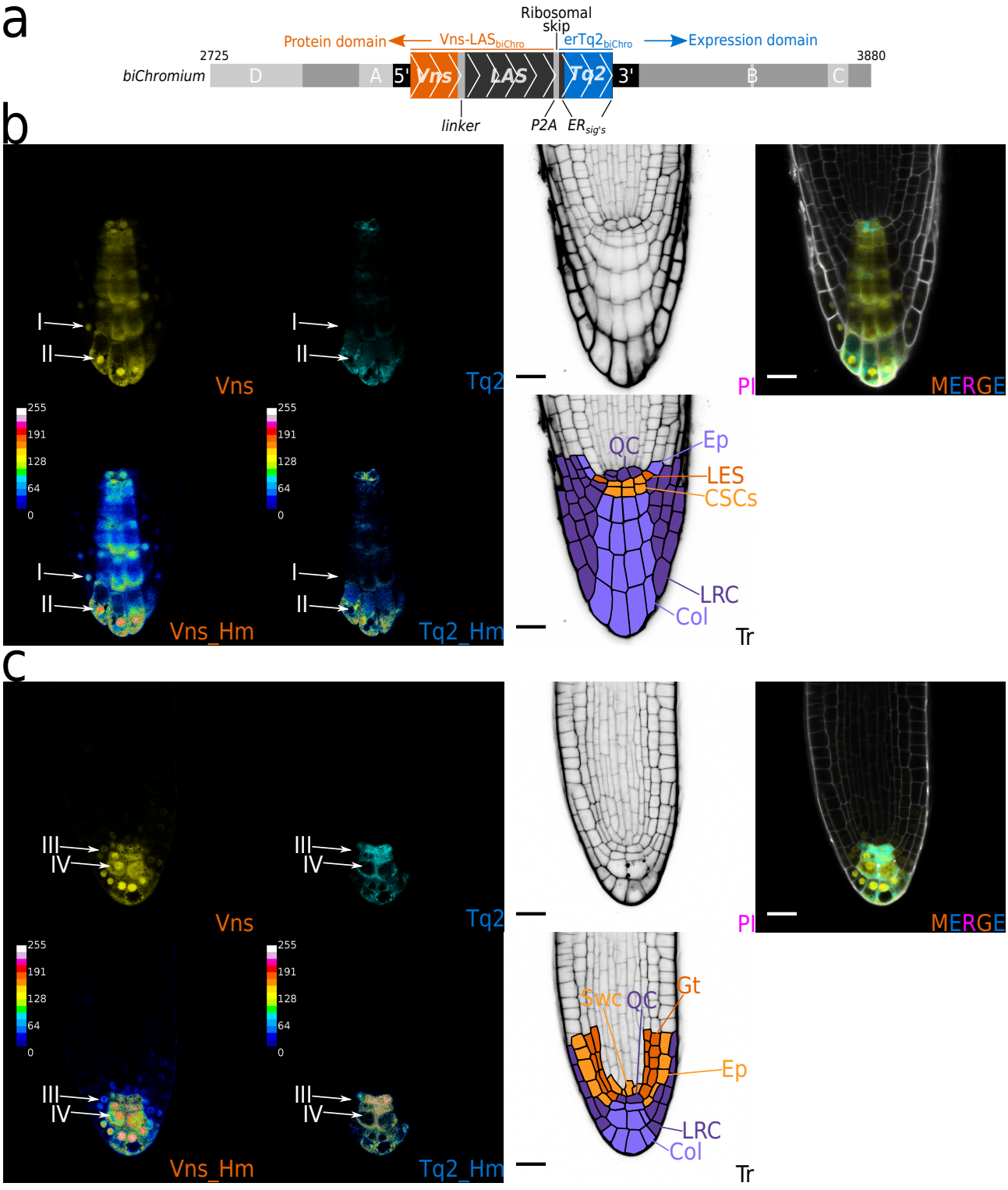


Figure 8: Cell-to-cell movement of LAS protein. CLSM of *biChromium* expression in root tips of transgenic plants. **a**, Cartoon of *biChromium* composition. The *LAS* promoter described by Raatz et al. (2011) including endogenous UTRs of the *LAS* locus, drives expression of a bi-cistronic artificial *LAS* gene. N-terminal *Vns* is connected via a flexible 99 bp *linker* sequence described by Daum et al. (2014), with the *LAS* genomic sequence. This first unit is connected via the 66 bp 2A sequence from porcine teschovirus-1 (P2A), with the second unit consisting of an ER-targeted Tq2. Tips of open triangles show 5' to 3' orientation of the *biChromium* ORF. **b**, Detection of Vns-LAS$_{biChro}$ and erTq2$_{biChro}$ in the primary root tip. Arrows point to identical coordinates in each panel denoting cells with presence of both *biChromium* proteins (Arrow II) or only Vns-LAS$_{biChro}$ (Arrow I). FIGURE CONTINUES ON THE NEXT PAGE ...

Figure 8: continued. **c**, Detection of Vns-LAS$_{biChro}$ and erTq2$_{biChro}$ in the tip of a young LR. Arrows point to identical coordinates in each panel denoting cells with presence of both *biChromium* proteins (Arrow IV) or only Vns-LAS$_{biChro}$ (Arrow III). Two independent *biChromium* lines (180111_1 and 180111_3) in the Col-0 background were analyzed, 7-8 days after germination and representative images are displayed in (**b**) and (**c**). For (**b**) and (**c**), first row, panels from left to right: Vns channel with yellow pseudo color, Tq2 channel with teal pseudo color, PI channel, image of merged Vns, Tq2 and PI channels. Second row, panels from left to right: Vns channel with grey value heat map, Tq2 channel with grey value heat map and cell tracings (Tr). In (**c**) only cell lineages are traced without explicitly denoting stem cells. Scale bars at the bottom corners of panels represent 18 μm. Col = columella, CSCs = columella stem cells, Ep = epidermis, Gt = ground tissue, LES = lateral root cap/epidermis stem cell, LRC = lateral root cap, QC = quiescent center, Swc = shootward stem cell.

young LRs. Simultaneously, Vns-LAS$_{biChro}$ accumulated in the cytosol and the nucleus of cell lineages that were also covered by erTq2$_{biChro}$. However, the Vns-LAS$_{biChro}$ domain was further extended along the shootward-rootward axis and the radial axis compared to erTq2$_{biChro}$. Vns-LAS$_{biChro}$ localization in this extended domain was mainly restricted to the nucleus (Fig. 8c). Thus, the Vns-LAS$_{biChro}$ domain and cellular localization mirrored the behavior of Vns-LAS in tips of young LRs. This suggested that, both *biChromium* proteins act like their mono-cistronic counterparts. Further, this demonstrated that translocation of *LAS* gene products, happened on protein level.

3.2 Phenotypic analysis of *las-4* root system development

Loss of *LATERAL SUPPRESSOR* effects the orientation of lateral roots

To analyze *LAS* function during *Arabidopsis* root development a multi-trait phenotyping approach was used, to compare root system development between Col-0 and *las-4* at quantitative level. The *las-4* allele was chosen, because it is presumably an *LAS* loss-of-function allele (Greb et al., 2003). Based on the root expression domains of *las-4* (Section 3.1), traits describing primary and lateral root development were monitored over a period of 14 days (Table S6 and Fig. 9a). Interestingly only traits describing LR development displayed significant differences between Col-0 and *las-4*.

The first trait that showed a significant difference between Col-0 and *las-4* was the LR branching angle (LRBA). This angle describes the space enclosed by the primary root and a LR at its emerging position (Fig. 9b). Calculation of the LRBA does not rely on a reference point like gravity, but requires vectorized positional data of the primary root and LRs. In *las-4* the LRBA was significantly decreased from 74.2° to 62.7° (Fig. 9c). This implied that LRs in *las-4* had a higher probability to display increased vertical growth trajectories.

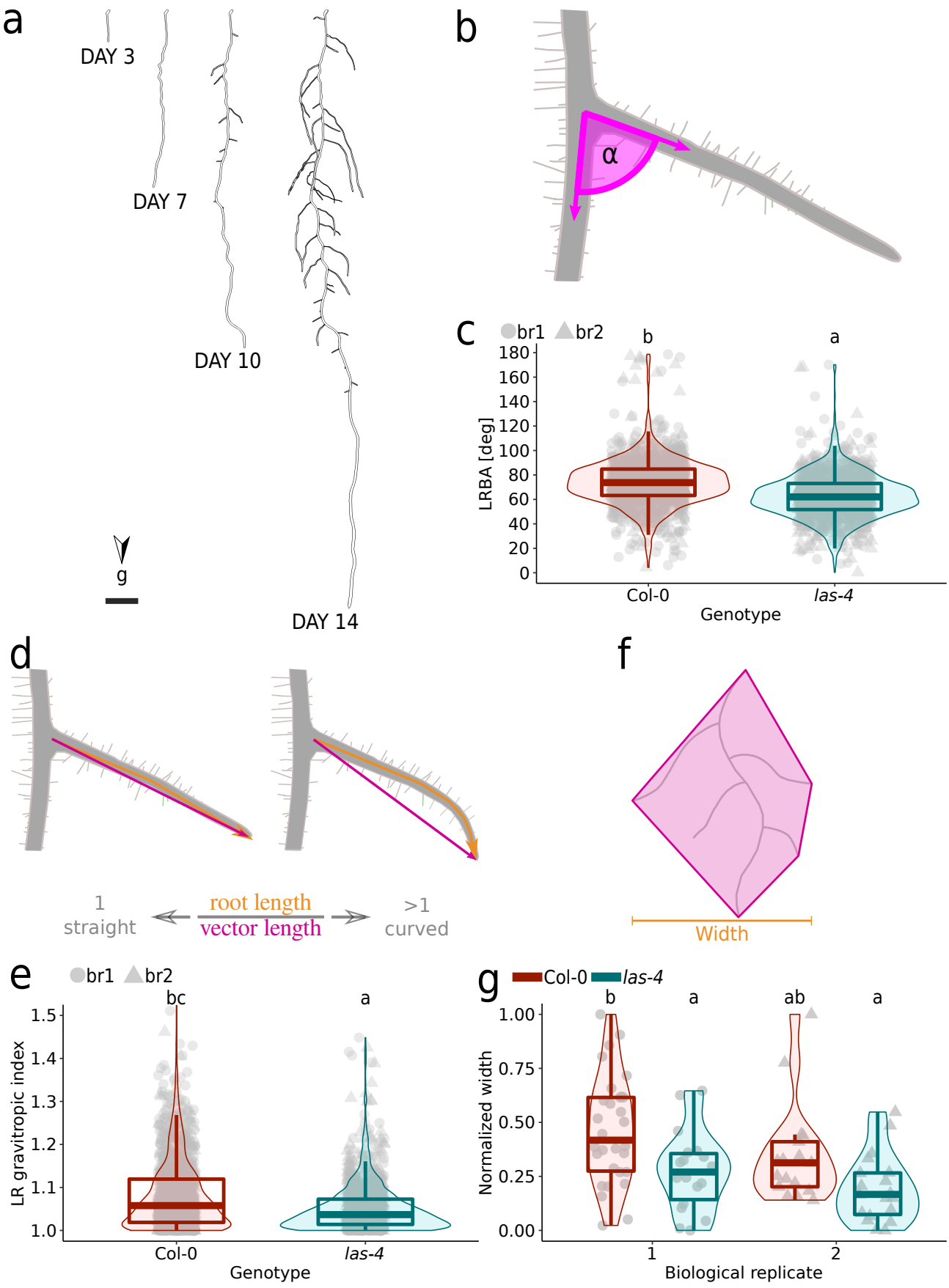


Figure 9: *las-4* causes a reduction in the lateral root branching angle and less curvature during lateral root growth. Multitrait phenotyping of 14 days old Col-0 and *las-4* root systems, grown in vertical orientation on the surface of MS-medium. **a**, Root system development time series of a Col-0 plant. Scale bar: 5 mm. g = direction of the gravity vector. **b**, Cartoon of the LRBA. **c**, LRBA in Col-0 and *las-4*, p(genotype) $< 2e^{-16}$. FIGURE CONTINUES ON THE NEXT PAGE ...

Figure 9: continued. **d**, Cartoon illustrating calculation of the gravitropic index (GI). **e**, GI of LRs in Col-0 and *las-4*, p(genotype) $< 2e^{-16}$. **f**, Cartoon illustrating the convex hull polygon of an arbitrary root system. The width is calculated as the maximal distance between two vertices, represented through a straight line that is parallel to the horizontal direction. **g**, Normalized convex hull width (for each group: largest value = 1 and smallest value = 0) in Col-0 and *las-4* root systems. Because this trait showed variation between biological replicates the data was plotted separately, p(genotype) ≈ 0.0004. Box plots in (**c**), (**e**) and (**g**) show the first and third quartiles separated by the median. Whiskers extend to the largest or smallest value within 1.5 * inter-quartile range (IQR, distance between the first and third quartiles) from the edges of the box. Violin plot in (**c**), (**e**) and (**g**) show the kernel density function of plotted data. Dots in (**c**), (**e**) and (**g**) represent individual LRs. In (**c**), (**e**) and (**g**) statistical significance was determined using unbalanced two-way ANOVA. The letters above the boxes (a–c) indicate the results of a post hoc Tukey test, groups with the same letter are indistinguishable at $> 95\%$ confidence using a 0.05 significance level. In (**c**), (**e**) and (**g**) data of both biological replicates was pooled prior to analysis. Summary statistics are described in table S16.

The second trait that was significantly reduced in *las-4* was the gravitropic index, which is a measure of tortuosity (Fig. 9e). The gravitropic index describes a root's growth path in relation to a straight line. With increasing deviation from a straight line, through directional changes during root growth, the gravitropic index increases (Fig. 9d). Translated to lateral root growth this meant that LRs in *las-4* grew with less changes in direction compared to Col-0. The growth direction of vertical grown primary roots is closely aligned with the gravity vector (Fig. 9a), whereas LRs especially in the early phase of outgrowth follow a more horizontal trajectory (Rosquete et al., 2013; Roychoudhry et al., 2013).

In combination, the LRBA and the gravitropic index can be used as predictors of LR growth trajectory. LRs matching the pattern observed in *las-4*, displaying a decreased LRBA and a decreased gravitropic index, should cover less horizontal space compared to wild type-like LRs, where both parameters displayed higher values. Therefore it was tested, whether changes in these traits would have an effect on root system architecture (RSA). Root system shape in two dimensions was approximated by calculating the convex hull polygon (Fig. 9F). Convex hull width appeared to be a trait with considerable variation, because the results of both biological replicates did not match each other. Only in biological replicate one the width in *las-4* root systems was significantly reduced, whereas in biological replicate there was no difference between root systems (Fig. 9g).

Increased vertical growth trajectories in *las-4* lateral roots

The decreased LRBA and the decreased LR gravitropic index in *las-4*, indicated a closer alignment with the gravity vector compared to LRs in Col-0. To test this, growth angle profiles of LRs with respect to gravity were analyzed. For the calculation of growth angle profiles, LRs were divided into 2.5 mm segments, starting from their emergence point. For each individual segment the growth angle was calculated, resulting in a quantitative growth angle profile, covering all captured LRs (Fig. 10a). In both genotypes, Col-0 and *las-4*, growth angle profiles

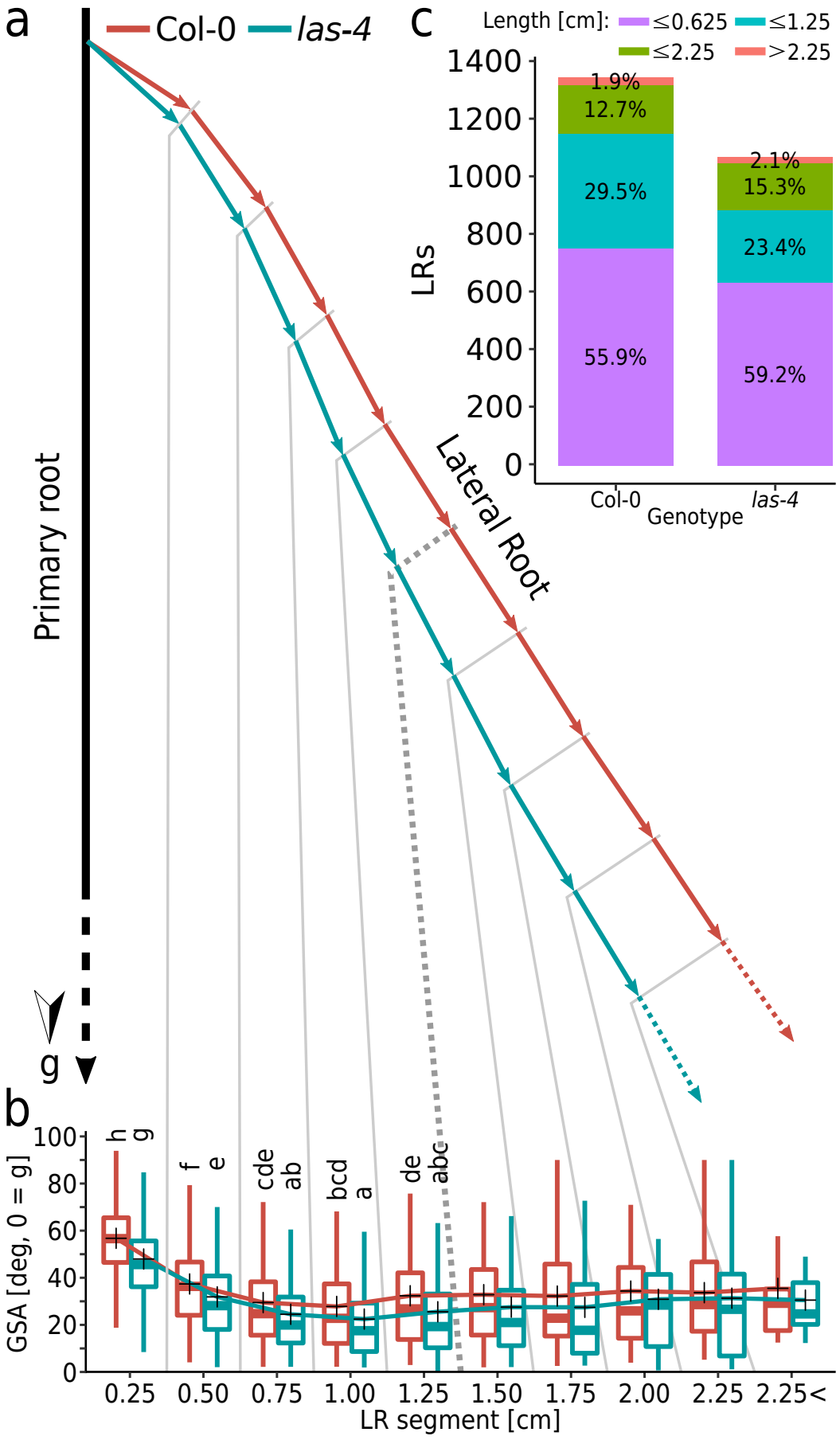


Figure 10: Lateral roots in *las-4* display increased vertical growth trajectories. Growth angle profiles of 14 days old Col-0 and *las-4* root systems, grown in vertical orientation on the surface of MS-medium. **a**, Cartoon of the growth angle profiles in LRs of Col-0 and *las-4* root systems. FIGURE CONTINUES ON THE NEXT PAGE ...

Figure 10: continued. Growth angle of individual segments correspond to the averaged growth angles for each segment (+ symbols in (**b**)). g = direction of the gravity vector. **b**, Growth angle profiles of LRs in Col-0 and *las-4* root systems. Straight lines connect mean values of sample populations (plus signs), p(genotype) $< 2e^{-16}$. **c**, Proportions of LRs grouped according to size in the LR sample population. For a description of box plots see Fig. 9. In (**b**) statistical significance was determined using unbalanced two-way ANOVA. The letters above the boxes (a–h) indicate the results of a post hoc Tukey test, groups with the same letter are indistinguishable at $> 95\%$ confidence using a 0.05 significance level. In (**b**) and (**c**) data of both biological replicates was pooled prior to analysis. Summary statistics are described in table S16.

followed the stereotypic pattern described for LRs in *Arabidopsis*. During the early phase of LR outgrowth, growth angles were less vertical and gradually became more vertical with increasing length of the root (Fig. 10a; Rosquete et al., 2013; Roychoudhry et al., 2013). Notably, LRs in *las-4* displayed significantly increased vertical growth (growth direction is closer to the gravity vector) during the first 1.25 cm of outgrowth (Fig. 10b). This trend continued in segments covering LR parts greater than 1.25 cm, even though growth directions were not significantly different anymore (Fig. 10b). To asses the consequences of a more vertical growth angle profile for a plant, LRs were grouped into categories according to their length. Because LRs grow more vertical with increased length, LRs in *las-4* would have to be considerably longer compared to Col-0, to cover the same horizontal (orthogonal to gravity) space. The fractions of LRs with different lengths were very similar between Col-0 and *las-4* (Fig. 10c). This indicated that in *las-4* increased vertical growth is not compensated through increased LR length, and therefore, *las-4* root systems might be at a disadvantage under conditions that require or trigger increased horizontal root spread, like nitrate deficiency (Roychoudhry et al., 2017).

3.3 Analysis of cell differentiation in the root apical meristem after ectopic *LATERAL SUPPRESSOR* expression

Rossmann et al. (2015) compared cell fate in distal leaflet boundaries, a tissue that is affected by loss of Ls, in wild-type and ls mutant backgrounds. The results presented in that study, suggested that Ls might act as an inhibitor of cell differentiation (Rossmann et al., 2015). To test this hypothesis, the *Arabidopsis* RAM was chosen as an experimental system to assess the consequences of *LAS* misexpression in relation to cell differentiation. Alterations in RAM activity correlate well with certain root traits like primary root length, primary root growth rate and gravity aligned growth direction, making it simple to monitor LAS induced changes on macroscopic level. Further, on cellular level, certain features making the *Arabidopsis* root tip, encompassing the RAM and differentiation zone, an attractive model system for studying developmental processes (Sabatini et al., 2003; Dello Ioio et al., 2007). First, cellular organization is simple with concentric (radial symmetric) single layered tissues enclosing the central bilateral symmetric vasculature. Second, cells are organized in files and each file is generated

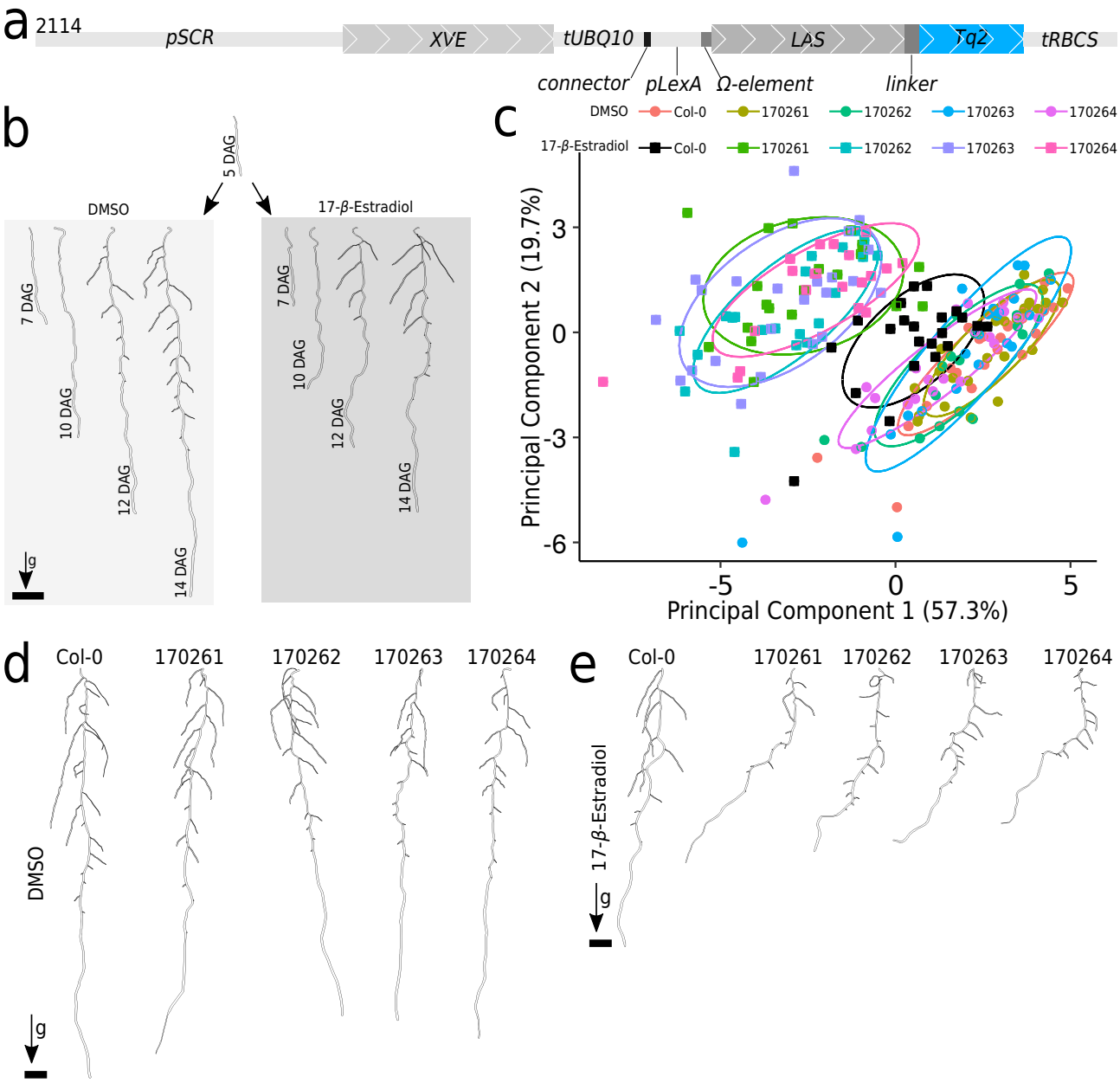


Figure 11: Driving *LAS* expression by the *SCR* promoter changes root system architecture. Phenotypic analysis of root architecture in *pSCR>>LAS-Tq2* plants after *LAS* induction. **a**, *pSCR>>LAS-Tq2* composition. The *XVE* driving- and *LAS* responding-cassette were combined on the same T-DNA, linked by a 44 bp *connector*. 2114 bp 5' of the *SCR* start codon were used as the *SCR* the promoter. Sequences of > symbols denote ORF 5' to 3' direction. **b**, Phenotyping experiment set-up, showing two Col-0 root systems. Plants were grown on AMS, at 5 DAG plants were transferred on new AMS that was either supplemented with DMSO or 10 μM 17-β-estradiol and scanned for the first time. Further, root systems were scanned on indicated time points. LRs were only traced for the 12 and 14 DAG time points. **c**, PCA analysis of root traits described in table S6. Normal probability ellipses drawn for all observation groups, encompassing the central 68% of the data. Sample size ranged between 20 to 26 plants for each line/treatment combination. **d**, Images of randomly picked root systems of all lines after 14 DAG on AMS supplemented with DMSO. **e**, Images of randomly picked root systems of all lines after 14 DAG on AMS supplemented with 10 μM 17-β-estradiol. For (**c**) to (**e**) 170261 to 170264 represent four independent transgenic lines in the Col-0 background, carrying *pSCR>>LAS-Tq2*. Arrows in (**b**), (**d**) and (**e**) denoted with g, indicate the direction of the gravity vector. Black bars in (**b**), (**d**) and (**e**) represent 5 mm.

from a single stem cell that is located in the root tip. This division pattern leads to a linear developmental timeline, reducing multi-dimensionality of development (three dimensional tissue organization that changes over time) to one dimension. Third, being a transparent organ, observations on cellular scale as well as monitoring whole organ development are easy to perform (Benfey and Schiefelbein, 1994; Bennett and Scheres, 2010).

Tissue specific *LAS* expression was achieved by deploying the *SCR* promoter in combination with an estradiol-inducible expression system (Fig. 11a). By using the *SCR* promoter, *LAS* expression could be induced specifically in the root endodermis, covering the whole developmental timeline of the endodermal cell lineage from stem cells over transient amplifying cells to differentiated cells. Further, the SCR expression domain includes the QC and LR primordia (LRPs) throughout LR morphogenesis (Di Laurenzio et al., 1996; Wysocka-Diller et al., 2000; Goh et al., 2016). As a side note, *SCR* expression domains in the QC and LRP overlap with endogenous *LAS* expression domains. Using this set-up, the following questions have been addressed:

1. Does ectopic *LAS* expression results in phenotypic alterations during root development?

2. Which cells in the root tip are responsive to *LAS* expression, e.g. only certain sub populations like meristematic cells, or respond cells independent of their differentiation status?

3. What is the consequence of *LAS* expression for individual cells?

The effect of *LAS* induction in the *SCR* expression domain was first analyzed on phenotypic level. Root system phenotyping followed the basic set up, described in section 3.2. Plants were monitored over a period of 14 days. 5 days after germination, plants were transferred either on medium supplemented with DMSO (control group) or 17-β-estradiol (treatment group), to continue growth in inducing conditions (Fig. 11b). Captured traits are summarized in table S6.

Exploring the root trait data set with principal component analysis (PCA) along the first and second principal components (explaining 54 and 15% of the variation, respectively), revealed a sharp partition of plants based on treatment. The first group included only root systems from the control group, the second group contained exclusively root systems of the treatment group. Non-transgenic plants of the treatment group assembled in a sub group, between both major groups. This sub group overlapped partially with the control group, indicating a closer relation of the sub group root systems with the control group root systems, in comparison to the root systems of the treatment group (Fig. 11c). Transgenic plants in the treatment group uniformly responded to the 17-β-estradiol treatment through deviation from gravity oriented root growth. Notably, all plants responded similarly by redirecting growth in the same direction with respect to gravity (Fig. 11d-e and Fig. S7a).

Prolonged 17-β-estradiol treatment leads to a reduced primary root growth rate in non-transgenic plants

Next, the effect of 17-β-estradiol treatment on non-transgenic plants was assessed. This is an important control step to discriminate growth aberrations that were caused either by 17-β-estradiol's *in vivo* effect on plant physiology, or by the induction of *LAS*. Based on PCA analysis 17-β-estradiol application, caused differences in root development between the control group plants and the treatment group plants. Non-transgenic plants assembled in a sub-group, that partially overlapped with plants of the control group (Fig. 11c). On single trait level, only traits in the root system dynamics category were specifically affected by 17-β-estradiol in non-transgenic plants of the treatment group. AT 14 DAG, non-transgenic plants of the treatment group showed minor but statistically not significant reductions in primary root length, in root system length and in lateral root length (Fig. 12a-c). For the primary root, growth rates were statistically significantly reduced, throughout all measuring points (Fig. 12d-g). In contrast, cumulative growth rate of LRs was slightly but not statistically significantly reduced (Fig. 12i). Therefore, the statistically significant difference in root system growth rate was mainly caused by reduced primary root growth rate (Fig. 12h). To summarize, in the used growth conditions 17-β-estradiol had a dampening effect on primary root growth rates of non-transgenic plants. Reduced root growth rates in turn, had only low impact on root length during the analyzed time interval, because differences in root length between treatments were not statistically significant. Probably, differences in root length would become more apparent when 17-β-estradiol exposure would be monitored over an extended period of time. In previous studies that used the estradiol-inducible expression system, similar effects on wild type *Arabidopsis* root growth were observed after prolonged 17-β-estradiol exposure (Siligato et al., 2016).

Ectopic *LAS* expression in the root endodermis is sufficient to reduce growth rates in primary and lateral roots

Induction of LAS in the *SCR* expression domain had a dampening effect on root growth. In contrast to the effect caused by 17-β-estradiol alone, the LAS-caused effect was clearly enhanced. Four independent transgenic lines carrying the *pSCR>>LAS-Tq2* transgene were assayed during the experiment. At 14 DAG, primary root length was significantly reduced in transgenic lines treated with 17-β-estradiol, compared to plants of the control group and non-transgenic plants of the treatment group (Fig. 12a). This difference in primary root length between non-transgenic and transgenic plants was caused by significant reduced growth rates between 5 to 10 days after germination (Fig. 12d-e). Interestingly, for the 5 to 7 DAG time window, a significant decrease in growth rates, were observed for transgenic plants of the control group as well. This might indicate increased sensitivity of transgenic plants to the stress imposed by the transfer from standard to modified growth medium (Fig. 12d). Over the course of the experiment, group specific growth rates settled down on the same level, in the control group from 7 DAG onwards, and in the treatment group from 10 DAG onwards (Fig. 12e-f).

A reduction in LR growth rates caused by ectopic *LAS* expression could not unambiguously evaluated, because only in line 170263 the LR growth rate was statistically significantly reduced (Fig. 12i). To achieve higher resolution compared to the cumulative LR growth rate, individual growth rates of LRs were calculated in 14 day old root systems. Using this approach, an effect of LAS on LR development was detected. This effect was masked, when only the cumulative LR length was applied as a descriptor of LRs. In general, LR length and growth rate displayed positive correlation. *LAS* induction led to a decreased maximal LR length of approximately 1 cm at 14 DAG. This was accompanied by a decreased maximal growth rate (Fig. S7b).

Based on the above described results, the dampening effect of *LAS* induction on root system length and root system growth rate was largely caused by decreased primary growth rate and to a smaller extent by decreased LR growth. At 14 DAG, the *Arabidopsis* root system just starts to develop into a complex branched structure. As the contribution of LR growth to root system growth will increase over time in relation to the contribution of primary root growth, the effect of *LAS* induction on LR growth would be more notable under prolonged treatment conditions, covering longer periods than 14 days of root system development.

SCR is expressed in LRPs throughout LR morphogenesis (Goh et al., 2016). LRs that emerge through the epidermis of the primary root, are considered as the final stage of LR morphogenesis. During LR morphogenesis, the LRP has to grow from the pericycle through overlying tissues of the primary root, to final make contact with the surrounding soil (Casimiro et al., 2003). Because the number of LRs was unaffected in transgenic plants of the treatment group, it is plausible to assume that the number of LRPs was unaffected as well (Fig. 13a). Therefore, the emergence of LRPs was probably unaffected by *LAS* induction. Transgenic plants of the treatment group had an overall decreased primary root length, leading to an increased LR density (Fig. 12a and Fig. 13b). Interestingly, the average distance between out branching LRs (LRs that were emerged from the epidermis and exploring the surrounding medium) along the primary root was only slightly reduced without being statistically significantly different. Only the transgenic line 170263 showed a statistically significant reduction of LR interbranch distance, after *LAS* expression was induced (Fig. 13c). Nevertheless, the interbranch distance was not statistically significantly different from other plants in the treatment group. Based on preserved interbranch distance across different treatments, priming of LRP founder cells, a process that occurs in the oscillation zone (OZ) is probably unaffected by *LAS* expression. The oscillation zone describes a specific region in the primary root tip that displays oscillating gene expression. The OZ is comprised of the basal RAM (RAM close to the transition zone) and the early differentiation zone (Moreno-Risueno et al., 2010). To achieve a similar interbranch distance for primary roots of different length, which have the same number of LRs, a compensation mechanism is required. One possible way to enlarge the zone of emerged LRs along the primary root, is to utilize the root segment in between the most apical emerged LR and the root tip. There is usually a considerable gap between the root tip and the first emerged LR in Col-0 (Fig. 9a, 10 and 14 DAG). This gap was statistically significantly

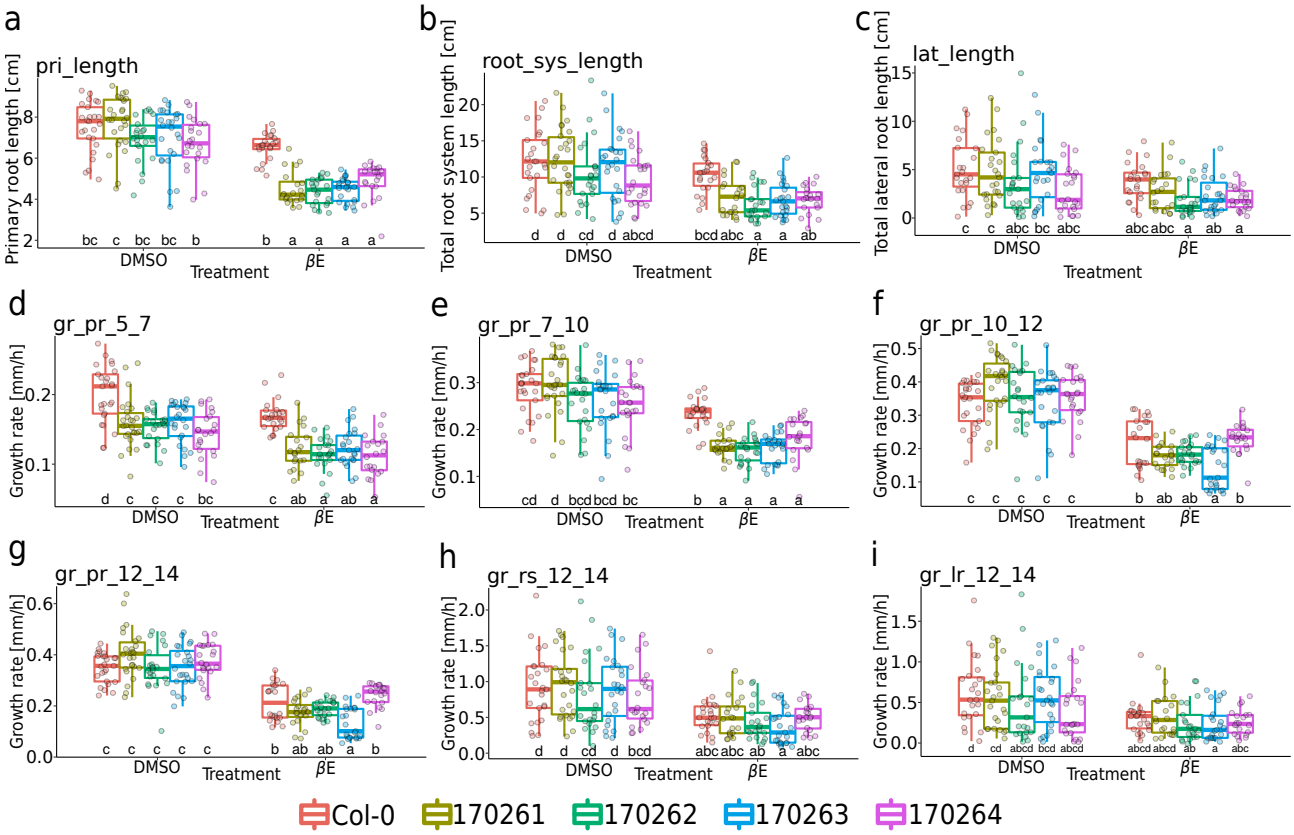


Figure 12: 17-β-estradiol and induction of *LAS* expression reduce root growth. Phenotypic analysis of root growth in *pSCR>>LAS-Tq2* plants after *LAS* induction on single trait level. (**a**) to (**i**) show root traits described in table S6. For a description of box plots see Fig. 9. Dots represent individual root systems. Sample size ranged between 20 to 26 plants for each line/treatment combination. Statistical significance was determined using unbalanced two-way ANOVA. The letters below the boxes (a–d) indicate the results of a post hoc Tukey test, groups with the same letter are indistinguishable at $> 95\%$ confidence using a 0.05 significance level. 170261 to 170264 represent four independent transgenic lines in the Col-0 background, carrying *pSCR>>LAS-Tq2*. Summary statistics are described in table S16.

decreased in transgenic plants of the treatment group, indicating that LRs develop closer to the RAM as a consequence of *LAS* induction (Fig. 13d).

Ectopic *LAS* expression promotes increased horizontal growth in lateral roots

Interestingly, *LAS* induction led to an increased LRBA (Fig. 14a). This was in contrast to the reduction in LRBA seen in *las-4* (Fig. 9c). Transgenic plants of the treatment group showed a shift in LRBA distribution towards larger angels. For two out of the four transgenic lines, this shift led to a statistically significant difference between control and treatment groups (Fig. 14a). Similar to *las-4*, a different LRBA might be an indicator for a change in the LR growth angle. Therefore, the growth angle profiles of LRs in control and treatment groups were calculated. As indicated by the LRBA, transgenic plants in the treatment group displayed statistically significantly enlarged horizontal growth angles compared to the non-transgenic plants in the

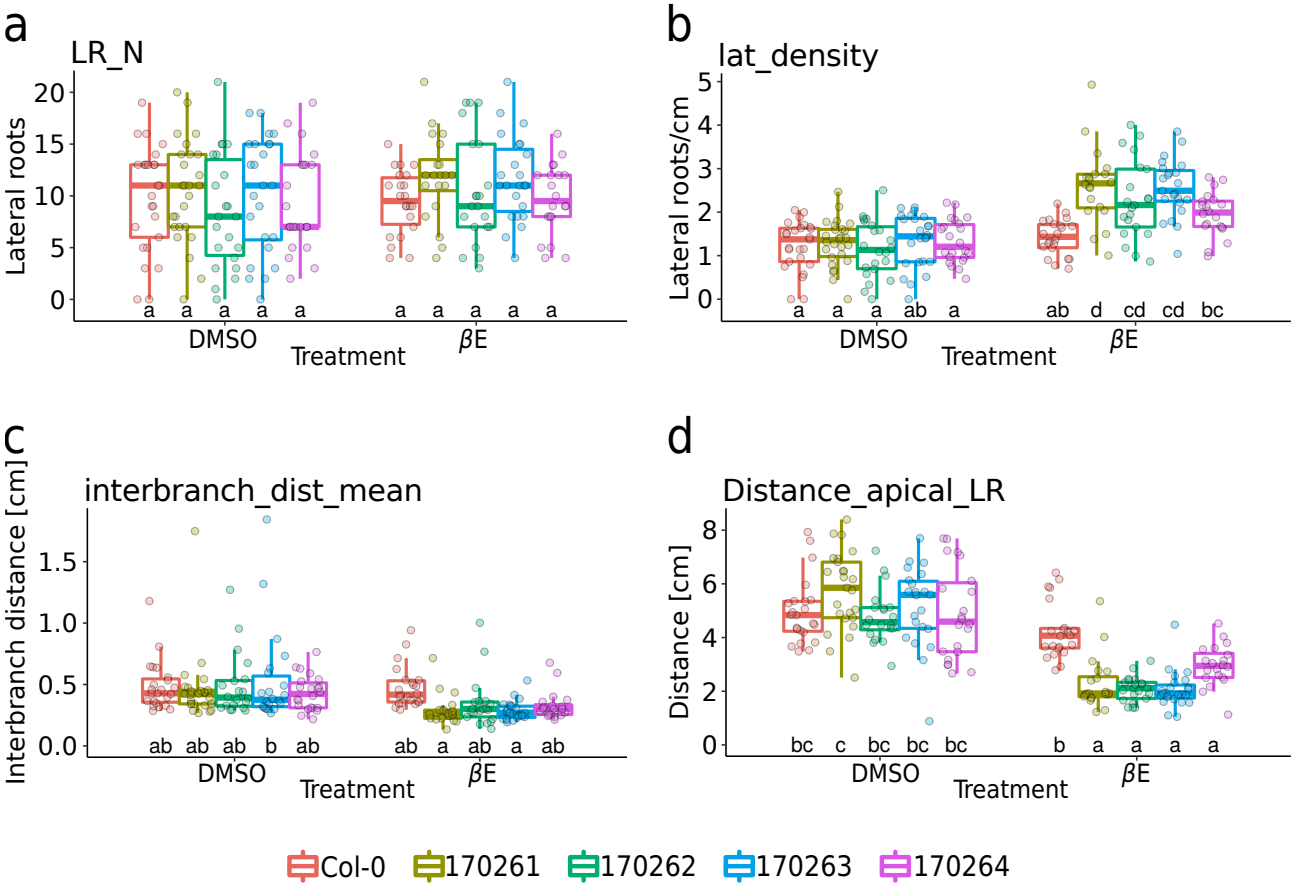


Figure 13: Induced *LAS* expression has no effect on LR number. Phenotypic analysis of root growth in *pSCR>>LAS-Tq2* plants after *LAS* induction on single trait level. (**a**) to (**c**) show root traits described in table S6. Dots represent individual root systems. **d**, Distance between the most apical (most rootwards) emerged LR and the root tip. Dots represent individual LRs. For a description of box plots see Fig. 9. Sample size ranged between 20 to 26 plants for each line/treatment combination. Statistical significance was determined using unbalanced two-way ANOVA. The letters below the boxes (a–d) indicate the results of a post hoc Tukey test, groups with the same letter are indistinguishable at $> 95\%$ confidence using a 0.05 significance level. 170261 to 170264 represent four independent transgenic lines in the Col-0 background, carrying *pSCR>>LAS-Tq2*. Summary statistics are described in table S16.

treatment group and the plants in the control group (Fig. 14b-d).

In shoot tissues the *SCR* promoter confers, expression in the starch containing endodermal cells, which are important for gravity sensing of the shoot (Wysocka-Diller et al., 2000). All transgenic lines displayed shoot-specific phenotypic alterations, like increased lobbing of rosette leaves, defective inflorescence phyllotaxy and an increased number of floral organs (data not shown). Interestingly, these phenotypic alterations occurred without any induction treatment, indicating a certain degree of leaky *LAS* expression arising from *pSCR>>LAS-Tq2* in shoot tissues of transgenic plants. Further, it has been shown that mutants with an aberrant LR growth angle also displayed changes in the growth angles of side shoots. Further, side shoot growth angle control is dependent on auxin signaling in the shoot endodermis (Roychoudhry et al., 2013). Because LAS had an impact on LR growth trajectory, more vertical in the mutant and more horizontal when ectopically expressed, growth angles of side shoots were analyzed. Notably, increased horizontal growth were observed for side shoots arising from cauline leaves of the lines 170262 and 170264, even though this phenotype has still to be quantified in greater detail (Fig. S8a and b). Similar to the before mentioned shoot-specific phenotypic alterations, transgenic plants were not treated with 17-β-estradiol and the aberrant phenotype was caused through leakiness of *pSCR>>LAS-Tq2*.

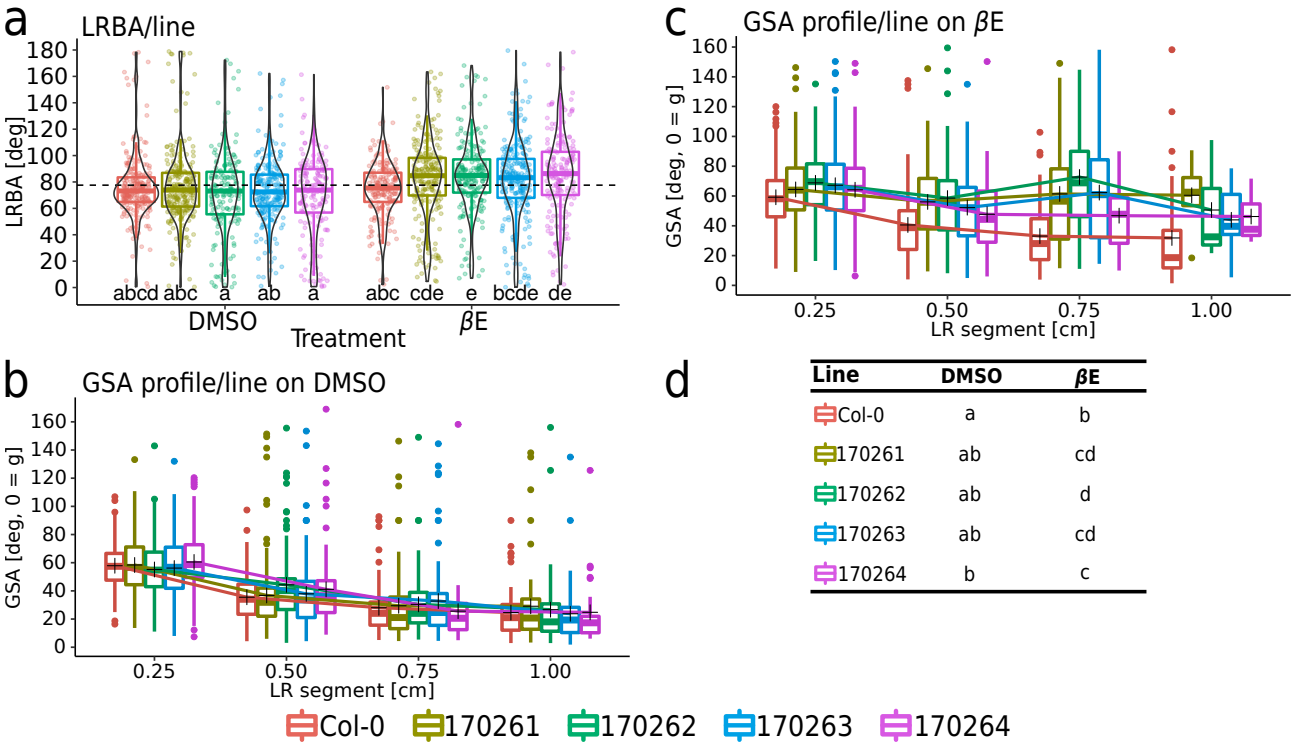


Figure 14: LRs display enlarged horizontal growth angles after induction of *LAS* expression. LRBA and LR growth angle analysis in *pSCR>>LAS-Tq2* plants after *LAS* induction. **a**, LRBA of LRs. Dots represent individual LRs. **b**, Growth angle profiles of LRs from plants growing on DMSO. Straight lines connect mean values of sample populations (plus signs). **c**, Growth angle profiles of LRs from plants growing on 10 μM βE. Straight lines connect mean values of sample populations (plus signs). Dots in (**b**) and (**c**) represent individual LR segments. For a description of box plots and violin plots see Fig. 9. Sample size ranged between 20 to 26 plants for each line/treatment combination. Statistical significance was determined using unbalanced two-way ANOVA. The letters below the boxes (a–e) for (**a**) or in the table (**d**) for (**b**) and (**c**) indicate the results of a post hoc Tukey test, groups with the same letter are indistinguishable at $> 95\%$ confidence using a 0.05 significance level. 170261 to 170264 represent four independent transgenic lines in the Col-0 background, carrying *pSCR>>LAS-Tq2*. Summary statistics are described in table S16.

LAS-Tq2 is ubiquitously detected in the root apical meristem and not restricted to the endodermis

To validate endodermis specific expression of the cloned *SCR* promoter, a control construct *pSCR>>SCR-Tq2* driving the *SCR* gene, was introduced into the *scr-3* mutant background (Fig. 15a). Analyzing protein localization of LAS-Tq2 in comparison to SCR-Tq2, based on Tq2 fluorescence, revealed that both proteins behaved very differently under the spatial control of the *SCR* promoter. SCR-Tq2 protein was detected mainly in the endodermis and within endodermal cells, SCR-Tq2 protein was restricted to the nucleus. In addition, residual Tq2 fluorescence was detected in nuclei of the youngest cells in the middle cortex lineage (Fig. 15b). This demonstrated that the *SCR* promoter driven, estradiol-inducible system, recreated the endogenous SCR domain and should be suitable to confer endodermis specific expression to *LAS*. In contrast, LAS-Tq2 detection was not restricted to the endodermis. Fluorescence was detected in additional root tissues, and was fanning out from the endodermis, the tissue with the strongest fluorescence, to neighboring tissues. In neighboring tissues, fluorescence decreased gradually with increasing distance to the endodermis, leading to a radial gradient of LAS-Tq2 towards more outer and more inner located tissues in relation to the endodermis (Fig.15c). Further, LAS-Tq2 localization on cellular level was different between tissues with high fluorescence and low fluorescence. In the endodermis and endodermis-bordering tissues the LAS-Tq2 fluorescence was detected in the cytosol and the nucleus. In tissues located in radial in greater distance to the endodermis, fluorescence was restricted mainly to the nucleus (Fig.15c). LAS-Tq2 fluorescence displayed a second gradient along the longitudinal direction with the highest fluorescence in the the QC and ground tissue stem cells. With increasing distance to the QC, fluorescence gradually decreased. Along the longitudinal root axis, the lateral range of the radial gradient decreased with further distance from the QC (Fig.15c). Interestingly, LAS-Tq2 fluorescence was detected in cells located rootwards from the QC, covering the columella cell lineages. The *SCR* promoter is not active in columella cell lineages. These observations provide additional proof that LAS is a cell-to-cell mobile protein (Section 3.1). Differences in protein behavior were dependent on the gene product driven by the *SCR* promoter. Only the *LAS* containing transgene displayed ubiquitously LAS-Tq2 fluorescence, in contrast to the endodermis specific SCR-Tq2. RAM ground tissue organization, displayed a unique behavior in response to *LAS* expression. Plants expressing LAS-Tq2, generated frequently four ground tissue layers. In contrast, plants with the corresponding SCR-Tq2 transgene, generated a maximum of three ground tissue layers (Fig.15c and e). This indicated that LAS in contrast to SCR promoted additional formative divisions in the ground tissue cell lineage.

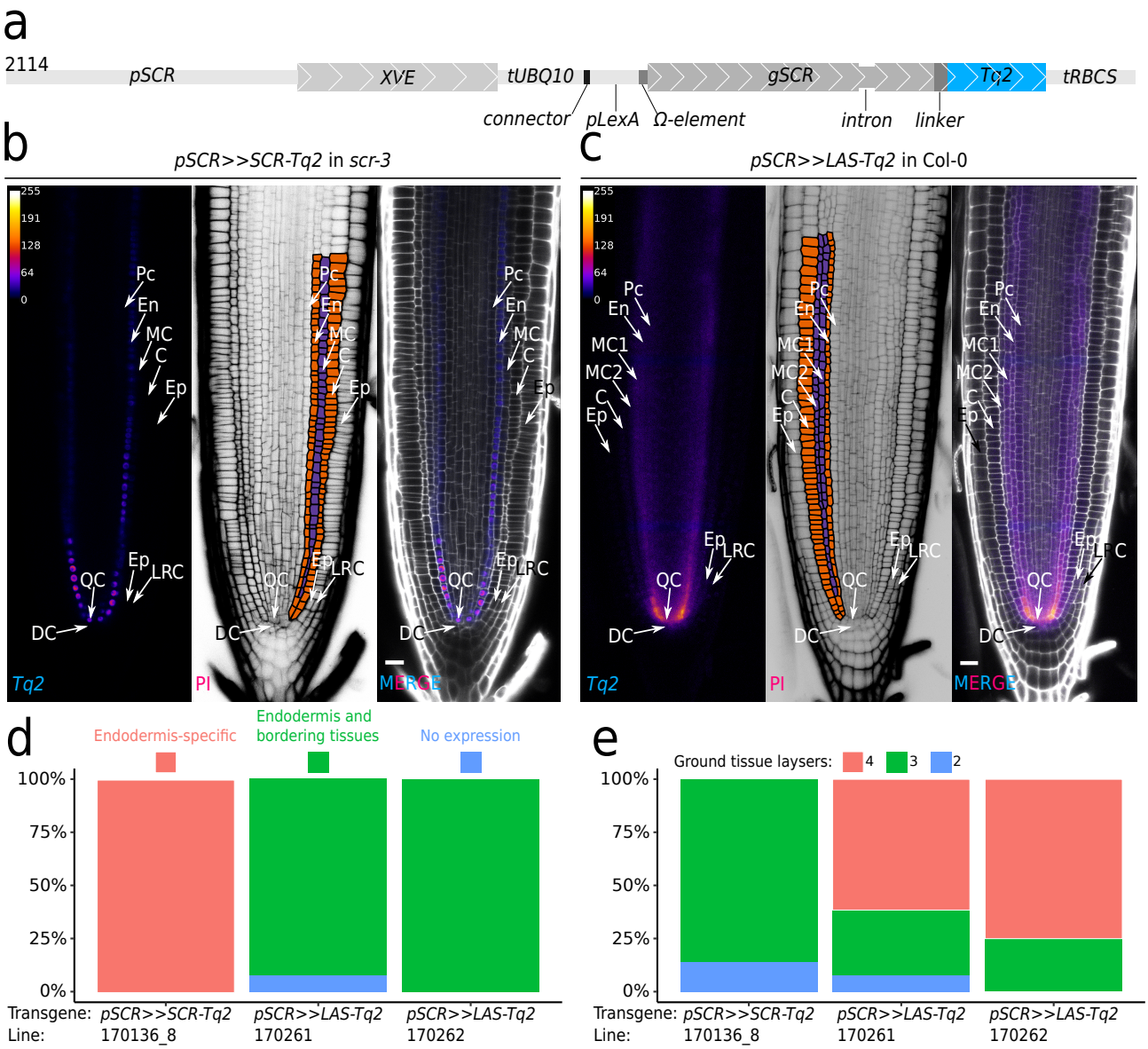


Figure 15: *SCR* promoter driven *LAS* does not reproduce the endogenous SCR domain. CLSM of LAS-Tq2 and SCR-Tq2 accumulation in the RAM of transgenic plants. **a**, *pSCR>>SCR-Tq2* composition. In comparison to *pSCR>>LAS-Tq2*, *LAS* ORF was replaced with *SCR* genomic sequence. (**b**) to (**c**), Representative images of root tips from 9 days old plants, carrying *pSCR>>SCR-Tq2* in the *scr-3* background, line 170136_8 (**b**) and *pSCR>>LAS-Tq2* in Col-0, line 170262 (**c**). 60 h prior to live-imaging plants were transferred on MS medium, containing 10 μM 17-β-estradiol. Left panel displays Tq2 fluorescence intensity, middle panel displays propidium iodide (PI) fluorescence and right panel displays a merged image of the left and middle panels. White bar in the bottom left corner of the right panel represents 18 μm. In the middle panel, the ground tissue cell lineage is traced. Orange tagged cell columns represent cortex and endodermis, purple denotes middle cortex. **d**, Categorization of transgene expression domains endodermal, extended in neighboring tissues or none, after induction with 17-β-estradiol. **e**, Quantification of the number of ground tissue cell layers (ground tissue tracings (**b**) to (**c**)) in transgenic lines after 17-β-estradiol induction. Line 170136_8, n = 7; line 170261, n = 13; line 170262, n = 8. Cell lineage/tissue abbreviations: C = cortex, DC = distal cells, En = endodermis, Ep = epidermis, LRC = lateral root cap, MC = middle cortex, Pc = pericycle, QC = quiescent center.

LAS-Tq2 promotes stem cell differentiation in the root stem cell niche

Cellular organization in the RAM was analyzed with the modified pseudo-Schiff propidium iodide (mPSPI) staining method. mPSPI staining is one of the most frequently used methods to study cellular organisation and amyloplast accumulation within cells in the RAM. Amyloplast accumulation is a useful marker for cell differentiation and cell fate, because in wild type *Arabidopsis* roots only mature columella and LRC cells develop amyloplasts (Truernit et al., 2008; Stahl et al., 2013). Sometimes staining artifacts arose within cells, which were distinct from amyloplasts based on size and form (Fig. S9b and c). Almost in every study that utilized the mPSPI staining method, staining artifacts appeared as a byproduct. In the stem cell niche, ectopic presence of amyloplasts in the columella stem cells, indicates premature stem cell differentiation (Stahl et al., 2013). In all transgenic plants, induction of LAS led to amyloplast accumulation in the first cell row, that borders the QC in rootwards direction (Fig. 16b and c). Presence of amyloplasts was also observed under non-inducing conditions in ca. 30% of assayed plants in line 170261 (Fig. 16c). In the other transgenic lines, ectopic amyloplast accumulation was not observed in the columella stem cells under non-inducing conditions (Fig. 16a and c). This indicated, that induction of LAS either promoted stem cell differentiation, or inhibited stem cell maintenance of the columella cell lineage. A second stem cell population, that displayed ectopic amyloplast accumulation under inducing conditions, were the epidermis/LRC stem cells. Induction of LAS, led to accumulation of amyloplasts in this stem cell population, as well as in the youngest cells of the epidermal cell lineage (Fig. 16b and d). This was never observed under non-inducing conditions, indicating that LAS induction had a similar effect in the epidermis/LRC stem cells as in the CSCs. Further, the origin of epidermal cells could not always unambiguously traced back to the epidermal/LRC stem cell. In these special cases, it appeared that epidermal cells might be generated through an ectopic division in the cortex cell lineage (Fig. 16b). Amyloplast accumulation in the QC was observed with low frequency under inducing conditions (Fig. 16f and Fig. S9a). This indicated, that LAS might promote ectopic cell fate acquisition in the QC, or inhibit maintenance of QC fate. The second morphological attribute of interest, was the number of ground tissue cell layers. As shown above, roots of CLSM-imaged transgenic plants, grown under inducing conditions displayed supernumerary ground tissue layers (Fig.15c and e). This was also observed in mPSPI stained root tips. Transgenic plants, grown under inducing conditions, displayed with higher frequency four ground tissue layers, in contrast to the three ground tissue layers seen under non-inducing conditions (Fig. 16b and e). This indicated that LAS might promote the initiation of the middle cortex lineage. Usually, the middle cortex tissue is generated from meristematic endodermal cells and indicates the transition from juvenile to mature roots, which happens in 7-day old plants (Drapek et al., 2017).

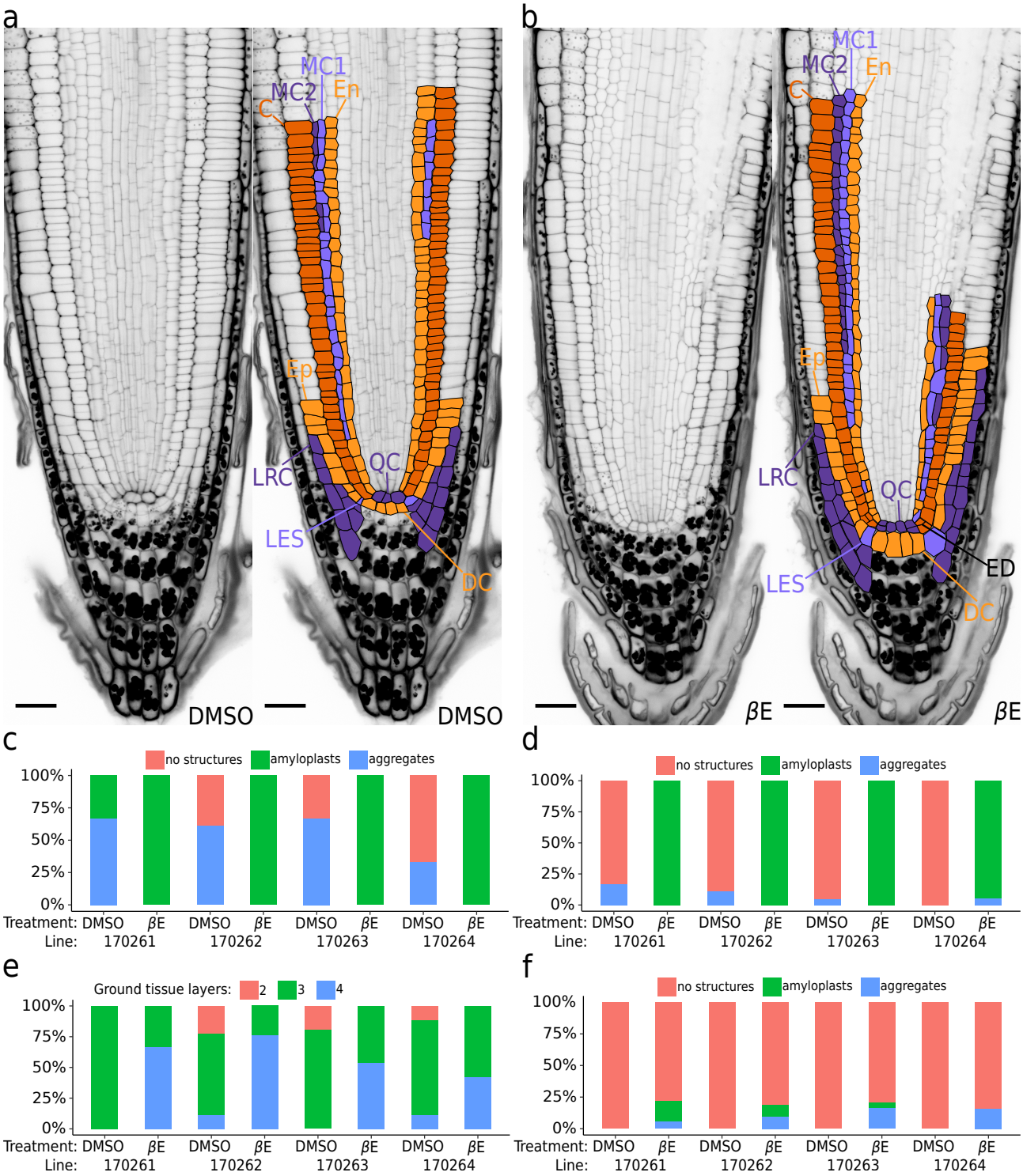


Figure 16: LAS promotes differentiation of stem cells and promotes formative divisions in the ground tissue. (**a**) and (**b**), representative images of mPSPI stained root tips from line 170262. In (**a**) and (**b**) cell lineages are traced in the right panel. Bordering cells of one color group represent a specific tissue. Left panels display the same root tip without tracings. Black bars in the lower left corner represent 25 μm. (**c**) to (**f**), Quantification of morphological hallmarks after mPS-PI staining. In (**c**), the presence of amyloplasts or aggregates in the first row of columella cells (DC), in physical contact with the QC was quantified. In (**d**), the presence of amyloplasts or aggregates in the epidermal cell lineage (LES and Ep) was quantified. In (**e**), the number of ground tissue cell layers (C, En and MC) was quantified. In (**f**), the presence of amyloplasts or aggregates in the QC was quantified. FIGURE CONTINUES ON THE NEXT PAGE ...

Figure 16: continued. Differences between amyloplasts and aggregates are illustrated in Fig. S9b and c. Plants of all four transgenic lines were stained 8 days after germination. Prior to staining, plants were grown for either 120 h (170261 and 170262) or 72 h (170263 and 170264) on medium supplemented with DMSO or 10 μM 17-β-estradiol. Summary statistics are described in table S16. Cell lineage/tissue abbreviations: C = cortex, DC = distal cells, ED = ectopic division, En = endodermis, Ep = epidermis, LES = lateral root cap/epidermis stem cell, LRC = lateral root cap, MC = middle cortex, QC = quiescent center.

3.4 Analyzing LATERAL SUPPRESSOR function in tomato root development

In *Arabidopsis las-4* mutants, LRs displayed increased vertical growth trajectories compared to wild type (Section 3.2). In contrast, other tissues with *LAS* expression, like the primary root tip or the pericycle, displayed no obvious phenotypic alterations in the *las-4* mutant. This posed the question about the relationship between *LAS* expression domains and protein function. Assuming that *LAS* expression has an, yet, undiscovered biological relevance during root development, two possible scenarios could be considered for explaining the lack of a phenotype in the majority of root expression domains:

1. Presence of a redundant mechanism that compensates for the loss of *las*.
2. Situation specific requirement of LAS, e.g. response to abiotic stimuli, that was not triggered in standard growth conditions.

In tomato, the *ls-1* mutant displays pleiotropic phenotypic deviations during shoot development, which are not occurring in *Arabidopsis las-4* mutants, like SAM termination and defective flower development (Schumacher et al., 1999; Greb et al., 2003). Therefore, tomato root development in *ls-1* was analyzed to test whether loss of Ls had, similarly to the shoot, more global effects on root development, compared to *las-4* in *Arabidopsis*.

The *ls-1* mutant displays altered growth trajectories in primary and lateral roots

Growth trajectories in tomato were analyzed with the recently described average absolute angle (avgAbsAng) method (Fig. 17c; Toal et al., 2018). Using this method growth trajectories can be approximated with a single value, which accounts for all directional changes the root did during its growth. It also reflects the major directions of growth, because growth trajectories are weighted according to the distance the root grew in that particular direction. Otherwise, the avgAbsAng describes growth trajectories similar to the GSA notation described above. An avgAbsAng of 0° describes a root that grows parallel to the gravity vector, whereas an avgAbsAng of 90° would indicate a root growing in orthogonal direction (horizontally) with respect to gravity (Fig. 17c).

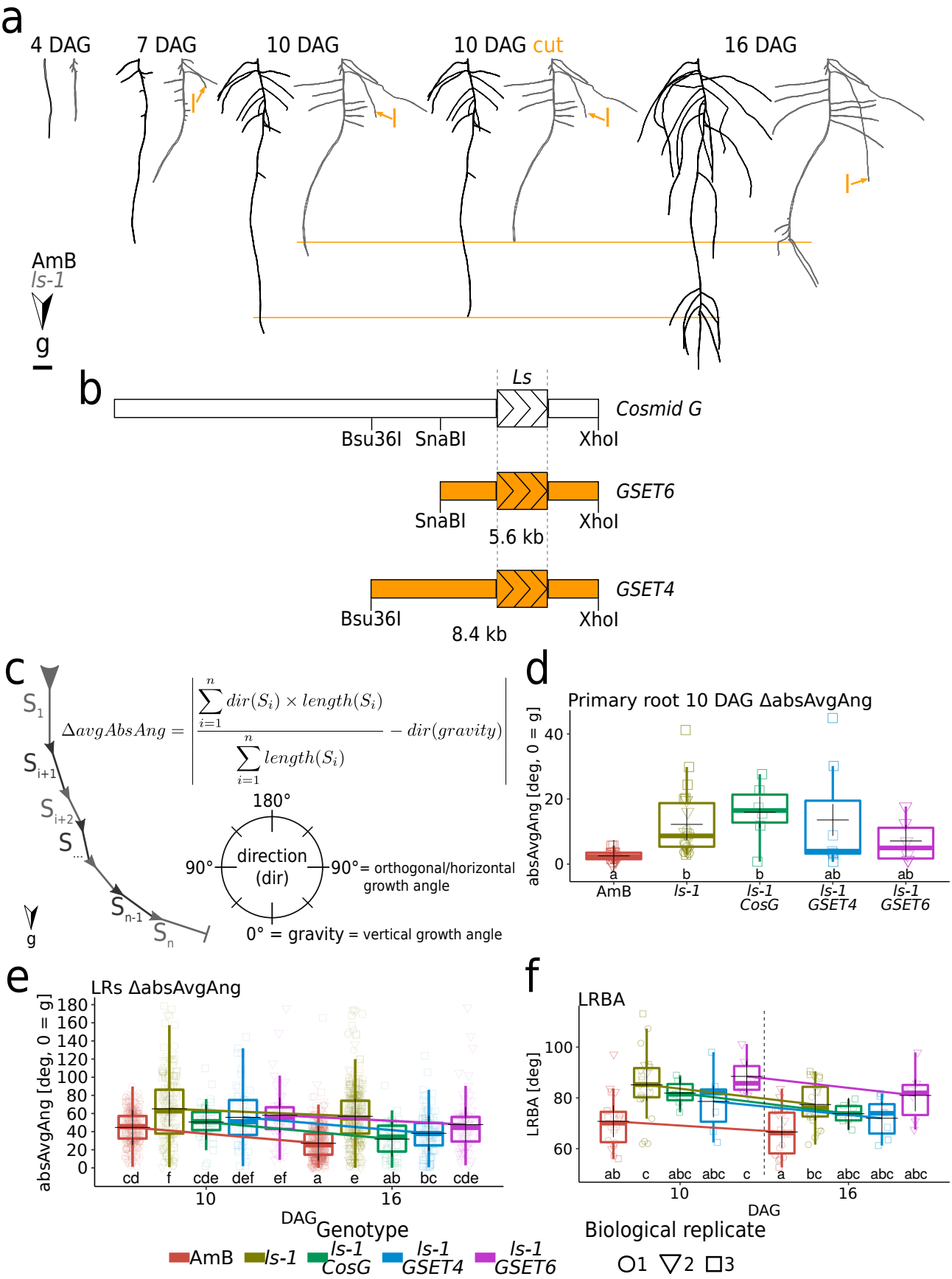


Figure 17: Increased horizontal growth trajectories of roots in the *ls-1* mutant. Phenotypic analysis of root system development in vertically grown wt and *ls-1* plants. **a**, Time series of AmB (black) and *ls-1* mutant (grey) root system development. Representative root systems are shown for wt and *ls-1*. At '10 DAG CUT' 1 cm of the primary root apex was decapitated. FIGURE CONTINUES ON THE NEXT PAGE ...

Figure 17: Continuation. Arrow I: Example of an LR that changed its growth angle, after reflection from a second crossing LR. Arrowhead in the bottom left corner indicates the direction of gravity (g). Scale bar: 1 cm. **b**, Figure is recreated from Schumacher et al. (1999). Shaded constructs *GSET4* and *GSET6* represent segments of *CosG*. Tips of open triangles indicate 5' to 3' orientation of the *Ls* CDS. **c**, Representative root tracing, illustrating the division of the tracing into individual segments based on directional change. Formula for avgAbsAng calculation adapted from Toal et al. (2018). Calculation is normalized against the direction of the gravity vector, so that an avgAbsAng of 0° indicates growth parallel to the direction of gravity. Clock representation of growth angle direction assignment. **d**, avgAbsAng of primary roots at 10 DAG. **e**, avgAbsAng of LRs at 10 DAG and 16 DAG. **f**, Average LRBA of root systems at 10 DAG and 16 DAG. For a description of box plots see Fig. 9. Dots represent individual primary roots (**d** and **f**) or LRs (**e**). Straight lines connect mean values of sample populations (plus signs). Statistical significance was determined using unbalanced two-way ANOVA. The letters below the boxes (a–f) indicate the results of a post hoc Tukey test, groups with the same letter are indistinguishable at $> 95\%$ confidence using a 0.05 significance level. For each time point data from three independent biological replicates was pooled prior to analysis. Sample size ranged between 5 to 8 root systems per genotype for each biological replicate. Summary statistics are described in table S16.

In primary roots of vertical grown 10 days old plants, the avgAbsAng in *ls-1* was statistically significantly increased to 12.2° compared to the 2.5° in wt (Fig. 17d). Interestingly, this phenotype was quite variable between different biological replicates, and even within sample populations. Phenotypes covered the whole range from wt-like vertical avgAbsAngs to nearly horizontally oriented avgAbsAngs, representing a severe mutant phenotype (Fig. 17d). It has been shown that the AM initiation defect in *ls-1* could be complemented with transgenes that harbor ample 5' and 3' regulatory sequences driving *Ls* expression (Schumacher et al., 1999). Three different transgenic lines, each harboring a different construct, were tested for their ability to complement the primary root avgAbsAng defect in *ls-1* (Fig. 17b). All three constructs have been reported to fully complement the AM initiation defect in *ls-1* (Schumacher et al., 1999). Notably, none of the transgenic lines was able to fully complement the primary root phenotype of the *ls-1* mutant. The phenotypic variation seen in the pure *ls-1* background was still present in plant populations of all tested transgenic lines. Based on statistical analysis, the line *ls-1 Cosmid G* (*CosG*), was classified as not/weak complementing, and the lines *ls-1 GSET4* and *ls-1 GSET6* as partially complementing, with respect to the avgAbsAng defect of the primary root (Fig. 17d).

The most notable phenotypic deviation displayed the LRs in *ls-1*. Similar to *Arabidopsis*, LRs in tomato change their growth trajectory in a gradual fashion with increasing age. Young LRs (just emerged or short in length) display horizontal growth trajectories that change with age (increased length) towards more vertical growth trajectories (Fig. 17a). This pattern was severely disrupted in *ls-1*. At 10 DAG, LRs in *ls-1* had an avgAbsAng of 65.1° and visually resembled straight lines (Fig. 17a and e). In contrast, the avgAbsAng of 44.6° in wt LRs, was statistically significantly lower and their appearance was similar to a down bending curve (Fig. 17a and e). Again, the three transgenic lines *ls-1 CosG*, *ls-1 GSET4* and *ls-1 GSET6* were not

able to fully complement the avgAbsAng defect of LRs in *ls-1* (Fig. 17e). In contrast to the primary root, *CosG* showed the strongest complementation, whereas *GSET4* and *GSET6* only conferred weak to no complementation (Fig. 17e). As previously shown (Sections 3.2 and **??**), the LRBA is a useful diagnostic tool to predict growth trajectories of LRs. An increased LRBA would indicate a trend towards more horizontal growth trajectories, vice versa, a decreased LRBA would indicate a trend towards more vertical growth trajectories. At 10 DAG, the LRBA in *ls-1* was statistically significantly increased compared to wt (Fig. 17f), corroborating the positive correlation between LRBA and growth trajectory/avgAbsAng measurements. Once more, the three transgenic lines displayed either only partial complementation of the mutant phenotype (*ls-1 CosG*, *ls-1 GSET4*) or showed no complementation (*ls-1 GSET6*, Fig. 17f).

To test whether LRs in *ls-1* displayed a delayed adjustment of growth trajectory towards gravity, the primary root tip was removed (Fig. 17a). This served two purposes: First, ablation of the main auxin sink induces formation of additional LRs close to the cutting site to replace the lacking primary root tip. This mechanism is also referred to as root apical dominance (Aloni et al., 2006; Rosquete et al., 2013). Second, it stimulates growth of LRs already present in the decapitated root system. For all tested plants, root tip decapitation led to increased vertical growth trajectories of LRs. This was seen in the avgAbsAng, as well as the LRBA (Fig. 17e and f). The LRBA does not change once a root is grown out, therefore the drop in LRBA size seen at 16 DAG was solely caused through newly initiated LRs. Further, this partially explained the increased vertical avgAbsAng of LRs at 16 DAG, based on the positive correlation between LRBA and avgAbsAng. LRs that were grown out prior to the decapitation, responded by becoming displaying more vertical growth trajectories, as well. Nevertheless, the mean decrease in LR avgAbsAng of 8.3° in *ls-1* is statistically significantly less, compared to the 17.4° in wt (Fig. 17e). This indicated, that LRs in *ls-1* were less sensitive to primary root tip decapitation. Interestingly, the transgenic lines *ls-1 CosG* and *ls-1 GSET4* both displayed a wt-like response with a mean avgAbsAng decrease of 18.8° and 17.6°, respectively. In contrast the transgenic line *ls-1 GSET6*, displayed only weak complementation of LR growth trajectory adjustment, with a mean avgAbsAng decrease of 10.3° (Fig. 17e).

Reduced primary root growth rate, but no reduction of LR number in *ls-1*

At 10 DAG, primary root length was significantly decreased in *ls-1* mutants. Reduced primary root length was caused through a statistically significantly decreased growth rate during both analyzed time intervals (Fig. 18a). Growth rates in *ls-1* stayed constant for both time intervals, whereas in the wt, growth rates started to decelerate in the 7-to-10-DAG time interval (Fig. 18a). Regarding the complementation of the mutant phenotype, the transgenic lines were split into two groups. Line *ls-1 GSET4* fully complemented the growth rate defect in *ls-1*, whereas the lines *ls-1 CosG* and *ls-1 GSET6* failed in that regard (Fig. 18a). Prior to the start of the phenotyping experiment, germination of seeds was timed to be simultaneous, through selection

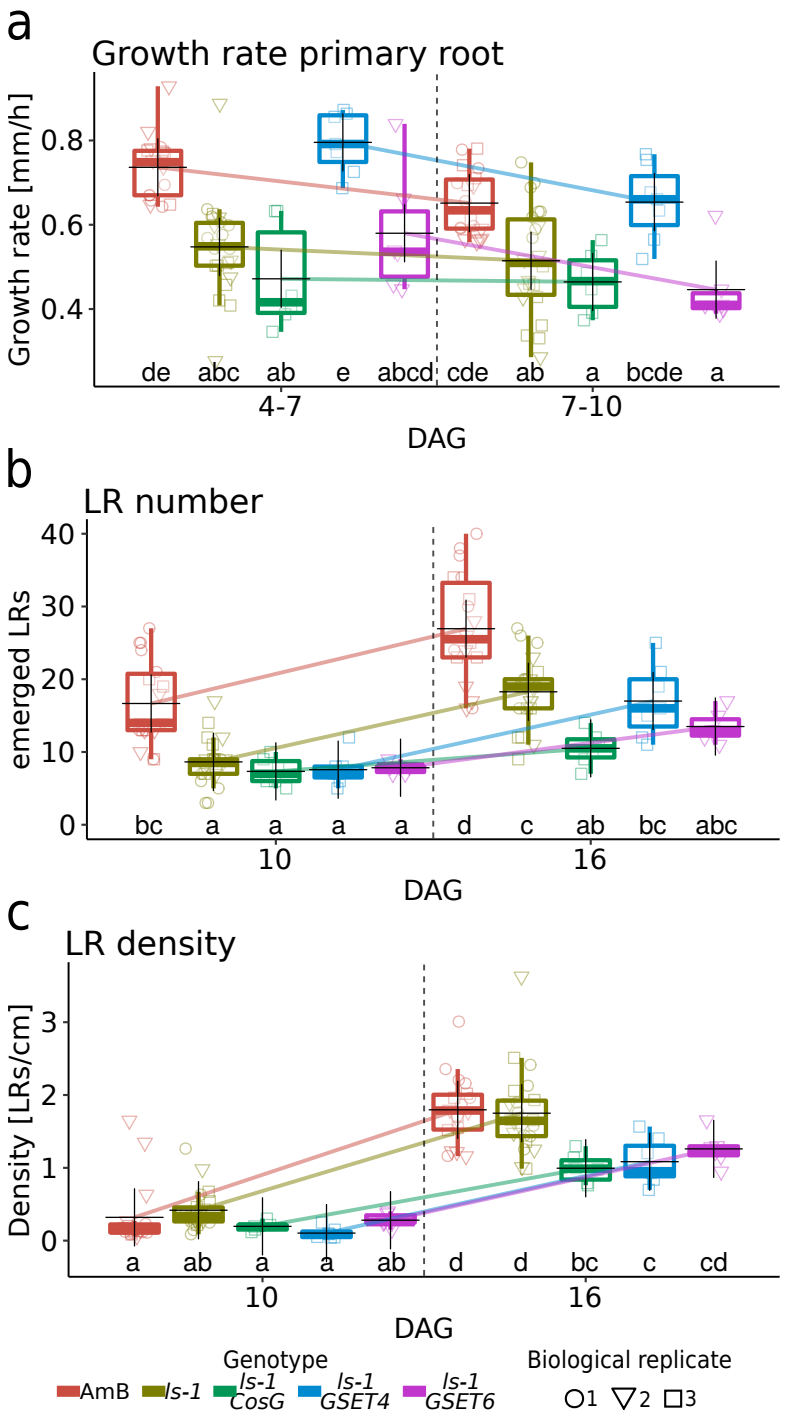


Figure 18: Reduced growth rate, but no reduction in LR number. Phenotypic analysis of root system development in vertically grown wt and *ls-1* plants. **a**, Primary root growth rate. **b**, LR number before (10 DAG) and after (16 DAG) release of root apical dominance. **c**, LR density before (10 DAG) and after (16 DAG) release of root apical dominance. For a description of box plots see Fig. 9. Dots represent individual primary roots. Straight lines connect mean values of sample populations (plus signs). Statistical significance was determined using unbalanced two-way ANOVA. The letters below the boxes (a–e) indicate the results of a post hoc Tukey test, groups with the same letter are indistinguishable at $> 95\%$ confidence using a 0.05 significance level. For each time point data from three independent biological replicates was pooled prior to analysis. Sample size ranged between 5 to 8 root systems per genotype for each biological replicate. Summary statistics are described in table S16.

of seeds that reached a comparable developmental stage. This excluded the effect of differential germination times as a causal factor for differential growth rates.

At 10 DAG, LR number was statistically significantly decreased in *ls-1* (Fig. 18b). Decreased LR number was probably a secondary effect of the decreased primary root length in *ls-1*, because LR density displayed no statistically significant differences (Fig. 18c). This indicated that LR number was not affected in *ls-1*. After release of root apical dominance, the number of newly initiated LRs was similar between wt and *ls-1* (Fig. 18b). This was also reflected in the LR density that increased equally in wt and *ls-1* (Fig. 18c). The increase in LR density was caused by the increased number of LRs, and the shortening of the primary root by decapitation.

Surprisingly, the transgenic lines appeared to have a slightly inhibitory effect on LR number. At 10 DAG, all transgenic lines had the same number of LRs as *ls-1* (Fig. 18b). For the lines *ls-1 CosG* and *ls-1 GSET6* this was expected, because of their reduced primary root length. However, for line *ls-1 GSET4* with a wt-like primary root length this was unexpected, and an indication of an inhibitory effect. LR density failed to show an inhibitory defect, because all analyzed plants displayed nearly identical LR density at 10 DAG, close to the absolute minimum (Fig. 18c). This is problematic for detecting inhibitory effects, because they would only cause a very subtle drop in density. To reliable calculate differences on these small scales, one would need to drastically increase sample size. Nevertheless, after releasing root apical dominance the number of newly initiated LRs in the transgenic lines was slightly lower compared to *ls-1* (Fig. 18b). The inhibitory effect of transgenic lines became obvious in the LR density, which was statistically significantly reduced compared to wt/*ls-1* at 16 DAG (Fig. 18c).

Minor reduction of gravitropism in primary roots of *ls-1* mutants

The increased avgAbsAng in primary roots of *ls-1* mutants indicated a defect in gravity sensing. Reorientation was used to analyze the response of roots to changes in the direction of the gravity vector. Roots were rotated for 90° and the growth angle of the root tip was measured before and 48 h after the rotation. This was followed by a second 90° rotation in reverse direction, back to the original orientation of the root (Fig. 19a). This set up is sufficient to test the response to gravity, but lacks the resolution to detect differences in the dynamics of the gravitropic response.

Root tip orientation was described with two angles for each time point in the rotation series. The gravity angle (gravAng) measures the deviation from the gravity vector. A gravAng of 0° would indicate perfect alignment of the root tip with the gravity vector, and a gravAng of 90° would indicate horizontal orientation of the root tip. The response angle (respAng) measures the deviation from a reference point. This reference point is aligned with the gravity vector for the first time point, and changes its position for subsequent time points based on the rotational direction and the amount of rotation (Fig. 19a). If the respAng change between two time points, the root tip responded to gravity. In contrast, a constant respAng between two time points indicates a gravity insensitive root tip.

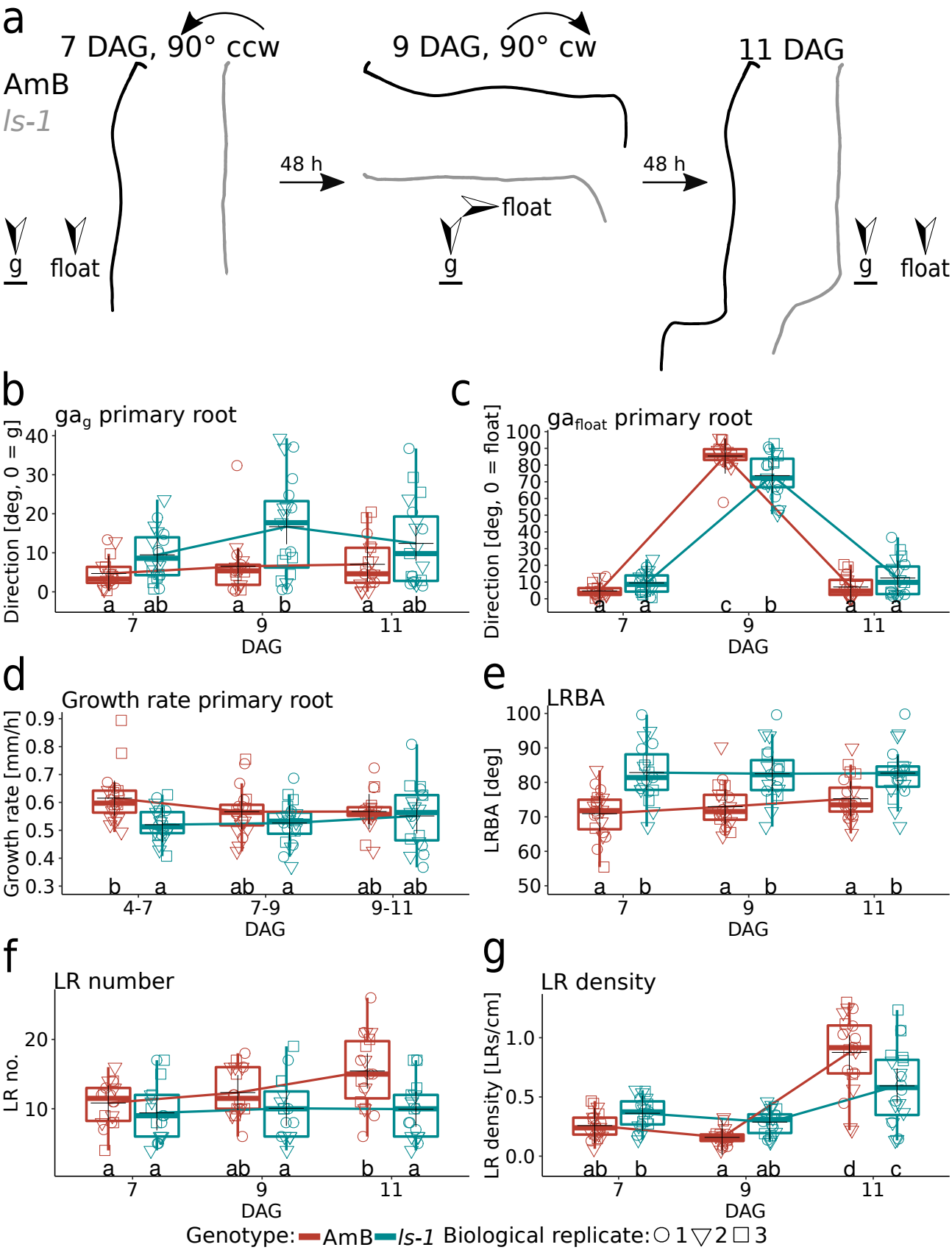


Figure 19: Minor reduction of gravitropic response and less LR development in primary roots of the *ls-1* mutant after root bending. Analysis of gravitropic response of wt and *ls-1* primary roots in response to two subsequent 90° rotations. **a**, Reorientation time series of AmB (black) and *ls-1* mutant (grey) root systems. The 4 DAG time point is not shown. For simplicity, LRs were removed from the root systems, to visualize the bare primary root. FIGURE CONTINUES ON THE NEXT PAGE ...

Figure 19: Continuation. The same root systems with accompanying LRs are displayed in Fig. 20a. At 7 DAG plants were imaged and immediately after that rotated 90° in counter clockwise (ccw) direction. 48 h later (9 DAG) plants were imaged again and immediately after that rotated 90° in clockwise (cw) direction. Plants were imaged once more after additional 48 h (11 DAG). Representative primary roots are shown from the two analyzed sample populations. Arrowheads indicate the direction of the gravity (g) vector and the position of the reference point (float) for each time point. Scale bar: 1 cm. **b**, gravAng of wt and *ls-1* mutant primary root tips at indicated time points. **c**, respAng of wt and *ls-1* mutant primary root tips at indicated time points. (**d**) to (**g**), quantification of root traits (plot titles) described in Table S6. For a description of box plots see Fig. 9. Dots represent individual primary roots. Straight lines connect mean values of sample populations (plus signs). Statistical significance was determined using unbalanced two-way ANOVA. The letters below the boxes (a–d) indicate the results of a post hoc Tukey test, groups with the same letter are indistinguishable at $> 95\%$ confidence using a 0.05 significance level. For each time point data from three independent biological replicates was pooled prior to analysis. Sample size ranged between 5 to 8 root systems per genotype for each biological replicate. Summary statistics are described in table S16.

The reorientation experiment was initiated at 7 DAG, because from this time point onwards growth rates of wt and *ls-1* primary roots should be comparable (Fig. 18a and Fig. 19d). Wt primary root tips maintained a gravAng of 6.1° for all analyzed reorientation time points, indicating continuous orientation towards gravity (Fig. 19b). Similarly, the respAng amplitude of 79.5° indicated, that wt root tips reoriented their growth trajectory two times in a row for nearly 90°. This reflected the two 90° rotations, that the plants experienced in course of the reorientation experiment. *ls-1* primary root tips displayed a minor, but not statistically significant increased gravAng at 7 and 11 DAG. However, at 9 DAG, the gravAng was statistically significantly increased (Fig. 19b). This indicated that *ls-1* primary root tips displayed a reduced orientation towards gravity. The respAng amplitude of 62.7° was statistically significantly decreased compared to the wt amplitude, confirming a reduction in gravitropism (Fig. 19c).

Notably, at 11 DAG, wt root systems had developed significantly more LRs compared to *ls-1*. This was unexpected, because at the start of the reorientation experiment (7 DAG), wt and *ls-1* had a similar number of LRs (Fig. 19f). Primary roots in *ls-1* were shorter than wt roots, due to the decreased root growth rate during the first week after germination. Thus, LR density was slightly increased in *ls-1* mutants compared to wt, at 7 and 9 DAG. At 11 DAG, both genotypes displayed increased LR densities compared to the previous time points, but LR density in the wt was significantly elevated compared to *ls-1* (Fig. 19g). This reversed the situation seen in the proceeding time points, indicating a strong boost in LR numbers that happened only in the wt. LRs in the *ls-1* mutant displayed a significantly increased LRBA throughout all time points (Fig. 19e). This was in line with the above described increased horizontal growth trajectories of LRs in *ls-1*.

Lateral roots in *ls-1* display a severe reduction in gravitropism

LRs in *ls-1* mutants displayed a notably different growth behavior compared to LRs in the wt. For terminology, depending on the side of emergence and their subsequent growth trajectory, LRs were classified as east or west (the naming is arbitrary; Fig. 20a). Sorting of LRs according to their growth trajectory was necessary for the calculation of gravAng and respAng. As an example, after the first counter clockwise 90° rotation, east facing LRs grew in the opposite direction of gravity, whereas west facing LRs grew in parallel with the gravity vector. This difference in growth trajectory would be reflected in the response of a specific LR to the gravity vector.

During the 7-to-9-DAG interval, growth rate was equal between east- and west-facing LRs within each genotype. LRs in the *ls-1* mutant had a statistically significantly reduced growth rate in comparison to the wt during this interval (Fig. S10a and b). In the 9-to-11-DAG interval, growth rates developed differently between east- and west-facing LR populations. In east-facing LRs, wt LRs displayed statistically significantly accelerated growth rates, compared to their growth rates during the 7-to-9-DAG interval. In contrast, east-facing LRs in *ls-1* kept their growth rate constant (Fig. S10a). In west-facing LRs, wt LRs kept a constant growth rate, but *ls-1* mutant LRs statistically significantly accelerated their growth rate to the level of the wt (Fig. S10b).

After the first reorientation, east-facing LRs in the wt maintained their original growth trajectory with respect to gravity. At 7 and 9 DAG, gravAng in wt LRs displayed 49.5°, indicating a graviresponse of 90° (Fig. 20b). This was also reflected in the respAng, which displayed nearly 45° for both time points, and the bend in the growth path of east-facing LRs in the 7-9-DAG interval (Fig. 20a and c). Roots that display growth trajectories with 45° offsets from gravity, and a 90° graviresponse after reorientation, are expected to behave exactly like the east-facing wt LRs in the 7-9-DAG interval. In contrast, east-facing LRs in the *ls-1* mutant did statistically significantly change their gravAng from 74.8° at 7 DAG to 128.6° at 9 DAG after the first reorientation (Fig. 20b). The accompanying respAng did not change in the 7-9-DAG interval, indicating that the rotation caused the differences in gravAng and not gravitropism (Fig. 20c). This was also confirmed visually, because east-facing LRs in *ls-1* remained straight after the reorientation (Fig. 20a). After the second reorientation in reverse direction, east-facing LRs in the wt statistically significantly decreased their gravAng from 54.9° at 9 DAG to 16.2° at 11 DAG. This indicated that the second graviresponse resulted in a smaller change in the growth trajectory (Fig. 20b). Contribution of the rotation to the altered growth trajectory could be excluded, because the respAng also statistically significantly decreased between 9 and 11 DAG (Fig. 20c). Visually, the graviresponse is recognizable by a small bend in eastwards direction (Fig. 20a). This was also a nice example of GSA control through AGO, because this eastward bend was only possible through altering the growth trajectory against the direction of gravity. After the second reorientation in reverse direction, east facing LRs in the *ls-1* mutant displayed a statistically significantly decreased gravAng at 11 DAG compared to 9 DAG (Fig. 20b). In conjunction with the constant respAng for all time points of the reorientation experiment, this

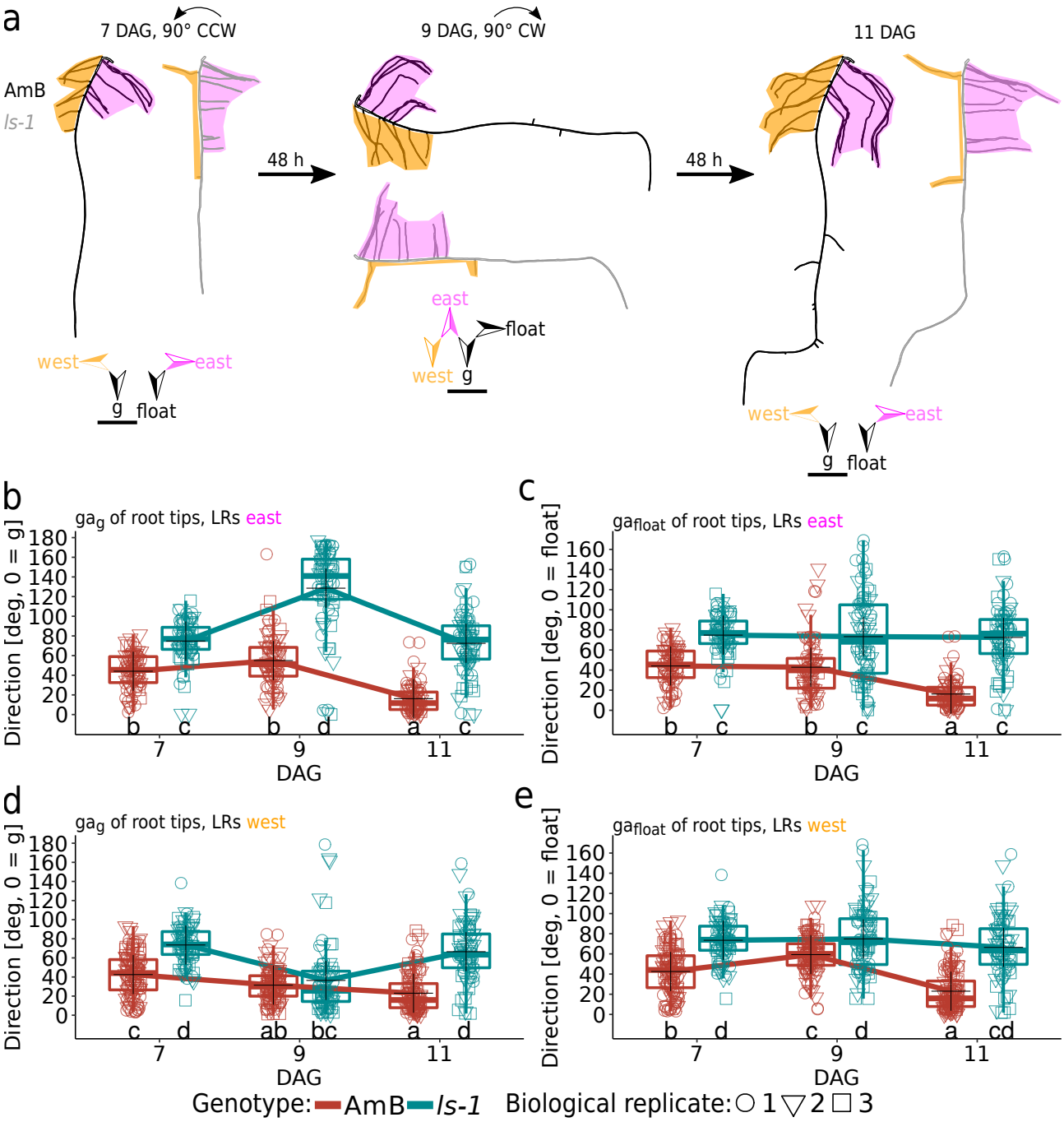


Figure 20: Loss of gravitropism in LRs of *ls-1* mutants. Analysis of gravitropic response of wt and *ls-1* lateral roots in response to two subsequent 90° rotations. **a**, Root systems and experimental set-up were described in Fig. 19a. Here, the LRs missing in Fig. 19a are displayed and color coded according to their growth trajectory. Graviresponse was only analyzed in LRs already present at 7 DAG. Arrowhead and cross indicate the direction of the gravity (g) vector and the position of the reference point (float) for each time point, respectively. Scale bar: 1 cm. **b**, gravAng of east facing LRs (tips), in wt and *ls-1* mutants at indicated time points. A gravAng of 0° indicates vertical growth along the gravity vector. **c**, respAng of east facing LRs (tips), in wt and *ls-1* mutants at indicated time points. **d**, gravAng of west facing LR (tips), in wt and *ls-1* mutants at indicated time points. A gravAng of 0° indicates vertical growth along the gravity vector. **e**, respAng of west facing LRs (tips), in wt and *ls-1* mutants at indicated time points. For a description of box plots see Fig. 9. Dots represent individual LRs. Straight lines connect mean values of sample populations (plus signs). Statistical significance was determined using unbalanced two-way ANOVA. FIGURE CONTINUES ON THE NEXT PAGE ...

Figure 20: Continuation. The letters below the boxes (a–d) indicate the results of a post hoc Tukey test, groups with the same letter are indistinguishable at $> 95\%$ confidence using a 0.05 significance level. For each time point data from three independent biological replicates was pooled prior to analysis. Sample size ranged between 5 to 8 root systems per genotype for each biological replicate. Summary statistics are described in table S16.

indicated that the alterations in growth trajectory after the second reverse rotation was caused, again, through the rotation, and not by gravitropism (Fig. 20c). Also visually, east-facing LRs still resembled straight lines at 11 DAG (Fig. 20a).

West facing LRs in wt displayed a gravAng of 42.5° at 7 DAG. This was similar to the gravAng of east facing LRs at this time point (Fig. 20d). After the first reorientation, the gravAng dropped statistically significantly to 31.5° indicative of a graviresponse. The accompanying respAng, statistically significantly increased from 7 DAG to 9 DAG, confirming an active graviresponse (Fig. 20e). Also visually, alterations in growth trajectories are recognizable as a bend in the growth path, indicative of a graviresponse (Fig. 20a). West facing LRs in *ls-1* mutants statistically significantly decreased their gravAng from 73.5° at 7 DAG to 36.4° at 9 DAG (Fig. 20e). Again, the corresponding respAng did not change in the 7-9-DAG interval, indicating that the rotation caused the change in gravAng. After the second reorientation in reverse direction, the gravAng of west-facing LRs in the wt dropped further to 23.0° (Fig. 20d). The corresponding respAng, statistically significantly decreased in the 9-11-DAG interval, indicating a graviresponse (Fig. 20e). Again, visually the graviresponse is clearly recognizable as a bend in the growth path (Fig. 20a). The gravAng of west-facing LRs in *ls-1*, statistically significantly increased in the 9-11-DAG interval (Fig. 20d). However, the corresponding respAng displayed only a very moderate change, indicating that the main cause for changes in gravAng was the rotation and not a graviresponse (Fig. 20e).

Calculation of the avgAbsAng as an alternative approach for growth trajectory measurement, corroborated the difference between wt and *ls-1* LR behavior, in response to gravity, described above. First, LRs in *ls-1* displayed an statistically significantly increased avgAbsAng compared to wt LRs at 7 and 11 DAG, indicating elevated horizontal growth trajectories for these time points (Fig. S10c and d). The development of the avgAbsAng over the course of the reorientation experiment further supported these results. The avgAbsAng of wt LRs statistically significantly decreased during the 7-to-11 DAG interval from 49.4° to 15.9°, indicating directional change through gravitropism. In contrast, the avgAbsAng of *ls-1* LRs in the remained constant at 72.2° during this interval, indicating that LRs did not change their growth trajectories at all (Fig. S10c and d).

To sum it up, wt LRs were able to respond to changes in the direction of the gravity vector by gravitropism. In contrast, *ls-1* LRs were either strongly insensitive to gravity or impaired in graviresponse.

Detection of an *Ls/LAS* antisense transcript in root tips of tomato and *Arabidopsis*

From the root systems described in the previous subsection, 1 cm of primary root tissue starting at the root apex was sampled at the end of the reorientation experiment for RNA seq analysis. Filtering for differentially expressed genes (DEGs) between wt and *ls-1* yielded only a very low number of candidate genes for further analysis (Table S11). Functional analysis of these DEGs is still ongoing, but so far none of them has been reported to be associated with gravity sensing in roots. Differential expression of all DEGs followed the same pattern, being up regulated in the *ls-1* mutant and not expressed in the wt. This suggested that *Ls* might act as a transcriptional repressor. One unexpected finding was the expression of an *Ls* antisense transcript. Analyzing read alignment at the *Ls* locus, showed the prevalent expression of an *Ls* antisense transcript (*asLs*; Fig. S12a-c). The transcription of *asLs* was further supported through 5' rapid amplification of cDNA ends (RACE; S13c). Repeating the 5' RACE for the *Arabidopsis LAS* locus revealed the expression of an *asLAS* transcript. This suggested that antisense transcription from the *Ls/LAS* loci is a conserved feature. Sequence analysis of the *Ls/LAS* reverse strands, detected only very short putative CDSs, indicating that *asLs/asLAS* encode long noncoding RNAs (lncRNAs).

Next, the ability of *LAS* regulatory elements to promote expression of an antisense transcript was tested, by cloning an *asLAS* reporter (*aspLAS:erSclt*) for CLSM. *aspLAS:erSclt* is based on the endogenous *LAS* regulatory regions, driving the expression of an ER-targeted Scarlet, which is inserted in reverse orientation in relation to the endogenous *LAS* CDS (Fig. 21a). The first 190 bp of the *LAS* 3' UTR were removed, because the majority of TSSs were mapped further downstream and most of the putative TATA-box motives accumulated in a region 220 bp - 315 bp downstream of the *LAS* stop (Fig. S13a). In the primary root tip, *aspLAS:erSclt* signal was detected in the same domain as *pLAS:erGFP* (6a). This domain contained the QC, CSCs and columella (Fig. 21d and e). In independent T1 plants, *aspLAS:erSclt* signal in the columella showed a certain degree of variation. *aspLAS:erSclt* fluorescence was either detected only in the two central columella cell files (Fig. 21b), or in all columella cell files (Fig. 21c). In tips of just emerged LRs, *aspLAS:erSclt* signal was detected in a domain very similar to the domain indicated by *pLAS:erGFP*. Cells within this domain were the QC, CSCs and columella, reflecting the *asLAS* expression domain seen in the primary root tip (Fig. S14a and b). Further, *aspLAS:erSclt* signal was detected with variable frequency in additional cell lineages like the ground tissue (Fig. S14a) or the LRC (Fig. S14b), which led to asymmetric expression domains. This was again reminiscent of *pLAS:erGFP*. A third expression domain of *aspLAS:erSclt* was detected in the primary root, in tissues that surround the central vasculature, namely pericycle, endodermis and cortex (Fig. S14c and d). Expression in these tissues was limited to parts of the root where cells were differentiated. This domain also displayed variation concerning tissue specific *aspLAS:erSclt* signal, between independent T1 plants. This includes plants with strong signal in all three tissues (Fig. S14c) and plants with signal mainly located in the pericycle (Fig. S14d).

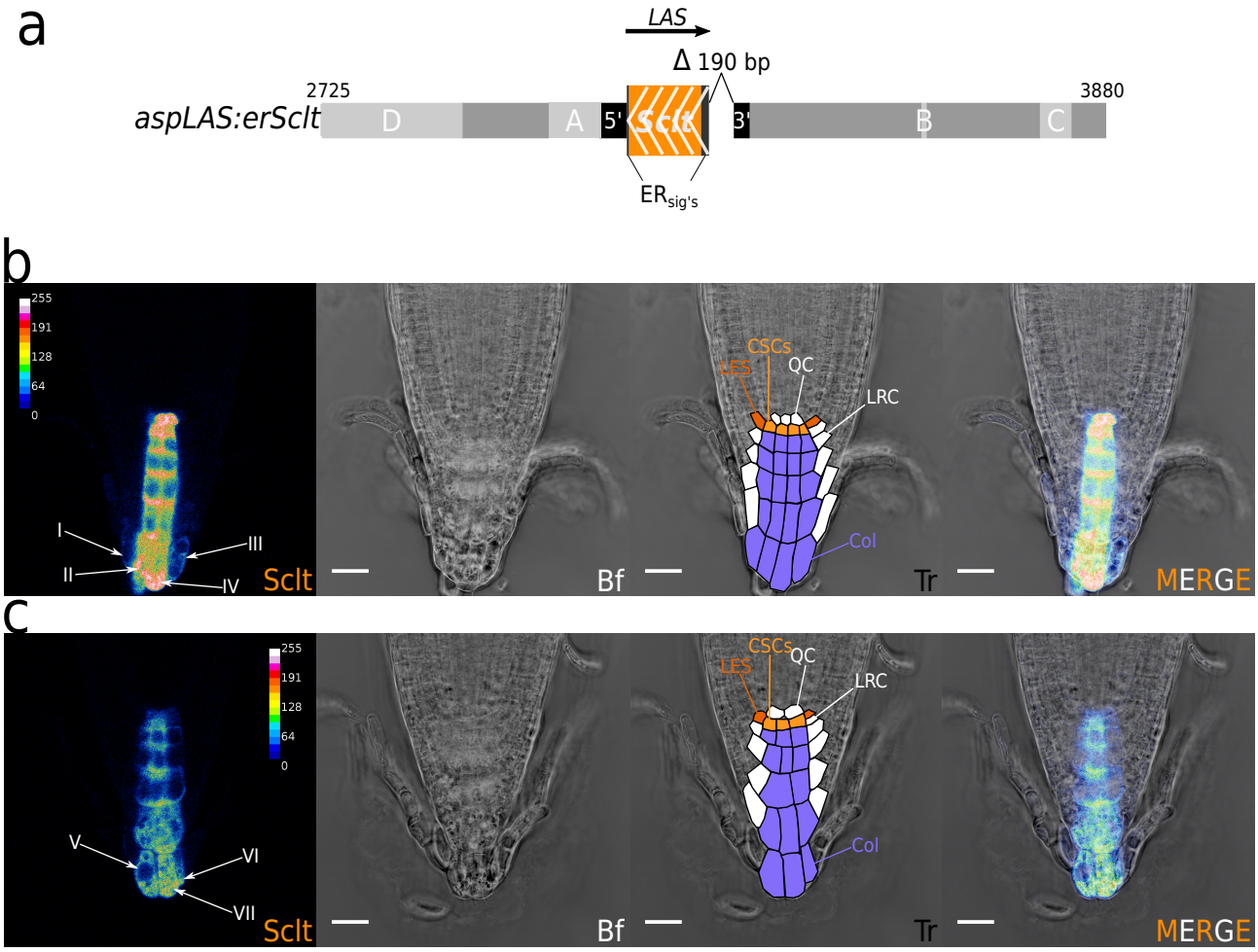


Figure 21: *asLAS* is expressed in the same domain as *LAS*. CLSM of *aspLAS:erSclt* expression in root tips of transgenic plants. **a**, Cartoon of the transcriptional reporter *aspLAS:erSclt*. *LAS* promoter described by Raatz et al. (2011) and endogenous UTRs of the *LAS* locus, drive expression of an ER-targeted *Sclt*. Tips of open triangles show 5' to 3' orientation of the *Sclt* CDS. The black arrow indicates the endogenous orientation of the *LAS* CDS. **b**, *aspLAS:erSclt* expression in the primary root tip. Arrows I and III point to columella cell files without or weak erSclt signal. Arrows II and IV point to columella cell files with strong erSclt signal. **c**, *aspLAS:erSclt* expression in the primary root tip of a different transgenic plant than (**a**). Arrows V to VII point to columella cell files with strong erSclt signal. 19 independent T1 *aspLAS:erSclt* plants in the Col-0 background were analyzed, 9-10 days after germination and representative images are displayed in (**b**) and (**c**). For (**b**) and (**c**), panels from left to right: Sclt channel with grey value heat map, brightfield (Bf) channel, cell tracings (Tr) , image of merged Sclt and Bf channels. Scale bars at the bottom corners of panels represent 25 μm. Col = columella, CSCs = columella stem cells, LES = lateral root cap/epidermis stem cell, LRC = lateral root cap, QC = quiescent center.

3.5 Biological relevance of LAS movement in the context of axillary meristem initiation

Inhibition of LAS movement

To evaluate biological relevance of LAS movement, the protein was tethered C-terminally to a duplicated SIMIAN VIRUS 40 (SV40) NUCLEAR LOCALIZATION SIGNAL (NLS) and N-terminally to either a Tq2 (Tq2-LAS-NLS) or a tandem Tomato (tdTom-LAS-NLS) under the control of the described *LAS* promoter (Fig. 22a). The NLS signal is expected to strongly promote protein accumulation in the nucleus. Using this approach movement is inhibited through control of protein localization, by trapping it in the nucleus, hence preventing trafficking through plasmodesmata (Gallagher et al., 2004; Balkunde et al., 2017). Alternatively, movement might be blocked through modification of protein size, like the attachment of a triple GFP to the protein of interest, making it physically to large to fit through plasmodesmata (Mähönen et al., 2014). The difference between both LAS-NLS versions was the size of the fluorescent tag. Tq2 (239 amino acids) has only half the size as tdTom (476 amino acids), making the tdTom-LAS-NLS version the probably more immobile version compared to Tq2-LAS-NLS.

LAS-NLS versions rescue axillary meristem initiation in a dose dependent manner

Next, both LAS-NLS versions were inserted into the *las-4* mutant to analyze their ability to complement the deficient axillary meristem initiation in this mutant. As controls, the non-NLS modified LAS versions Vns-LAS and LAS-Vns (Section 3.1) were used. AM scoring was done in plants of segregating T2 populations, excluding the non-transgenic null segregants. Col-0 plants developed AMs nearly in all rosette leaf axils, whereas rosettes of *las-4* mutant plants lacked AMs in nearly every leaf axil (Fig. 22b). In Col-0 the fraction of empty rosette leaf axils never exceeded 20% (filling index = 0.8), which was used as a threshold value for full complementation (Fig. 22c). Following that scheme, transgenic plants were grouped according to their filling index into four categories. Each category reflected the degree of complementation of a specific transgene in an individual plant (Fig. 22c). The filling index is a quantitative trait indicating the amount of filled leaf axils in an individual plant. However, it does not provide insight into the spatial distribution (sequence) of filled versus empty leaf axils within the rosette.

las-4 plants with a filling index above 0.8 were observed for all of the four introduced LAS versions. However, transgenes encoding different LAS versions led to varying frequencies of fully complemented *las-4* mutants. Mutant plants carrying *pLAS:LAS-Vns* (described in Section 3.1) were very similar to Col-0 plants, and never displayed a filling index below 0.8. This was true for plants of all four analyzed independent transgenic lines (Fig. 22b, c and Fig. S15a, b). Only two out of four analyzed independent lines carrying *pLAS:Vns-LAS* (described in Section 3.1)

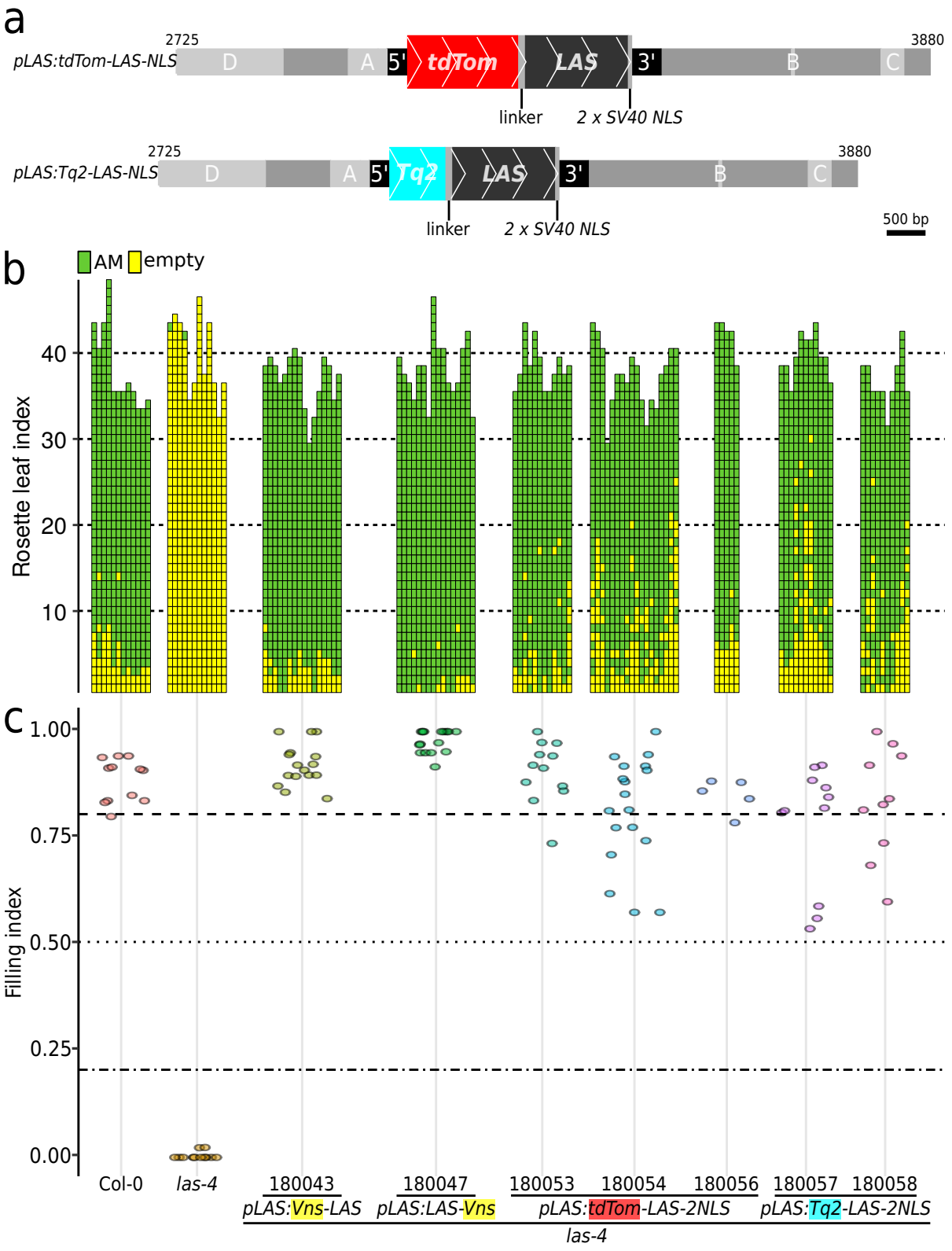


Figure 22: LAS-NLS versions partially rescue the *las-4* AM initiation defect. Scoring of axillary bud formation in rosette leaf axils of Col-0 and *las-4* plants. **a**, Cartoon of the two LAS-NLS versions *pLAS:tdTom-LAS-NLS* and *pLAS:Tq2-LAS-NLS*. The *LAS* promoter described by Raatz et al. (2011) and endogenous UTRs of the *LAS* locus, drive expression of a translational fusion protein. The fusion protein consists of three parts. N-terminal *tdTom* or *Tq2* is connected via a flexible 99 bp *linker* sequence described by Daum et al. (2014), with the *LAS* genomic sequence, and is followed C-terminal by a duplicated SV40 NLS.

FIGURE CONTINUES ON THE NEXT PAGE ...

Figure 22: continued. Tips of open triangles show 5' to 3' orientation of the *LAS-NLS* ORF. **b**, Scoring plots representing the presence or absence of axillary buds in rosette leaf axils, from the oldest (rosette leaf index = 1) to the youngest rosette leaf. Each column represents an individual plant and each square within a column represents a phytomer with a filled (green) or empty (yellow) leaf axil. **c**, Filling index of plants displayed in (**b**). Circles represent individual plants. The filling index is calculated as the ratio of filled leaf axils over the total number of rosette leaf axils. All plants with a filling index greater than 0.8 (dashed line) were considered as fully complemented. Plants with a filling index between 0.8 and 0.5 (dotted line) were considered as partially complemented. Plants with a filling index between 0.5 and 0.2 (dashed-dotted line) were considered as weakly complemented. Plants with a filling index below 0.2 were considered as not complemented. All scored plants were grown at the same time and each number indicates an independent transgenic line. Plants were grown for six weeks under short day conditions. After that period, plants were transferred to long day conditions and scored when the the shoot started to bolt.

displayed a filling index above 0.8 in all analyzed plants (Fig. 22b, c and Fig. S15a, b). Out of the 13 analyzed independent lines expressing one of the two LAS-NLS versions, just a single line (180056, pLAS:tdTom-LAS-NLS) displayed a filling index above 0.8 in all analyzed plants (Fig. 22b and c). This demonstrated that the addition of the duplicated NLS led to a decrease of LAS function during AM initiation, even though this effect appeared to be variable.

AM initiation in transgenic lines consisting of plant populations with a minimal filling index of 0.5 (lines 180045, 180053, 180054, 180057 and 180058) followed an interesting pattern. The fraction of partial complementing plants (filling index: 0.5 to 0.8) in these lines had barren leaf axils, especially in the older half of the rosette (Fig. 22b and Fig. S15a). This showed that the older leaf axils were more susceptible to the modification of LAS, caused through the addition of the NLS.

Notably, among the lines expressing either Vns-LAS (N-terminal tagged LAS version) or one of the two LAS-NLS versions, a third pattern with respect to the complementation of the AM initiation defect was observed. Plant populations in this third category showed variable phenotypes among individuals, covering the whole phenotypic range from no complementation to full complementation (Fig. 23b and c). These *las-4* looking plants were not T2 null segregants, because transgenic seeds were preselected based on the expression of the seed coat marker (Shimada et al., 2010). Additionally, all plants were genotyped for the presence of the transgene. The variation in these lines was reminiscent of segregation, and the penetrance of the complementation phenotype might be explained by differences in transgene zygosity in individual plants. To test that, copy number qPCR was conducted in all lines that were grouped into the third category. It is worth mentioning that copy number estimation based on qPCR is reliable for detecting differences in zygosity and might be imprecise when analyzing the number of inserted transgenes (Bubner and Baldwin, 2004; Głowacka et al., 2016). Positive correlation between high transgene copy number and a *las-4*-like phenotype was found for the lines 180044, 180051 and 180052, whereas the line 180060 displayed positive correlation between low transgene copy number and the *las-4*-like phenotype (Fig. 23a and b). For the lines 180050,

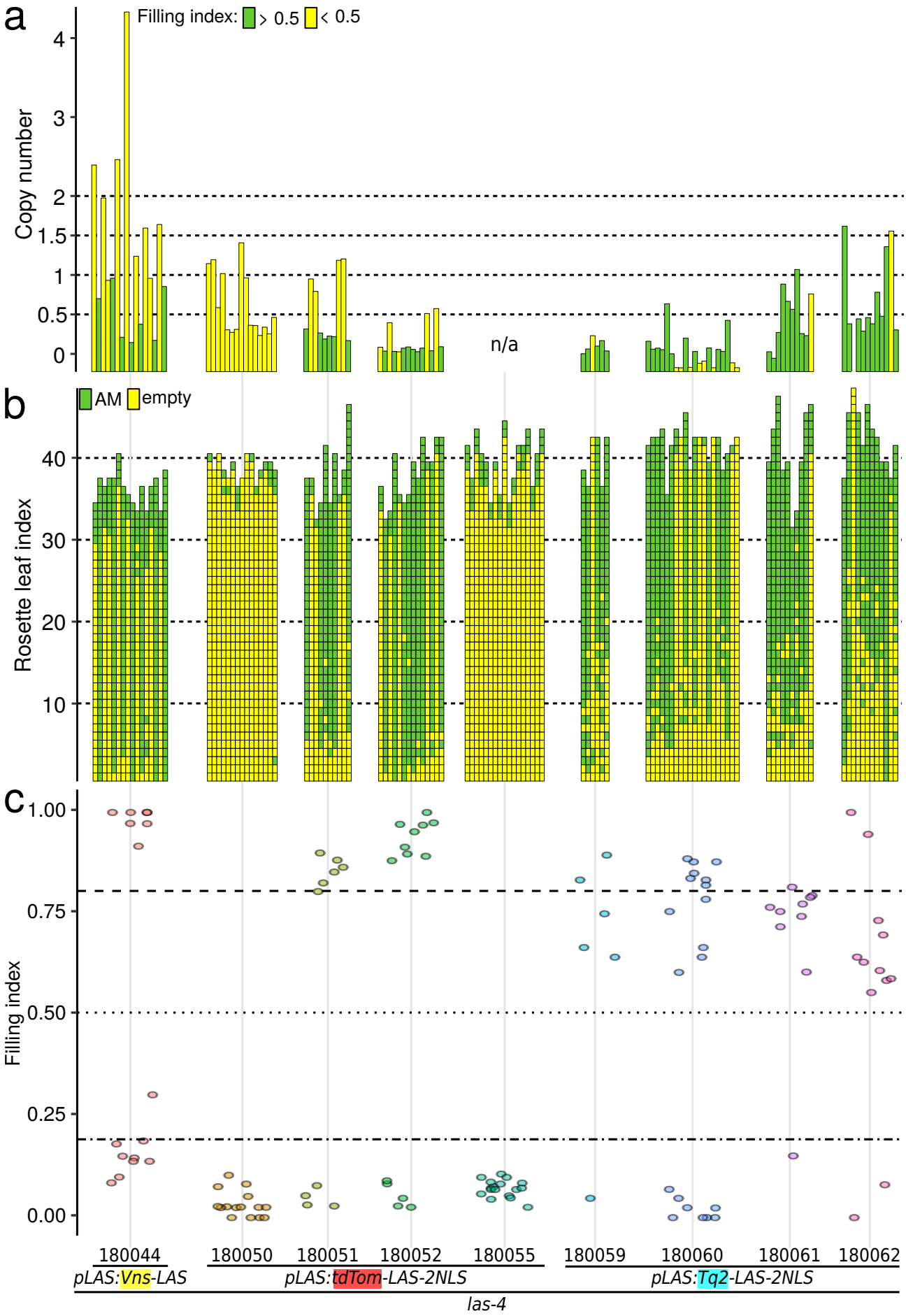


Figure 23: Correlation between transgene zygosity and AM initiation rescue. FIGURE CONTINUES ON THE NEXT PAGE ...

Figure 23: continued. Scoring of axillary bud formation in rosette leaf axils of *las-4* plants and determination of transgene copy number. **a**, Transgene copy-number determination with qPCR. The single-copy gene *SICKLE* (*SIC*; Zhan et al., 2012) was used as reference. Each bar represent an individual plant. **b**, Scoring plots representing the presence or absence of axillary buds in rosette leaf axils, from the oldest (rosette leaf index = 1) to the youngest rosette leaf. Each column represents an individual plant and each square within a column represents a phytomer with a filled (green) or empty (yellow) leaf axil. **c**, Filling index of plants displayed in (**b**). The filling index is calculated as the ratio of filled leaf axils over the total number of rosette leaf axils. All plants with a filling index greater than 0.8 (dashed line) were considered as fully complemented. Plants with a filling index between 0.8 and 0.5 (dotted line) were considered as partially complemented. Plants with a filling index between 0.5 and 0.2 (dashed-dotted line) were considered as weakly complemented. Plants with a filling index below 0.2 were considered as not complemented. Plants in (**a**) and (**b**) are plotted in the same order. All scored plants were grown at the same time and each number indicates an independent transgenic line. Plants were grown for six weeks under short day conditions. After that period, plants were transferred to long day conditions and scored when the the shoot started to bolt. Plants displayed in this figure belong to the same experiment as plants displayed in Fig. 22. n/a = not analyzed.

180059, 180061 and 180062 no correlation between copy number and phenotype was observed. The lines 180050 and 180055, both expressing tdTom-LAS-NLS, completely failed to rescue the AM initiation defect in the *las-4* mutant (Fig. 23b and c). Plants of line 180050 also displayed different zygosity levels, yet indicating no correlation between zygosity and phenotype.

Next the same segregating T2 lines, that were used for AM phenotyping, were analyzed with CLSM to monitor cellular localization of the modified LAS versions. Additionally, this served as a control to exclude the possibility of gene silencing in lines with variable phenotypes (Fig. 23). In all lines, transgene expression was detected in 100% of the monitored plants (Fig. S15c). Even though imaging was restricted to primary roots and LRs, it strongly promoted the view that the *las-4* like phenotype in transgenic plants was not due to gene silencing. Unique for line 180055 was an extended expression domain of tdTom-LAS-NLS, compared to the *LAS* expression domain described in Section 3.1. Ectopic expression was observed in the LRC, the epidermis and the ground tissue cell lineages in primary roots as well as LRs (Fig. S15d and e). This observation indicated that in line 180055 the transgene inserted at a genomic locus, which promoted ectopic expression of tdTom-LAS-NLS. Interestingly, in none of the transgenic lines expressing one of the LAS-NLS versions, the NLS seemed to have an effect on protein localization. In the columella, LAS-NLS was detected in the cytosol as well as the nucleus (Fig. S15d-g). Further, the transgenic protein was still detected in nuclei of LRC cells, indicating that protein trafficking was not inhibited (Fig. S15d-g). Thus either the NLS might be inactive due to its C-terminal position in the fusion protein, or alternatively, a part of the LAS C-terminus might be modified through proteolysis, leading to a removal of the NLS.

4. Discussion

4.1 Cellular differences in *LATERAL SUPPRESSOR* expression domains in leaf axils and root tips

The *LAS* expression domain in the tips of primary and lateral roots showed two major differences with respect to the leaf axil/boundary. First, the relation between *LAS* and auxin levels/auxin signaling does not correlate. For instance in the shoot, the vegetative rosette leaf axil is described in general as a low auxin environment, having both, low auxin levels and low auxin regulated gene expression (Wang et al., 2014b,c). Therefore, during the leaf boundary establishment, *LAS* is expressed in an auxin depleted domain within the shoot apex. However, a recent report showed contradictory data, where the P1 leaf axil displayed an auxin response maximum Burian et al. (2016). To solve this issue it would be useful to analyze the *in vivo* coexpression of *LAS* and auxin reporters. In contrast, the spatial relation between *LAS* expression and auxin distribution shows a positive correlation in the root. The LAS transcriptional reporter, *pLAS:erGFP*, displays promoter activity in the QC, the CSCs and all columella cells (Fig. 6). Thus, the *LAS* expression domain overlaps with the root auxin maxima, found at the tips of primary and lateral roots. The focal point of the auxin maximum is the QC, which has high auxin levels and a maximum of auxin regulated gene expression. In addition, the CSCs and the columella cells are part of the tip-specific auxin maximum, giving rise to a cone-shaped domain (Sabatini et al., 1999; Brunoud et al., 2012). Support for a contribution of auxin signaling to the regulation of *LAS* expression comes from the analysis of the recently developed synthetic auxin-TRANSPORT INHIBITOR RESISTANT 1 (TIR1) pair. In this system, auxin signaling is triggered through an specifically-designed auxin analog, called convex auxin indole-3-acetic acid (cvxIAA). cvxIAA is not recognized by endogenous TIR1/AUXIN SIGNALING F-BOX (TIR1/AFB) F-box proteins. Only a modified version of the TIR1 auxin coreceptor, called concave TIR1 (ccvTIR1), recognizes cvxIAA and initiates the auxin signaling cascade. By a comparative RNAseq experiment including *35S:ccvTIR1* Col-0 plants treated with cvxIAA, *LAS* was found within the differentially upregulated genes (Uchida et al., 2018). In the root, the prime candidates as upstream regulators of *LAS* expression, would be transcription factors that bind to motifs located in the regulatory region B of the *LAS* locus. *LAS* expression in the tips of primary and lateral roots requires region B, but in the shoot, its contribution is still obscure. Thus, region B might directly and/or indirectly be targeted by tissue specific AUXIN RESPONSE FACTORS (ARFs). Two *LAS*-regulating upstream candidates

would be ARF10 and ARF16, which both display root cap specific expression domains. In the root tip ARF10/ARF16 are involved in gravity sensing, cell division repression and columella cell differentiation (Wang et al., 2005). Although, the RNAseq experiment suggests that *LAS* expression is promoted through a specific TIR1-based auxin response module, the treatment of Col-0 plants with IAA has no effect on *LAS* expression level, suggesting the presence of a second *LAS* repressing or balancing auxin response module. The interaction between different auxin response modules might explain the differences in *LAS* expression levels, observed when comparing primary and lateral roots. However, contribution of auxin signaling modules for the *LAS* expression in low auxin environments, like in the vegetative leaf axil, would probably be insignificant. For future studies, *LAS* might represent an interesting candidate gene to analyze the regulation of tissue-specific expression in an organism-wide context.

Second, cell populations displaying *LAS* expression showed different statuses of differentiation, when comparing root and shoot domains. Even though the differentiation status of cells residing in shoot boundary tissues is not well defined, it is assumed that these cells are undifferentiated and probably pluripotent (Wang et al., 2016). In contrast, the cone shaped *LAS* expression domain typical for root tips, covers the whole range of cell differentiation, from undifferentiated, pluripotent stem cells to fully differentiated cells. In addition, *LAS* is expressed in the QC, the root stem cell niche organizer a different kind of undifferentiated cells compared to stem cells, based on cell division frequency analysis, cell ablation studies and transcriptome profiling (van den Berg et al., 1995, 1997; Nawy et al., 2005; Cruz-Ramírez et al., 2013; Denyer et al., 2019). If LAS performs the same function throughout the plant in a tissue- and cell-independent context, this function is probably not linked to the differentiation stage of cells. Alternatively, LAS function could be variable with different functions dependent on the differentiation stage of cells.

4.2 LATERAL SUPPRESSOR - a putative suppressor of auxin signaling or modifier of auxin fluxes?

The significantly increased vertical growth trajectory of LRs in *las-4* described in this study, resembles the phenotype of young LRs, in mutants or treatment conditions, which display or cause an elevation in the auxin signaling input, respectively. In *Arabidopsis*, LR growth is tightly linked with differential auxin signaling input, that in turn, correlates with differences in growth trajectory. LRs can be grouped into various categories, based on their length, growth trajectory and other developmental hallmarks, like the appearance of root hairs (Rosquete et al., 2013). For simplification, I will only discriminate between young LRs and old LRs. Young LRs comprise LRs that have just emerged from the primary root and display growth trajectories that are usually closer to a horizontal orientation. On the other hand, the term older LRs describes longer LRs with a distinctive shift in their growth trajectory towards a more vertical orientation (this study; Mullen and Hangarter, 2003; Rosquete et al., 2013; Roychoudhry et al., 2013). By following different reporters for auxin signaling during LR development, it has been

reported that AUX/IAA degradation and transcriptional auxin response were at a lower level in tips of young LRs compared to tips of older LRs (Roychoudhry et al., 2017; Ruiz Rosquete and Kleine-Vehn, 2018). The correlation between the level of auxin signaling and LR growth trajectory was further corroborated through analysis of mutants that have been shown to be affected in either auxin synthesis/conjugation, reception or response. Mutants that accumulate higher endogenous levels of auxin, like *yucca-1D* (*yuc-1D*), display increased vertical growth trajectories in young LRs (Zhao et al., 2001; Mashiguchi et al., 2011; Roychoudhry et al., 2013). Similarly, mutants with an expected higher level of auxin response, like *auxin-resistant3-10* (*axr3-10*), a null allele of the AUX/IAA transcriptional coregulator IAA17, display increased vertical growth trajectories in young LRs (Leyser et al., 1996; Knox et al., 2003; Roychoudhry et al., 2013). Alternatively, one can enforce increased vertical growth trajectories in young LRs through artificial elevation of auxin signaling by pharmacological treatments of wt *Arabidopsis* roots with IAA or the synthetic auxin analog 2,4-dichlorophenoxyacetic acid (2,4-D; Rosquete et al., 2013; Roychoudhry et al., 2013). This indicates that loss of LAS function might cause an increased sensitivity of the young LR tip to the endogenous auxin input. This putative increase in auxin sensitivity might ultimately lead to an increased vertical growth trajectory during the early stage of LR growth. According to this view, LAS would function as a negative regulator of auxin signaling during growth trajectory determination in young LRs. It has been shown, that auxin reception in columella cells is key for LR growth trajectory control. For example, expression of the auxin insensitive axr3-1 protein (dominant negative AUX/IAA) in the columella of LRs induced increased vertical LR growth trajectories, nicely demonstrating the relationship between columella-specific auxin signaling and LR growth trajectory control (Roychoudhry et al., 2013). Transcriptional auxin response in the columella changes throughout LR development, with low auxin response in young LRs and increased auxin response in older LRs (Roychoudhry et al., 2017; Ruiz Rosquete and Kleine-Vehn, 2018). If LAS would act as a negative regulator of auxin signaling, one would expect an increased auxin response during early LR development in *las-4*. Also, increased auxin response in older LRs should correlate with a reduced level of *LAS* expression in the columella cells. However, both of these assumptions have to be tested experimentally. Expression analysis of the translational reporter Vns-LAS indeed supports the idea, that the level of *LAS* expression or protein accumulation has an effect on LR growth trajectory determination. In the primary root, the GSA is close to 0° (or perfect vertical growth trajectory), and in the columella Vns-LAS was hardly detectable. In contrast, in young LRs, which display increased horizontal GSAs (or horizontal growth trajectories), Vns-LAS accumulation in columella cells was significantly increased.

Induction of *LAS* expression in the 17-β-estradiol responsive *pSCR>>LAS-Tq2* line, had unexpected effects on growth trajectories of primary and lateral roots. After induction, primary roots started to display oblique growth trajectories, in contrast to their pre-treatment vertical growth trajectories. Intriguingly, growth trajectories were not randomly distributed, as one would expect in agravitropic mutants, like higher order *PIN* mutant combinations (Santelia et al., 2008). Instead, primary roots displayed growth trajectories that were very similar with

respect to direction and deviation from gravity-steered growth. This excludes that induction of *LAS* expression in *pSCR>>LAS-Tq2* resulted in agravitropic roots. More likely, a specific tropic response mechanism triggered by *SCR*-driven *LAS* expression might override primary root gravitropism as the main determinant for root growth trajectory. Both, halotropism and phototropism interfere with PIN recycling to the plasma membrane through integration of environmental cues, resulting in modification of gravity steered root growth. PIN internalization reduces polar auxin transport in the stimulus-facing side of the RAM, causing tissue wide asymmetric auxin distribution and root bending (Sassi et al., 2012; Galvan-Ampudia et al., 2013). To test, whether induction of *LAS* expression in *pSCR>>LAS-Tq2* would have a similar effect on intracellular PIN localization, behavior of tagged-PIN proteins should be analyzed in *pSCR>>LAS-Tq2*. Modification of PIN membrane localization in LR columella cells would be an alternative mechanism, explaining the increased vertical LR growth trajectory in *las* mutants. When LRs grow at a specific GSA (stable or linear growth trajectory), columella cells display a balanced polarized localization of PIN3 and PIN7, resulting in a symmetric auxin distribution in the LR RAM. Displacement of the LR through rotation, results in phosphorylation-dependent relocalization of PIN3 in the columella cells, without affecting PIN7 polarization, towards the gravity-facing side of the root. The amount of PIN3 phosphorylation is dependent on the difference of the growth trajectory to the gravity vector The bigger the difference between growth trajectory and the gravity vector, the more PIN3 is phosphorylated, resulting in increased auxin flow towards the gravity-facing side of the LR and disturbs the auxin symmetry (Roychoudhry et al., 2019). Interpreting the *las* mutant phenotype with respect to PIN polarization, LAS could be seen as a control factor, determining the polarization of PIN protein distribution at the plasma membrane with respect to gravity, within the LR columella cells. Control of auxin fluxes through LAS-dependent control of PIN polarization would be an attractive model to explain establishment and maintenance of the low auxin environment in the vegetative leaf axil, to facilitate AM initiation. Polar localization of PIN1, the prevalent PIN in the *Arabidopsis* and tomato SAM, is required to channel auxin outflow away from the leaf axil, to generate the required low auxin environment (Wang et al., 2014b). For both proposed functions of LAS during GSA/growth trajectory control of LRs, the molecular mechanisms by which LAS would interfere with auxin signaling or would control polar PIN localization are not clear and should be addressed in further studies.

4.3 Comparison of *Arabidopsis las-4* mutants and tomato *ls-1* mutants

With respect to phenotypic aberration, comparison of *Arabidopsis las* mutants and tomato *ls-1* mutants, reveals a general pattern in shoot and root development. In *Arabidopsis* shoot development, loss of LAS function is associated with a single affected trait, defective AM initiation during vegetative development, whereas in tomato, the *ls-1* mutant shows additional defects in

reproductive development (Schumacher et al., 1999; Greb et al., 2003). In root system development, this pattern holds true, when comparing *las-4* and *ls-1*. In *Arabidopsis*, significantly increased vertical LR growth trajectories are the only root-specific phenotypic aberration in *las* mutants, whereas in tomato *ls-1* mutants, root system development is compromised in LRs and in the primary root.

Tomato primary root development displayed two phenotypic alterations in *ls-1*. First, a slight reduction of growth rate during the first days after germination, which is usually an indicator of a reduced RAM size (Dello Ioio et al., 2007). Second, oblique growth trajectories of primary roots, a trait that displayed variable penetrance in the assayed plant populations. Classic reorientation assays demonstrated that oblique growth trajectories were not caused by loss of gravitropism, because *ls-1* mutant primary roots responded to changes in the direction of the gravity vector. The dynamics of the gravitropic response may differ between wild type and *ls-1*, because growth paths of roots during the gravitropic response were quite different. In comparison to *ls-1*, wild type primary roots showed a faster readjustment of growth direction. However, a different experimental set up would be needed to analyze the dynamics of the gravitropic response. Growth rate is an important factor when comparing dynamics of gravitropic responses, because directional change (gravitropism) includes a distance variable. Short time intervals between measurements, which should not exceed 30 min to reach high temporal resolution, would be required to properly normalize gravitropic response over distance against the growth rate (Schöller et al., 2018). Even though gaps between measurements during the reorientation experiment spanned 48 h, growth rate was calculated as a control variable to ensure that analyzed roots were actively growing and able to respond to changes in the direction of the gravity vector. Interestingly, *Solanum pennellii* (*S. penn.*), the wild relative of cultivated tomato, develops shallow root systems through long-term oblique primary root growth. Long-term oblique growth was found to be differentially regulated compared to short-term gravitropic response. Introgression lines derived from a cross between cv. M82 and *S. penn.* were used to identify the genetic loci that control long-term oblique primary root growth (Eshed and Zamir, 1995; Toal et al., 2018). *PURPLE ACID PHOSPHATASE27-4a* (*SlPAP27*) was identified as a candidate gene, causing long-term oblique primary root growth. Overexpression of the *Arabidopsis* orthologue AtPAP27 resulted in increased oblique root growth in *Arabidopsis*, similar to the changes in root growth trajectories seen in *pSCR>>LAS-Tq2* after 17-β-estradiol induction. Acid phosphatases, including purple acid phosphatases, belong to the set of genes, which are upregulated during phosphate stress response (Toal et al., 2018). Toal et al. (2018) hypothesized, that long-term oblique growth might be an adaptation to the sandy coastal regions and dry rocky regions of Peru and Chile, the natural habitats of *S. penn.* (Peralta and Spooner, 2005). To successfully thrive in such environments, root systems have to maximize their abilities to capture phosphorus, a low abundance nutrient, and water. The top most soil layers are rich in phosphate compared to deeper layers, and plants that forage for phosphorous will often develop root systems that cover the horizontal space close to the soil surface (Lynch and Brown, 2001). In dry soils, available water, for example after a precipitation event, usually

does not penetrate deep into the soil, but stays at the surface and rapidly flows away in surface cracks and ditches. In such environments, shallow and surface-near root systems might have a higher water capturing ability (Toal et al., 2018). Therefore, the long-term oblique growth phenotype in *ls-1*, suggests that Ls might be involved in sensing or integrating nutrient availability in the surrounding soil. Ls might translate soil status information into corresponding adaptations of root growth.

The LR growth aberration seen in the tomato *ls-1* mutants is quite different compared to the LR growth defects in *Arabidopsis las* mutants. In tomato *ls-1* mutants, LR display significantly increased horizontal growth trajectories. This is in sharp contrast to the growth defect in *Arabidopsis las* mutants, which display significantly increased vertical growth trajectories. Interestingly, the growth angle defect in tomato appeared to be caused through a reduction in gravitropism. LRs in tomato *ls-1*, appeared to be agravitropic, because they did not respond to changes in the direction of the gravity vector. This is unexpected, because *Arabidopsis las* mutants do not display defective gravitropism in primary or lateral roots, and primary roots in *ls-1* are still graviresponsive. However, using the model system *Arabidopsis* as a reference might not in all instances be informative with respect to conserved growth responses. One example illustrating differential root growth responses is growth in a low phosphate environment. In *Arabidopsis*, low phosphorous conditions trigger increased vertical growth of LRs, similar to the LR phenotype of *las* mutants. In contrast, basal roots of bean display increased horizontal growth under low phosphorus conditions, more similar to the LR phenotype in *ls-1* (Lynch and Brown, 2001; Roychoudhry et al., 2017). Taken together, both, LAS and Ls seem to affect LR growth trajectories, but the mechanistic basis might be different or cause opposite responses.

Alternatively, either *las-4* in *Arabidopsis* or *ls-1* in tomato might not be a loss-of-function mutant. *las-4* harbors a frame shift in the first third of the *LAS* CDS, making it unlikely to encode a functional protein (Greb et al., 2003). In contrast, *ls-1* harbors a 1.5 kb deletion, spanning 995 bp of the presumptive promoter sequence and the first 555 bp of the *Ls* CDS (Schumacher et al., 1999). Analysis of *Ls* CDS in *ls-1* reveals that the partial CDS would still be able to encode for a truncated Ls protein. Synthesis of a truncated protein would require an alternative transcription start site upstream of the 1.5 kb deletion. In both *las-4* and *ls-1*, *LAS*/*Ls* transcript can be detected. Interestingly, *Ls* transcript abundance is increased in *ls-1* (Raatz et al., 2011; Rossmann, 2013). Hence, the deletion in *ls-1* might cause the elevated expression of a truncated Ls protein with residual/partial function. In *Arabidopsis*, increased *LAS* expression correlates with an increased horizontal LR growth trajectory. This would be in line with the increased LR growth trajectories in *ls-1*. To clarify this situation, root system development in mutants harboring different *Ls* alleles, for instance the *ls-3* and *ls-8* mutants in the cv. M82, should be analyzed (Rossmann, 2013). Another indication that *ls-1* might not be a standard loss-of-function allele comes from the analysis of complementation lines. Schumacher et al. (1999) generated different transgenes, consisting of *Ls* and different promoter and enhancer sequences, that were able to rescue the AM initiation defect. Interestingly, these complementing lines were not able to rescue the growth defects in the primary root tip and

only weakly rescued the LR growth angle defect. Surprisingly, complementing lines had an inhibitory effect on LR number of *ls-1* mutants, a trait that normally was not affected in *ls-1*.

4.4 Potential LATERAL SUPPRESSOR functions - deduced from ectopic expression analysis

The molecular function of LAS is still obscure. Studies on cell morphology and marker gene expression in the distal leaflet boundary, suggest that LAS acts as a suppressor of cell differentiation. Distal leaflet boundaries are capable to develop ectopic shoots, and in the case of leaf detachment, this provides a means of clonal propagation. In *ls-1*, ectopic shoot formation is suppressed, indicating that axillary shoot and ectopic shoot formation are mechanistically closely related processes, further, cells located in the distal leaflet boundary, differentiate into trichomes or stomata. In contrast, cells located in the distal leaflet boundary in wild type, do not develop trichomes or stomata. Further, expression of *Histone H4*, a cell division marker, was down-regulated in *ls-1* distal leaflet boundaries. From these experiments it was concluded that cells in distal leaflet boundaries and similarly in the leaf axil have to be kept in an undifferentiated state. Only cells with high developmental potential are able to initiate axillary meristems (Rossmann et al., 2015).

Here, the proposed function of LAS, to act as an inhibitor of cell differentiation, was tested in the RAM. The RAM is a powerful system to study cell lineage-specific differentiation processes, because of its simple structure. Each individual cell file originates from a single stem cell, located in the stem cell niche at the root tip. Differentiation state can be easily deduced from cell position within a cell file, cell length, presence of trichomes in epidermal cells, presence of amyloplasts, staining for cell wall modifications and differential gene expression. This division pattern leads to a linear developmental timeline, reducing multi-dimensionality of development (three dimensional tissue organization that changes over time) to one dimension (Dolan et al., 1993; Benfey and Schiefelbein, 1994; Brady et al., 2007; Bennett and Scheres, 2010; Stahl et al., 2013; Kamiya et al., 2015; Liberman et al., 2015; Denyer et al., 2019). The tissue of choice for ectopic expression of *LAS* was the root endodermis, because it is a well characterized model for cell differentiation (Drapek et al., 2017).

Interestingly, induction of ectopic *LAS* expression in *pSCR>>LAS-Tq2* led to a reduced root growth rate, indicating that RAM size might be decreased (Dello Ioio et al., 2007). Decreased RAM indicates a shift in the position of the transition zone from meristematic to differentiating cells closer to the QC, suggesting that ectopic *LAS* expression would accelerate cell differentiation, showing a contrary molecular function compared to Rossmann et al. (2015). Further, it was quite intriguing that endodermis-specific expression of *LAS* was sufficient to affect cell differentiation in the whole RAM. Monitoring LAS-Tq2 protein localization after induction of ectopic expression in *pSCR>>LAS-Tq2* revealed that the fusion protein can be detected in all tissues of the RAM.

The QC represented an exception in the ectopic expression assay, because within the QC, the *SCR* expression domain intersects with the endogenous *LAS* expression domain. Thus, induction of *LAS* expression in *pSCR>>LAS-Tq2* leads to an artificial elevation of *LAS* expression in the QC. The QC appeared to be unaffected in the majority of *pSCR>>LAS-Tq2* plants, after the induction of *LAS* expression. However, a small fraction of plants displayed amyloplast accumulation in single QC cells, indicating a partial loss of QC identity. Loss of QC identity was probably only a temporary event, because root growth was not affected as severely as one would expect for loss of QC specification and maintenance seen in strong *scr* and *shr* single mutants or *plt1 plt2* double mutants (Helariutta et al., 2000; Sabatini et al., 2003; Aida et al., 2004). Still, this might indicate that elevation of *LAS* expression in the QC interferes temporarily with the QC specification and maintenance pathways. Auxin signaling in the QC is necessary to promote the expression of PLT1/PLT2 through ARF7/NPH4 (Aida et al., 2004). This would further promote the hypothesis that LAS might act as a modifier of auxin-regulated developmental processes, either through modification of auxin signaling or polar auxin transport.

The most striking effect of induced *LAS* expression in *pSCR>>LAS-Tq2* was seen in the CSCs and the lateral root cap/epidermis stem cells (LESs). Both stem cell populations are not included by the endogenous *SCR* expression domain, suggesting that LAS is able to act non-cell autonomously through protein movement. In *pSCR>>LAS-Tq2* plants, LAS-Tq2 is detected in CSCs and the LESs, a property that was not observed in the control *pSCR>>SCR-Tq2* plants, again demonstrating cell-to-cell movement of LAS. Similar to the situation in the QC, LAS protein accumulation in CSCs did not represent an ectopic protein accumulation domain, but an artificial addition of LAS to the endogenous LAS pool already present in CSCs. In contrast, LAS protein accumulation in the LESs represents an ectopic protein accumulation. In both stem cell populations, ectopic accumulation of amyloplasts indicates premature differentiation. Further, stem cells of the columella and epidermis/LRC lineages were not just temporarily lost, but were not detectable at all. Premature stem cell differentiation might be either caused through loss of the QC mediated stem cell cues to neighboring stem cell. Alternatively, elevation of LAS levels might promote differentiation into columella-like cells, indicated by the accumulation of amyloplasts. With respect to the columella cell lineage, it is intriguing that elevating LAS levels, in a domain that displays endogenous LAS expression already, has such dramatic effects. This kind of observations suggest that LAS function is dosage-dependent. Similar dosage-dependent protein function was described for the related GRAS gene *SHR*. In the root, SHR was found to act in three distinct developmental pathways. SHR is required for QC maintenance, specification of the endodermal lineage and the formative (periclinal) cell divisions that form the middle cortex in more mature roots (Helariutta et al., 2000; Sabatini et al., 2003; Paquette and Benfey, 2005). Interestingly, in heterozygous *SHR/shr-2* plants and in *short-root interacting embryonic lethal siel* mutants, in which SHR movement is reduced, premature middle cortex formation is observed. Further, live-imaging revealed that a reduction in SHR protein levels precede the formative middle cortex division in the endodermis. Based on these observations

it was concluded that high levels of SHR protein in the endodermis inhibit middle cortex formation, whereas later in root development, reduction of SHR protein level promotes middle cortex formation (Koizumi et al., 2011, 2012).

Notably, middle cortex formation was the third process affected through ectopic *LAS* expression in *pSCR>>LAS-Tq2*. Eight day old plants, that grew for 72-120 h on inducing medium, displayed increased middle cortex formation. The majority of control plants, which were grown on non-inducing medium, displayed one middle cortex layer. Often this single middle cortex layer was still patchy and noncontinuous, indicating an early stage of middle cortex formation (Paquette and Benfey, 2005). In contrast, plants grown on inducing medium, displayed consistently two middle cortex layers. Notably, middle cortex formation was restricted to the endodermal lineage, indicating that only the endodermis was responsive to ectopic LAS expression, with respect to periclinal divisions resulting in extra middle cortex layers. Thus, to promote formative divisions, LAS is dependent on other pathways, and it is not sufficient to promote formative divisions on its own. This is quite different from ectopic RAM-wide *SHR* expression, which results in the formation of supernumerary *SCR* expressing ground tissue cell layers (Helariutta et al., 2000). Several different pathways converge during root development to regulate the timing of middle cortex formation, thus there is quite a spectrum of putative scenarios to integrate LAS function.

The core middle cortex regulatory module involves three GRAS genes. The dosage-dependent role of SHR was already mentioned before. *scr* and *scarecrow-like 3* (*scl3*) single mutants display premature middle cortex formation, indicating that SCR and SCL3 repress middle cortex formation, similar to high endodermal SHR protein levels (Wysocka-Diller et al., 2000; Paquette and Benfey, 2005). The transcriptional coregulator SEUSS (SEU) maintains sufficient levels of *SHR*, *SCR* and *SCL3* by binding directly their promoters to suppress middle cortex formation. *seu* mutants display also a high frequency of premature middle cortex formation. *SEU* expression in turn is inhibited by gibberellic acid signaling, which promotes middle cortex formation (Paquette and Benfey, 2005; Gong et al., 2016). A second mechanism contributing to the regulation of middle cortex formation is epigenetic regulation. A set of directly regulated SCR targets was also regulated by LIKE HETEROCHROMATIN PROTEIN 1 (LHP1), a transcriptional repressor. Accordingly, *lhp1* mutants display premature middle cortex formation. Interestingly, the binding profiles of both proteins, obtained through chromatin immunoprecipitation, overlap considerably at common target genes, suggesting a direct interaction. Further, the *spindly* (*spy*) mutant also displays premature middle cortex formation. The animal SPY orthologue is part of a multimeric complex that contains histone deacetylases (HDACs). Histone deacetylation represses gene expression. Notably, treatment of *Arabidopsis* roots with the histone deacetylase inhibitor Trichostatin A, induces premature middle cortex formation (Cui and Benfey, 2009b,a). LAS might either block middle cortex inhibiting factors or promote middle cortex promoting factors in the regulatory network outlined above. Recently, epigenetic regulation was shown to be involved in the regulation of AM initiation, suggesting that their

might be common features between LAS mediated middle cortex formation and AM initiation (Lopez Marin, 2017).

4.5 The role of the *LAS/Ls* antisense transcript

A novel finding was the detection of a long noncoding RNA (lncRNA), transcribed in reverse orientation from the *LAS/Ls* loci. Construction and evaluation of a transcriptional reporter showed that the *asLAS* expression domain is indistinguishable from the *LAS* expression domain. This excluded the possibility, that *asLAS* spatially restricts *LAS* expression to a specific group of cells. An example of a restrictive mechanism is the direct SHR target miR165/6. SHR activates miR165/6 expression in the endodermis, and miR165/6 acts non-cell autonomously in the provasculature and the pericycle to degrade, in a dosage dependent manner, its target mRNAs. miR165/6 targets are the transcripts of HD-ZIP transcription factors. The resulting gradual distribution of HD-ZIP transcripts, is important for proper xylem differentiation (Carlsbecker et al., 2010). Some lncRNAs are indeed described to act as microRNA precursors, like the lncRNA H19 in mice. In general, lncRNAs are capable to act in cis or in trans. However, for the majority of lncRNAs, there is nothing known about the molecular mechanism (Lee, 2012). lncRNAs have the ability to target a unique locus or allele, because of their sequence length. In contrast, transcription factors are able to bind efficiently to DNA, based on the recognition of short motifs. By chance, these short motifs occur thousands of times in the genome, resulting in possible regulation of many genes at once. Binding sites of lncRNAs, occur usually only once, enabling gene regulation at a unique 'address'. The model example for such a process is X-chromosome inactivation in female mammals, to balance expression of X-chromosome encoded genes. X-inactive-specific transcript (Xist) encodes for an lncRNA that coats the inactive X-chromosome. Xist mediates the inactivation through direct interaction with Polycomb repressive complex 2 (PRC2), which is responsible for trimethylation of histone H3 (H3K27me3; Lee, 2012).

Regulation of gene expression by antisense transcripts is also frequently found during plant development. One example, demonstrating the conservation of an antisense-directed developmental decisions is the female-to-male sex conversion in *Marchantia polymorpha*. *FEMALE GAMETOPHYTE MYB* (*MpFGMYB*) promotes female gametophyte development and loss of *MpFGMYB* function converts female gametophytes into male gametophytes. To induce male gametophyte development, expression of *MpFGMYB* has to be suppressed by a cis-acting lncRNA antisense transcript, called *SUPPRESSOR OF FEMINIZATION* (*SUF*). However, the mechanistic basis of *SUF* mediated *MpFGMYB* expression is not characterized in great detail, yet (Hisanaga et al., 2019). In the case of the *MpFGMYB/SUF* sense-antisense pair, different promoter elements were identified, that control either *MpFGMYB* or *SUF* expression. This suggests, that sense and antisense transcripts compete during transcription via RNA polymerase II directed expression for obstacle-free transcription (Hisanaga et al., 2019). In contrast,

LAS/*asLAS* expression might be regulated by a different mechanism. Here, different transcription factors, promoting expression of either the sense or the antisense transcript, might compete for docking sites at a common regulatory element, for example regulatory element B. This would imply transcription factor dependent DNA looping, that would either promote initiation of *LAS* transcription or promote the initiation of *asLAS* transcription.

A different mode of transcriptional interplay, constituting a possible regulatory mechanism between *LAS* and *asLAS*, is described for the sense/antisense pair *FLOWERING LOCUS C* (*FLC*)/*COOLAIR*. *COOLAIR* encodes an lncRNA that regulates the expression of *FLC*. Prolonged growth under cold conditions induces *COOLAIR* expression, which in turn represses *FLC* transcription. FLC acts as a repressor of the floral transition. Expression of *COOLAIR* is regulated via R loop formation (Sun et al., 2013). R loops can be formed during RNA polymerase II directed transcription from nascent transcripts behind the elongating RNA polymerase II. Nascent transcripts can invade the DNA double strand and hybridize with the respective template strand, leading to the formation of a RNA-DNA hybrid. The RNA-DNA hybrid blocks out the DNA nontemplate strand, resulting in the formation of a protrusion of the single stranded DNA. Such three-stranded DNA-RNA hybrids are termed R loops (Skourti-Stathaki and Proudfoot, 2014). In the case of *COOLAIR* repression, R loops are detected in the *COOLAIR* promoter region. Additionally, the single-strand-binding protein ATNDX stabilizes R loops at the *COOLAIR* promoter through binding of the RNA-replaced single stranded DNA. This R loop inhibits *COOLAIR* expression (Sun et al., 2013).

Indeed, sense-antisense pairs a quite common in *Arabidopsis*. A recent study identified 37,238 of such pairs, of which 70 % belong to annotated mRNAs. Querying the published dataset for *LAS* revealed the presence of an *asLAS* transcript (Wang et al., 2014a), confirming the observations described above. In comparison, querying the dataset for *SCR* or *SHR* yielded no result. Expression of a subsection of those pairs was light responsive, and changes in expression level were correlated with histone acetylation at these loci (Wang et al., 2014a). Similarly, the ratio of *LAS* and *asLAS* expression might be under environmental control integrating, for example, nutrient availability in the surrounding soil. Depending on soil properties, LR growth trajectories may be adjusted based on the level of LAS protein accumulation as a consequence of differential *LAS*/*asLAS* expression. To further dissect the function of *LAS* and *asLAS* expression in root development an interesting approach might be the generation of alleles that abolish either *LAS* or *asLAS* expression without affecting expression of the counterpart. This might be achieved through CRISPR/CAS9 mediated gene editing.

4.6 Does LATERAL SUPPRESSOR movement plays a role during axillary meristem formation?

One of the novel findings in this study was the ability of the LAS protein to move from the columella cells into the LRC. Lucas et al. (1995) initially described the first moving transcription factor, KNOTTED1 (KN1), in maize. Since then, movement, or cell-to-cell trafficking, has been

shown for additional transcription factors. Other proteins displaying short-range movement, describing protein movement over a range of one to several cells, are STM, LEAFY (LFY), SHR and WUS (Sessions et al., 2000; Kim et al., 2003; Nakajima et al., 2001; Daum et al., 2014). In plants, most evidence points to plasmodesmata as mediators of cell-to-cell movement. Plasmodesmata are tunnel-like connections between neighboring cells that are lined by plasma membrane, thereby establishing a symplastic continuum. Two models provide different modes that might operate to allow protein movement through plasmodesmata. Plasmodesmata might restrict the size of molecules traveling through them by the size-exclusion limit, which selects by molecule size. Alternatively, transcription factors might increase the size-exclusion limit through direct modification of the plasmodesmata structure. However, the molecular mechanisms underlying protein movement through plasmodesmata are still obscure (Zambryski and Crawford, 2000; Zambryski, 2004; Daum et al., 2014). A different type of transcription factor movement includes long range transport through a combination of plasmodesmata and vasculature, like in the case of ELONGATED HYPOCOTYL5 (HY5), a bZIP transcription factor. HY5 is a shoot-to-root mobile signal, which traffics through the phloem to modulate root development (root growth and LR outgrowth) and nitrate uptake, in response to light signaling in the shoot (Chen et al., 2016; van Gelderen et al., 2018).

LAS most likely belongs to the first category, meaning it acts as a short range signal. It was shown that the family-defining GRAS domain, is a necessity for SHR movement and promotes protein movement in a general fashion. Swapping the unrelated variable N-termini of SCR and SHR was sufficient to enable SCR movement. Similarly, deleting the variable N-terminus in SCR, resulted in movement of the truncated SCR GRAS domain protein. Interestingly, interference with SHR nuclear accumulation, through mutations altering the GRAS domain, also prevented protein movement. These observations suggested, that domains which promote movement and nuclear localization overlap, or that nuclear localization promotes protein movement based on a shared mechanism for protein translocation (Gallagher and Benfey, 2009). In comparison to these examples, LAS is more similar to SHR, because the variable N-terminus in LAS does not inhibit movement, like in the case of SCR. In columella cells, LAS protein accumulates in the nucleus as well as the cytoplasm. In contrast, in the LRC it becomes restricted to the nucleus. This pattern of protein localization is similar to SHR, which displays cytoplasmic and nuclear localization in provasculature and pericycle and gets restricted to the nucleus in the endodermis. This might indicate a similar mechanistic basis, regulating SHR and LAS movement in their specific tissue contexts.

Observation of protein movement always implies the question of its biological relevance. In many cases, protein movement and protein function appear to be unrelated with respect to plant development, like the non-targeted diffusion of LFY (Wu et al., 2003). Because LAS movement and intracellular localization were not known previously, it was tested whether these characteristics have implications for LAS function during AM initiation. Interestingly, the addition of NLS domains to LAS did result in unexpected phenotypes. Standard LAS translational fusion proteins fully complemented the branching defect in *las-4*. In contrast the addition of

an NLS domain to the LAS fusion protein resulted in a loss of complementation ability. In extreme cases, all plants in a specific transgenic line displayed the mutant *las-4* phenotype and none of the independent transgenic lines expressing LAS-NLS versions displayed complementation in the whole population. In all analyzed plants, LAS-NLS fusion proteins were detectable in root tips via live-imaging, demonstrating that failure of rescue was not due to transgene silencing. However, addition of an NLS domain to LAS did not inhibit LAS movement, because LAS-NLS was still present in the LRC. Further, two transgenic lines displayed ectopic LAS-NLS expression throughout the RAM. All plants of these two lines displayed the *las-4* phenotype. Intriguingly, a second category of transgenic LAS-NLS lines displayed segregation of complementation. These observations suggested that the level of LAS protein might be critical for AM initiation. In the lines without complementation, the transgene might have inserted at a genomic locus, which promotes excessive transgene expression, also in ectopic domains. Alternatively, there might me multiple transgene insertions, which additively raise LAS levels. To test this hypothesis, LAS-NLS lines that displayed segregation of complementation were analyzed with respect to transgene copy number. Indeed, transgene copy number correlated with phenotype. High copy number, usually resulted in loss of *las-4* complementation. This suggested that copy number and consequently LAS dosage has profound consequences for AM initiation. The expression level might be variable and to initiate an AM, *LAS* levels have to be kept in a dynamic range with an upper and a lower threshold. High transgene expression levels above the upper threshold might be caused either through insertion at a genomic locus that enhances transgene expression, through alterations in T-DNA copy number or through differences in zygosity.

This experiment corroborates that LAS protein abundance might be directly related to the exerted function. A simple model may assume that increased LAS accumulation results in a spillover effect, which counteracts standard LAS function. The spillover-model would rely on one (simple case) hypothetical LAS-interacting protein (IPX). IPX possesses two properties: First, the IPX expression domain overlaps with the endogenous *LAS* expression domain. Second, IPX abundance stays constant within the cell, and the IPX level is equal to or higher than the LAS level. LAS has high affinity for IPX, and both proteins form a complex, which is necessary for proper LAS function. IPX has to be in excess compared to LAS, to buffer potential lower-affinity interactions with other proteins. If LAS levels exceed IPX levels, IPX loses its buffer function and LAS might interact with other proteins. Potential IPX candidates might be SCR or LAS itself, based on Y2H studies (Greb, 2003). For instance, *SCR* is expressed in the L1 layer in the shoot apex and may interact with LAS in the leaf axil (Wysocka-Diller et al., 2000). Formation of these secondary low-affinity protein complexes inhibits or counteracts LAS-IPX function.

4.7 Conclusions

This study demonstrates that LAS functions as a regulator of LR growth direction by regulating LR growth angles. Furthermore, an emergent property related to LAS function seems to be the level of *LAS* expression or protein abundance. Various experimental data point to a dosage-dependent function of LAS. In LRs, *LAS* expression is significantly increased, compared to primary roots, correlating with the differential integration of gravity. Artificial elevation of *LAS* expression in its endogenous expression domains, resulted in cell differentiation, further corroborating the relationship between LAS protein level and LAS function. Following this trend, rescue of AM initiation in *las-4* was sensitive to high LAS levels. Further, evidence was provided that LAS protein is able to move from cell to cell and that an *LAS* antisense transcript is expressed in the same domain. Protein movement and antisense transcription are two previously unknown characteristics providing new avenues to further analyze LAS function in the future.

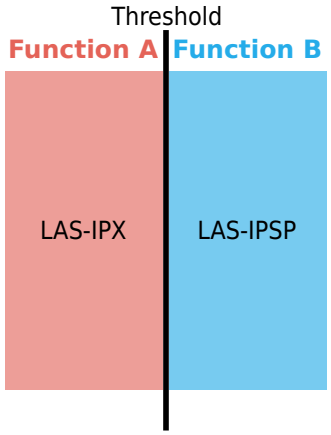


Figure 24: Spillover model. Cartoon of the Spillover model illustrating the dosage-dependent function of the LAS protein. Important is the threshold (black line), which determines when IPX loses its buffering capacity and LAS is able to form secondary low affinity complexes with other interacting partners, exemplified here by the spillover interacting protein (IPSP). The LAS-IPSP complex executes a different function than the LAS-IPX complex.

5. Supplementary Data

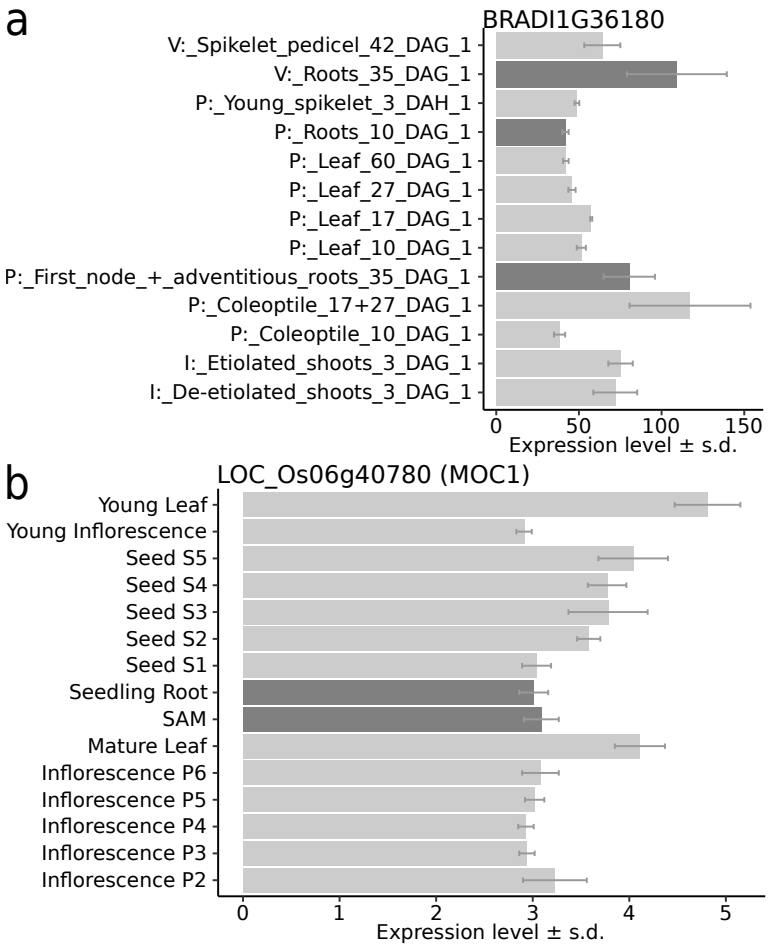


Figure S1: Expression of *LATERAL SUPPRESSOR* orthologues in monocots. Online expression data for rice and *Brachypodium LAS* orthologues. **a**, Expression of *BdLAS* (BRADI1G36180) in various *Brachypodium* tissues. Expression data was downloaded from the *Brachypodium distachyon* eFP browser (Winter et al., 2007; Sibout et al., 2017). **b**, Expression of *MOC1* in various rice tissues. Expression data was downloaded from the rice eFP browser, using the 'rice rma' data source (Winter et al., 2007).

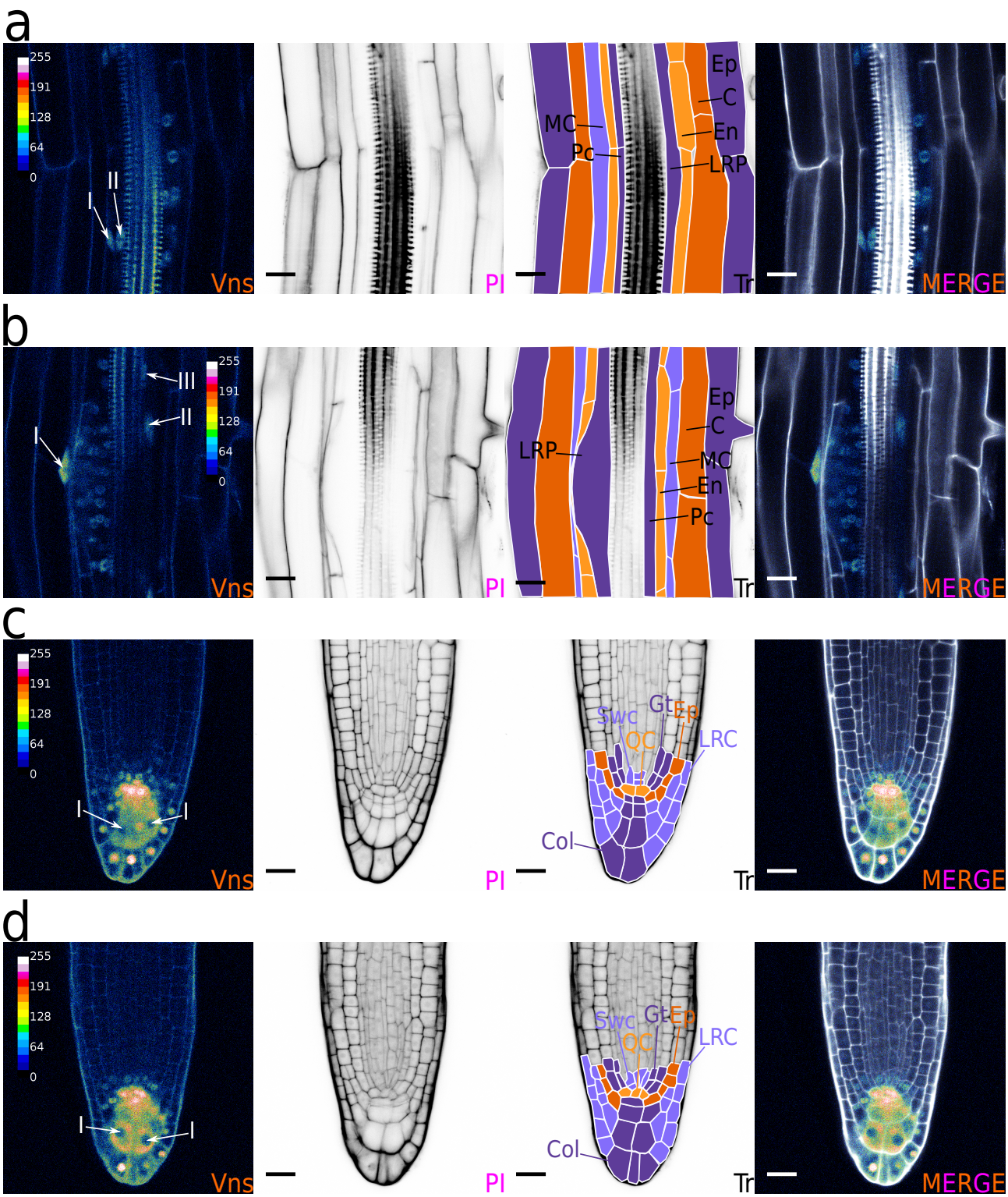


Figure S2: Vns-LAS localization during lateral root morphogenesis. CLSM of Vns-LAS expression in LRP and LR tips of transgenic *las-4* plants. **a**, Stage II LRP. Vns-LAS fluorescence in nuclei of cells comprising the LRP and in cells unrelated to the LRP (arrows). Arrow I: Nucleus of endodermal cell. Arrow II: Nucleus of pericycle cell. **b**, Stage IV LRP. Vns-LAS fluorescence in nuclei of cells comprising the LRP and in cells unrelated to the LRP (arrows). Arrow I: Nucleus of cortex cell, that is in physical contact with LRP. Arrow II: Nucleus of endodermal cell. Arrow III: Nucleus of pericycle cell. **c**, Vns-LAS fluorescence in the tip of a LR longer than 5 mm. Arrows I indicate columella/LRC cells that display fluorescence in the cytosol, but not in the nucleus. **d**, The same as in (**c**), but LR from a different root system. In (**a**) to (**d**) images were taken from roots of *las-4* mutant plants transformed with *pLAS:Vns-LAS* (line 170138_4), 10 days after germination. FIGURE CONTINUES ON THE NEXT PAGE ...

Figure S2: continued. (**a**) to (**d**), panels from left to right: Vns channel with grey value heat map, PI channel, cell tracings (Tr) and image of merged Vns and PI channels. Stages of LR morphogenesis in (**a**) and (**b**) according to Malamy and Benfey (1997). In (**c**) and (**d**) only cell lineages are traced, without denoting stem cells. Based on cellular organization, discrimination of the columella and LRC lineage is not in all cases unambiguous. Scale bars at the bottom corners of panels represent 18 μm. C = cortex, Col = columella, En = endodermis, Ep = epidermis, Gt = ground tissue, LRC = lateral root cap, LRP = lateral root primordium, MC = middle cortex, Pc = pericycle, QC = quiescent center, Swc = shootward stem cell.

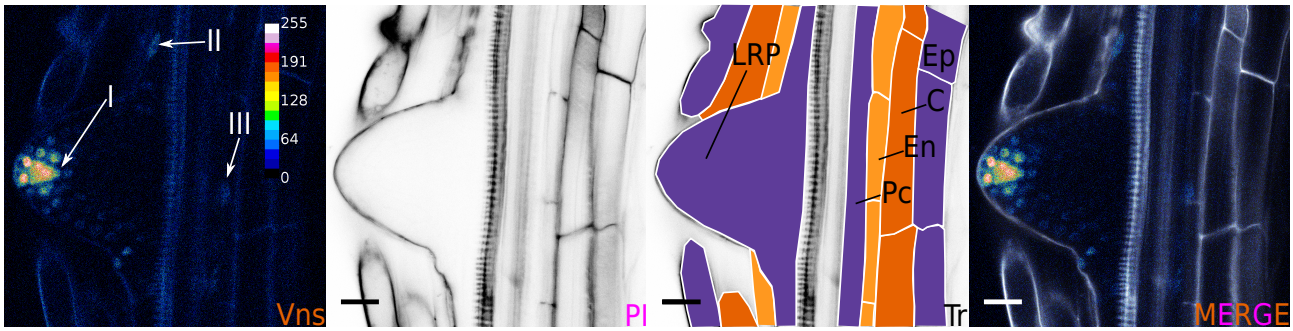


Figure S3: LAS-Vns signal during lateral root primordium emergence. Representative image displaying LAS-Vns signal during the emergence of a LRP from the epidermis. This event marks also the transition of a LRP to a LR. Arrow I: Restricted domain, with increased LAS-Vns fluorescence intensity. Arrow II: LAS-Vns signal in a pericycle cell in the LRP periphery. Arrow III: LAS-Vns signal in an endodermal cell. The image was taken from a root of a *las-4* mutant plant transformed with *pLAS:LAS-Vns* (line 170200_1), 10 days after germination. Panels from left to right: Vns channel with grey value heat map, PI channel, cell tracings (Tr) and image of merged Vns and PI channels. Scale bars at the bottom corners of panels represent 18 μm. C = cortex, En = endodermis, Ep = epidermis, LRP = lateral root primordium, Pc = pericycle.

Arbeitsgruppe von Prof. Dr. Klaus Theres

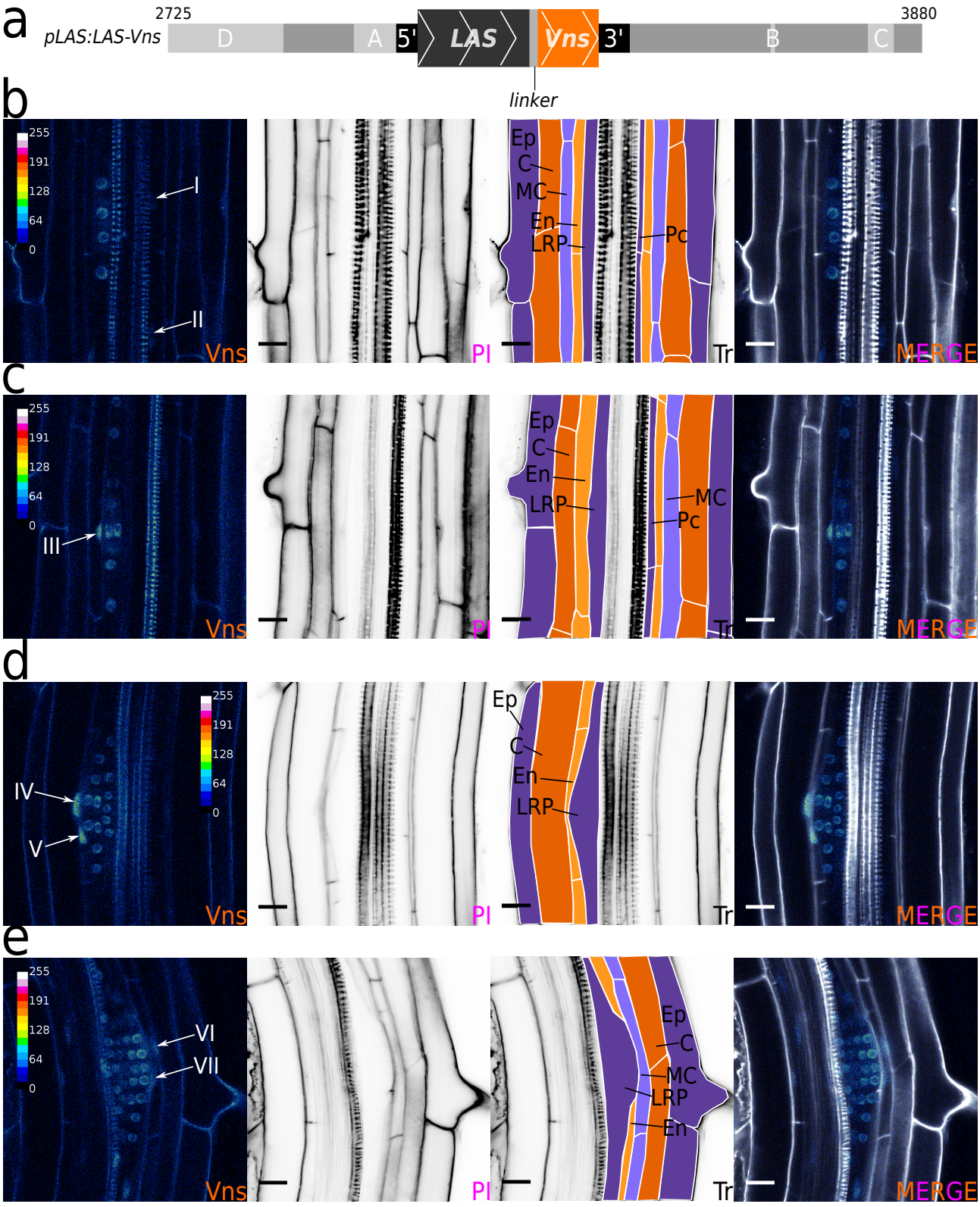


Figure S4: LAS-Vns protein localization during lateral root morphogenesis. CLSM of LAS-Vns expression in LRP of transgenic *las-4* plants. **a**, Cartoon of the translational reporter *pLAS:LAS-Vns*. The only difference to *pLAS:Vns-LAS* described in Fig. 7a is the composition of the translational fusion protein. The fusion protein consists of three parts. The *LAS* genomic sequence is connected via a flexible 99 bp *linker* sequence described by Daum et al. (2014), with a C-terminal Vns. Tips of open triangles show 5' to 3' orientation of the *LAS-Vns* ORF. **b**, Stage I LRP. LAS-Vns fluorescence in nuclei of cells comprising the LRP and in cells unrelated to the LRP (arrows). Arrow I and II: Nuclei of pericycle cells without physical contact to the LRP. **c**, Stage II LRP. FIGURE CONTINUES ON THE NEXT PAGE ...

Figure S4: continued. LAS-Vns fluorescence in nuclei of cells comprising the LRP and in overlaying cortex cell with physical contact to the LRP. Arrow III: Nucleus of cortex cell. **d**, Stage III LRP. LAS-Vns fluorescence in nuclei of cells comprising the LRP and in overlaying cortex and endodermis cells with physical contact to the LRP. Arrow IV: Nucleus of cortex cell. Arrow V: Nucleus of endodermal cell. **e**, Stage IV LRP. LAS-Vns fluorescence in nuclei of cells comprising the LRP and in overlaying middle cortex and endodermis cells with physical contact to the LRP. Arrow VI: Nucleus of middle cortex cell. Arrow VII: Nucleus of endodermal cell. In (**b**) to (**e**) images were taken from roots of *las-4* mutant plants transformed with *pLAS:LAS-Vns* (line 170200_1), 10 days after germination. (**b**) to (**e**), panels from left to right: Vns channel with grey value heat map, PI channel, cell tracings (Tr) and image of merged Vns and PI channels. Stages of LR morphogenesis in (**a**) and (**b**) according to Malamy and Benfey (1997). Scale bars at the bottom corners of panels represent 18 μm. C = cortex, En = endodermis, Ep = epidermis, LRP = lateral root primordium, MC = middle cortex, Pc = pericycle.

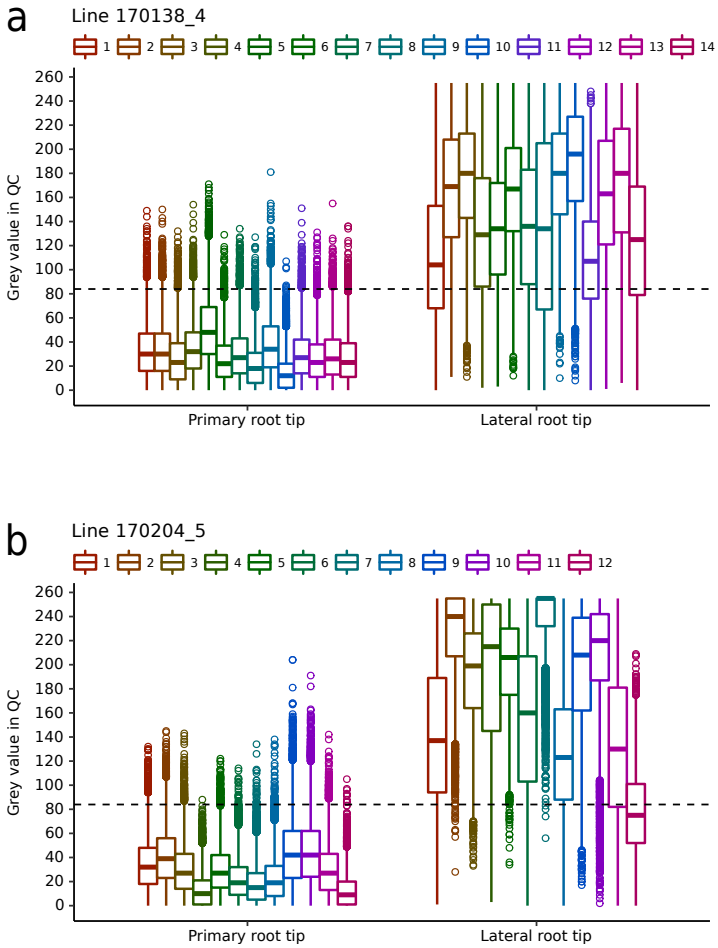


Figure S5: Differences in Vns-LAS protein levels between primary and lateral root QCs. (**a**) and (**b**), Pairwise grey value quantification of Vns-LAS signal intensity in selected QCs from individual root systems. Grey value distributions in the QC of the primary root and the most rootwards LR, that has a similar developmental stage as the LR depicted in Fig. 7c were determined. Two independent transgenic lines (plot titles, *pLAS:Vns-LAS* in *las-4*) were assayed. Colors represent individual root systems. For a description of box plots see Fig. 9. Circles represent outlier grey values. Dashed line depicts the mean grey value across all pixels assayed during the experiment. Plants were imaged 7 days after germination.

Trait	Description	Unit	Reference
Root system morphology			
pri_length	Length of the primary root	cm	-
pri_gravi_indx	Gravitropic index, ratio of primary root length over vector length	-	Barbez et al. (2017)
lat_gravi_indx	Mean gravitropic index of all lateral roots in a root system	-	-
Root system geometry			
convex hull	Smallest convex polygon of a root system	cm^2	Galkovskyi et al. (2012)
width	Maximal horizontal expansion of a root system	cm	Lobet et al. (2017)
depth	Maximal vertical expansion of a root system	cm	Lobet et al. (2017)
width_depth_ratio	Ratio of width over depth	-	Lobet et al. (2017)
Root system topology			
root_sys_length	Overall length of the root system (pri_length and lat_length)	cm	Delory et al. (2016)
lat_length	Cumulative length of all lateral roots in a root system	cm	Delory et al. (2016)
LRBA	The LR branching angle (LRBA) describes the angle enclosed by the primary root and the LR at its emergence position. Direction of the gravity vector does not matter for LRBA calculation, because reference points are the orientations of the primary root and the LR.	°	Lobet et al. (2011)
LR_N	Number of lateral roots in a root system	-	-
lat_density	Ratio of lateral root number over primary root length	cm^{-1}	-
interbranch_dist_mean	Describes the primary root segment with emerged LRs. Measure of the average distance between lateral root emergence positions within this segment	cm	Delory et al. (2016)
Root system dynamics			
gr_rs	Growth rate of the root system during scanning intervals	$mm\ h^{-1}$	Delory et al. (2016)
gr_pr	Growth rate of the primary root during scanning intervals	$mm\ h^{-1}$	-
gr_lr	Growth rate of the lateral roots during scanning intervals	$mm\ h^{-1}$	Delory et al. (2016)

Figure S6: Root traits. Description of root traits used for root system phenotyping. Categories are based on Lobet (2015). The following traits were usually only extracted from the last time point in the time series: pri_gravi_indx, lat_gravi_indx, convex hull, width, depth, width_depth_ratio, LRBA, LR_N, lat_density and interbranch_dist_mean.

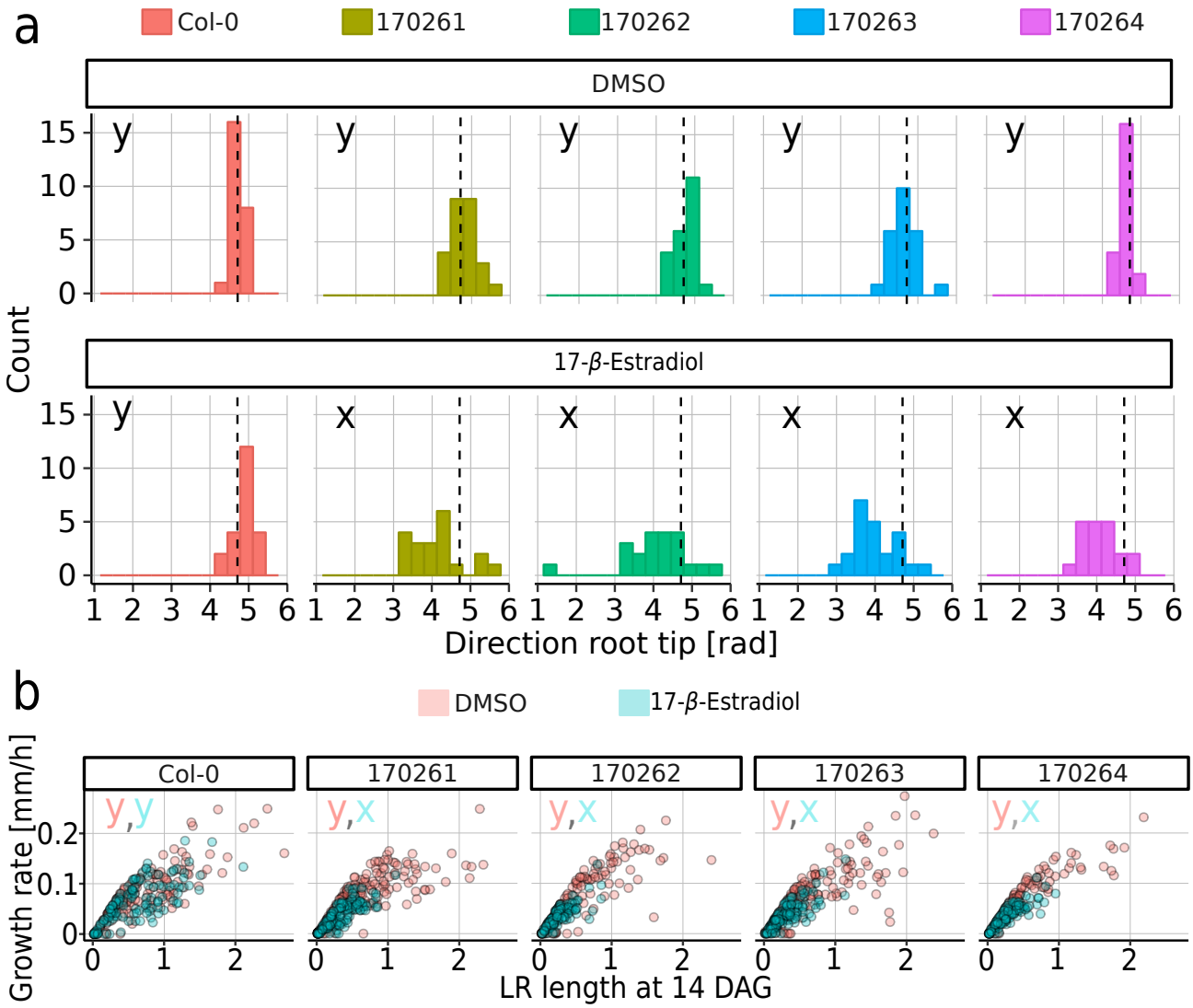


Figure S7: Specific deviation from gravity oriented growth and effect on LR growth rate in *pSCR>>LAS-Tq2* plants after *LAS* induction. Analysis of primary root tip growth direction and LR growth rates in *pSCR>>LAS-Tq2* plants after *LAS* induction. **a**, Histograms of root tip orientations after 14 DAG. Plants were either treated with DMSO or 10 μM 17-β-estradiol from 5 DAG onwards. Dashed line indicates root tip orientation parallel to the gravity vector (4.71 rad). **b**, Scatter plots of LR length at 14 DAG in relation to growth rate. Points represent individual LRs. Plants are the same as in (**a**). In (**a**) and (**b**) statistical significance was determined using unbalanced two-way ANOVA. The letters in the upper left plot corners (x or y, in (**b**) color-coded based on treatment) indicate the results of a post hoc Tukey test, groups with the same letter are indistinguishable at $> 95\%$ confidence using a 0.05 significance level. Sample size ranged between 20 to 26 plants for each line/treatment combination. 170261 to 170264 represent four independent transgenic lines in the Col-0 background, carrying *pSCR>>LAS-Tq2*. Summary statistics are described in table S16.

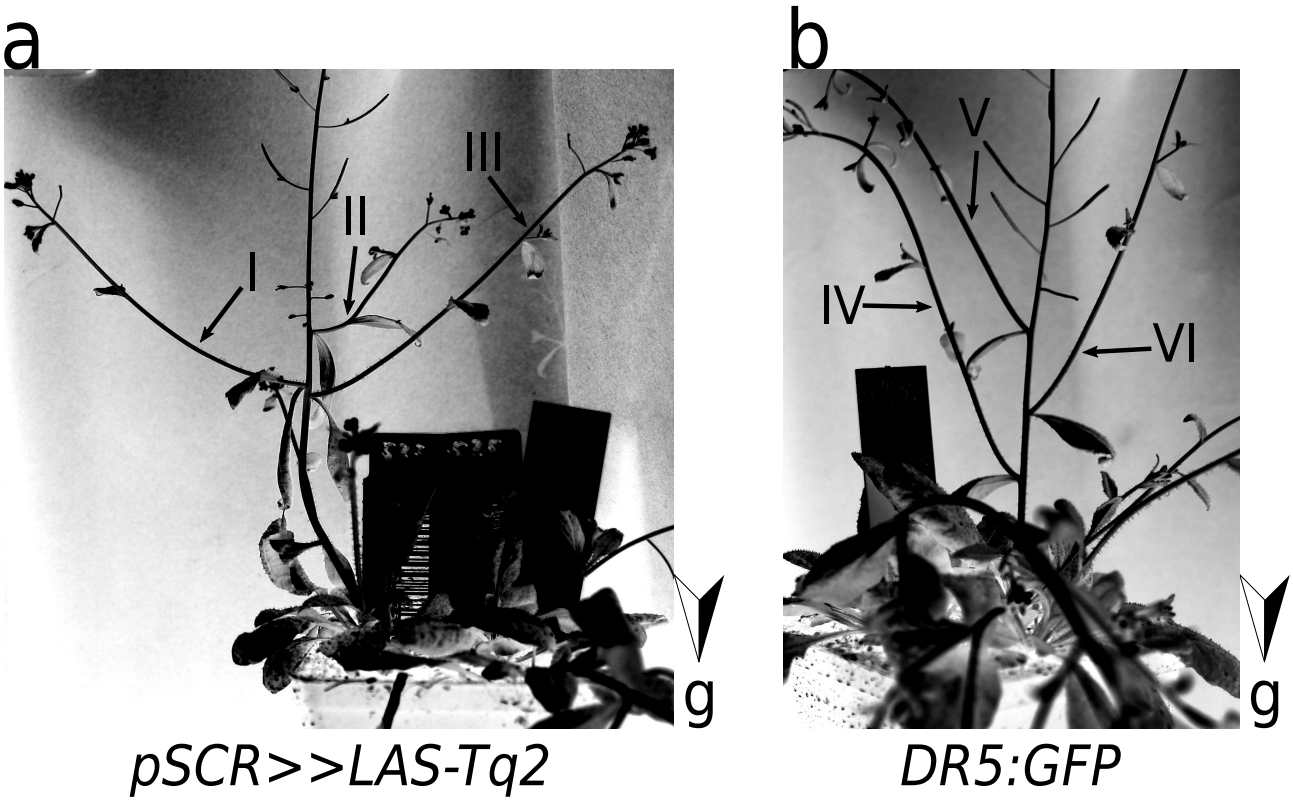


Figure S8: Increased horizontal growth in side shoots of plants expressing *pSCR>>LAS-Tq2*. Display of cauline leaf side shoots in *pSCR>>LAS-Tq2* and *DR5:erGFP*. **a**, Col-0 plant expressing *pSCR>>LAS-Tq2*, without any induction treatment. Arrows I - III indicate the three youngest side shoots, before flowers are initiated from the inflorescence. Image was taken from a representative plant from line 170262. **b**, Col-0 plant expressing *DR5:erGFP*, without any induction treatment. Arrows IV - VI indicate the three youngest side shoots, before flowers are initiated from the inflorescence. Plants in (**a**) and (**b**) were grown simultaneously under the same conditions in the green house. Arrowheads denote the direction of gravity. n = 23 plants/line.

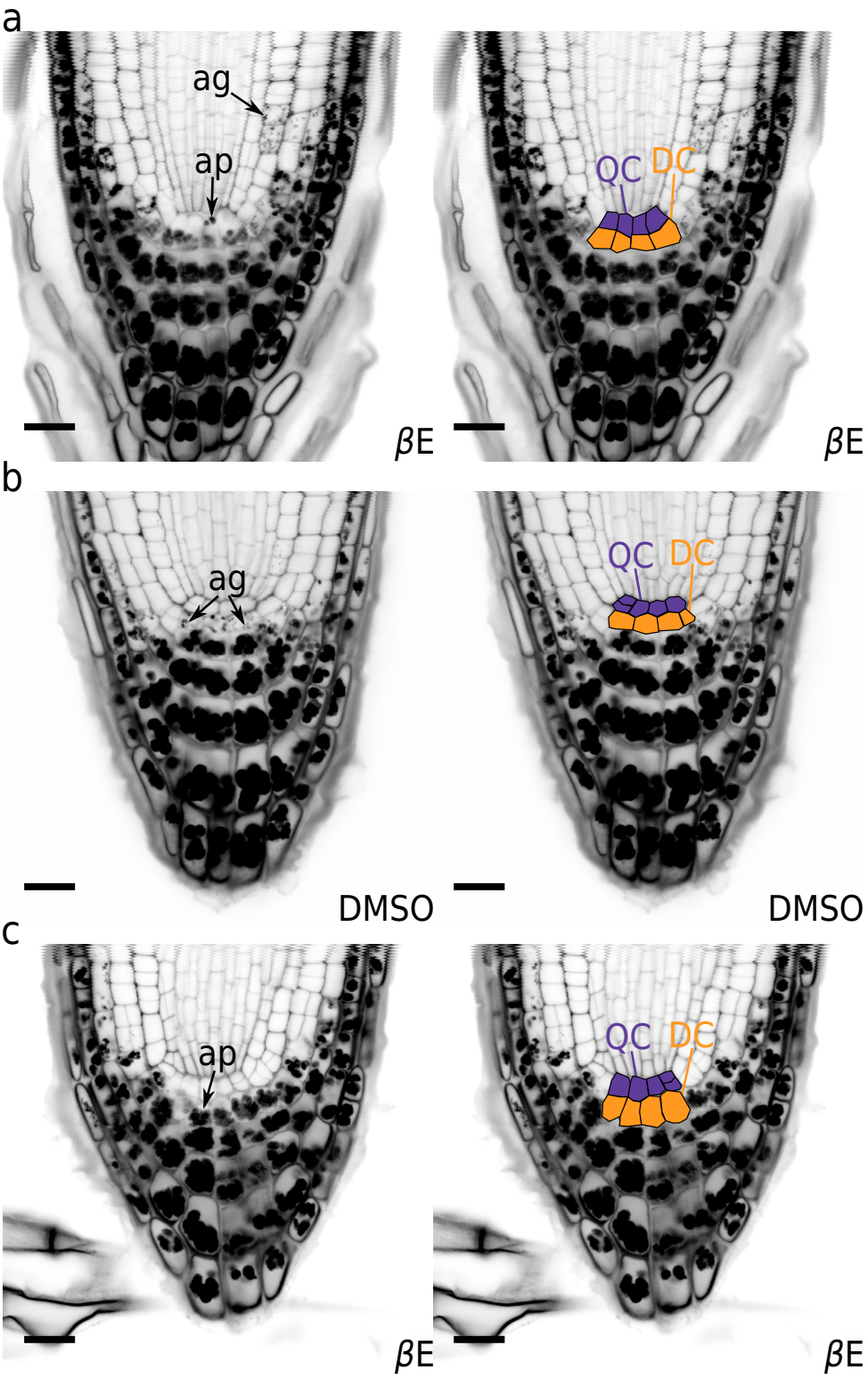


Figure S9: Loss of QC fate in LAS inducing conditions. **a**, mPSPI stained amyloplasts in QC cells. **b**, Representative image of aggregates in distal cells, after mPSPI staining. **c**, Representative image of amyloplasts in distal cells, after mPSPI staining. In (**a**) to (**c**), cell lineages are traced in the right panel. Left panels display the same root tip without tracings. Black bars in the lower left corner represent 18 μm. Root tip images in (**a**) to (**c**) came from line 170261, that is described in Fig. 16. βE and DMSO indicate inducing and non-inducing conditions, respectively. ag = aggregates, ap = amyloplasts, DC = distal cells, QC = quiescent center.

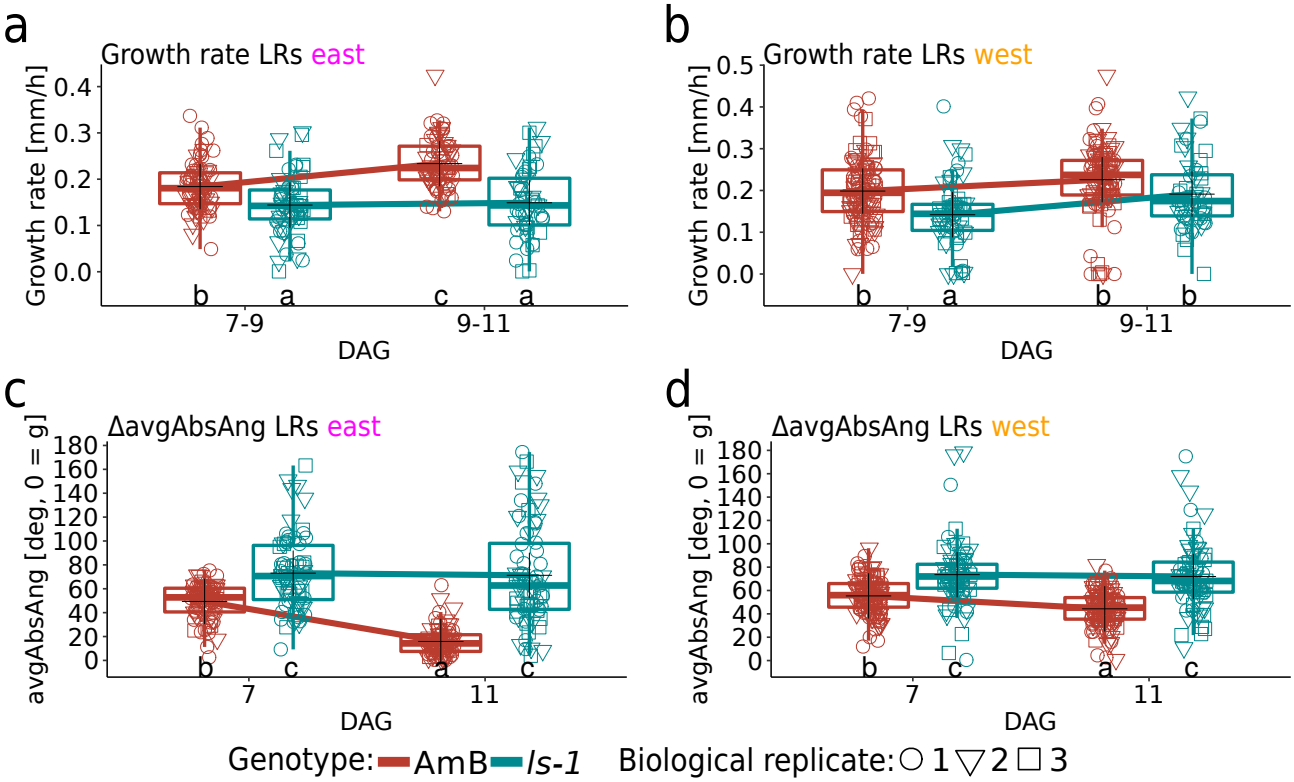


Figure S10: LRs in the *ls-1* mutant did not respond to gravity. **a**, growth rate of east facing LRs, in wt and *ls-1* mutants at indicated time intervals. **b**, growth rate of west facing LRs, in wt and *ls-1* mutants at indicated time intervals. **c**, avgAbsAng of east facing LRs, in wt and *ls-1* mutants at indicated time points. **d**, avgAbsAng of east facing LRs, in wt and *ls-1* mutants at indicated time points. Analyzed root systems are described in Fig. 20. For a description of box plots see Fig. 9. Dots represent individual LRs. Straight lines connect mean values of sample populations (plus signs). Statistical significance was determined using unbalanced two-way ANOVA. The letters below the boxes (a–d) indicate the results of a post hoc Tukey test, groups with the same letter are indistinguishable at $> 95\%$ confidence using a 0.05 significance level. For each time point data from three independent biological replicates was pooled prior to analysis. Sample size ranged between 5 to 8 root systems per genotype for each biological replicate.

Gene	$\log_2$FC	AmB_br1	AmB_br2	AmB_br3	*ls-1*_br1	*ls-1*_br2	*ls-1*_br3	p value	q value
Solyc06g035940.3	6.345337	0	0	0	59.444160	69.509865	89.440125	$8.104461e-06$	0.015823959
Solyc05g006370.1	4.132439	0	0	0	13.971774	15.012501	17.675827	$4.736512e-06$	0.015823959
Solyc08g075560.1	3.444878	0	0	0	9.624366	9.960014	9.905534	$1.884500e-07$	0.001272839
Solyc05g009200.2	3.250500	0	0	0	8.244841	8.231915	8.680717	$2.173007e-07$	0.001272839
Solyc10g012210.2	2.958679	0	0	0	7.048996	6.138143	7.000710	$3.223697e-05$	0.040000970

Figure S11: DEGs in *ls-1* mutant primary root tips. DEGs identified after filtering results of the differential expression analysis according to the following criteria: $\log_2$ fold change (FC) ≥ 2.5 and FDR (q value) < 0.05. Columns 3 to 8 display FPKM values of individual samples.

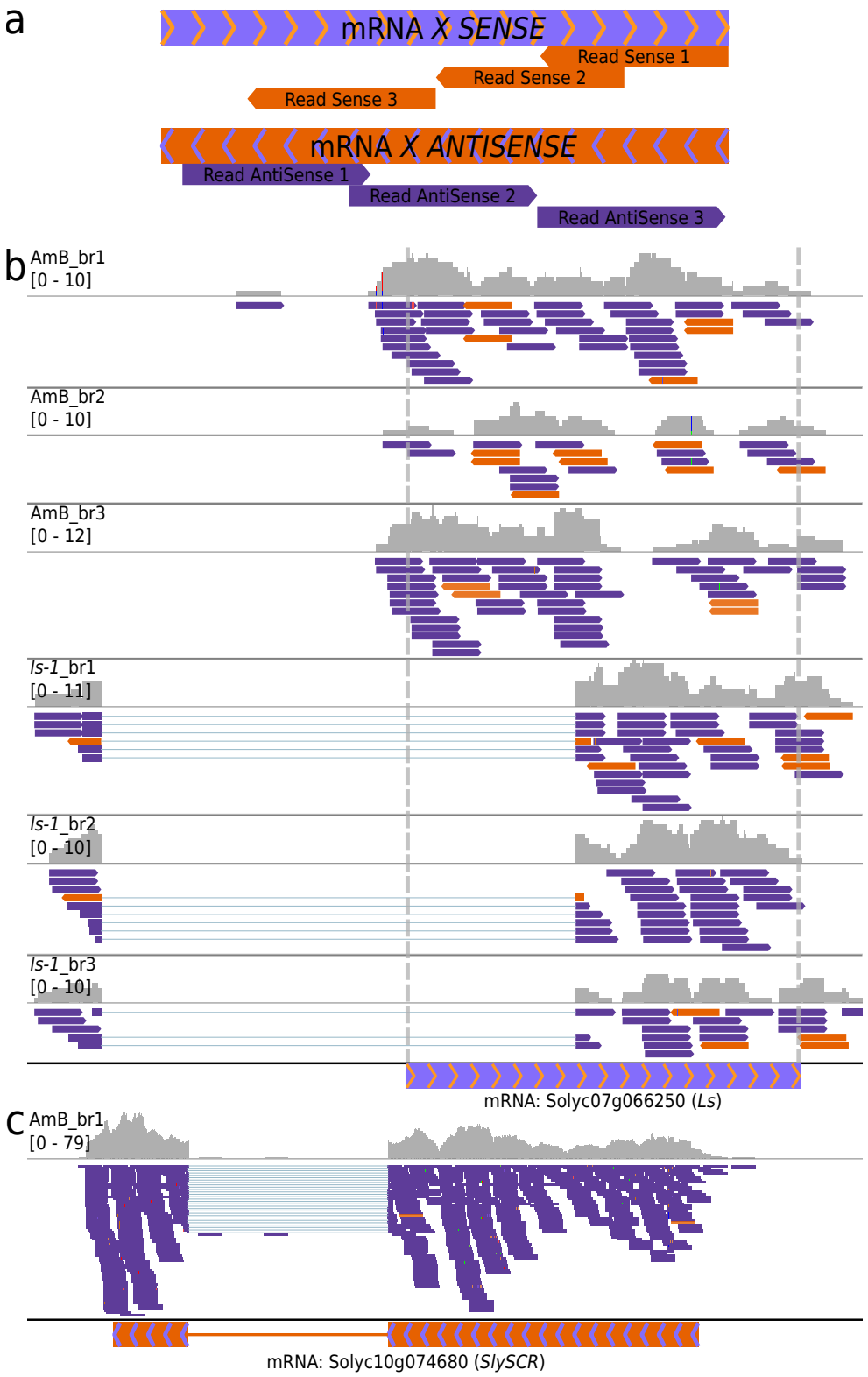


Figure S12: *Ls* antisense transcript in tomato roots. **a**, Cartoon illustrates directional relation between mRNA and strand specific reads. Depicted are sense and antisense transcripts of a hypothetical gene *X*. Reads will always face in the opposite direction, in relation to the mRNA that was sequenced. **b**, Read mapping at the *Ls* locus in the wt (AmB) and *ls-1* mutant background. **c**, Read mapping at the *SlySCR* locus in br1 of the wt. For (**b**) and (**c**) raw read mappings without adjustment of library size are displayed. Text panels in upper left corners indicate genetic background, biological replicate and the range of the coverage plot. Color encoding of transcript and read orientation in (**a**) is maintained throughout (**b**) and (**c**).

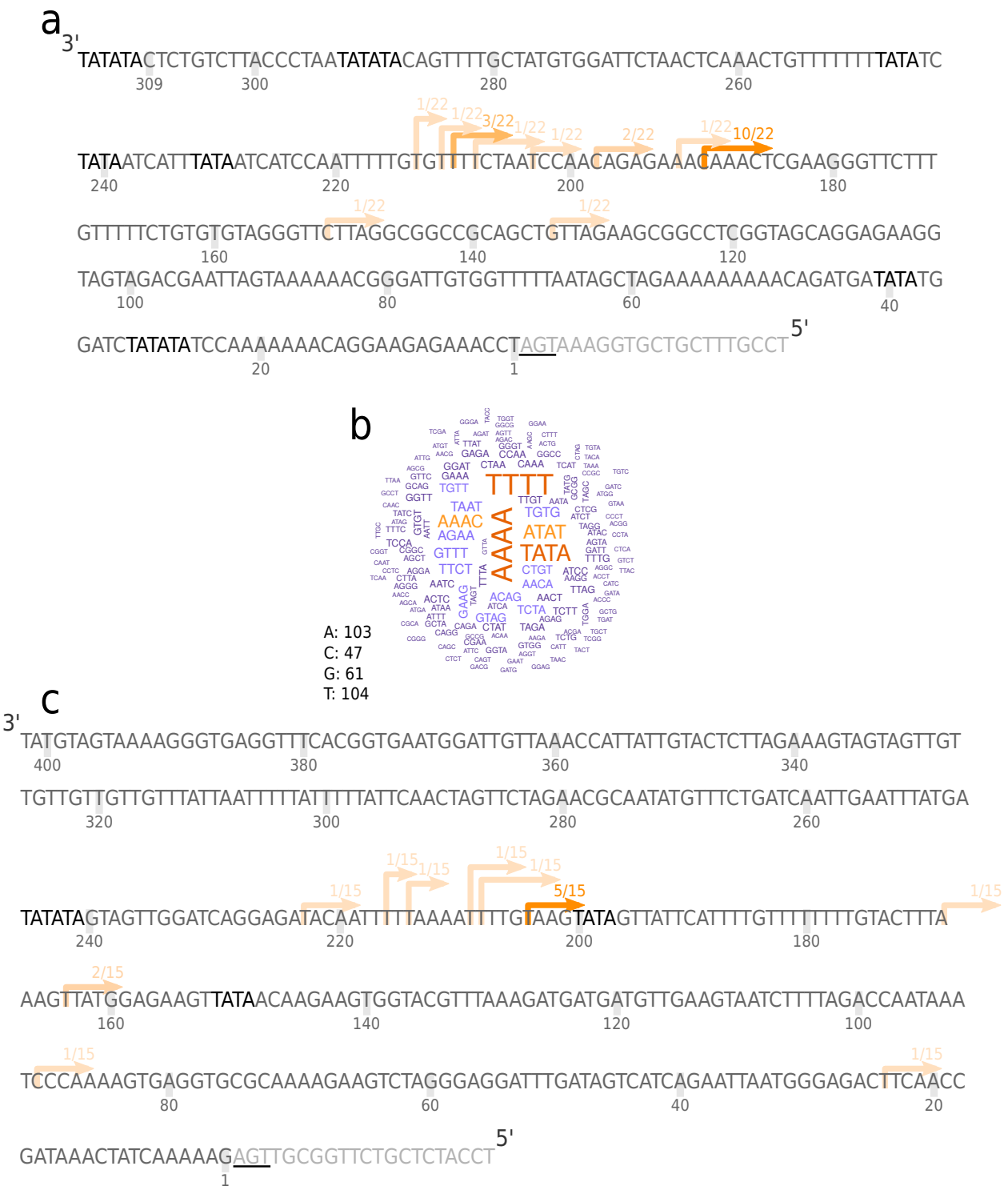


Figure S13: 5′ RACE of *asLAS* and *asLs* transcripts. mRNA sequence of *LAS*/*Ls* antisense transcripts, showing the 5′ UTRs detected with 5′ RACE based on sequenced clones. **a**, *LAS* sense strand in 3′ to 5′ orientation. Displayed are the final codons of the *LAS* CDS in light grey font, the stop codon is underlined. The *LAS* 3′ UTR has a length of 309 bp indicated by positional marks. Orange arrows depict the detected TSSs, with associated frequencies. Black font highlights putative TATA-boxes. **b**, Word cloud representation of a sliding window frequency analysis of 4-mer oligonucleotides in 3′ to 5′ direction of the sequence shown in (**a**) without *LAS* CDS. Table sums up count data for individual bases. **c**, *Ls* sense strand in 3′ to 5′ orientation. Displayed are the final codons of the *Ls* CDS in light grey font, the stop codon is underlined. 402 bp downstream of *Ls* stop are indicated by positional marks. Orange arrows depict the detected TSSs, with associated frequencies. Black font highlights TATA-boxes.

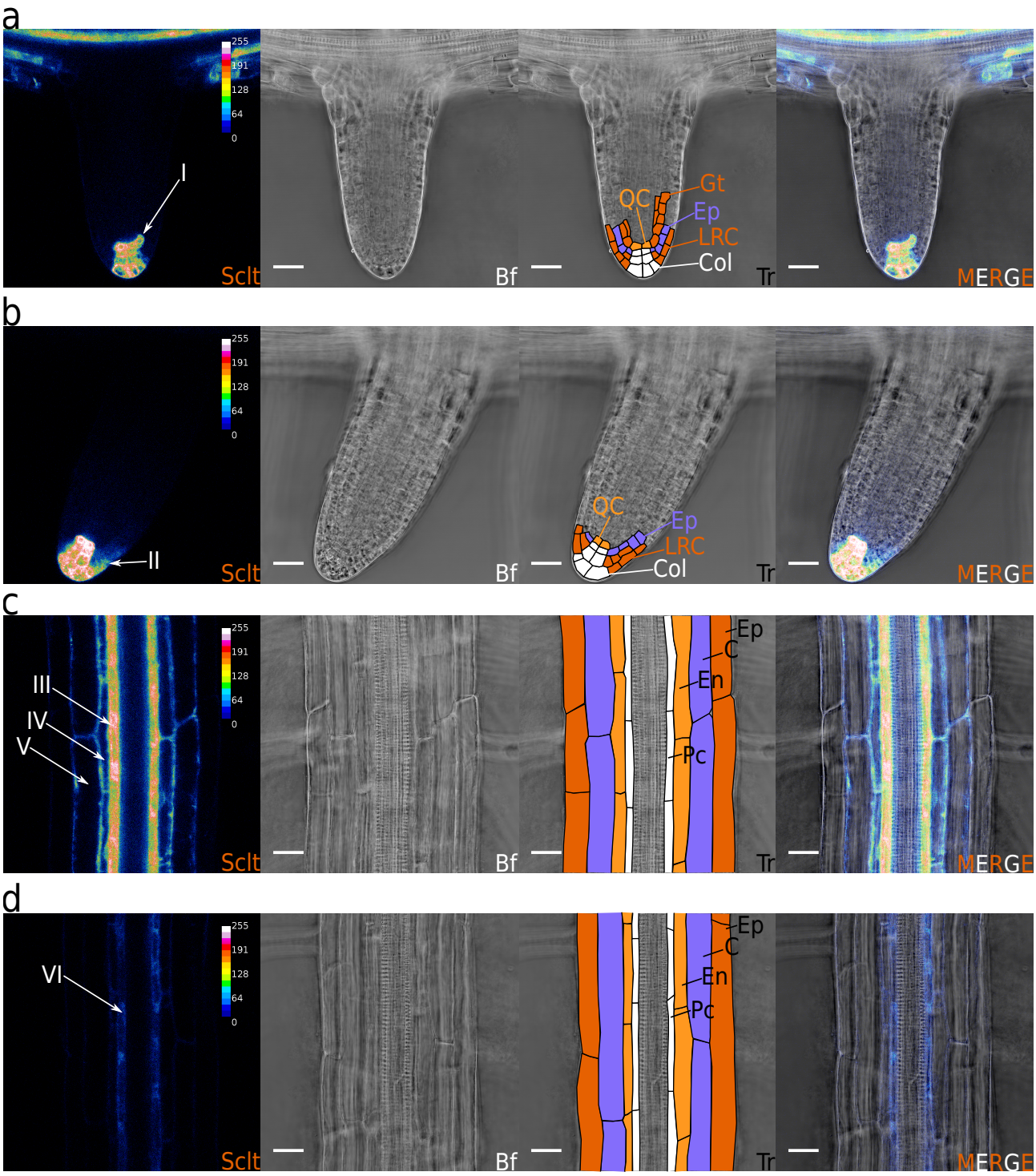


Figure S14: *aspLAS:erSclt* expression in LRs and pericycle/ground tissue cell lineages. (**a**) and (**b**), *aspLAS:erSclt* expression in just emerged LRs from two independent transgenic plants. Expression in QC, CSCs and the columella. Variable asymmetric expression in the ground tissue (arrow I) or the LRC (arrow II). (**a**) and (**b**), *aspLAS:erSclt* expression in the primary root, in areas with differentiated cells. This expression domain displayed variation between different transgenic plants. In (**c**) a transgenic plant with expression in the pericycle (arrow III), the endodermis (arrow IV) and the cortex is shown (arrow V). In (**d**) a transgenic plant with strong *aspLAS:erSclt* signal mainly in the pericycle is displayed (arrow VI). 19 independent T1 *aspLAS:erSclt* plants in the Col-0 background were analyzed, 9-10 days after germination and representative images are displayed in (**a**) to (**d**). FIGURE CONTINUES ON THE NEXT PAGE ...

Figure S14: continued. For (**a**) to (**d**), panels from left to right: Sclt channel with grey value heat map, brightfield (Bf) channel, Bf channel with cell tracings (Tr) , image of merged Sclt and Bf channels. Scale bars at the bottom corners of panels represent 25 μm. Stem cells of different cell lineages were not traced in LRs. C = cortex, Col = columella, En = endodermis, Ep = epidermis, LRC = lateral root cap, Pc = pericycle, QC = quiescent center.

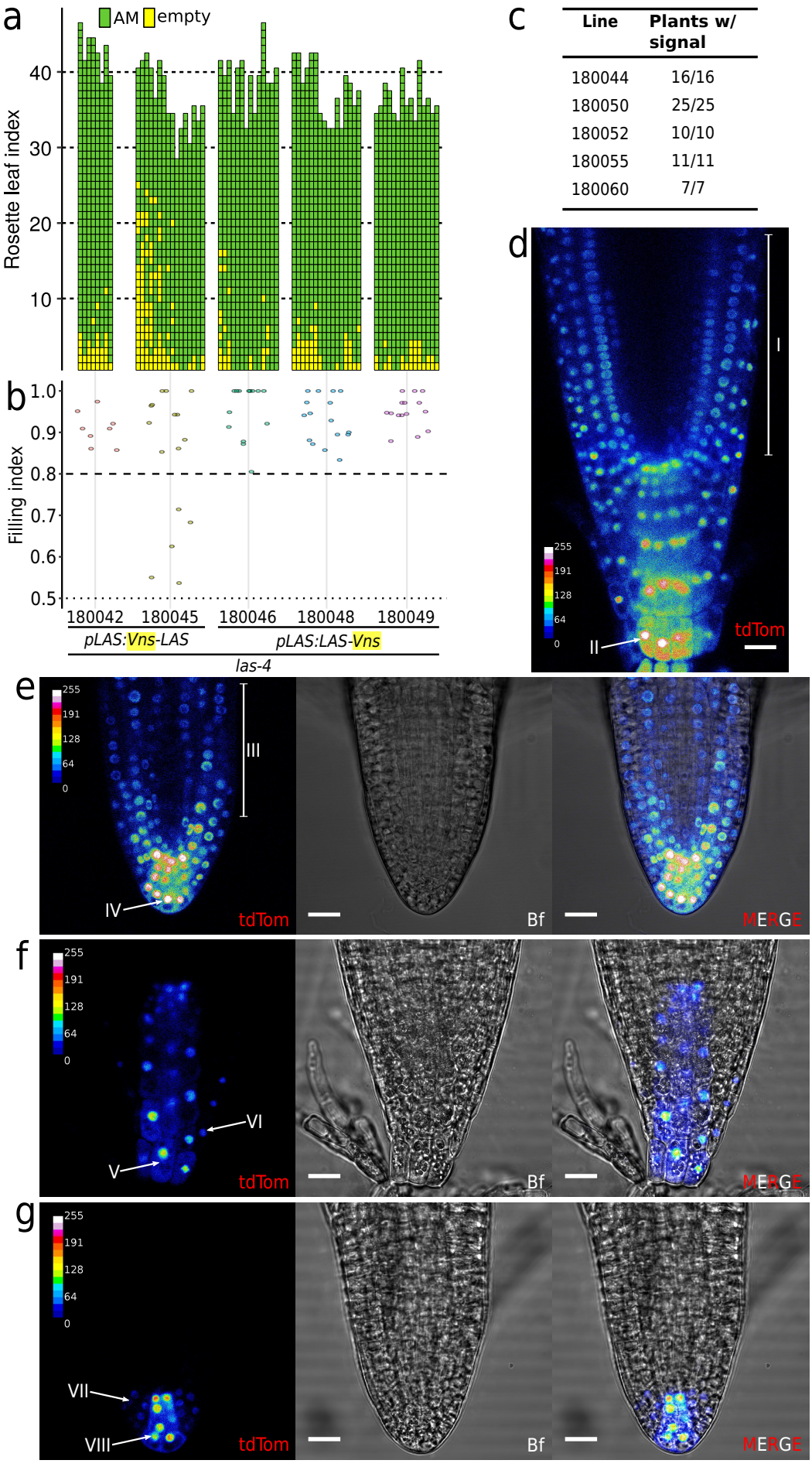


Figure S15: LAS-NLS versions are expressed in endogenous root expression domains. Figure continues on the next page ...

Figure S15: continued. Scoring of axillary bud formation in rosette leaf axils of *las-4* plants in (**a**) and (**b**) and live-imaging of *las-4* plants expressing LAS-NLS versions (**c**) - (**g**). **a**, Scoring plots representing the presence or absence of axillary buds in rosette leaf axils, from the oldest (rosette leaf index = 1) to the youngest rosette leaf. Each column represents an individual plant and each square within a column represents a phytomer with a filled (green) or empty (yellow) leaf axil. **b**, Filling index of plants displayed in (**a**). Circles represent individual plants. The filling index is calculated as the ratio of filled leaf axils over the total number of rosette leaf axils. All plants with a filling index greater than 0.8 (dashed line) were considered as fully complemented. Plants with a filling index between 0.8 and 0.5 (dotted line) were considered as partially complemented. All scored plants were grown at the same time and each number indicates an independent transgenic line. Plants were grown for six weeks under short day conditions. After that period, plants were transferred to long day conditions and scored when the the shoot started to bolt. Plants displayed in (**a**) and (**b**) belong to the same experiment as plants displayed in Fig. 22. **c**, The table summarizes frequency counts of transgene expressing plants for each of the indicated independent lines, based on the detection of fluorescence during live-imaging. Only primary roots and LRs were analyzed. **d**, Primary root tip of a plant from line 180055 (pLAS:tdTom-LAS-NLS). Line I: Ectopic tdTom-LAS-NLS domain in the LRC, epidermis and ground tissue cell lineages. Arrow II: Representative columella cell with tdTom-LAS-NLS signal in the cytosol and the nucleus. **e**, LR tip of a plant from line 180055 (pLAS:tdTom-LAS-NLS). Line III: Ectopic tdTom-LAS-NLS domain in the LRC, epidermis and ground tissue cell lineages. Arrow IV: Representative columella cell with tdTom-LAS-NLS signal in the cytosol and the nucleus. **f**, Primary root tip of a plant from line 180050 (pLAS:tdTom-LAS-NLS). Arrow V: Representative columella cell with tdTom-LAS-NLS signal in the cytosol and the nucleus. Arrow VI: Representative LRC cell with tdTom-LAS-NLS signal restricted to the nucleus. **g**, LR tip of a plant from line 180050 (pLAS:tdTom-LAS-NLS). Arrow VII: Representative LRC cell with tdTom-LAS-NLS signal restricted to the nucleus. Arrow VIII: Representative columella cell with tdTom-LAS-NLS signal in the cytosol and the nucleus. For (**c**) to (**g**), plants were imaged 7-10 days after germination and representative images were chose for display. For (**d**) to (**g**), panels from left to right: tdTom channel with grey value heat map, brightfield (Bf) channel, and image of merged tdTom and Bf channels. Scale bars at the bottom corners of panels represent 19 μm.

Figure	Test	Model	p values	Biological replicate	Genotype/ Line	PR (n)	LR (n)	Sum PR (n)	Sum LR (n)
9c	two-way ANOVA	$Pty_{\mathbf{LRBA}} = Gty + br + Gty \times br$	$p(Gty) < 2e^{-16}$ $p(br) = 0.09692$ $p(Gty \times br) = 0.66903$	1	Col-0	30	909	84	2420
					las-4	18	523		
				2	Col-0	17	439		
					las-4	19	549		
9e	two-way ANOVA	$Pty_{\mathbf{gravitropic\ index}} = Gty + br + Gty \times br$	$p(Gty) < 2e^{-16}$ $p(br) = 0.010375$ $p(Gty \times br) = 0.003007$	see Fig. 9c	see Fig. 9c	see Fig. 9c	see Fig. 9c	see Fig. 9c	see Fig. 9c
9g	two-way ANOVA	$Pty_{\mathbf{width}} = Gty + br + Gty \times br$	$p(Gty) = 0.0004051$ $p(br) = 0.0391648$ $p(Gty \times br) = 0.7215274$	see Fig. 9c	see Fig. 9c	see Fig. 9c	see Fig. 9c	see Fig. 9c	see Fig. 9c
10b	two-way ANOVA	$Pty_{\mathbf{growth\ angle\ profile}} = Gty + catg + Gty \times catg$	$p(Gty) < 2e^{-16}$ $p(br) < 2e^{-16}$ $p(Gty \times catg) = 0.05138$	see Fig. 9c	see Fig. 9c	see Fig. 9c	see Fig. 9c	see Fig. 9c	see Fig. 9c
12a	two-way ANOVA	$Pty_{\mathbf{pri_length}} = line + trmt + line \times trmt$	$p(line) = 2.005e^{-09}$ $p(trmt) < 2e^{-16}$ $p(line \times trmt) = 8.044e^{-06}$	1	Col-0, 140260	25 on DMSO	245 on DMSO	225	2275
					Col-0, 170261	26 on DMSO	271 on DMSO		
					Col-0, 170262	22 on DMSO	187 on DMSO		
					Col-0, 170263	24 on DMSO	244 on DMSO		
					Col-0, 170264	22 on DMSO	206 on DMSO		
					Col-0, 140260	22 on βE	207 on βE		
					Col-0, 170261	20 on βE	236 on βE		
					Col-0, 170262	21 on βE	217 on βE		
					Col-0, 170263	23 on βE	268 on βE		
					Col-0, 170264	20 on βE	194 on βE		

Figure S16: Summary statistics. FIGURE CONTINUES ON THE NEXT PAGE ...

Figure	Test	Model	p values	Biological replicate	Genotype/ Line	PR (n)	LR (n)	Sum PR (n)	Sum LR (n)
12b	two-way ANOVA	$Pty_{\mathbf{root_sys_length}} = line + trmt + line \times trmt$	p(line) = 0.0002355 p(trmt) = $1.33e^{-13}$ p(line × trmt) = 0.1560775	1	see Fig. 12a	see Fig. 12a	see Fig. 12a	see Fig. 12a	see Fig. 12a
12c	two-way ANOVA	$Pty_{\mathbf{lat_length}} = line + trmt + line \times trmt$	p(line) = 0.001986 p(trmt) = $2.327e^{-06}$ p(line × trmt) = 0.706855	1	see Fig. 12a	see Fig. 12a	see Fig. 12a	see Fig. 12a	see Fig. 12a
12d	two-way ANOVA	$Pty_{\mathbf{gr_pr_5_7}} = line + trmt + line \times trmt$	p(line) < $2e^{-16}$ p(trmt)< $2e^{-16}$ p(line × trmt) = 0.9605	1	see Fig. 12a	see Fig. 12a	see Fig. 12a	see Fig. 12a	see Fig. 12a
12e	two-way ANOVA	$Pty_{\mathbf{gr_pr_7_10}} = line + trmt + line \times trmt$	p(line) = $9.22e^{-07}$ p(trmt)< $2e^{-16}$ p(line × trmt) = 0.001255	1	see Fig. 12a	see Fig. 12a	see Fig. 12a	see Fig. 12a	see Fig. 12a
12f	two-way ANOVA	$Pty_{\mathbf{gr_pr_10_12}} = line + trmt + line \times trmt$	p(line) = 0.0074656 p(trmt)< $2e^{-16}$ p(line × trmt) = 0.0009691	1	see Fig. 12a	see Fig. 12a	see Fig. 12a	see Fig. 12a	see Fig. 12a
12g	two-way ANOVA	$Pty_{\mathbf{gr_pr_12_14}} = line + trmt + line \times trmt$	p(line) = 0.0001974 p(trmt)< $2e^{-16}$ p(line × trmt) = 0.0004744	1	see Fig. 12a	see Fig. 12a	see Fig. 12a	see Fig. 12a	see Fig. 12a
12h	two-way ANOVA	$Pty_{\mathbf{gr_rs_12_14}} = line + trmt + line \times trmt$	p(line) = 0.4735 p(trmt) = $7.965e^{-14}$ p(line × trmt) = 0.6766	1	see Fig. 12a	see Fig. 12a	see Fig. 12a	see Fig. 12a	see Fig. 12a
12i	two-way ANOVA	$Pty_{\mathbf{gr_lr_12_14}} = line + trmt + line \times trmt$	p(line) = 0.2583 p(trmt) = 3.976^{-08} p(line × trmt) = 0.7538	1	see Fig. 12a	see Fig. 12a	see Fig. 12a	see Fig. 12a	see Fig. 12a

Figure S16: continued. FIGURE CONTINUES ON THE NEXT PAGE ...

Figure	Test	Model	p values	Biological replicate	Genotype/ Line	PR (n)	LR (n)	Sum PR (n)	Sum LR (n)
13a	two-way ANOVA	$\text{Pty}_{\textbf{LR_N}} = \text{line} + \text{trmt} + \text{line} \times \text{trmt}$	p(line) = 0.2579 p(trmt) = 0.1426 p(line × trmt) = 0.7796	1	see Fig. 12a	see Fig. 12a	see Fig. 12a	see Fig. 12a	see Fig. 12a
13b	two-way ANOVA	$\text{Pty}_{\textbf{lat_density}} = \text{line} + \text{trmt} + \text{line} \times \text{trmt}$	p(line) = $3.220e^{-05}$ p(trmt) < $2e^{-16}$ p(line × trmt) = $7.035e^{-05}$	1	see Fig. 12a	see Fig. 12a	see Fig. 12a	see Fig. 12a	see Fig. 12a
13c	two-way ANOVA	$\text{Pty}_{\textbf{interbranch_dist_mean}} = \text{line} + \text{trmt} + \text{line} \times \text{trmt}$	p(line) = 0.1609 p(trmt) = $6.31e^{-06}$ p(line × trmt) = 0.1239	1	see Fig. 12a	see Fig. 12a	see Fig. 12a	see Fig. 12a	see Fig. 12a
13d	two-way ANOVA	$\text{Pty}_{\textbf{Distance_apical_LR}} = \text{line} + \text{trmt} + \text{line} \times \text{trmt}$	p(line) = $5.363e^{-05}$ p(trmt)< $2e^{-16}$ p(line × trmt) = $2.272e^{-07}$	1	see Fig. 12a	see Fig. 12a	see Fig. 12a	see Fig. 12a	see Fig. 12a
14a	two-way ANOVA	$\text{Pty}_{\textbf{LRBA}} = \text{line} + \text{trmt} + \text{line} \times \text{trmt}$	p(line) = 0.4794683 p(trmt) = $2.206e^{-10}$ p(line × trmt) = 0.0001697	1	see Fig. 12a	see Fig. 12a	see Fig. 12a	see Fig. 12a	see Fig. 12a
14b-d	two-way ANOVA	$\text{Pty}_{\textbf{growth angle profile}} = \text{line} + \text{trmt} + \text{line} \times \text{trmt}$	p(line) < $2e^{-16}$ p(trmt)< $2e^{-16}$ p(line × trmt) = $1.365e^{-13}$	1	see Fig. 12a	see Fig. 12a	see Fig. 12a	see Fig. 12a	see Fig. 12a

Figure S16: continued. FIGURE CONTINUES ON THE NEXT PAGE ...

Figure	Test	Model	p values	Biological replicate	Genotype/ Line	PR (n)	LR (n)	Sum PR (n)	Sum LR (n)
16c-f	n/a	n/a	n/a	1	Col-0, 170261	12 on DMSO	n/a	151	n/a
					Col-0, 170262	18 on DMSO			
					Col-0, 170263	21 on DMSO			
					Col-0, 170264	18 on DMSO			
					Col-0, 170261	18 on βE			
					Col-0, 170262	21 on βE			
					Col-0, 170263	24 on βE			
					Col-0, 170264	19 on βE			
17d	one-way ANOVA	$\text{Pty}_{\mathbf{\Delta avgAbsAng}} = \text{Gty}$	$p(\text{Gty}) = 0.004367$	1, 2, 3	AmB	18 at 10 DAG	300 at 10 DAG	59	634 at 10 DAG 1149 at 16 DAG
				1, 2, 3	*ls-1*	22 at 10 DAG	190 at 10 DAG		
				3	*ls-1 CosG*	6 at 10 DAG	44 at 10 DAG		
				3	*ls-1 GSET4*	7 at 10 DAG	53 at 10 DAG		
				2	*ls-1 GSET6*	6 at 10 DAG	47 at 10 DAG		
				1, 2, 3	AmB	18 at 16 DAG	485 at 16 DAG		
				1, 2, 3	*ls-1*	22 at 16 DAG	401 at 16 DAG		
				3	*ls-1 CosG*	6 at 16 DAG	63 at 16 DAG		
				3	*ls-1 GSET4*	7 at 16 DAG	119 at 16 DAG		
				2	*ls-1 GSET6*	6 at 16 DAG	81 at 16 DAG		
17e	two-way ANOVA	$\text{Pty}_{\mathbf{\Delta avgAbsAng}} = \text{Gty} + \text{ti_po} + \text{Gty} \times \text{ti_po}$	$p(\text{Gty}) < 2e^{-16}$ $p(\text{ti_po}) < 2e^{-16}$ $p(\text{Gty} \times \text{ti_po}) = 0.01474$	see Fig. 17d	see Fig. 17d	see Fig. 17d	see Fig. 17d	see Fig. 17d	see Fig. 17d
17f	two-way ANOVA	$\text{Pty}_{\mathbf{LRBA}} = \text{Gty} + \text{ti_po} + \text{Gty} \times \text{ti_po}$	$p(\text{Gty}) = 6.385e^{-07}$ $p(\text{ti_po}) = 0.0006133$ $p(\text{Gty} \times \text{ti_po}) = 0.9437882$	see Fig. 17d	see Fig. 17d	see Fig. 17d	see Fig. 17d	see Fig. 17d	see Fig. 17d

Figure S16: continued. FIGURE CONTINUES ON THE NEXT PAGE ...

Figure	Test	Model	p values	Biological replicate	Genotype/ Line	PR (n)	LR (n)	Sum PR (n)	Sum LR (n)
18a	two-way ANOVA	$\mathrm{Pty}_{\mathbf{Growth\ rate}} = \mathrm{Gty} + \mathrm{ti_po} + \mathrm{Gty} \times \mathrm{ti_po}$	$p(\mathrm{Gty}) = 2.374e^{-14}$ $p(\mathrm{ti_po}) = 0.0004197$ $p(\mathrm{Gty} \times \mathrm{ti_po}) = 0.2455955$	see Fig. 17d	see Fig. 17d	see Fig. 17d	see Fig. 17d	see Fig. 17d	see Fig. 17d
18b	two-way ANOVA	$\mathrm{Pty}_{\mathbf{LR\ number}} = \mathrm{Gty} + \mathrm{ti_po} + \mathrm{Gty} \times \mathrm{ti_po}$	$p(\mathrm{Gty}) = 8.764ee^{-16}$ $p(\mathrm{ti_po}) < 2e^{-16}$ $p(\mathrm{Gty} \times \mathrm{ti_po}) = 0.1639$	see Fig. 17d	see Fig. 17d	see Fig. 17d	see Fig. 17d	see Fig. 17d	see Fig. 17d
18c	two-way ANOVA	$\mathrm{Pty}_{\mathbf{LR\ density}} = \mathrm{Gty} + \mathrm{ti_po} + \mathrm{Gty} \times \mathrm{ti_po}$	$p(\mathrm{Gty}) = 1.645ee^{-05}$ $p(\mathrm{ti_po}) < 2e^{-16}$ $p(\mathrm{Gty} \times \mathrm{ti_po}) = 0.04863$	see Fig. 17d	see Fig. 17d	see Fig. 17d	see Fig. 17d	see Fig. 17d	see Fig. 17d
19b	two-way ANOVA	$\mathrm{Pty}_{\mathbf{ga}_g} = \mathrm{Gty} + \mathrm{ti_po} + \mathrm{Gty} \times \mathrm{ti_po}$	$p(\mathrm{Gty}) = 9.063e^{-05}$ $p(\mathrm{ti_po}) = 0.07433$ $p(\mathrm{Gty} \times \mathrm{ti_po}) = 0.35224$	1, 2, 3	AmB *ls-1*	20 20	199 at 7 DAG 226 at 9 DAG 284 at 11 DAG 167 at 7 DAG 170 at 9 DAG 175 at 11 DAG	40	366 at 7 DAG 396 at 9 DAG 459 at 11 DAG
19c	two-way ANOVA	$\mathrm{Pty}_{\mathbf{ga}_{float}} = \mathrm{Gty} + \mathrm{ti_po} + \mathrm{Gty} \times \mathrm{ti_po}$	$p(\mathrm{Gty}) = 0.7644$ $p(\mathrm{ti_po}) < 2.2e^{-16}$ $p(\mathrm{Gty} \times \mathrm{ti_po}) = 7.038e^{-05}$	see Fig. 19b	see Fig.19b	see Fig. 19b	see Fig.19b	see Fig. 19b	see Fig. 19b
19d	two-way ANOVA	$\mathrm{Pty}_{\mathbf{Growth\ rate}} = \mathrm{Gty} + \mathrm{ti_po} + \mathrm{Gty} \times \mathrm{ti_po}$	$p(\mathrm{Gty}) = 0.001161$ $p(\mathrm{ti_po}) = 0.514510$ $p(\mathrm{Gty} \times \mathrm{ti_po}) = 0.107850$	see Fig. 19b	see Fig.19b	see Fig. 19b	see Fig.19b	see Fig. 19b	see Fig. 19b
19e	two-way ANOVA	$\mathrm{Pty}_{\mathbf{LRBA}} = \mathrm{Gty} + \mathrm{ti_po} + \mathrm{Gty} \times \mathrm{ti_po}$	$p(\mathrm{Gty}) = 7.328e^{-11}$ $p(\mathrm{ti_po}) = 0.4261$ $p(\mathrm{Gty} \times \mathrm{ti_po}) = 0.3897$	see Fig. 19b	see Fig.19b	see Fig. 19b	see Fig.19b	see Fig. 19b	see Fig. 19b

Figure S16: continued. FIGURE CONTINUES ON THE NEXT PAGE ...

Figure	Test	Model	p values	Biological replicate	Genotype/ Line	PR (n)	LR (n)	Sum PR (n)	Sum LR (n)
19f	two-way ANOVA	$Pty_{\textbf{LR number}} = Gty + ti_po + Gty \times ti_po$	p(Gty) = 0.6259 p(ti_po) = 0.0318372 p(Gty × ti_po) = 0.0993096	see Fig. 19b	see Fig.19b	see Fig. 19b	see Fig.19b	see Fig. 19b	see Fig. 19b
19g	two-way ANOVA	$Pty_{\textbf{LR density}} = Gty + ti_po + Gty \times ti_po$	p(Gty) = 0.0002645 p(ti_po) < $2.2e^{-16}$ p(Gty × ti_po) = $1.462e^{-05}$	see Fig. 19b	see Fig.19b	see Fig. 19b	see Fig.19b	see Fig. 19b	see Fig. 19b
20b	two-way ANOVA	$Pty_{ga_g\ \textbf{LRs east}} = Gty + ti_po + Gty \times ti_po$	p(Gty) < $2.2e^{-16}$ p(ti_po) < $2.2e^{-16}$ p(Gty × ti_po) = $6.857e^{-10}$	1, 2, 3	AmB *ls-1*	20 20	74 at 7 DAG 71 at 7 DAG	40	145
20c	two-way ANOVA	$Pty_{ga_{float}\ \textbf{LRs east}} = Gty + ti_po + Gty \times ti_po$	p(Gty) < $2.2e^{-16}$ p(ti_po) = $2.649e^{-06}$ p(Gty × ti_po) = $5.045e^{-05}$	see Fig. 20b	see Fig. 20b	see Fig. 20b	see Fig. 20b	see Fig. 20b	see Fig. 20b
20d	two-way ANOVA	$Pty_{ga_g\ \textbf{LRs west}} = Gty + ti_po + Gty \times ti_po$	p(Gty) < $2.2e^{-16}$ p(ti_po) = $1.475e^{-15}$ p(Gty × ti_po) = $3.451e^{-12}$	1, 2, 3	AmB *ls-1*	20 20	107 at 7 DAG 75 at 7 DAG	40	182
20e	two-way ANOVA	$Pty_{ga_{float}\ \textbf{LRs west}} = Gty + ti_po + Gty \times ti_po$	p(Gty) < $2.2e^{-16}$ p(ti_po) < $2.2e^{-16}$ p(Gty × ti_po) = $5.224e^{-07}$	see Fig. 20d	see Fig. 20d	see Fig. 20d	see Fig. 20d	see Fig. 20d	see Fig. 20d
S7a	two-way ANOVA	$Pty_{\textbf{Direction root tip}} = line + trmt + line \times trmt$	p(line) = $3.282e^{-05}$ p(trmt) = $1.452e^{-12}$ p(line × trmt) = $6.518e^{-05}$	1	see Fig. 12a	see Fig. 12a	see Fig. 12a	see Fig. 12a	see Fig. 12a
S7b	two-way ANOVA	$Pty_{\textbf{LR growth rate}} = line + trmt + line \times trmt$	p(line) = $3.548e^{-05}$ p(trmt) < $2.2e^{-16}$ p(line × trmt) = $6.175e^{-05}$	1	see Fig. 12a	see Fig. 12a	see Fig. 12a	see Fig. 12a	see Fig. 12a

Figure S16: continued. FIGURE CONTINUES ON THE NEXT PAGE ...

Figure	Test	Model	p values	Biological replicate	Genotype/ Line	PR (n)	LR (n)	Sum PR (n)	Sum LR (n)
S10a	two-way ANOVA	$\text{Pty}_{\textbf{Growth rate LRs east}} = \text{Gty} + \text{ti_po} + \text{Gty} \times \text{ti_po}$	$p(\text{Gty}) = 3.123e^{-14}$ $p(\text{ti_po}) = 0.0001028$ $p(\text{Gty} \times \text{ti_po}) = 0.0037348$	see Fig. 19b	see Fig.20b	see Fig. 20b	see Fig. 20b	see Fig. 20b	see Fig. 20b
S10b	two-way ANOVA	$\text{Pty}_{\textbf{Growth rate LRs west}} = \text{Gty} + \text{ti_po} + \text{Gty} \times \text{ti_po}$	$p(\text{Gty}) = 1.701e^{-06}$ $p(\text{ti_po}) = 0.0001353$ $p(\text{Gty} \times \text{ti_po}) = 0.2466284$	see Fig. 20d	see Fig.20d	see Fig. 20d	see Fig. 20d	see Fig. 20d	see Fig. 20d
S10c	two-way ANOVA	$\text{Pty}_{\textbf{}\Delta\textbf{avgAbsAng LRs east}} = \text{Gty} + \text{ti_po} + \text{Gty} \times \text{ti_po}$	$p(\text{Gty}) < 2.2e^{-16}$ $p(\text{ti_po}) = 6.996e^{-08}$ $p(\text{Gty} \times \text{ti_po}) = 1.760e^{-06}$	see Fig. 20b	see Fig.20b	see Fig. 20b	see Fig. 20b	see Fig. 20b	see Fig. 20b
S10d	two-way ANOVA	$\text{Pty}_{\textbf{}\Delta\textbf{avgAbsAng LRs west}} = \text{Gty} + \text{ti_po} + \text{Gty} \times \text{ti_po}$	$p(\text{Gty}) < 2.2e^{-16}$ $p(\text{ti_po}) = 0.001812$ $p(\text{Gty} \times \text{ti_po}) = 0.041607$	see Fig. 20d	see Fig.20d	see Fig. 20d	see Fig. 20d	see Fig. 20d	see Fig. 20d

Figure S16: continued. Supplementing information for all statistical analysis employed in this thesis. **For a human readable form of this table use the online version available @ Universitäts- und Stadtbibliothek Köln.** The linear statistical model to explain differences in phenotype (Pty), takes the contribution of the genotype (Gty), an additional factor variable (biological replicate, treatment, category or time point) and a possible interaction between Gty and the factor variable into account. PR(n) = number of primary roots analyzed; LR(n) = number of LRs analyzed. catg = category, ti_po = time point, trmt = treatment.

References

Aida, M., Ishida, T., Fukaki, H., Fujisawa, H., and Tasaka, M. Genes involved in organ separation in Arabidopsis: an analysis of the *cup-shaped cotyledon* mutant. *The Plant Cell*, 9(6):841–857, 1997. doi: 10.1105/tpc.9.6.841. URL http://www.plantcell.org/content/9/6/841.

Aida, M., Beis, D., Heidstra, R., Willemsen, V., Blilou, I., Galinha, C., Nussaume, L., Noh, Y.-S., Amasino, R., and Scheres, B. The *PLETHORA* Genes Mediate Patterning of the *Arabidopsis* Root Stem Cell Niche. *Cell*, 119(1):109 – 120, 2004. doi: 10.1016/j.cell.2004.09.018. URL http://www.sciencedirect.com/science/article/pii/S0092867404008931.

Aloni, R., Aloni, E., Langhans, M., and Ullrich, C. I. Role of Cytokinin and Auxin in Shaping Root Architecture: Regulating Vascular Differentiation, Lateral Root Initiation, Root Apical Dominance and Root Gravitropism. *Ann Bot*, 97(5):883–893, May 2006. doi: 10.1093/aob/mcl027. URL http://dx.doi.org/10.1093/aob/mcl027.

Balkunde, R., Kitagawa, M., Xu, X. M., Wang, J., and Jackson, D. SHOOT MERISTEMLESS trafficking controls axillary meristem formation, meristem size and organ boundaries in Arabidopsis. *The Plant Journal*, 90(3):435–446, 2017. doi: 10.1111/tpj.13504. URL https://doi.org/10.1111/tpj.13504.

Banerji, J., Olson, L., and Schaffner, W. A Lymphocyte-Specific Cellular Enhancer is Located Downstream of the Joining Region in Immunoglobulin Heavy Chain Genes. *Cell*, 33(3):729–740, Jul 1983. doi: 10.1016/0092-8674(83)90015-6. URL https://doi.org/10.1016/0092-8674(83)90015-6.

Barbez, E., Dünser, K., Gaidora, A., Lendl, T., and Busch, W. Auxin steers root cell expansion via apoplastic pH regulation in Arabidopsis thaliana. *Proceedings of the National Academy of Sciences*, 2017. doi: 10.1073/pnas.1613499114. URL http://dx.doi.org/10.1073/pnas.1613499114.

Baskin, T. I., Peret, B., Baluska, F., Benfey, P. N., Bennett, M., Forde, B. G., Gilroy, S., Helariutta, Y., Hepler, P. K., Leyser, O., Masson, P. H., Muday, G. K., Murphy, A. S., Poethig, S., Rahman, A., Roberts, K., Scheres, B., Sharp, R. E., and Somerville, C. Shootward and rootward: peak terminology for plant polarity. *Trends in Plant Science*, 15(11):593–594, Nov 2010. doi: 10.1016/j.tplants.2010.08.006. URL https://doi.org/10.1016/j.tplants.2010.08.006.

Benfey, P. N. and Schiefelbein, J. W. Getting to the root of plant development: the genetics of *Arabidopsis* root formation. *Trends in Genetics*, 10(3):84 – 88, 1994. doi: 10.1016/0168-9525(94)90230-5. URL http://dx.doi.org/10.1016/0168-9525(94)90230-5.

Bennett, T. and Scheres, B. Chapter Three - Root Development—Two Meristems for the Price of One? In *Plant Development*, volume 91 of *Current Topics in Developmental Biology*, pages 67 – 102. Academic Press, 2010. doi: 10.1016/S0070-2153(10)91003-X. URL http://www.sciencedirect.com/science/article/pii/S007021531091003X.

Berhin, A., de Bellis, D., Franke, R. B., Buono, R. A., Nowack, M. K., and Nawrath, C. The Root Cap Cuticle: A Cell Wall Structure for Seedling Establishment and Lateral Root Formation. *Cell*, 176(6):1367–1378.e8, Mar 2019. doi: 10.1016/j.cell.2019.01.005. URL https://doi.org/10.1016/j.cell.2019.01.005.

Bleckmann, A., Weidtkamp-Peters, S., Seidel, C. A., and Simon, R. Stem Cell Signaling in Arabidopsis Requires CRN to Localize CLV2 to the Plasma Membrane. *Plant Physiology*, 152(1):166–176, 2010. doi: 10.1104/pp.109.149930. URL http://www.plantphysiol.org/content/152/1/166.

Brady, S. M., Orlando, D. A., Lee, J.-Y., Wang, J. Y., Koch, J., Dinneny, J. R., Mace, D., Ohler, U., and Benfey, P. N. A High-Resolution Root Spatiotemporal Map Reveals Dominant Expression Patterns. *Science*, 318(5851):801–806, 2007. doi: 10.1126/science.1146265. URL https://science.sciencemag.org/content/318/5851/801.

Brand, U., Fletcher, J. C., Hobe, M., Meyerowitz, E. M., and Simon, R. Dependence of Stem Cell Fate in *Arabidopsis* on a Feedback Loop Regulated by *CLV3* Activity. *Science*, 289(5479):617–619, 2000. doi: 10.1126/science.289.5479.617. URL http://science.sciencemag.org/content/289/5479/617.

Brunoud, G., Wells, D. M., Oliva, M., Larrieu, A., Mirabet, V., Burrow, A. H., Beeckman, T., Kepinski, S., Traas, J., Bennett, M. J., and Vernoux, T. A novel sensor to map auxin response and distribution at high spatio-temporal resolution. *Nature*, 482:103 EP –, Jan 2012. doi: 10.1038/nature10791. URL https://doi.org/10.1038/nature10791.

Bubner, B. and Baldwin, I. T. Use of real-time PCR for determining copy number and zygosity in transgenic plants. *Plant Cell Reports*, 23(5):263–271, Nov 2004. doi: 10.1007/s00299-004-0859-y. URL https://doi.org/10.1007/s00299-004-0859-y.

Burian, A., Barbier de Reuille, P., and Kuhlemeier, C. Patterns of Stem Cell Divisions Contribute to Plant Longevity. *Current Biology*, 26(11):1385 – 1394, 2016. doi: https://doi.org/10.1016/j.cub.2016.03.067. URL http://www.sciencedirect.com/science/article/pii/S0960982216303128.

Busch, B. L., Schmitz, G., Rossmann, S., Piron, F., Ding, J., Bendahmane, A., and Theres, K. Shoot Branching and Leaf Dissection in Tomato Are Regulated by Homologous Gene Modules. *The Plant Cell*, 23(10):3595–3609, 2011. doi: 10.1105/tpc.111.087981. URL http://www.plantcell.org/content/23/10/3595.

Carlsbecker, A., Lee, J.-Y., Roberts, C. J., Dettmer, J., Lehesranta, S., Zhou, J., Lindgren, O., Moreno-Risueno, M. A., Vatén, A., Thitamadee, S., Campilho, A., Sebastian, J., Bowman, J. L., Helariutta, Y., and Benfey, P. N. Cell signalling by microRNA165/6 directs gene dose-dependent root cell fate. *Nature*, 465:316 EP –, Apr 2010. doi: 10.1038/nature08977. URL https://doi.org/10.1038/nature08977.

Casimiro, I., Beeckman, T., Graham, N., Bhalerao, R., Zhang, H., Casero, P., Sandberg, G., and Bennett, M. J. Dissecting *Arabidopsis* lateral root development. *Trends in Plant Science*, 8(4):165 – 171, 2003. doi: 10.1016/S1360-1385(03)00051-7. URL http://www.sciencedirect.com/science/article/pii/S1360138503000517.

Chen, X., Yao, Q., Gao, X., Jiang, C., Harberd, N., and Fu, X. Shoot-to-Root Mobile Transcription Factor HY5 Coordinates Plant Carbon and Nitrogen Acquisition. *Current Biology*, 26(5):640–646, Mar 2016. doi: 10.1016/j.cub.2015.12.066. URL https://doi.org/10.1016/j.cub.2015.12.066.

Clark, S. E., Williams, R. W., and Meyerowitz, E. M. The *CLAVATA1* Gene Encodes a Putative Receptor Kinase That Controls Shoot and Floral Meristem Size in Arabidopsis. *Cell*, 89(4):575 – 585, 1997. doi: 10.1016/S0092-8674(00)80239-1. URL http://www.sciencedirect.com/science/article/pii/S0092867400802391.

Clough, S. J. and Bent, A. F. Floral dip: a simplified method for *Agrobacterium*-mediated transformation of *Arabidopsis thaliana*. *The Plant Journal*, 16(6):735–743, 1998. doi: 10.1046/j.1365-313x.1998.00343.x. URL https://onlinelibrary.wiley.com/doi/abs/10.1046/j.1365-313x.1998.00343.x.

Consortium, T. T. G. The tomato genome sequence provides insights into fleshy fruit evolution. *Nature*, 485:635 EP –, May 2012. doi: 10.1038/nature11119. URL https://doi.org/10.1038/nature11119.

Cruz-Ramírez, A., Díaz-Triviño, S., Wachsman, G., Du, Y., Arteága-Vázquez, M., Zhang, H., Benjamins, R., Blilou, I., Neef, A. B., Chandler, V., and Scheres, B. A SCARECROW-RETINOBLASTOMA Protein Network Controls Protective Quiescence in the Arabidopsis Root Stem Cell Organizer. *PLOS Biology*, 11 (11):1–12, Nov 2013. doi: 10.1371/journal.pbio.1001724. URL https://doi.org/10.1371/journal.pbio.1001724.

Cui, H. and Benfey, P. N. Cortex proliferation: Simple phenotype, complex regulatory mechanisms. *Plant Signal Behav*, 4(6):551–553, Jun 2009a. doi: 10.1111/j.1365-313X.2009.03839.x. URL https://www.ncbi.nlm.nih.gov/pubmed/19816127.

Cui, H. and Benfey, P. N. Interplay between SCARECROW, GA and LIKE HETEROCHROMATIN PROTEIN 1 in ground tissue patterning in the Arabidopsis root. *The Plant Journal*, 58(6):1016–1027, 2009b. doi: 10.1111/j.1365-313X.2009.03839.x. URL https://onlinelibrary.wiley.com/doi/abs/10.1111/j.1365-313X.2009.03839.x.

Daum, G., Medzihradszky, A., Suzaki, T., and Lohmann, J. U. A mechanistic framework for noncell autonomous stem cell induction in *Arabidopsis*. *Proceedings of the National Academy of Sciences*, 111(40):14619–14624, 2014. doi: 10.1073/pnas.1406446111. URL http://www.pnas.org/content/111/40/14619.abstract.

Dello Ioio, R., Linhares, F. S., Scacchi, E., Casamitjana-Martinez, E., Heidstra, R., Costantino, P., and Sabatini, S. Cytokinins Determine *Arabidopsis* Root-Meristem Size by Controlling Cell Differentiation. *Current Biology*, 17(8):678 – 682, 2007. doi: 10.1016/j.cub.2007.02.047. URL http://www.sciencedirect.com/science/article/pii/S0960982207010561.

Dello Ioio, R., Nakamura, K., Moubayidin, L., Perilli, S., Taniguchi, M., Morita, M. T., Aoyama, T., Costantino, P., and Sabatini, S. A Genetic Framework for the Control of Cell Division and Differentiation in the Root Meristem. *Science*, 322(5906):1380–1384, 2008. doi: 10.1126/science.1164147. URL https://science.sciencemag.org/content/322/5906/1380.

Delory, B. M., Baudson, C., Brostaux, Y., Lobet, G., du Jardin, P., Pagès, L., and Delaplace, P. archiDART: an R package for the automated computation of plant root architectural traits. *Plant and Soil*, 398(1):351–365, Jan 2016. doi: 10.1007/s11104-015-2673-4. URL https://doi.org/10.1007/s11104-015-2673-4.

Denay, G., Tichtinsky, G., Le Masson, M., Chahtane, H., Huguet, S., Lopez-Vidriero, I., Wenzl, C., Franco-Zorrilla, J.-M., Simon, R., Lohmann, J. U., and Parcy, F. Control of stem-cell niche establishment in Arabidopsis flowers by REVOLUTA and the LEAFY-RAX1 module. *bioRxiv*, 2018. doi: 10.1101/488114. URL https://www.biorxiv.org/content/early/2018/12/06/488114.

Denyer, T., Ma, X., Klesen, S., Scacchi, E., Nieselt, K., and Timmermans, M. C. Spatiotemporal Developmental Trajectories in the *Arabidopsis* Root Revealed Using High-Throughput Single-Cell RNA Sequencing. *Developmental Cell*, 48(6):840 – 852.e5, 2019. doi: 10.1016/j.devcel.2019.02.022. URL http://www.sciencedirect.com/science/article/pii/S1534580719301455.

Deyoung, B. J. and Clark, S. E. BAM receptors regulate stem cell specification and organ development through complex interactions with CLAVATA signaling. *Genetics*, 180(2):895–904, Oct 2008. doi: 10.1534/genetics.108.091108. URL https://www.ncbi.nlm.nih.gov/pubmed/18780746.

DeYoung, B. J., Bickle, K. L., Schrage, K. J., Muskett, P., Patel, K., and Clark, S. E. The CLAVATA1-related BAM1, BAM2 and BAM3 receptor kinase-like proteins are required for meristem function in Arabidopsis. *The Plant Journal*, 45(1):1–16, 2006. doi: 10.1111/j.1365-313X.2005.02592.x. URL https://onlinelibrary.wiley.com/doi/abs/10.1111/j.1365-313X.2005.02592.x.

Di Laurenzio, L., Wysocka-Diller, J., Malamy, J. E., Pysh, L., Helariutta, Y., Freshour, G., Hahn, M. G., Feldmann, K. A., and Benfey, P. N. The *SCARECROW* Gene Regulates an Asymmetric Cell Division That

Is Essential for Generating the Radial Organization of the Arabidopsis Root. *Cell*, 86(3):423–433, Aug 1996. doi: 10.1016/S0092-8674(00)80115-4. URL https://doi.org/10.1016/S0092-8674(00)80115-4.

Di Mambro, R., De Ruvo, M., Pacifici, E., Salvi, E., Sozzani, R., Benfey, P. N., Busch, W., Novak, O., Ljung, K., Di Paola, L., Marée, A. F. M., Costantino, P., Grieneisen, V. A., and Sabatini, S. Auxin minimum triggers the developmental switch from cell division to cell differentiation in the *Arabidopsis* root. *Proceedings of the National Academy of Sciences*, 114(36):E7641–E7649, 2017. doi: 10.1073/pnas.1705833114. URL https://www.pnas.org/content/114/36/E7641.

Di Mambro, R., Svolacchia, N., Ioio, R. D., Pierdonati, E., Salvi, E., Pedrazzini, E., Vitale, A., Perilli, S., Sozzani, R., Benfey, P. N., Busch, W., Costantino, P., and Sabatini, S. The Lateral Root Cap Acts as an Auxin Sink that Controls Meristem Size. *Current Biology*, 29(7):1199 – 1205.e4, 2019. doi: 10.1016/j.cub.2019.02.022. URL http://www.sciencedirect.com/science/article/pii/S0960982219301617.

Digby, J. and Firn, R. D. The gravitropic set-point angle (GSA): the identification of an important developmentally controlled variable governing plant architecture*. *Plant, Cell & Environment*, 18(12):1434–1440, 1995. doi: 10.1111/j.1365-3040.1995.tb00205.x. URL https://onlinelibrary.wiley.com/doi/abs/10.1111/j.1365-3040.1995.tb00205.x.

Dolan, L., Janmaat, K., Willemsen, V., Linstead, P., Poethig, S., Roberts, K., and Scheres, B. Cellular organisation of the *Arabidopsis thaliana* root. *Development*, 119(1):71–84, 1993. URL http://dev.biologists.org/content/119/1/71.

Donnelly, M. L. L., Luke, G., Mehrotra, A., Li, X., Hughes, L. E., Gani, D., and Ryan, M. D. Analysis of the aphthovirus 2A/2B polyprotein 'cleavage' mechanism indicates not a proteolytic reaction, but a novel translational effect: a putative ribosomal 'skip'. *Journal of General Virology*, 82(5):1013–1025, 2001. doi: 10.1099/0022-1317-82-5-1013. URL http://jgv.microbiologyresearch.org/content/journal/jgv/10.1099/0022-1317-82-5-1013.

Drapek, C., Sparks, E. E., and Benfey, P. N. Uncovering Gene Regulatory Networks Controlling Plant Cell Differentiation. *Trends in Genetics*, 33(8):529 – 539, 2017. doi: 10.1016/j.tig.2017.05.002. URL http://www.sciencedirect.com/science/article/pii/S0168952517300835.

Edwards, K., Johnstone, C., and Thompson, C. A simple and rapid method for the preparation of plant genomic DNA for PCR analysis. *Nucleic acids research*, 19(6):1349–1349, Mar 1991. doi: 10.1093/nar/19.6.1349. URL https://www.ncbi.nlm.nih.gov/pubmed/2030957.

Eshed, Y. and Zamir, D. An introgression line population of Lycopersicon pennellii in the cultivated tomato enables the identification and fine mapping of yield-associated QTL. *Genetics*, 141(3):1147–1162, 1995. URL https://www.genetics.org/content/141/3/1147.

Evans, M. L. Gravitropism: Interaction of Sensitivity Modulation and Effector Redistribution. *Plant Physiology*, 95(1):1–5, 1991. doi: 10.1104/pp.95.1.1. URL http://www.plantphysiol.org/content/95/1/1.

Fambrini, M., Salvini, M., and Pugliesi, C. Molecular cloning, phylogenetic analysis, and expression patterns of *LATERAL SUPPRESSOR-LIKE* and *REGULATOR OF AXILLARY MERISTEM FORMATION-LIKE* genes in sunflower (*Helianthus annuus* L.). *Development Genes and Evolution*, 227(2):159–170, Mar 2017. doi: 10.1007/s00427-016-0571-2. URL https://doi.org/10.1007/s00427-016-0571-2.

Fletcher, J. C., Brand, U., Running, M. P., Simon, R., and Meyerowitz, E. M. Signaling of Cell Fate Decisions by *CLAVATA3* in *Arabidopsis* Shoot Meristems. *Science*, 283(5409):1911–1914, 1999. doi: 10.1126/science.283.5409.1911. URL http://science.sciencemag.org/content/283/5409/1911.

Forzani, C., Aichinger, E., Sornay, E., Willemsen, V., Laux, T., Dewitte, W., and Murray, J. WOX5 Suppresses *CYCLIN D* Activity to Establish Quiescence at the Center of the Root Stem Cell Niche. *Current Biology*, 24(16):1939 – 1944, 2014. doi: 10.1016/j.cub.2014.07.019. URL http://www.sciencedirect.com/science/article/pii/S0960982214008458.

Fukaki, H., Wysocka-Diller, J., Kato, T., Fujisawa, H., Benfey, P. N., and Tasaka, M. Genetic evidence that the endodermis is essential for shoot gravitropism in *Arabidopsis thaliana*. *The Plant Journal*, 14(4):425–430, 1998. doi: 10.1046/j.1365-313X.1998.00137.x. URL https://onlinelibrary.wiley.com/doi/abs/10.1046/j.1365-313X.1998.00137.x.

Galinha, C., Hofhuis, H., Luijten, M., Willemsen, V., Blilou, I., Heidstra, R., and Scheres, B. PLETHORA proteins as dose-dependent master regulators of *Arabidopsis* root development. *Nature*, 449:1053 EP –, Oct 2007. doi: 10.1038/nature06206. URL https://doi.org/10.1038/nature06206.

Galkovskyi, T., Mileyko, Y., Bucksch, A., Moore, B., Symonova, O., Price, C. A., Topp, C. N., Iyer-Pascuzzi, A. S., Zurek, P. R., Fang, S., Harer, J., Benfey, P. N., and Weitz, J. S. GiA Roots: software for the high throughput analysis of plant root system architecture. *BMC Plant Biology*, 12(1):116, Jul 2012. doi: 10.1186/1471-2229-12-116. URL https://doi.org/10.1186/1471-2229-12-116.

Gallagher, K. L. and Benfey, P. N. Both the conserved GRAS domain and nuclear localization are required for SHORT-ROOT movement. *The Plant Journal*, 57(5):785–797, 2009. doi: 10.1111/j.1365-313X.2008.03735.x. URL https://onlinelibrary.wiley.com/doi/abs/10.1111/j.1365-313X.2008.03735.x.

Gallagher, K. L., Paquette, A. J., Nakajima, K., and Benfey, P. N. Mechanisms Regulating SHORT-ROOT Intercellular Movement. *Current Biology*, 14(20):1847 – 1851, 2004. doi: 10.1016/j.cub.2004.09.081. URL https://doi.org/10.1016/j.cub.2004.09.081.

Galvan-Ampudia, C., Julkowska, M., Darwish, E., Gandullo, J., Korver, R., Brunoud, G., Haring, M., Munnik, T., Vernoux, T., and Testerink, C. Halotropism Is a Response of Plant Roots to Avoid a Saline Environment. *Current Biology*, 23(20):2044–2050, Oct 2013. doi: 10.1016/j.cub.2013.08.042. URL https://doi.org/10.1016/j.cub.2013.08.042.

Głowacka, K., Kromdijk, J., Leonelli, L., Niyogi, K. K., Clemente, T. E., and Long, S. P. An evaluation of new and established methods to determine T-DNA copy number and homozygosity in transgenic plants. *Plant Cell Environ*, 39(4):908–917, Apr 2016. doi: 10.1111/pce.12693. URL http://dx.doi.org/10.1111/pce.12693.

Goh, T., Toyokura, K., Wells, D. M., Swarup, K., Yamamoto, M., Mimura, T., Weijers, D., Fukaki, H., Laplaze, L., Bennett, M. J., and Guyomarc'h, S. Quiescent center initiation in the *Arabidopsis* lateral root primordia is dependent on the *SCARECROW* transcription factor. *Development*, 143(18):3363–3371, 2016. doi: 10.1242/dev.135319. URL http://dev.biologists.org/content/143/18/3363.

Goldshmidt, A., Alvarez, J. P., Bowman, J. L., and Eshed, Y. Signals Derived from *YABBY* Gene Activities in Organ Primordia Regulate Growth and Partitioning of *Arabidopsis* Shoot Apical Meristems. *The Plant Cell*, 20(5):1217–1230, 2008. doi: 10.1105/tpc.107.057877. URL http://www.plantcell.org/content/20/5/1217.

Gong, X., Flores-Vergara, M. A., Hong, J. H., Chu, H., Lim, J., Franks, R. G., Liu, Z., and Xu, J. SEUSS Integrates Gibberellin Signaling with Transcriptional Inputs from the SHR-SCR-SCL3 Module to Regulate Middle Cortex Formation in the Arabidopsis Root. *Plant Physiology*, 170(3):1675–1683, 2016. doi: 10.1104/pp.15.01501. URL http://www.plantphysiol.org/content/170/3/1675.

Greb, T. *Untersuchungen zur Rolle des Gens LATERAL SUPPRESSOR in der Seitentriebentwicklung von Arabidopsis thaliana H. und der Tomate (Lycopersicon esculentum M.)*. PhD thesis, Universität zu Köln, 2003. URL https://kups.ub.uni-koeln.de/681/1/11w1421.pdf.

Greb, T., Clarenz, O., Schäfer, E., Müller, D., Herrero, R., Schmitz, G., and Theres, K. Molecular analysis of the *LATERAL SUPPRESSOR* gene in *Arabidopsis* reveals a conserved control mechanism for axillary meristem formation. *Genes & Development*, 17(9):1175–1187, 2003. doi: 10.1101/gad.260703. URL http://genesdev.cshlp.org/content/17/9/1175.abstract.

Guo, Y., Han, L., Hymes, M., Denver, R., and Clark, S. E. CLAVATA2 forms a distinct CLE-binding receptor complex regulating Arabidopsis stem cell specification. *The Plant Journal*, 63(6):889–900, 2010. doi: 10.1111/j.1365-313X.2010.04295.x. URL https://onlinelibrary.wiley.com/doi/abs/10.1111/j.1365-313X.2010.04295.x.

Haecker, A., Groß-Hardt, R., Geiges, B., Sarkar, A., Breuninger, H., Herrmann, M., and Laux, T. Expression dynamics of *WOX* genes mark cell fate decisions during early embryonic patterning in *Arabidopsis thaliana*. *Development*, 131(3):657–668, 2004. doi: 10.1242/dev.00963. URL http://dev.biologists.org/content/131/3/657.

Hall, T. A. et al. BioEdit: a user-friendly biological sequence alignment editor and analysis program for Windows 95/98/NT. 1999.

Hanahan, D. Studies on transformation of *Escherichia coli* with plasmids. *Journal of Molecular Biology*, 166 (4):557 – 580, 1983. doi: 10.1016/S0022-2836(83)80284-8. URL http://www.sciencedirect.com/science/article/pii/S0022283683802848.

Heidstra, R. and Sabatini, S. Plant and animal stem cells: similar yet different. *Nature Reviews Molecular Cell Biology*, 15:301 EP –, Apr 2014. doi: 10.1038/nrm3790. URL https://doi.org/10.1038/nrm3790.

Helariutta, Y., Fukaki, H., Wysocka-Diller, J., Nakajima, K., Jung, J., Sena, G., Hauser, M.-T., and Benfey, P. N. The *SHORT-ROOT* Gene Controls Radial Patterning of the *Arabidopsis* Root through Radial Signaling. *Cell*, 101(5):555 – 567, 2000. doi: 10.1016/S0092-8674(00)80865-X. URL http://www.sciencedirect.com/science/article/pii/S009286740080865X.

Hisanaga, T., Okahashi, K., Yamaoka, S., Kajiwara, T., Nishihama, R., Shimamura, M., Yamato, K. T., Bowman, J. L., Kohchi, T., and Nakajima, K. A *cis*-acting bidirectional transcription switch controls sexual dimorphism in the liverwort. *The EMBO Journal*, 38(6), 2019. doi: 10.15252/embj.2018100240. URL http://emboj.embopress.org/content/38/6/e100240.

Hobert, O. Gene Regulation: Enhancers Stepping Out of the Shadow. *Current Biology*, 20(17):R697 – R699, 2010. doi: 10.1016/j.cub.2010.07.035. URL http://www.sciencedirect.com/science/article/pii/S0960982210009371.

Hong, S. H., Kim, H. J., Ryu, J. S., Choi, H., Jeong, S., Shin, J., Choi, G., and Nam, H. G. CRY1 inhibits COP1-mediated degradation of BIT1, a MYB transcription factor, to activate blue light-dependent gene expression in Arabidopsis. *The Plant Journal*, 55(3):361–371, 2008. doi: 10.1111/j.1365-313X.2008.03508.x. URL https://onlinelibrary.wiley.com/doi/abs/10.1111/j.1365-313X.2008.03508.x.

Horstman, A., Willemsen, V., Boutilier, K., and Heidstra, R. AINTEGUMENTA-LIKE proteins: hubs in a plethora of networks. *Trends in Plant Science*, 19(3):146 – 157, 2014. doi: 10.1016/j.tplants.2013.10.010. URL http://www.sciencedirect.com/science/article/pii/S1360138513002513.

Ikeda, Y., Banno, H., Niu, Q.-W., Chua, N.-H., and Howell, S. H. The *ENHANCER OF SHOOT REGENERATION 2* gene in *Arabidopsis* Regulates *CUP-SHAPED COTYLEDON 1* at the Transcriptional Level and Controls Cotyledon Development . *Plant and Cell Physiology*, 47(11):1443–1456, Nov 2006. doi: 10.1093/pcp/pcl023. URL https://doi.org/10.1093/pcp/pcl023.

Jeifetz, D., David-Schwartz, R., Borovsky, Y., and Paran, I. *CaBLIND* regulates axillary meristem initiation and transition to flowering in pepper. *Planta*, 234(6):1227–1236, Dec 2011. doi: 10.1007/s00425-011-1479-8. URL https://doi.org/10.1007/s00425-011-1479-8.

Jeong, S., Trotochaud, A. E., and Clark, S. E. The Arabidopsis *CLAVATA2* Gene Encodes a Receptor-like Protein Required for the Stability of the *CLAVATA1* Receptor-like Kinase. *The Plant Cell*, 11(10):1925–1933, 1999. doi: 10.1105/tpc.11.10.1925. URL http://www.plantcell.org/content/11/10/1925.

Jürgens, G. Axis Formation in Plant Embryogenesis: Cues and Clues. *Cell*, 81(4):467–470, 1995. doi: 10.1016/0092-8674(95)90065-9. URL http://dx.doi.org/10.1016/0092-8674(95)90065-9.

Kamiya, T., Borghi, M., Wang, P., Danku, J. M. C., Kalmbach, L., Hosmani, P. S., Naseer, S., Fujiwara, T., Geldner, N., and Salt, D. E. The MYB36 transcription factor orchestrates Casparian strip formation. *Proceedings of the National Academy of Sciences*, 112(33):10533–10538, 2015. doi: 10.1073/pnas.1507691112. URL https://www.pnas.org/content/112/33/10533.

Kasschau, K. D., Xie, Z., Allen, E., Llave, C., Chapman, E. J., Krizan, K. A., and Carrington, J. C. P1/HC-Pro, a Viral Suppressor of RNA Silencing, Interferes with *Arabidopsis* Development and miRNA Function. *Developmental Cell*, 4(2):205 – 217, 2003. doi: 10.1016/S1534-5807(03)00025-X. URL http://www.sciencedirect.com/science/article/pii/S153458070300025X.

Kayes, J. and Clark, S. *CLAVATA2*, a regulator of meristem and organ development in *Arabidopsis*. *Development*, 125(19):3843–3851, 1998. URL http://dev.biologists.org/content/125/19/3843.

Kim, J. H., Lee, S.-R., Li, L.-H., Park, H.-J., Park, J.-H., Lee, K. Y., Kim, M.-K., Shin, B. A., and Choi, S.-Y. High Cleavage Efficiency of a 2A Peptide Derived from Porcine Teschovirus-1 in Human Cell Lines, Zebrafish and Mice. *PLOS ONE*, 6(4):1–8, 04 2011. doi: 10.1371/journal.pone.0018556. URL https://doi.org/10.1371/journal.pone.0018556.

Kim, J.-Y., Yuan, Z., and Jackson, D. Developmental regulation and significance of KNOX protein trafficking in *Arabidopsis*. *Development*, 130(18):4351–4362, 2003. doi: 10.1242/dev.00618. URL http://dev.biologists.org/content/130/18/4351.

Knox, K., Grierson, C. S., and Leyser, O. *AXR3* and *SHY2* interact to regulate root hair development. *Development*, 130(23):5769–5777, 2003. doi: 10.1242/dev.00659. URL http://dx.doi.org/10.1242/dev.00659.

Koizumi, K., Wu, S., MacRae-Crerar, A., and Gallagher, K. An Essential Protein that Interacts with Endosomes and Promotes Movement of the SHORT-ROOT Transcription Factor. *Current Biology*, 21(18):1559 – 1564, 2011. doi: 10.1016/j.cub.2011.08.013. URL http://www.sciencedirect.com/science/article/pii/S0960982211008888.

Koizumi, K., Hayashi, T., Wu, S., and Gallagher, K. L. The SHORT-ROOT protein acts as a mobile, dose-dependent signal in patterning the ground tissue. *Proceedings of the National Academy of Sciences*, 109(32):13010–13015, 2012. doi: 10.1073/pnas.1205579109. URL https://www.pnas.org/content/109/32/13010.

Koncz, C. and Schell, J. The promoter of T_L-DNA gene *5* controls the tissue-specific expression of chimaeric genes carried by a novel type of *Agrobacterium* binary vector. *Molecular and General Genetics MGG*, 204(3):383–396, Sep 1986. doi: 10.1007/BF00331014. URL https://doi.org/10.1007/BF00331014.

Kwiatkowska, D. Structural integration at the shoot apical meristem: models, measurements, and experiments. *American Journal of Botany*, 91(9):1277–1293, 2004. doi: 10.3732/ajb.91.9.1277. URL https://bsapubs.onlinelibrary.wiley.com/doi/abs/10.3732/ajb.91.9.1277.

Lampropoulos, A., Sutikovic, Z., Wenzl, C., Maegele, I., Lohmann, J. U., and Forner, J. GreenGate - A Novel, Versatile, and Efficient Cloning System for Plant Transgenesis. *PLoS One*, 8(12):e83043, Dec 2013. doi: 10.1371/journal.pone.0083043. URL http://www.ncbi.nlm.nih.gov/pmc/articles/PMC3869738/.

Landrein, B., Formosa-Jordan, P., Malivert, A., Schuster, C., Melnyk, C. W., Yang, W., Turnbull, C., Meyerowitz, E. M., Locke, J. C. W., and Jönsson, H. Nitrate modulates stem cell dynamics in *Arabidopsis* shoot meristems through cytokinins. *Proceedings of the National Academy of Sciences*, 115(6):1382–1387, 2018. doi: 10.1073/pnas.1718670115. URL https://www.pnas.org/content/115/6/1382.

Laux, T., Mayer, K., Berger, J., and Jürgens, G. The *WUSCHEL* gene is required for shoot and floral meristem integrity in *Arabidopsis*. *Development*, 122(1):87–96, 1996. URL http://dev.biologists.org/content/122/1/87.

Lee, J. T. Epigenetic Regulation by Long Noncoding RNAs. *Science*, 338(6113):1435–1439, 2012. doi: 10.1126/science.1231776. URL https://science.sciencemag.org/content/338/6113/1435.

Lenhard, M., Jürgens, G., and Laux, T. The *WUSCHEL* and *SHOOTMERISTEMLESS* genes fulfil complementary roles in *Arabidopsis* shoot meristem regulation. *Development*, 129(13):3195–3206, 2002. URL http://dev.biologists.org/content/129/13/3195.

Leyser, H. O., Pickett, F. B., Dharmasiri, S., and Estelle, M. Mutations in the *AXR3* gene of *Arabidopsis* result in altered auxin response including ectopic expression from the *SAUR-AC1* promoter. *The Plant Journal*, 10(3):403–413, 1996. doi: 10.1046/j.1365-313x.1996.10030403.x. URL http://dx.doi.org/10.1046/j.1365-313x.1996.10030403.x.

Li, X., Qian, Q., Fu, Z., Wang, Y., Xiong, G., Zeng, D., Wang, X., Liu, X., Teng, S., Hiroshi, F., Yuan, M., Luo, D., Han, B., and Li, J. Control of tillering in rice. *Nature*, 422:618–621, Apr 2003. doi: 10.1038/nature01518. URL http://dx.doi.org/10.1038/nature01518.

Liberman, L. M., Sparks, E. E., Moreno-Risueno, M. A., Petricka, J. J., and Benfey, P. N. MYB36 regulates the transition from proliferation to differentiation in the *Arabidopsis* root. *Proceedings of the National Academy of Sciences*, 112(39):12099–12104, 2015. doi: 10.1073/pnas.1515576112. URL https://www.pnas.org/content/112/39/12099.

Lobet, G. Structural Root Modelling. Nov 2015. doi: 10.6084/m9.figshare.1594792.v3. URL https://figshare.com/articles/Structural_Plant_Modelling/1594792/3.

Lobet, G., Pagès, L., and Draye, X. A Novel Image-Analysis Toolbox Enabling Quantitative Analysis of Root System Architecture. *Plant Physiology*, 157(1):29–39, 2011. doi: 10.1104/pp.111.179895. URL http://www.plantphysiol.org/content/157/1/29.

Lobet, G., Koevoets, I. T., Noll, M., Meyer, P. E., Tocquin, P., Pagès, L., and Périlleux, C. Using a Structural Root System Model to Evaluate and Improve the Accuracy of Root Image Analysis Pipelines. *Frontiers in Plant Science*, 8:447, 2017. doi: 10.3389/fpls.2017.00447. URL https://www.frontiersin.org/article/10.3389/fpls.2017.00447.

Long, J. and Barton, M. Initiation of Axillary and Floral Meristems in *Arabidopsis*. *Developmental Biology*, 218(2):341 – 353, 2000. doi: http://dx.doi.org/10.1006/dbio.1999.9572. URL http://www.sciencedirect.com/science/article/pii/S0012160699995726.

Long, J. A., Moan, E. I., Medford, J. I., and Barton, M. K. A member of the KNOTTED class of homeodomain proteins encoded by the *STM* gene of *Arabidopsis*. *Nature*, 379(6560):66–69, 1996. doi: 10.1038/379066a0. URL https://doi.org/10.1038/379066a0.

Lopez Marin, H. D. *Genetic and functional analysis of the tomato shoot branching regulator Super determinant 1 (Sde1)*. PhD thesis, Dec 2017. URL https://kups.ub.uni-koeln.de/9197/.

Lucas, W. J., Bouché-Pillon, S., Jackson, D. P., Nguyen, L., Baker, L., Ding, B., and Hake, S. Selective Trafficking of KNOTTED1 Homeodomain Protein and Its mRNA Through Plasmodesmata. *Science*, 270(5244): 1980–1983, 1995. doi: 10.1126/science.270.5244.1980. URL http://science.sciencemag.org/content/270/5244/1980.

Lynch, J. P. and Brown, K. M. Topsoil foraging - an architectural adaptation of plants to low phosphorus availability. *Plant and Soil*, 237(2):225–237, Dec 2001. doi: 10.1023/A:1013324727040. URL https://doi.org/10.1023/A:1013324727040.

Malamy, J. and Benfey, P. Organization and cell differentiation in lateral roots of *Arabidopsis thaliana*. *Development*, 124(1):33–44, 1997. URL http://dev.biologists.org/content/124/1/33.

Mashiguchi, K., Tanaka, K., Sakai, T., Sugawara, S., Kawaide, H., Natsume, M., Hanada, A., Yaeno, T., Shirasu, K., Yao, H., McSteen, P., Zhao, Y., Hayashi, K.-i., Kamiya, Y., and Kasahara, H. The main auxin biosynthesis pathway in *Arabidopsis*. *Proc Natl Acad Sci U S A*, 108(45):18512–18517, Nov 2011. doi: 10.1073/pnas.1108434108. URL http://dx.doi.org/10.1073/pnas.1108434108.

Mayer, K. F. X., Schoof, H., Haecker, A., Lenhard, M., Jürgens, G., and Laux, T. Role of *WUSCHEL* in Regulating Stem Cell Fate in the *Arabidopsis* Shoot Meristem. *Cell*, 95(6):805–815, Dec 1998. doi: 10.1016/S0092-8674(00)81703-1. URL https://doi.org/10.1016/S0092-8674(00)81703-1.

McSteen, P. and Leyser, O. Shoot Branching. *Annual Review of Plant Biology*, 56(1):353–374, 2005. doi: 10.1146/annurev.arplant.56.032604.144122. URL http://dx.doi.org/10.1146/annurev.arplant.56.032604.144122.

Medford, J. I. Vegetative Apical Meristems. *Plant Cell*, 4(9):1029–1039, Sep 1992. doi: 10.1105/tpc.4.9.1029. URL https://www.ncbi.nlm.nih.gov/pubmed/12297667.

Mizzotti, C., Galliani, B. M., Dreni, L., Sommer, H., Bombarely, A., and Masiero, S. ERAMOSA controls lateral branching in snapdragon. *Scientific Reports*, 7:41319, Feb 2017. doi: 10.1038/srep41319. URL http://dx.doi.org/10.1038/srep41319.

Moreno-Risueno, M. A., Van Norman, J. M., Moreno, A., Zhang, J., Ahnert, S. E., and Benfey, P. N. Oscillating Gene Expression Determines Competence for Periodic *Arabidopsis* Root Branching. *Science*, 329(5997):1306–1311, 2010. doi: 10.1126/science.1191937. URL http://science.sciencemag.org/content/329/5997/1306.

Morita, M. T. Directional Gravity Sensing in Gravitropism. *Annual Review of Plant Biology*, 61(1):705–720, 2010. doi: 10.1146/annurev.arplant.043008.092042. URL https://doi.org/10.1146/annurev.arplant.043008.092042.

Morita, M. T. and Tasaka, M. Gravity sensing and signaling. *Current Opinion in Plant Biology*, 7(6):712 – 718, 2004. doi: 10.1016/j.pbi.2004.09.001. URL http://www.sciencedirect.com/science/article/pii/S1369526604001220.

Mullen, J. and Hangarter, R. Genetic Analysis Of The Gravitropic Set-point Angle In Lateral Roots Of *Arabidopsis*. *Advances in Space Research*, 31(10):2229 – 2236, 2003. ISSN 0273-1177. doi: 10.1016/S0273-1177(03)00249-7. URL https://doi.org/10.1016/S0273-1177(03)00249-7. Space Life Sciences: Gravity-Related Processes in Plants.

Müller, D., Schmitz, G., and Theres, K. *Blind* Homologous *R2R3 Myb* Genes Control the Pattern of Lateral Meristem Initiation in *Arabidopsis*. *The Plant Cell*, 18(3):586–597, 2006. doi: 10.1105/tpc.105.038745. URL http://www.plantcell.org/content/18/3/586.

Müller, R., Bleckmann, A., and Simon, R. The Receptor Kinase CORYNE of *Arabidopsis* Transmits the Stem Cell–Limiting Signal CLAVATA3 Independently of CLAVATA1. *The Plant Cell*, 20(4):934–946, 2008. doi: 10.1105/tpc.107.057547. URL http://www.plantcell.org/content/20/4/934.

Mähönen, A. P., Tusscher, K. t., Siligato, R., Smetana, O., Diaz-Trivino, S., Salojarvi, J., Wachsman, G., Prasad, K., Heidstra, R., and Scheres, B. PLETHORA gradient formation mechanism separates auxin responses. *Nature*, 515(7525):125–129, Nov 2014. doi: 10.1038/nature13663. URL http://dx.doi.org/10.1038/nature13663.

Nagaya, S., Kawamura, K., Shinmyo, A., and Kato, K. The *HSP* Terminator of *Arabidopsis thaliana* Increases Gene Expression in Plant Cells. *Plant and Cell Physiology*, 51(2):328–332, Dec 2009. doi: 10.1093/pcp/pcp188. URL https://doi.org/10.1093/pcp/pcp188.

Nakajima, K., Sena, G., Nawy, T., and Benfey, P. N. Intercellular movement of the putative transcription factor SHR in root patterning. *Nature*, 413:307–311, Sep 2001. doi: 10.1038/35095061. URL http://dx.doi.org/10.1038/35095061.

Nawy, T., Lee, J.-Y., Colinas, J., Wang, J. Y., Thongrod, S. C., Malamy, J. E., Birnbaum, K., and Benfey, P. N. Transcriptional Profile of the Arabidopsis Root Quiescent Center. *The Plant Cell*, 17(7):1908–1925, 2005. doi: 10.1105/tpc.105.031724. URL http://www.plantcell.org/content/17/7/1908.

Nimchuk, Z. L., Tarr, P. T., and Meyerowitz, E. M. An Evolutionarily Conserved Pseudokinase Mediates Stem Cell Production in Plants. *The Plant Cell*, 23(3):851–854, 2011. doi: 10.1105/tpc.110.075622. URL http://www.plantcell.org/content/23/3/851.

Nimchuk, Z. L., Zhou, Y., Tarr, P. T., Peterson, B. A., and Meyerowitz, E. M. Plant stem cell maintenance by transcriptional cross-regulation of related receptor kinases. *Development*, 142(6):1043–1049, 2015. doi: 10.1242/dev.119677. URL http://dev.biologists.org/content/142/6/1043.

Niu, Y., Zhao, T., Xu, X., and Li, J. Genome-wide identification and characterization of GRAS transcription factors in tomato (*Solanum lycopersicum*). *PeerJ*, 5:e3955, Nov 2017. doi: 10.7717/peerj.3955. URL https://doi.org/10.7717/peerj.3955.

Ogawa, M., Shinohara, H., Sakagami, Y., and Matsubayashi, Y. *Arabidopsis* CLV3 Peptide Directly Binds CLV1 Ectodomain. *Science*, 319(5861):294–294, 2008. doi: 10.1126/science.1150083. URL http://science.sciencemag.org/content/319/5861/294.

Pacifici, E., Di Mambro, R., Dello Ioio, R., Costantino, P., and Sabatini, S. Acidic cell elongation drives cell differentiation in the *Arabidopsis* root. *The EMBO Journal*, 37(16), 2018. doi: 10.15252/embj.201899134. URL http://emboj.embopress.org/content/37/16/e99134.

Paquette, A. J. and Benfey, P. N. Maturation of the Ground Tissue of the Root Is Regulated by Gibberellin and *SCARECROW* and Requires *SHORT-ROOT*. *Plant Physiology*, 138(2):636–640, 2005. doi: 10.1104/pp.104.058362. URL http://www.plantphysiol.org/content/138/2/636.

Peralta, I. E. and Spooner, D. M. Morphological characterization and relationships of wild tomatoes (*Solanum* L. Sect. *Lycopersicon*). *Monographs In Systematic Botany*, 104:227, 2005. URL https://vcru.wisc.edu/spoonerlab/pdf/Peralta%20and%20Spooner%20D'Arcy%20volume.pdf.

Peret, B. Primary and lateral root.ai. Jul 2017. doi: 10.6084/m9.figshare.5143987.v4. URL https://figshare.com/articles/Primary_and_lateral_root_ai/5143987.

Pertea, M., Kim, D., Pertea, G. M., Leek, J. T., and Salzberg, S. L. Transcript-level expression analysis of RNA-seq experiments with HISAT, StringTie and Ballgown. *Nature Protocols*, 11:1650 EP –, Aug 2016. doi: 10.1038/nprot.2016.095. URL https://doi.org/10.1038/nprot.2016.095.

Pi, L., Aichinger, E., van der Graaff, E., Llavata-Peris, C., Weijers, D., Hennig, L., Groot, E., and Laux, T. Organizer-Derived WOX5 Signal Maintains Root Columella Stem Cells through Chromatin-Mediated Repression of *CDF4* Expression. *Developmental Cell*, 33(5):576 – 588, 2015. doi: 10.1016/j.devcel.2015.04.024. URL http://www.sciencedirect.com/science/article/pii/S1534580715002889.

Picard, D. and Schaffner, W. Correct transcription of a cloned mouse immunoglobulin gene *in vivo*. *Proc Natl Acad Sci U S A*, 80(2):417–421, Jan 1983. URL https://www.ncbi.nlm.nih.gov/pubmed/6300842.

Pysh, L. D., Wysocka-Diller, J. W., Camilleri, C., Bouchez, D., and Benfey, P. N. The GRAS gene family in Arabidopsis: sequence characterization and basic expression analysis of the *SCARECROW-LIKE* genes. *The Plant Journal*, 18(1):111–119, 1999. doi: 10.1046/j.1365-313X.1999.00431.x. URL https://onlinelibrary.wiley.com/doi/abs/10.1046/j.1365-313X.1999.00431.x.

Raatz, B., Eicker, A., Schmitz, G., Fuss, E., Müller, D., Rossmann, S., and Theres, K. Specific expression of LATERAL SUPPRESSOR is controlled by an evolutionarily conserved 3' enhancer. *The Plant Journal*, 68(3):400–412, 2011. doi: 10.1111/j.1365-313X.2011.04694.x. URL http://dx.doi.org/10.1111/j.1365-313X.2011.04694.x.

Raman, S., Greb, T., Peaucelle, A., Blein, T., Laufs, P., and Theres, K. Interplay of miR164, *CUP-SHAPED COTYLEDON* genes and *LATERAL SUPPRESSOR* controls axillary meristem formation in *Arabidopsis thaliana*. *The Plant Journal*, 55(1):65–76, 2008. doi: 10.1111/j.1365-313X.2008.03483.x. URL https://onlinelibrary.wiley.com/doi/abs/10.1111/j.1365-313X.2008.03483.x.

Ratcliffe, O. J., Riechmann, J. L., and Zhang, J. Z. *INTERFASCICULAR FIBERLESS1* Is the Same Gene as *REVOLUTA*. *The Plant Cell*, 12(3):315–317, 2000. doi: 10.1105/tpc.12.3.315. URL http://www.plantcell.org/content/12/3/315.

Reddy, G. V., Heisler, M. G., Ehrhardt, D. W., and Meyerowitz, E. M. Real-time lineage analysis reveals oriented cell divisions associated with morphogenesis at the shoot apex of *Arabidopsis thaliana*. *Development*, 131(17):4225–4237, 2004. doi: 10.1242/dev.01261. URL http://dev.biologists.org/content/131/17/4225.

Rosquete, M. R., von Wangenheim, D., Marhavý, P., Barbez, E., Stelzer, E. K., Benková, E., Maizel, A., and Kleine-Vehn, J. An Auxin Transport Mechanism Restricts Positive Orthogravitropism in Lateral Roots. *Current Biology*, 23(9):817–822, May 2013. doi: 10.1016/j.cub.2013.03.064. URL https://doi.org/10.1016/j.cub.2013.03.064.

Rossmann, S. *Analysis of the Lateral suppressor pathway in tomato axillary meristem formation.* Phd thesis, Universität Köln, Nov 2013. URL https://kups.ub.uni-koeln.de/5358/.

Rossmann, S., Kohlen, W., Hasson, A., and Theres, K. Lateral suppressor and Goblet act in hierarchical order to regulate ectopic meristem formation at the base of tomato leaflets. *The Plant Journal*, 81(6):837–848, Feb 2015. doi: 10.1111/tpj.12782. URL https://onlinelibrary.wiley.com/doi/abs/10.1111/tpj.12782.

Roychoudhry, S. and Kepinski, S. Shoot and root branch growth angle control—the wonderfulness of lateralness. *Current Opinion in Plant Biology*, 23:124 – 131, 2015. doi: 10.1016/j.pbi.2014.12.004. URL http://dx.doi.org/10.1016/j.pbi.2014.12.004.

Roychoudhry, S., Del Bianco, M., Kieffer, M., and Kepinski, S. Auxin Controls Gravitropic Setpoint Angle in Higher Plant Lateral Branches. *Current Biology*, 23(15):1497 – 1504, 2013. doi: 10.1016/j.cub.2013.06.034. URL http://dx.doi.org/10.1016/j.cub.2013.06.034.

Roychoudhry, S., Kieffer, M., Del Bianco, M., Liao, C.-Y., Weijers, D., and Kepinski, S. The developmental and environmental regulation of gravitropic setpoint angle in Arabidopsis and bean. *Scientific Reports*, 7:42664 EP –, Mar 2017. doi: 10.1038/srep42664. URL https://doi.org/10.1038/srep42664.

Roychoudhry, S., Sageman-Furnas, K., Wolverton, C., Goodman, H. L., Grones, P., Mullen, J., Hangarter, R., Friml, J., and Kepinski, S. Antagonistic and auxin-dependent phosphoregulation of columella PIN proteins controls lateral root gravitropic setpoint angle in Arabidopsis. *bioRxiv*, 2019. doi: 10.1101/594838. URL https://www.biorxiv.org/content/early/2019/03/31/594838.

Ruiz Rosquete, M. and Kleine-Vehn, J. PIN7 auxin carrier is a terminator of radial root expansion in *Arabidopsis thaliana*. *bioRxiv*, 2018. doi: 10.1101/253807. URL https://www.biorxiv.org/content/early/2018/01/25/253807.

Sabatini, S., Beis, D., Wolkenfelt, H., Murfett, J., Guilfoyle, T., Malamy, J., Benfey, P., Leyser, O., Bechtold, N., Weisbeek, P., and Scheres, B. An Auxin-Dependent Distal Organizer of Pattern and Polarity in the *Arabidopsis* Root. *Cell*, 99(5):463–472, Nov 1999. ISSN 0092-8674. doi: 10.1016/S0092-8674(00)81535-4. URL https://doi.org/10.1016/S0092-8674(00)81535-4.

Sabatini, S., Heidstra, R., Wildwater, M., and Scheres, B. SCARECROW is involved in positioning the stem cell niche in the *Arabidopsis* root meristem. *Genes Dev*, 17(3):354–358, Feb 2003. doi: 10.1101/gad.252503. URL https://www.ncbi.nlm.nih.gov/pubmed/12569126.

Sambrook, J. and Russel, D. W. *Molecular cloning: A laboratory manual*. Cold Spring Harbor Lab. Press, NY, 3 edition, 2001.

Santelia, D., Henrichs, S., Vincenzetti, V., Sauer, M., Bigler, L., Klein, M., Bailly, A., Lee, Y., Friml, J., Geisler, M., and Martinoia, E. Flavonoids Redirect PIN-mediated Polar Auxin Fluxes during Root Gravitropic Responses. *The Journal of Biological Chemistry*, 283(45):31218–31226, Nov 2008. doi: 10.1074/jbc.M710122200. URL http://www.ncbi.nlm.nih.gov/pmc/articles/PMC2662185/.

Sarkar, A. K., Luijten, M., Miyashima, S., Lenhard, M., Hashimoto, T., Nakajima, K., Scheres, B., Heidstra, R., and Laux, T. Conserved factors regulate signalling in *Arabidopsis thaliana* shoot and root stem cell organizers. *Nature*, 446:811 EP –, Apr 2007. doi: 10.1038/nature05703. URL https://doi.org/10.1038/nature05703.

Sassi, M., Lu, Y., Zhang, Y., Wang, J., Dhonukshe, P., Blilou, I., Dai, M., Li, J., Gong, X., Jaillais, Y., Yu, X., Traas, J., Ruberti, I., Wang, H., Scheres, B., Vernoux, T., and Xu, J. COP1 mediates the coordination of root and shoot growth by light through modulation of PIN1- and PIN2-dependent auxin transport in *Arabidopsis*. *Development*, 139(18):3402–3412, 2012. doi: 10.1242/dev.078212. URL http://dev.biologists.org/content/139/18/3402.

Schmitz, G., Tillmann, E., Carriero, F., Fiore, C., Cellini, F., and Theres, K. The tomato *Blind* gene encodes a MYB transcription factor that controls the formation of lateral meristems. *Proceedings of the National Academy of Sciences*, 99(2):1064–1069, 2002. doi: 10.1073/pnas.022516199. URL https://www.pnas.org/content/99/2/1064.

Schöller, M., Sarkel, E., Kleine-Vehn, J., and Feraru, E. *Root Development: Methods and Protocols*, chapter Growth Rate Normalization Method to Assess Gravitropic Root Growth, pages 199–208. Springer New York, 2018. ISBN 978-1-4939-7747-5. doi: 10.1007/978-1-4939-7747-5_15. URL https://doi.org/10.1007/978-1-4939-7747-5_15.

Schoof, H., Lenhard, M., Haecker, A., Mayer, K. F., Jürgens, G., and Laux, T. The Stem Cell Population of *Arabidopsis* Shoot Meristems Is Maintained by a Regulatory Loop between the *CLAVATA* and *WUSCHEL* Genes. *Cell*, 100(6):635 – 644, 2000. doi: https://doi.org/10.1016/S0092-8674(00)80700-X. URL http://www.sciencedirect.com/science/article/pii/S009286740080700X.

Schumacher, K., Schmitt, T., Rossberg, M., Schmitz, G., and Theres, K. The *Lateral suppressor* (*Ls*) gene of tomato encodes a new member of the VHIID protein family. *Proceedings of the National Academy of Sciences*, 96(1):290–295, 1999. doi: 10.1073/pnas.96.1.290. URL http://www.pnas.org/content/96/1/290.

Sessions, A., Yanofsky, M. F., and Weigel, D. Cell-Cell Signaling and Movement by the Floral Transcription Factors LEAFY and APETALA1. *Science*, 289(5480):779–781, 2000. doi: 10.1126/science.289.5480.779. URL https://science.sciencemag.org/content/289/5480/779.

Shi, B., Zhang, C., Tian, C., Wang, J., Wang, Q., Xu, T., Xu, Y., Ohno, C., Sablowski, R., Heisler, M. G., Theres, K., Wang, Y., and Jiao, Y. Two-Step Regulation of a Meristematic Cell Population Acting in Shoot Branching in *Arabidopsis*. *PLOS Genetics*, 12:1–20, 2016. doi: 10.1371/journal.pgen.1006168. URL https://doi.org/10.1371/journal.pgen.1006168.

Shimada, T. L., Shimada, T., and Hara-Nishimura, I. A rapid and non-destructive screenable marker, FAST, for identifying transformed seeds of *Arabidopsis thaliana*. *The Plant Journal*, 61(3):519–528, 2010. doi: 10.1111/j.1365-313X.2009.04060.x. URL http://dx.doi.org/10.1111/j.1365-313X.2009.04060.x.

Shinohara, H. and Matsubayashi, Y. Reevaluation of the CLV3-receptor interaction in the shoot apical meristem: dissection of the CLV3 signaling pathway from a direct ligand-binding point of view. *The Plant Journal*, 82 (2):328–336, 2015. doi: 10.1111/tpj.12817. URL https://onlinelibrary.wiley.com/doi/abs/10.1111/tpj.12817.

Sibout, R., Proost, S., Hansen, B. O., Vaid, N., Giorgi, F. M., Ho-Yue-Kuang, S., Legée, F., Cézart, L., Bouchabké-Coussa, O., Soulhat, C., Provart, N., Pasha, A., Le Bris, P., Roujol, D., Hofte, H., Jamet, E., Lapierre, C., Persson, S., and Mutwil, M. Expression atlas and comparative coexpression network analyses reveal important genes involved in the formation of lignified cell wall in *Brachypodium distachyon*. *New Phytologist*, 215(3):1009–1025, 2017. doi: 10.1111/nph.14635. URL https://nph.onlinelibrary.wiley.com/doi/abs/10.1111/nph.14635.

Siligato, R., Wang, X., Yadav, S. R., Lehesranta, S., Ma, G., Ursache, R., Sevilem, I., Zhang, J., Gorte, M., Prasad, K., Wrzaczek, M., Heidstra, R., Murphy, A., Scheres, B., and Mähönen, A. P. MultiSite Gateway-Compatible Cell Type-Specific Gene-Inducible System for Plants. *Plant Physiology*, 170(2):627–641, 2016. doi: 10.1104/pp.15.01246. URL http://www.plantphysiol.org/content/170/2/627.abstract.

Skourti-Stathaki, K. and Proudfoot, N. J. A double-edged sword: R loops as threats to genome integrity and powerful regulators of gene expression. *Genes & Development*, 28(13):1384–1396, 2014. doi: 10.1101/gad.242990.114. URL http://genesdev.cshlp.org/content/28/13/1384.abstract.

Sparks, E. Cross section of an *Arabidopsis* root. Feb 2017a. doi: 10.6084/m9.figshare.4688371.v1. URL https://figshare.com/articles/Cross_section_of_an_Arabidopsis_root/4688371.

Sparks, E. The stem cell niches of *Arabidopsis*. Feb 2017b. doi: 10.6084/m9.figshare.4688404.v1. URL https://figshare.com/articles/The_stem_cell_niches_of_Arabidopsis/4688404.

Stahl, Y. and Simon, R. Plant stem cell niches. *International Journal of Developmental Biology*, 49(5-6): 479–489, 2004. doi: 10.1387/ijdb.041929ys. URL http://dx.doi.org/10.1387/ijdb.041929ys.

Stahl, Y., Wink, R. H., Ingram, G. C., and Simon, R. A Signaling Module Controlling the Stem Cell Niche in *Arabidopsis* Root Meristems. *Current Biology*, 19(11):909 – 914, 2009. doi: https://doi.org/10.1016/j.cub.2009.03.060. URL http://www.sciencedirect.com/science/article/pii/S0960982209009142.

Stahl, Y., Grabowski, S., Bleckmann, A., Kühnemuth, R., Weidtkamp-Peters, S., Pinto, K., Kirschner, G., Schmid, J., Wink, R., Hülsewede, A., Felekyan, S., Seidel, C., and Simon, R. Moderation of *Arabidopsis* Root Stemness by CLAVATA1 and ARABIDOPSIS CRINKLY4 Receptor Kinase Complexes. *Current Biology*, 23(5):362 – 371, 2013. doi: 10.1016/j.cub.2013.01.045. URL http://www.sciencedirect.com/science/article/pii/S0960982213000808.

Sun, Q., Csorba, T., Skourti-Stathaki, K., Proudfoot, N. J., and Dean, C. R-Loop Stabilization Represses Antisense Transcription at the *Arabidopsis FLC* Locus. *Science*, 340(6132):619–621, 2013. doi: 10.1126/science.1234848. URL https://science.sciencemag.org/content/340/6132/619.

Takada, S., Hibara, K., Ishida, T., and Tasaka, M. The *CUP-SHAPED COTYLEDON1* gene of *Arabidopsis* regulates shoot apical meristem formation. *Development*, 128(7):1127–1135, 2001. URL http://dev.biologists.org/content/128/7/1127.

Talbert, P., Adler, H., Parks, D., and Comai, L. The *REVOLUTA* gene is necessary for apical meristem development and for limiting cell divisions in the leaves and stems of *Arabidopsis thaliana*. *Development*, 121 (9):2723–2735, 1995. URL http://dev.biologists.org/content/121/9/2723.

Tian, C., Zhang, X., He, J., Yu, H., Wang, Y., Shi, B., Han, Y., Wang, G., Feng, X., Zhang, C., Wang, J., Qi, J., Yu, R., and Jiao, Y. An organ boundary-enriched gene regulatory network uncovers regulatory hierarchies underlying axillary meristem initiation. *Molecular Systems Biology*, 10(10), 2014. doi: 10.15252/msb.20145470. URL http://msb.embopress.org/content/10/10/755.

Toal, T. W., Ron, M., Gibson, D., Kajala, K., Splitt, B., Johnson, L. S., Miller, N. D., Slovak, R., Gaudinier, A., Patel, R., de Lucas, M., Provart, N. J., Spalding, E. P., Busch, W., Kliebenstein, D. J., and Brady, S. M. Regulation of Root Angle and Gravitropism. *G3: Genes, Genomes, Genetics*, 8(12):3841–3855, 2018. doi: 10.1534/g3.118.200540. URL http://dx.doi.org/10.1534/g3.118.200540.

Truernit, E., Bauby, H., Dubreucq, B., Grandjean, O., Runions, J., Barthélémy, J., and Palauqui, J.-C. High-Resolution Whole-Mount Imaging of Three-Dimensional Tissue Organization and Gene Expression Enables the Study of Phloem Development and Structure in *Arabidopsis*. *The Plant Cell*, 20(6):1494–1503, 2008. doi: 10.1105/tpc.107.056069. URL http://www.plantcell.org/content/20/6/1494.

Uchida, N., Takahashi, K., Iwasaki, R., Yamada, R., Yoshimura, M., Endo, T. A., Kimura, S., Zhang, H., Nomoto, M., Tada, Y., Kinoshita, T., Itami, K., Hagihara, S., and Torii, K. U. Chemical hijacking of auxin signaling with an engineered auxin-TIR1 pair. *Nature Chemical Biology*, 14:299 EP –, Jan 2018. doi: 10.1038/nchembio.2555. URL https://doi.org/10.1038/nchembio.2555.

Untergasser, A., Cutcutache, I., Koressaar, T., Ye, J., Faircloth, B. C., Remm, M., and Rozen, S. G. Primer3—new capabilities and interfaces. *Nucleic Acids Research*, 40(15):e115–e115, Jul 2012. doi: 10.1093/nar/gks596. URL https://doi.org/10.1093/nar/gks596.

van den Berg, C., Willemsen, V., Hage, W., Weisbeek, P., and Scheres, B. Cell fate in the *Arabidopsis* root meristem determined by directional signalling. *Nature*, 378(6552):62–65, 1995. doi: 10.1038/378062a0. URL https://doi.org/10.1038/378062a0.

van den Berg, C., Willemsen, V., Hendriks, G., Weisbeek, P., and Scheres, B. Short-range control of cell differentiation in the *Arabidopsis* root meristem. *Nature*, 390(6657):287–289, 1997. doi: 10.1038/36856. URL https://doi.org/10.1038/36856.

van Gelderen, K., Kang, C., Paalman, R., Keuskamp, D., Hayes, S., and Pierik, R. Far-Red Light Detection in the Shoot Regulates Lateral Root Development through the HY5 Transcription Factor. *The Plant Cell*, 30 (1):101–116, 2018. doi: 10.1105/tpc.17.00771. URL http://www.plantcell.org/content/30/1/101.

Vroemen, C. W., Mordhorst, A. P., Albrecht, C., Kwaaitaal, M. A. C. J., and de Vries, S. C. The *CUP-SHAPED COTYLEDON3* Gene Is Required for Boundary and Shoot Meristem Formation in Arabidopsis. *The Plant Cell*, 15(7):1563–1577, 2003. doi: 10.1105/tpc.012203. URL http://www.plantcell.org/content/15/7/1563.

Waidmann, S., Rosquete, M. R., Schöller, M., Lindner, H., LaRue, T., Sarkel, E., Petřík, I., Dünser, K., Martopawiro, S., Sasidharan, R., Novak, O., Wabnik, K., Dinneny, J. R., and Kleine-Vehn, J. Cytokinin functions as an asymmetric and anti-gravitropic signal in lateral roots. *bioRxiv*, 2019. doi: 10.1101/572941. URL https://www.biorxiv.org/content/early/2019/03/09/572941.

Wang, H., Chung, P. J., Liu, J., Jang, I.-C., Kean, M. J., Xu, J., and Chua, N.-H. Genome-wide identification of long noncoding natural antisense transcripts and their responses to light in *Arabidopsis*. *Genome Research*, 24(3):444–453, 2014a. doi: 10.1101/gr.165555.113. URL http://genome.cshlp.org/content/24/3/444.abstract.

Wang, J.-W., Wang, L.-J., Mao, Y.-B., Cai, W.-J., Xue, H.-W., and Chen, X.-Y. Control of root cap formation by MicroRNA-targeted auxin response factors in Arabidopsis. *Plant Cell*, 17(8):2204–2216, Aug 2005. doi: 10.1105/tpc.105.033076. URL http://dx.doi.org/10.1105/tpc.105.033076.

Wang, Q., Kohlen, W., Rossmann, S., Vernoux, T., and Theres, K. Auxin Depletion from the Leaf Axil Conditions Competence for Axillary Meristem Formation in *Arabidopsis* and Tomato. *The Plant Cell*, 26(5):2068–2079, 2014b. doi: 10.1105/tpc.114.123059. URL http://www.plantcell.org/content/26/5/2068.

Wang, Q., Hasson, A., Rossmann, S., and Theres, K. *Divide et impera*: boundaries shape the plant body and initiate new meristems. *New Phytologist*, 209(2):485–498, 2016. doi: 10.1111/nph.13641. URL http://dx.doi.org/10.1111/nph.13641.

Wang, Y., Wang, J., Shi, B., Yu, T., Qi, J., Meyerowitz, E. M., and Jiao, Y. The Stem Cell Niche in Leaf Axils Is Established by Auxin and Cytokinin in *Arabidopsis*. *The Plant Cell*, 26(5):2055–2067, 2014c. doi: 10.1105/tpc.114.123083. URL http://www.plantcell.org/content/26/5/2055.

Weijers, D. and Wagner, D. Transcriptional Responses to the Auxin Hormone. *Annual Review of Plant Biology*, 67(1):539–574, 2016. doi: 10.1146/annurev-arplant-043015-112122. URL https://doi.org/10.1146/annurev-arplant-043015-112122.

Winter, D., Vinegar, B., Nahal, H., Ammar, R., Wilson, G. V., and Provart, N. J. An "Electronic Fluorescent Pictograph" Browser for Exploring and Analyzing Large-Scale Biological Data Sets. *PLOS ONE*, 2(8):1–12, Aug 2007. doi: 10.1371/journal.pone.0000718. URL https://doi.org/10.1371/journal.pone.0000718.

Wu, X., Dinneny, J. R., Crawford, K. M., Rhee, Y., Citovsky, V., Zambryski, P. C., and Weigel, D. Modes of intercellular transcription factor movement in the *Arabidopsis* apex. *Development*, 130(16):3735–3745, 2003. doi: 10.1242/dev.00577. URL http://dev.biologists.org/content/130/16/3735.

Wysocka-Diller, J., Helariutta, Y., Fukaki, H., Malamy, J., and Benfey, P. Molecular analysis of SCARECROW function reveals a radial patterning mechanism common to root and shoot. *Development*, 127(3):595–603, 2000. URL http://dev.biologists.org/content/127/3/595.

Yadav, R. K., Perales, M., Gruel, J., Girke, T., Jönsson, H., and Reddy, G. V. WUSCHEL protein movement mediates stem cell homeostasis in the *Arabidopsis* shoot apex. *Genes Dev*, 25(19):2025–2030, Oct 2011. doi: 10.1101/gad.17258511. URL http://www.ncbi.nlm.nih.gov/pmc/articles/PMC3197201/.

Zambryski, P. Cell-to-cell transport of proteins and fluorescent tracers via plasmodesmata during plant development. *The Journal of Cell Biology*, 164(2):165–168, 2004. doi: 10.1083/jcb.200310048. URL http://jcb.rupress.org/content/164/2/165.

Zambryski, P. and Crawford, K. Plasmodesmata: Gatekeepers for Cell-to-Cell Transport of Developmental Signals in Plants. *Annual Review of Cell and Developmental Biology*, 16(1):393–421, 2000. doi: 10.1146/annurev.cellbio.16.1.393. URL https://doi.org/10.1146/annurev.cellbio.16.1.393.

Zhan, X., Wang, B., Li, H., Liu, R., Kalia, R. K., Zhu, J.-K., and Chinnusamy, V. *Arabidopsis* proline-rich protein important for development and abiotic stress tolerance is involved in microRNA biogenesis. *Proceedings of the National Academy of Sciences*, 109(44):18198–18203, 2012. doi: 10.1073/pnas.1216199109. URL http://dx.doi.org/10.1073/pnas.1216199109.

Zhang, C., Wang, J., Wenkel, S., Chandler, J. W., Werr, W., and Jiao, Y. Spatiotemporal control of axillary meristem formation by interacting transcriptional regulators. *Development*, 145(24), 2018. doi: 10.1242/dev.158352. URL http://dev.biologists.org/content/145/24/dev158352.

Zhao, Y., Christensen, S. K., Fankhauser, C., Cashman, J. R., Cohen, J. D., Weigel, D., and Chory, J. A Role for Flavin Monooxygenase-Like Enzymes in Auxin Biosynthesis. *Science*, 291(5502):306–309, 2001. doi: 10.1126/science.291.5502.306. URL http://dx.doi.org/10.1126/science.291.5502.306.

Danksagung/Acknowledgments

Größer Dank gilt KlausTheres, mir die Möglichkeit gegeben zu haben, mich selbst weiterzuentwickeln, durch die Herausvorderung die Rolle von LAS in der Wurzel zu entschlüsseln. Du warst immer offen für Diskussionen und ein für mich prägender Satz war das 'Principle of Limited Sloppiness' von Max Delbrück, den du irgendwann zu Beginn meiner Arbeit an der Thesis zitiert hast. Die 'limited Sloppiness', als Bereitschaft neue Ideen auszuprobieren (meine Auslegung), war ausschlaggebend für die Weiterentwicklung des Projekts in Phasen des Stillstands.

Gerne möchte ich auch UteHöcker und WolfgangWerr für Ihre Bereitschaft zur Übernahme des Prüfungsvorsitzes und des Zweitgutachters danken.

I would particularly like to thank Udhaya and Hernán, as long-time office fellows and first-line witnesses of success or failure, for our nice informal discussions, and for sharing your nuts, cakes, choc late and biscuits with me.

Thanks to Susanne, Quan and Aman, for your feedback regarding my project and your encouragement.

I would like to thank Wouter, who was the first to become interested in LAS function in the root and set the seed for this project. You always supported the project, by being available for long and insightful discussions.

Ursula und Alex, vielen Dank für eure Unterstüzung im Labor und im Gewächshaus. Eure Hilfe hat mir Freiräume gegeben, um neue Ansätze oder Ideen zu entwickeln und auszuprobieren.

I would like to thank TomBeeckman and BarbaraMöller (both VIB, Ghent, Belgium) for their help during the initial phase of this study, by helping to get used to work with, and analyze, the hidden half of *Arabidopsis*.

Dem Gewächshaus-Team möchte ich meinen Dank dafür aussprechen, weil Ihr euch velässlich um meine *Arabidopsis* Pflanzen gekümmert habt.

Ich möchte meiner Familie und meinen Freunden für ihre Unterstützung danken.

Mein gößter Dank gilt meiner Freundin Lea. Danke, dass Du, in dieser von emotionalen Höhen und Tiefen geprägten Zeit, immer an mich geglaubt und mich unterstützt hast.

-If you're too sloppy, then you never get reproducible results, and then you never can draw any conclusions; but if you are just a little sloppy, then when you see something startling, (...) you nail it down (...). So I called it the 'Principle of Limited Sloppiness'.- Max Delbrück.

Eidesstattliche Erklärung

Ich versichere, dass ich die von mir vorgelegte Dissertation selbständig angefertigt, die benutzten Quellen und Hilfsmittel vollständig angegeben und die Stellen der Arbeit - einschließlich Tabellen, Karten und Abbildungen -, die anderen Werken im Wortlaut oder dem Sinn nach entnommen sind, in jedem Einzelfall als Entlehnung kenntlich gemacht habe; dass diese Dissertation noch keiner anderen Fakultät oder Universität zur Prüfung vorgelegen hat; dass sie - abgesehen von unten angegebenen Teilpublikationen - noch nicht veröffentlicht worden ist, sowie, dass ich eine solche Veröffentlichung vor Abschluss des Promotionsverfahrens nicht vornehmen werde. Die Bestimmungen der Promotionsordnung sind mir bekannt. Die von mir vorgelegte Dissertation ist von Prof. Dr. Klaus Theres betreut worden.

Köln, 20.05.2019

Rahere Thoma



BY NC SA